Ollscoil Chathair Bhaile Átha Cliath
Dublin City University

Copper(II) Phenanthrene and Naphthalene Oxidative Chemical Nucleases

Zara Molphy B.Sc (Hons)

A thesis submitted for the award of
Doctor of Philosophy

Primary Supervisor: Dr. Andrew Kellett
Co-supervisor: Dr. Niall Barron

School of Chemical Sciences
Dublin City University
January 2017

I hereby certify that this material, which I now submit for assessment on the programme of study leading to the award of Doctor of Philosophy is entirely my own work, and that I have exercised reasonable care to ensure that the work is original, and does not to the best of my knowledge breach any law of copyright, and has not been taken from the work of others save and to the extent that such work has been cited and acknowledged within the text of my work.

Signed: _____ (Candidate) ID No.: _____ Date: _____

In memory of my Nanny

ACKNOWLEDGEMENTS

The completion of this thesis allows me the opportunity to thank several people who have contributed to this research in many ways and to whom I am deeply grateful.

Firstly, I wish to offer my utmost thanks to to my supervisor Dr. Andrew Kellett for his unwavering support, guidance, encouragement and patience from the beginning of my 4th year research project through to the final year of my PhD programme. Thank you for always having your door open for a "quick chat"! Without his wisdom and counsel, this work would not have been possible. It was a pleasure joining the group at such an early stage to see it blossom into such an energetic and successful research group –a testament to his work ethic, ambition and most importantly his mentorship.

Thanks to my fellow Kellett Research Group colleagues both past and present. To the science/cat meme contributors in the "Chemical Hunger" group (you know who you are), thanks for the daily laughs. In particular I would like to say a huge thank you to Creina Slator and Tadhg McGivern for being a constant rock of support. The most challenging lab days are made easy with such great friends around. To both Shauna and David, for the many many coffee and scone breaks spanning our undergraduate and postgraduate careers together.

I would also like to thank my co-supervisor Dr. Niall Barron, Dr. Paul Kelly and Dr. Alan Griffith, for providing me with much needed advice in the early days of my biological career in 201. A big thank you to both Carol and Mairead for a warm welcome to the NICB everyday and also to Prof. Martin Clynes for his entertaining emails. To Prof. Vickie McKee, I really appreciate your contribution to my projects. I am also grateful to the technical support staff in the NICB, NRF and the School of Chemical Sciences – especially to Damien and Ambrose– for always being there with a joke and a smile.

To Steven, who ended up learning more about my PhD than he ever intended! Thank you for being so caring, patient, understanding of the late night graphing and for always making me laugh –even if it's at my own expense!

To my aunty, uncles and cousins for the weekend beach trips with the ponies and the Sunday dinner sweats! Finally, I would like to thank my parents for their unconditional love, encouragement, support and belief in me. I would not have been able to start or complete this chapter of my life without them.

PUBLICATIONS

- **Z. Molphy**, D. Montagner, C. Slator, A. Erxleben and A. Kellett. [Cu_2(*tetra*-(2-pyridyl)-naphthalene)Cl_4] Displays Non-Intercalative Major Groove Binding and Self-Activating Oxidative DNA Damage, *Nucleic Acids Research*, 2017 (Manuscript in preparation).

- A. Kellett, **Z. Molphy**, C. Slator, V. McKee and N. Farrell. Molecular Methods for Probing Cytotoxic Metallodrug-DNA Interactions, *Current Medicinal Chemistry*, 2017 (Accepted).

- N. McStay, **Z. Molphy**, A. Coughlan, A. Cafolla, V. McKee, N. Gathergood and A. Kellett. C_3-Symmetric Opioid Scaffolds are pH-Responsive DNA Condensation Agents, *Nucleic Acids Research*, 2017 (In press – DOI: 10.1093/nar/gkw1097).

- M. A. Terzidis, A. Prisecaru, **Z. Molphy**, N. Barron, A. Randazzo, E. Dumont, M. G. Krokidis, A. Kellett and C. Chatgilialoglu. Radical-induced purine lesion formation is dependent on DNA helical topology, *Free Radical Research*, 2016, **50**, S91-101.

- **Z. Molphy**, C. Slator, C. Chatgilialoglu and A. Kellett. DNA Oxidation Profiles of Copper Phenanthrene Chemical Nucleases, *Frontiers in Chemistry*, 2015, **3**, 1-9.

- **Z. Molphy**, A. Prisecaru, C. Slator, N. Barron, M. McCann, J. Colleran, D. Chandran, N. Gathergood and A. Kellett. Copper Phenanthrene Oxidative Chemical Nucleases, *Inorganic Chemistry*, 2014, **53**, 5392–5404.

- A. Prisecaru, **Z. Molphy**, R. Kipping, E. Peterson, Y. Qu, A. Kellett and N. Farrell. The Phosphate Clamp: sequence selective nucleic acid binding profiles and conformational induction of endonuclease inhibition by cationic Triplatin complexes, *Nucleic Acids Research*, 2014, **42**, 13474-13487.

- A. Kellett, A. Prisecaru, C. Slator, **Z. Molphy**, M. McCann. Metal-Based Antimicrobial Protease Inhibitors. *Current Medicinal Chemistry*, 2013, **20**, 3134-3151.

POSTER AND SCIENTIFIC TALKS

Poster Title:

- Z. Molphy, N. McStay, and A. Kellett. C_3-Symmetric Opioid Scaffolds are pH-Responsive DNA Condensation Agents. 68th Irish Universities Chemistry Research Colloquium, University College Cork, 23 – 24th June 2016.

- Z. Molphy, D. Montagner, C. Slator, A. Erxleben, and A. Kellett. 2015. [Cu_2(*tetra*-(2-pyridyl)-naphthalene)Cl_4] displays self-activating oxidative chemical nuclease activity at the major groove. ISABC International Symposium on Applied Bio-Inorganic Chemistry, National University of Ireland Galway, 12 – 15th June 2015.

- Z. Molphy, A. Prisecaru, C. Slator and A. Kellett. 2014. Copper Phenanthrene Oxidative Chemical Nucleases. Inorganic Ireland Symposium, Royal College of Surgeons in Ireland, 11th December 2014.

- Z. Molphy, A. Prisecaru, C. Slator, and A. Kellett. 2014. Copper Phenanthrene Oxidative Chemical Nucleases. MCB2014; Joining Forces in Pharmaceutical Analysis and Medicinal Chemistry, University of Groningen, The Netherlands, 25 – 26th August 2014.

- Z. Molphy, A. Prisecaru, C. Slator, and A. Kellett. 2014. The development of Copper(II) Phenanthrene Oxidative Chemical Nucleases. 66th Irish Universities Chemistry Research Colloquium, National University of Ireland Galway, 19 – 20th June 2014.

Scientific Talks:

- DNA Oxidation Profiles of Copper Phenanthrene Chemical Nucleases. 68th Irish Universities Chemistry Research Colloquium, University College Cork, 23 – 24th June 2016.

- DNA Oxidation Profiles of Copper Phenanthrene Chemical Nucleases. COST Action CM1201 Biomimetic Radical Chemistry, Carton House, Maynooth, 23 – 25th July 2015.

- The design and development of Copper Phenanthrene based Chemical Nucleases. Irish Institute for Metal Based Drugs (IIMBD), Royal College of Surgeons in Ireland, 1st November 2013.

AWARDS

Irish Research Council Government of Ireland Postgraduate Scholar GOIPG/2013/826, with the project title: Inorganic Molecular Scissors as Tools for Gene Knockout.

AIMS OF THE RESEARCH

The broad aim of this research was the development of new materials as potentially novel nucleic acid binding agents.

Firstly, a range of Cu^{2+} phenanthrene-based chemical nucleases were generated as potential anticancer agents and structure-activity relationship (SAR) studies were conducted in order to identify agents with augmented (i) nucleotide binding affinity, (ii) base specific targeting/DNA recognition, (iii) oxidative chemical nuclease activity, and (iv) cytotoxicity profiles using a number of newly developed molecular biology based techniques. Experiments were also designed such that the oxidative DNA cleavage mechanism and redox properties of the complexes could be elucidated relative to the control, Sigman's reagent $[Cu(phen)_2]^{2+}$. The influence of nuclearity on DNA binding and oxidative cleavage was also explored during this project.

The introduction of two or three metal centres into a complex scaffold has not only uncovered binding interactions not possible through the use of univalent complexes but has also transformed metallodrug transport and cellular accumulation properties. Therefore, the second aim of this project was to elucidate the nucleic acid interactions of a novel di-nuclear Cu^{2+} complex, $[Cu_2(\textit{tetra}\text{-}(2\text{-pyridyl})\text{-naphthalene})Cl_4]$, through a range of biophysical and electrophoretic techniques available to this group.

The final aim of this project was to uncover the DNA binding properties of C_3-symmetric opiate compounds and their potential use as novel gene delivery agents. A wide range of biophysical and molecular biological techniques including atomic force microscopy, on-chip microfluidics and absorbance-based spectroscopy were employed to uncover their binding mechanism.

CONTRIBUTION TO PEER-REVIEWED PUBLICATIONS

This thesis contains four original papers published in peer-reviewed journals conducted in collaboration with colleagues from the Kellett research group and through collaborations with other institutions.

My contribution to each paper presented in this thesis is outlined in the table below:

Thesis Chapter	Publication Title	Publication Status	Nature and Extent of Candidates Contribution
I	Molecular Methods for Probing Cytotoxic Metallodrug-DNA Interactions	Currrent Medicinal Chemistry, 2017, Accepted for publication.	Manuscript 2nd author. Contributed to writing sections of this review relevant to the work conducted during my PhD.
II	Copper Phenanthrene Chemical Oxidative Nucleases	Inorganic Chemistry, 2014, 53, 10, 5392-5404.	Manuscript joint 1st author. Conducted the synthesis of organic ligands and inorganic complexes, DNA binding studies, chemical nuclease, SOD and H_2O_2 breakdown assays.
III	DNA Oxidation Profiles of Copper Phenanthrene Chemical Nucleases	Frontiers in Chemistry, 2015, 3, 28.	Manuscript 1st author. Designed and conducted DNA cleavage studies and polymerase chain reaction inhibition studies. Collaborated with Miss. Creina Slator on 8-oxo-dG assay.
IV	$[Cu_2$(*tetra*-(2-pyridyl)-naphthalene)$Cl_4]$ Displays Self-Activating Oxidative Chemical Nuclease Activity at the Major Groove	Nucleic Acids Research, 2017, Manuscript in preparation.	Manuscript joint 1st author. Conducted DNA binding and cleavage assays and developed biophysical experiments to investigate drug-DNA interactions including circular dichroism spectroscopy.
V	C_3-Symmetric Opioid Scaffolds are pH-Responsive DNA Condensation Agents	Nucleic Acids Research, 2017, Accepted for publication.	Manuscript joint 1st author. Conducted condensation studies on a series of mono- , di- and tri-substituted mesitylene-linked opioid scaffolds. Collaborated with Miss. Natasha McStay on DNA binding assays.

THESIS OUTLINE

A detailed overview of each chapter is given below.

Chapter I

This chapter reviews a range of molecular methods currently employed within our laboratory to explore covalent and non-covalent nucleic acid interactions of novel copper^{2+} and platinum^{2+} metallodrugs. Molecular methods for probing these binding interactions include: *i*.) electrophoretic based techniques; *ii*.) fluorescence and absorbance based techniques; *iii*.) viscosity; *iv*.) mass spectrometry; *v*.) NMR spectroscopy; and *vi*.) *in cellulo* genotoxicity. These experimental concepts are discussed in detail and feature heavily in the following chapters.

Chapter II

This chapter describes the synthesis and characterisation of a series of novel, structurally related, copper^{2+} phenanthrene complexes whose nucleotide binding affinity, intercalative profile, and oxidative chemical nuclease activity were explored using a range of high-throughput biophysical and electrophoretic techniques. This chapter also describes the use of a microfluidic on-chip protocol to compare the DNA degradation profiles of the complex series. Furthermore, the cytotoxic properties of the complexes were determined on human SKOV3 ovarian cancer cells.

Chapter III

This chapter outlines mechanistic investigations into the oxidative DNA cleavage and redox properties of the previously reported *mono*-nuclear copper^{2+} phenanthrene complexes and the *di*-nuclear agent [{Cu(phen)$_2$}$_2$(μ-terph)](terph), Cu-Terph. In this study, complexes are directly compared to Sigman's reagent [Cu(phen)$_2$]$^{2+}$ through the use of both reactive oxygen species (ROS) scavangers and stabilisers and an ELISA protocol to determine the number of oxidative DNA lesions (8-oxo-dG) produced during complex exposure.

Chapter IV

This chapter describes the rational design, DNA binding activity, and antitumoural potential of a novel di-nuclear copper $^{2+}$ complex [Cu_2(*tetra*-(2-pyridyl)-naphthalene)Cl_4] (Cu_2TPNap). This complex binds DNA non-intercalatively at the major groove with high affinity, inducing major groove deformation. and oxidative DNA damage in the absence of exogenous oxidant or reductant through a superoxide-mediated process.

Chapter V

This chapter describes the synthesis and characterisation of a series of *mono*-substituted (C_1-symmetric), *di*-substitued (C_2-symmetric) and *tri*-substituted (C_3-symmetric) mesitylene-linked opioid scaffolds. The high affinity DNA binding and condensation properties observed were found to be dependant on the C_3 scaffold and formal 3+ cationic charge. These effects were determined through a number of biophysical techniques including gel electrophoresis, on-chip microfluidic analysis, turbidity, thermal melting, circular dichroism and atomic force microscopy.

Signed:

_____ _____

Candidate Principal Supervisor

_____

Secondary Supervisor

TABLE OF CONTENTS

TABLE OF FIGURES

TABLE OF TABLES

TABLE OF SCHEMES

ABBREVIATIONS

A	Adenine
ACN	Acetonitrile
A-DNA	Dehydrated DNA
BER	Base excision repair
bipy	2,2′-bipyridine
bp	Base pair
C	Cytosine
CD	Circular Dichroism Spectrometry
$CDCl_3$	Deuterated Chloroform
$CHCl_3$	Chloroform
CHN	Carbon hydrogen nitrogen analysis
Chrysi	5,6-chrysenequinone diimine
CpG	Cytosine-phosphate-guanine
ctDNA	Calf thymus DNA
CTR1	Copper uptake transport protein
$CuCl_2$	Copper chloride
Cu/Zn-SOD	Copper and Zinc superoxide dismutase
C_{50}	Concentration required to reduce fluorescence intensity by 50%
DBSs	Double stranded breaks
DDD	Dickerson Drew Dodecamer
DI H_2O	Deionised Water
DMSO	Dimethylsulfoxide
DMF	Dimethylformamide
DNA	Deoxyribose nucleic acid
dsDNA	Double stranded DNA
DPPN	Benzol [*l*] Dipyrido[3,2-*a*:2′,3′-c]phenazine
DPPZ	Dipyridol[3,2-*a*:2′,3′-c]phenazine
DPQ	Dipyrido[3,2-*f*:2′,3′-h]quinoxaline
D_2O	Deuterated water
EDTA	Ethylenediaminetetraacetic acid
EtBr	Ethidium bromide
Et^+	Ethidium cation
EtOH	Ethanol
G	Guanine
lcDNA	Linear
GC	Gas chromatography
lcDNA	Linear DNA
L*k*	Link number
ICL	Interstrand Crosslinking
ICD	Induced circular dichroism
IC_{50}	half maximal inhibitory concentration
IR	Infrared spectroscopy
HPLC	High pressure liquid chromatography
H_2O_2	Hydrogen Peroxide
H_2SO_4	Sulphuric acid
HNO_3	Nitric acid

LC	Liquid chromatography
K_{app}	Apparent binding constant
K_b	Binding constant
KBr	Potassium bromide
KI	Potassium Iodide
lcDNA	Linear DNA
mC	Methyl cytosine
MeOH	Methanol
ML-DNA	Micrococcus leuteus DNA
MP	Melting point
MS	Mass spectrometry
NaN_3	Sodium Azide
NaOH	Sodium hydroxide
NBT	Nitro blue tetrazolium
NER	Nucleotide excision repair
NMR	Nuclear magnetic resonance
ocDNA	Open circular DNA
$^1O_2$	Singlet oxygen
$^{\bullet}OH$	Hydroxyl radical
$O_2^{\bullet-}$	Superoxide radical
PCR	Polymerase chain reaction
Poly[(A-T)$_2$]	Poly(deoxyadenylic-thymidylic) acid sodium salt
Poly[(G-C)$_2$]	Poly(deoxyguanylic-deoxycytidylic) acid sodium salt
Phen	1,10-Phenanthroline
Phen-Dione	1,10-Phenanthroline-5,6-Dione
RNA	Ribonucleic acid
RNS	Reactive nitrogen species
ROS	Reactive oxygen species
rpm	rotations per minute
scDNA	Supercoiled DNA
SOD	Superoxide dismutase
SODm	Superoxide dismutase mimetic
ssDNA	Single stranded DNA
stDNA	Salmon Testes DNA
T	Thymine
Taq	Thermus aquaticus
Terph	Terephthalate
T_M	Thermal melting
Topo	Topoisomerase
Tw	Twist number
Wr	Writhe number
Z-DNA	Zigzag DNA

Units of Measurement

Å	Angstrom
Abs	Absorbance
cm	Centimeter
cm^{-1}	Reciprocal wavelength
cP	Centipoise
C_{50}	Concentration required to reduce 50% fluorescence
°C	Degrees Celcius
δ	Delta (NMR chemical shift)
ΔT_M	Difference in thermal melting
ε_{max}	molar absorption coefficient
g	Gram
h	Hour
Hz	Hertz
K_{app}	Apparent binding constant on DNA
K_{cat}	Apparent catalytic rate constant
L	Liter
M	Molar
mg	Milligram
MHz	Megahertz
min	Minute
ml	Millilitre
mmol	Milimolar
mM	Milimolar
mol	Mole
Mp	Melting point
ng	Nanogram
nM	Nanomole
nm	Nanometers
pH	Potential hydrogen
ppm	Parts per million
Q	Fluorescence quenching
r	[drug]/[DNA] ratio
s	Seconds
T_M	Thermal Melting
V	Volt
v/v	Volume per volume
U	Enzyme units
µL	Microliter
µM	Micromolar

ABSTRACT

Zara Molphy

Copper(II) Phenanthrene and Naphthalene Oxidative Chemical Nucleases

Since the structural elucidation of duplex DNA, the construction of small molecules that recognise and react at specific sites to modify DNA structure, reactivity and biological repair mechanisms has been an area of considerable research interest. The discovery of the first synthetic chemical nuclease $[Cu(phen)_2]^{2+}$ (where phen = 1,10-phenanthroline) has sparked intensive effort toward the development of new artificial metallonucleases. $[Cu(phen)_2]^{2+}$ binds both nucleic acids and proteins without specificity inducing general toxicity, and is thus considered a "promiscuous" agent. Accordingly, manipulation of this chemotype represents an interesting developmental challenge. The first part of this work thus reports a range of novel Cu^{2+} chemical nucleases of $[Cu(phen)(N,N')]^{2+}$ carrying designer phenazine type-intercalators (where N,N' = DPQ, DPPZ and DPPN) were developed to identify how systematic extension of the ligated phenanthrene group influences nucleotide binding affinity, base selectivity, oxidative chemical nuclease activity, and cytotoxicity within human cancer cells. Agents within this series showed potent intercalative selectivity with high-affinity binding constants among the highest reported to-date.

Since the introduction of two metal centres into complex scaffolds has uncovered nucleic acid binding interactions not possible through the use of simple univalent compounds—with recent examples including the cytotoxic 'self-activating' DNA oxidant $[Cu_2(\mu\text{-terephthalate})(phen)_4]^{2+}$—the development of new polynuclear complexes is an area of considerable research interest. With this in mind, the second part of this thesis reports a new *di*-Cu^{2+} complex $[Cu_2(tetra\text{-(2-pyridyl)-naphthalene})Cl_4]$ (Cu_2TPNap) that was rationally designed based on *i.*) the utility of a *tetra*-2-pyridine ligand scaffold for efficient nucleic acid catalytic cleavage within previously reported di-Zn^{2+} systems, and *ii.*) the introduction of an aromatic DNA binding moiety that can potentially enhance both nucleic acid targeting and binding affinity. Using a range of molecular biological and spectroscopic techniques, Cu_2TPNap was identified to bind DNA non-intercalatively at the major groove inducing guanine-cytosine specific deformation and condensation. The complex oxidatively damages DNA through a superoxide-mediated process leading to strand breakages in the absence of co-activating exogenous species.

The final part of this thesis reports the discovery of a new class of DNA condensation agent featuring a C_3-symmetric opioid scaffold. These agents, which may have potential gene transfection properties, were identified to collapse the tertiary structure of duplex DNA polymers through phosphate ionic interactions at a protonated piperidine site on the opioid molecule. Using a series of molecular biological and biophysical assays, the binding interactions and structural requirements for this new class of agent were uncovered and are described herein.

CHAPTER I.

Molecular methods for probing cytotoxic metallodrug-DNA interactions

---

This paper has been accepted for publication by *Current Medicinal Chemistry*, 2017, as part of a themed issue entitled "Throwing light on recent advances on metallodrugs: from deemed poisons to a striking hope for the future".

Andrew Kellett, Zara Molphy, Creina Slator, Vickie McKee and Nicholas P. Farrell.

My contribution to this paper involved preparation of sections; 1.1 Nucleic acid structure, 3. Electrophoretic-based techniques, 4. Fluorescence and absorbance based techniques and 5. Viscosity.

I. 1. Abstract

The binding of small molecule metallodrugs to discrete regions on nucleic acids is an important area of medicinal inorganic chemistry and the nature of these binding interactions allied with sequence and helical isoform selectivity form the backbone of modern metallodrug-DNA drug research. In this review we describe a range of molecular methods currently employed within our laboratories to explore covalent and non-covalent nucleic acid interactions of novel metallodrugs. At the outset, an introduction to DNA from a structural biological perspective is provided along with descriptions of covalent (short- and long-range platination) and non-covalent (intercalation, insertion, and phosphate clamping) metallodrug interactions. Molecular methods for probing these binding interactions are then organized between: *i*.) electrophoretic based techniques; *ii*.) fluorescence and absorbance based techniques; *iii*.) viscosity; *iv*.) mass spectrometry; *v*.) NMR spectroscopy; and *vi*.) *in cellulo* genotoxicity. In each method discussed, we provide an overview of the technique and its application toward the elucidation of new metallodrug-DNA interactions by copper(II) and platinum(II) complexes developed by our groups. As such, structure-activity factors in metal complex design become apparent and the consequences of unique binding and/or oxidation reactions at the nucleic acid interface often give rise to unique cytotoxic profiles that are subsequently followed using intracellular methods. Accordingly, a combination of molecular methods is often required to elucidate the nature of new metallodrug-DNA interactions and, from a drug discovery perspective, it is of particular relevance to identify whether metallodrug-DNA binding activity is conserved intracellularly, and is therefore applicable to cytotoxic action.

I. 2. Introduction

I. 2.1. Nucleic Acid Structure

Nucleic acids provide an intriguing molecular target for candidate antitumoral metallodrugs. Given their electron dense phosphate backbones, heterocyclic and exocyclic heteroatoms found within nucleobase structures, and intricate secondary and tertiary structures adopted upon Watson-Crick base pairing under action of ubiquitous enzymes, nucleic acids have a rich history of binding metal ions and discrete complexes.[1-4] From a medicinal chemistry perspective, therefore, the ability to probe metal complex coordination to DNA and RNA provides us with a powerful tool for developing new architectures to selectively target oligonucleotides. Furthermore, given the essentiality of

the DNA double-helix for the storage of genetic information and in mediating faithful cell replication, the interruption of processes essential to biogenesis at this primary juncture provides an important basis for metallodrug discovery.[5,6] Accordingly, the structure of the DNA double helix, in particular its predominant B-DNA form, is an important consideration for bioinorganic chemists. B-DNA comprises a right-handed double helix containing two antiparallel sugar-phosphate chains. The heteroaromatic bases found in the centre of the helix engage in hydrogen bonding to effectively bind the helical chains together and are supported by flanking van der Waals base contacts that result in their perpendicular orientation to the helical axis. These nucleobases obey Chargaff's rules being found in 1:1 ratio between specific purine-pyrimidine molecules (adenine (A) : thymine (T) and guanine : cytosine (C)).[7] Since the edges of the base pairs from where glyosidic bonds extend and their opposite edges differ in size, unequal grooves called the minor and major groove, respectively, are found (**Figure I-1C**)**.** These grooves are structurally distinct with the minor being narrow and the major being wide by comparison.[8,9] In B-DNA the 2′-deoxyribose ring exists in the C2′-*endo* twist conformation, in contrast to the C3′-*endo* twist conformation of both A and Z-form DNA (**Figure I-1B** and **C**).[10] Structural characteristics can be exploited for molecular recognition as the major groove (10.5 Å) is wider than the minor groove (4.8 Å) though their depths are identical. Between the base pairs of B-DNA there is an axial rise of 3.4 Å (0.34 nm) and a 34.5° twist angle associated with every residue rotation while the width of the helix diameter is 20 Å (**Figure I-1A**). A-DNA is the dehydrated form of B-DNA and is a more rigid and compacted structure consisting of 11 base pairs per helical turn with a distance of 2.25 Å between the bases.[11] Z-DNA is formed during the transcription process *in-vivo* due to the torsional strains generated as negative supercoils are created by RNA polymerase moving along the sequence of the DNA double helix. A radical difference exists between Z- and classical B-DNA as the helical sense flips from right- to left-handed DNA and this conformational change is due to bases alternating between the *syn*- and *anti*-conformation. Z-DNA is elongated and narrow, with a diameter of 18 Å and is composed of only one single narrow groove analogous to that of the minor groove of B-DNA; resulting in a zigzag arrangement of the backbone (hence Z-DNA) (**Figure I-1C**)**.**[12]

A.

Parameter	A-DNA	B-DNA	Z-DNA
Helical sense	Right	Right	Left
Residues per helical turn	11	10	12
Helix Pitch (Å)	28	34	45
Helix Diameter (Å)	23	20	18
Axial Rise (Å)	2.55	3.4	3.7
Rotation per residue (Å)	33	36	-30

B.

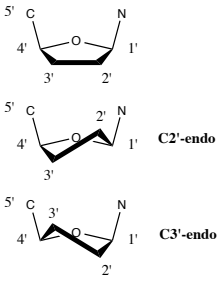

C.

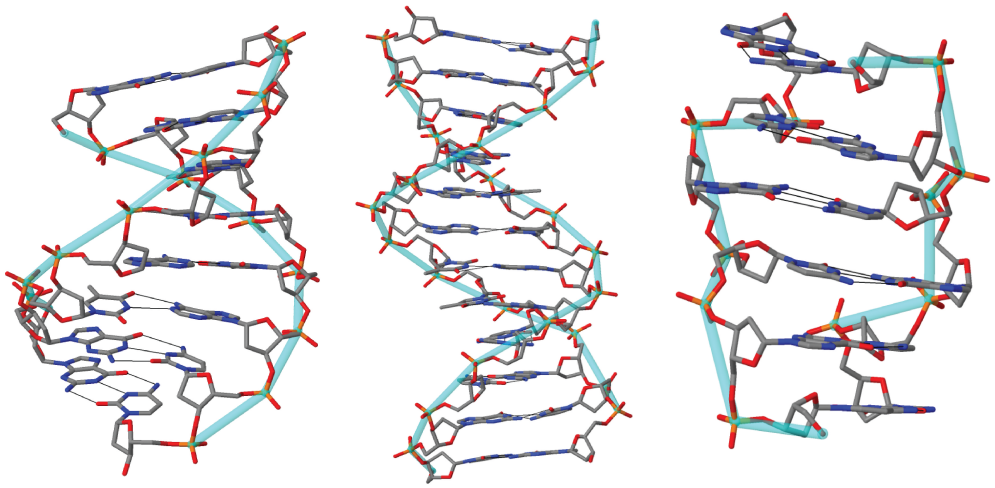

Figure I-1. A. Summary of structural differences between A-, B- and Z-DNA;[13] **B.** conformational preferences of the 2′-deoxyribose rings of DNA and **C.** X-ray structures of A-, B- and Z-DNA from PDB files 1VJ4, 1BNA and 2DCG, respectively.

Since great effort has been expended in recent years to determine how novel metallodrug molecules interact with nucleic acids, a number of complementary molecular methods have been developed to probe these reversible and non-reversible interactions. Additionally, in the absence of high resolution structural data including X-ray diffraction and NMR studies, the mode of binding can be inferred indirectly from molecular biological and biophysical solution studies. A wealth of information regarding the binding mode and sequence specificity of these interactions can therefore be determined and in this review we provide an overview of selected molecular methods to identify metallodrug-DNA interactions with particular emphasis on copper^{2+} and platinum^{2+} complexes developed within our laboratories within the past 25 years. A review of polynuclear Pt^{2+} (Triplatin) binding by X-ray diffraction was recently reported by Komeda *et al.* and, as such, is not discussed here.[14] Furthermore, while much elegant work has been conducted on Z-DNA, G-quadruplex and other non-canonical structures (including their targeting by selected metal complexes),[15-19] it is beyond the scope of this work.

I. 2.2. Nucleic acids as metallodrug targets

I. 2.2.1 Covalent Interactions by platinum(II) chemotherapeutics

Platinum-based drugs are currently used alone or in combination with other therapies for over half of cancer treatments[20] and over 23 platinum complexes have entered into clinical trials since 1970.[21] The era of platinum-based anticancer agents began with the serendipitous discovery of the antitumoral effects of cisplatin (**Figure I-2A**) by Rosenberg[6] and was the first transition metal-based agent approved by the FDA for chemotherapeutic treatment in 1978.[22] Subsequent generations of platinum research led to the development of carboplatin and oxaliplatin, both of which are globally used in clinical treatment,[20] whilst other complexes—nedaplatin, lobaplatin and heptaplatin—have gained approval for use within individual markets (**Figure I-2B**).[21] The restricted use of cisplatin stems from dose-limiting effects due to metabolic degradation and accelerated uptake in rapidly dividing cells; associated side-effects including nephrotoxicity, ototoxicity, myelosuppression (due to rapid rejuvenation of bone marrow), gastrointestinal tract toxicity and nausea.[21]

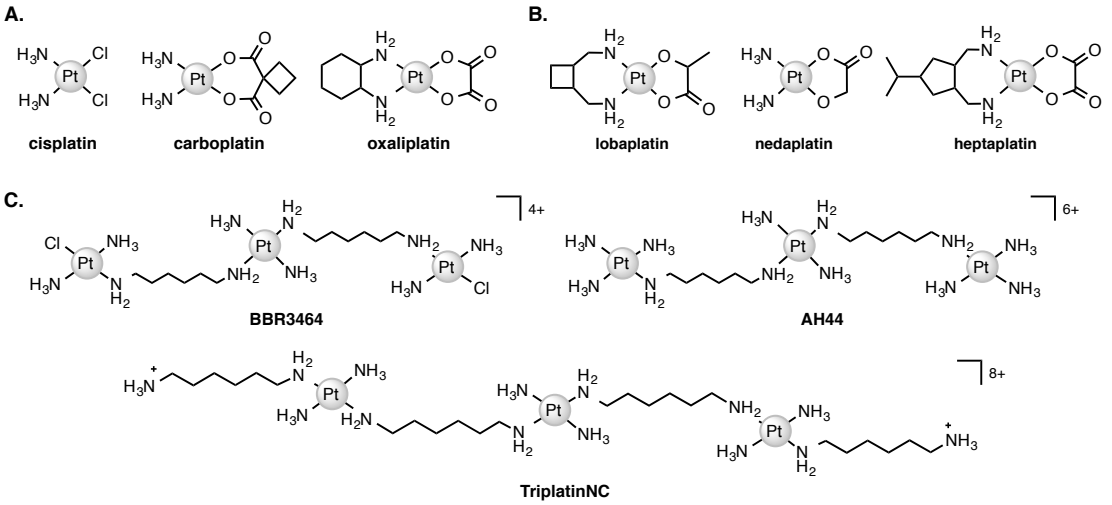

Figure I-2. Molecular structures of, **A.** globally approved Pt(II) complexes cisplatin, carboplatin and oxaliplatin and **B.** those approved in single markets lobaplatn, nedaplatin and heptaplatin, C. polynuclear platinum complexes (PPCs) $[\{trans\text{PtCl}(NH_3)_2\}_2\text{-}\mu\text{-}\{trans\text{-Pt}(NH_3)_2(NH_2(CH_2)_6NH_2)_2\}]^{4+}$ (Triplatin, BBR3464), $[\{Pt(NH_3)_3\}_2\text{-}\mu\text{-}\{\{trans\text{-Pt}(NH_3)_2(NH_2(CH_2)_6NH_2)_2\}]^{6+}$ (AH44), and $[\{trans\text{Pt}(NH_3)_2(NH_2(CH_2)_6NH_3)\}_2\text{-}\mu\text{-}(trans\text{-Pt}(NH_3)_2(NH_2(CH_2)_6NH_2)_2\}]^{8+}$ (TriplatinNC).

Cisplatin exists in the blood stream in its neutral form due to the innately high concentration of chloride ions (~100 mM) found therein.[23] The drug enters the cell *via* active or passive diffusion and is subsequently activated by aquation in a stepwise exchange of the labile chloride ligands to water or hydroxyl ions. This conversion is largely due to the compartmentalised nature of the cell where a decreased concentration

range of chloride ions exists (2-30 mM).[20,24,25] Accordingly, Pt(II) drugs containing chloride ions require hydrolysis prior to DNA platination,[26] a reaction that involves direct coordination of the platinum metal centre with electron rich sites on the nucleobase (**Figure I-3C**). The rate of hydrolysis of the chloride ligands can depend on surrounding environment concentration,[24,25] pH, electronic and steric effects of the non-leaving groups (i.e. am(m)ine ligands).[20] The subsequent formation of mono-functional or bi-functional adducts with DNA *via* platination is often considered akin to DNA alkylation. Mono-functional adducts arise from single coordination to either negatively charged oxygen atoms on the sugar phosphate backbone[27] or suitable donor atoms in the heterocyclic base.[22] Bi-functional adducts, however, are formed when platinum chelates DNA *via* two coordination sites on the pyridine and imidazole-like nitrogen atoms in the heterocyclic bases thus forming a crosslink between two bases of DNA yielding intrastrand (most common) or interstrand adducts (**Figure I-3ii**).[28] Cisplatin preferentially binds to N7 of guanine and adenine and typically results in 1,2-GG/AG intrastrand crosslinks with structural distortion through helical unwinding by 13°, and helical bending of 30 - 40° towards the major groove.[29,30] The structurally modified DNA strand is then recognised by repair enzymes[31] with excess excision of Pt-DNA adducts linked to the induction of apoptotic cell death (**Figure I-3D**).[32] Alternatively, bi-functional cross linking can occur to a lesser extent between DNA-Pt-protein through donor atoms on the axillary chains of protein termini.[33]

Ineligible or discontinued treatment of platinum-based therapies can occur from intrinsic or acquired resistance proceeding sub-lethal continuous exposure to the drug.[21] Furthermore, as carboplatin shares cross-resistance with cisplatin (both drugs are effective against the same population of solid epithelial tumours) limiting the efficacy of platinum drugs currently available in clinical treatment.[20] A culmination of various parameters is responsible for platinum resistance: *i.*) decreased cellular accumulation due to differential rates of cellular influx and efflux (**Figure I-3A** and **H**); *ii*.) detoxification by elevated levels of intra- and extraceullar reductants such as thiol-rich reductants glutathione (GSH) (**Figure I-3F** and **G**), *L*-cysteine,[34] ascorbic acid[35] and metallothionein (MET);[36] *iii.*) enhanced repair mechanisms and/or tolerance to platinated DNA adducts;[20,28] and *iv.*) full or partial bypass of 1,2-GG/AG or 1,3-GTG intrastrand crosslinks achieved by specialized polymerases in the replication process.[37]

BBR3464 (**Figure I-2C**) was the first multi-nuclear platinum complex to enter clinical trials capable of bi-functional DNA binding interactions in comparison to that of 'classical' mono-nuclear Pt(II) drugs. This compound produces long-range covalent inter- and intra-strand DNA platination and is entirely distinct from cisplatin's short range platination.[38] BBR3464-induced DNA distortions significantly different from cisplatin-DNA adducts, the latter of which leads to recruitment of recognition repair enzymes and adduct excision. Pre-association of BBR3464 to DNA is mediated by electrostatic interactions transiently engaging with phosphate groups in the minor groove, and is an important mechanistic feature determining the specificity and formation of covalent long-range crosslinks.[38,39] The complex has demonstrated excellent toxicity within *in-vitro* and *in-vivo* models with a broad spectrum of activity in cancers both sensitive and resistant to cisplatin and those with p53 mutants.[40] This novel activity ensured progression to phase II clinical trials, however, intracellular instability and metabolic byproducts structurally similar to cisplatin halted further advancement.[41]

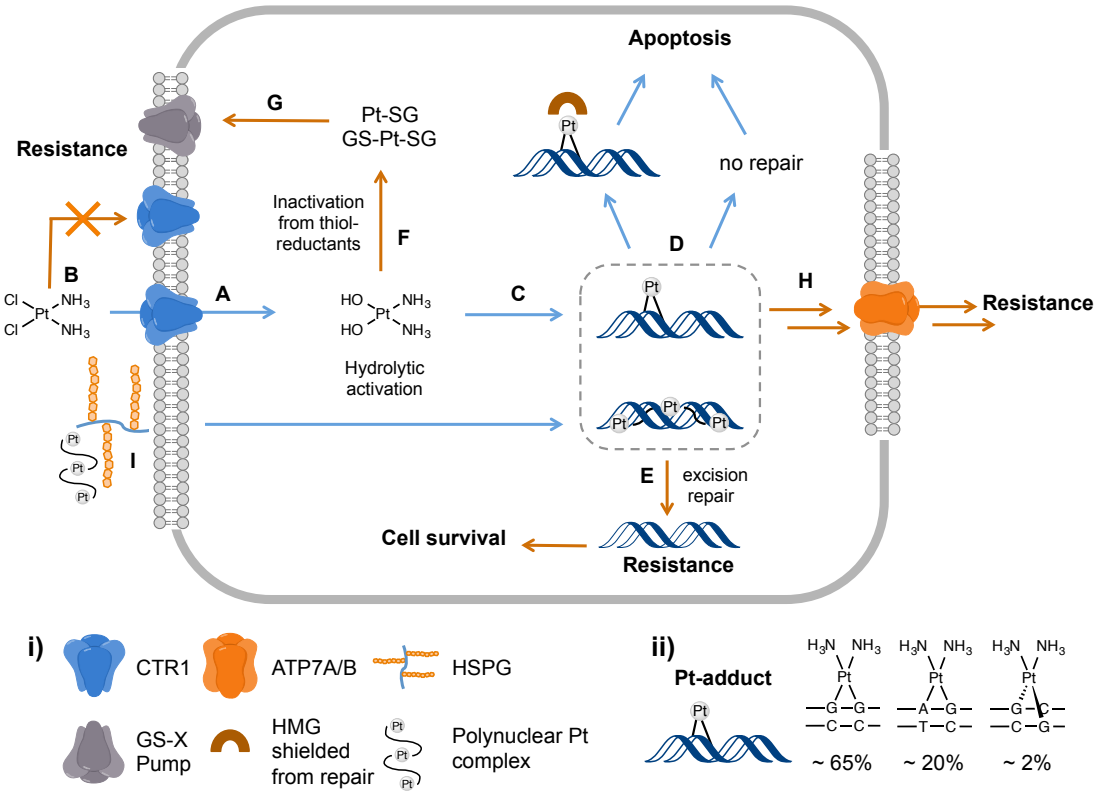

Figure I-3. Pathways of cisplatin cytotoxicity (blue arrows) and resistance (orange arrows). i) Membrane-bound afflux proteins (copper transport influx pump CTR1, efflux pump ATP7A/B and glutathione adducts afflux pump GS-X) and high mobility group proteins (HMG). ii) Pt-adducts in order of occurrence: 1,2-intrastrand G-G (60-65%) and A-G (20%) and 1,3 interstrand G-G (2%). Cisplatin is incorporated into the cell through CTR1 (A). Under-expression of CTR1 results in decreased cellular accumulation of cisplatin (B). Activation through hydrolysis (C), facilitating DNA platination and distortion (D) with no, or little, inhibition of enzymatic repair activity through HMG (D) resulting induced apoptotic cell death. Acquired resistance can occur from enhanced DNA repair mechanisms and Pt adduct excision (E). Other resistance factors such as inactivation through thiol-rich reductants (F), (GSH as example) and GS-Pt (and GS-Pt-SG) adduction elimination through GS-X pump (G). Accelerated efflux of cisplatin through overexpression of copper transporters, ATP7A/B (H). Membrane recognition and intracellular accumulation of polynuclear Pt complexes through heparan sulphate proteoglycans (HSPG) (I).

I. 2.2.2. Non-covalent interactions

I. 2.2.2.1 Metallointercalation and metalloinsertion

Intercalation involves insertion of a planar, usually aromatic ligand (or part thereof) between the stacked base pairs of DNA. This interaction was identified and characterised by Lerman in 1961[42] and many organic intercalators have been recognized since.[43,44] Intercalation of metal complexes also has a long history, the first structurally characterized (by X-ray diffraction by fibres) example being the 2-hydroxyethanethiolato(2,2′,2″terpyridine)-platinum(II) monocation[45,46] and a number of recent reviews have appeared describing intercalation by complexes of platinum, copper, ruthenium, rhodium[47] and osmium.[3,44,47-50] The essential structural requirement is that the intercalating group must engage in the base stacking interactions, the major factor stabilising the DNA structure. The nature of "π-stacking" is complex and influenced by, for example, electrostatic substituent effects and solvent[51-55] but generally requires both that the ligand is planar and (usually) that it contains a significant delocalized region. It is also necessary that the additional stabilisation on stacking the intercalating ligand outweighs the reorganization energy necessary to permit it. The intercalated groups orient approximately parallel to the plane of the base pairs, and the base pairing is not significantly disturbed. The principal effect on the DNA structure is to extend it by *ca*. 3.6 Å for each intercalated group (3.6 Å being the normal interplanar distance for π-stacking). To permit this, the DNA helix unwinds, reducing the helical twist across the intercalation site. There are also a number of smaller geometric changes[56,57] that together may reduce conformational flexibility in the adjacent portions of the helix, since it is observed that further intercalation does not occur at the neighbouring sites (the "nearest neighbour exclusion principle").[46,58] Structurally characterized metallointercalators are all bound from the major groove, though there is some NMR evidence for minor groove binding in solution.[59]

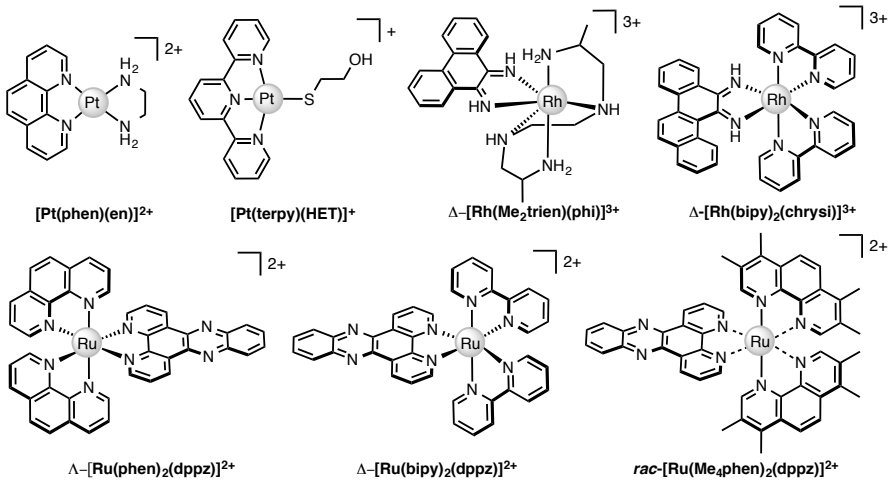

Figure I-4. Molecular structures of platinum(II), Rh(III) and Ru(II) intercalating and insertion complexes.

Since only the planar section of the ligand can intercalate, it needs to be large enough to achieve significant π-overlap, without bringing the remainder of the complex into unfavourable steric or electronic interaction. Ligands such as 1,10-phenanthroline (phen) and terpyridine (terpy) in square planar Pt complexes[3] are able to intercalate effectively but large ligands such as 9,10-phenanthrenequione diime (phi) or dipyridophenazine (dppz) are more effective for 6-coordinate complexes.[47] The orientation of the intercalator in the "slot" between two base pairs may be symmetrical, or laterally offset relative to the principal axis of the DNA helix,[60,61] presumably reflecting the best accessible set of stacking and other interactions, hence dependent on the detailed electronic structures of the intercalating ligand and the base pairs lining the intercalation site.[55,62,63] There are ten possible intercalation sites,[46] differing in existing π-interactions between base pairs[51,63] and their affinity for a specific intercalator. For example, in 1979 Lippard and co-workers showed that $[Pt(phen)(en)]^{2+}$ and $[Pt(terpy)(HET)]^{+}$ (where HET = 2-hydroxyethanethiolate) exhibit GC selectivity,[64] while $[Ru(phen)_2(dppz)]^{2+}$ (**Figure I-4**) displays preferential intercalation for poly-d(AT) over poly-d(GC).[65] The same complex intercalates symmetrically at the TA/TA step in $d(CCGGTACCGG)_2$ but not the AT/AT site in $d(CCGGATCCGG)_2$.[61] In fact, many metallointercalators bind preferentially to DNA at specific sites, and this function can be amplified by interaction of the ancillary ligands with the DNA duplex. In an early example, the photoactive complex Δ-α-$[Rh\{(R,R)\text{-}Me_2trien\}phi]^{3+}$ (where Me_2trien = 2,9-diamino-4,7-diazadecane, **Figure I-4**) was found to specifically cleave the sequence 5'-TGCA-3'.[66] The structural basis for this specificity was demonstrated in the X-ray structure of the complex bound to 5'-G(5|U)TGCAAC-3' (**Figure I-5A**) in the major groove specifically at the 5'-TG|CA-3' site

(where | indicates phi insertion).[57] The intercalation π-stacking is supported by H-bonds from the amines of the Me_2trien ancillary ligands to the guanine-O6 acceptors as well as to some ordered water molecules.

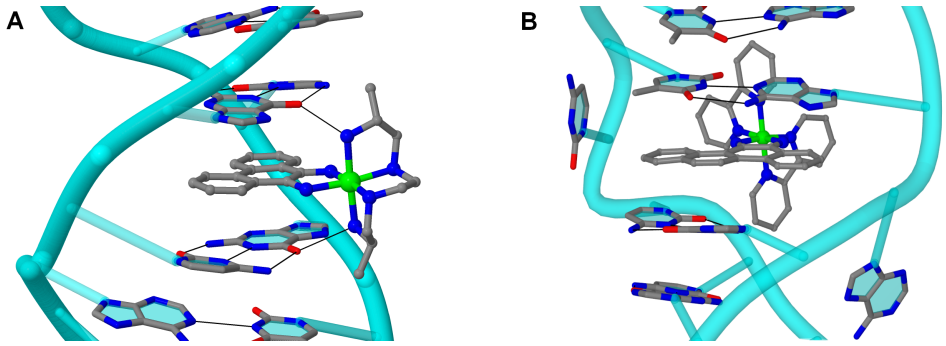

Figure I-5. Intercalation and insertion. **A.** Δ-α-[Rh{(R,R)-Me_2trien}phi]$^{3+}$ intercalated into 5'-G(5|U)TGCAAC-3' with additional stabilisation by H-bonds from the ancillary ligand (PDB 454d), black lines indicate hydrogen bonds[57] and **B.** Δ-[Rh(bpy)$_2$(chrysi)]$^{3+}$ inserted into (5'-CGG*A*AATT*C*CCG-3'), displacing a mismatched AC pair (PDB 2O1I).[67]

Metalloinsertion is closely related to intercalation, also involving incorporation of a ligand into the base pair stack. The main difference is that in metalloinsertion one base pair is ejected and replaced by the incoming ligand. This interaction was also predicted by Lerman[1] and first structurally characterized in a metal complex only in 2007 for Δ-[Rh(bpy)$_2$(chrysi)]$^{3+}$ (where chrysi = 5,6-chrysenequinone diimine, **Figure I-4** and **Figure I-5B**),[67] extended to a family of chrysi detivatives[68] and more recently for both Δ-[Ru(bipy)$_2$(dppz)]$^{2+}$[69] and Λ-[Ru(phen)$_2$(dppz)]$^{2+}$ (where bipy = 2,2′-bipyridine, **Figure I-4**),[61] in all three cases the insertion is at a mis-matched base pair and from the minor groove (in contrast to intercalation). The dppz complexes are capable of both intercalation and insertion and it may be that other known intercalators are also capable of insertion in the presence of base-pair mismatches. Insertion involves less modification to the helical structure of DNA than intercalation. There is no significant extension or change in helicity although the "flipped out" bases are free to interact in other ways with the DNA helix or the inserting complex. The stabilisations due to hydrogen bonding of the displaced base pair and its stacking interactions are both lost and need to be replaced by the new π-stacking interactions (plus any new interactions involving the flipped out base pair). Since base-stacking dominates DNA duplex stability and base pairing contributes relatively little stabilization,[52,63] the loss of the H-bonding component might not be expected to have a high cost. Nonetheless, metalloinsertion is observed to be specific for mismatched base

pairs, especially those where resulting base-pairing is poor (CC and CA). For example, D-$[Rh(bipy)_2(chrysi)]^{2+}$ (**Figure I-4**) can promote specific cleavage at a single mismatch site in a 2725 base pair linearized plasmid heteroduplex.[70] This specificity is useful in detection of mismatches and potentially diagnostic for cells with impaired mismatch repair (MMR) mechanisms; notably, the series of Rh-chrysi complexes shows selective cytotoxicity for MMR-deficient cancer cells.[68]

As for intercalation, interaction of the ancillary ligands with the DNA can be used to tune the binding properties of the inserting complex. For example, $[Ru(bipy)_2dppz]^{2+}$ binds to DNA *via* both intercalation and insertion at mismatch sites but $[Ru(Me_4phen)_2(dppz)]^{2+}$ (where Me_4phen = 3,4,7,8-tetramethyl-1,10-phenanthtroline, **Figure I-4**) is a mismatch-specific metalloinsertor where the methyl groups disfavour intercalation, due to steric interaction with the backbone, and also control the depth of dppz insertion.[71] As might be expected, the metalloinsertion correlates with the stability of the mismatch site, strongest for CC and CA (less stable), less striking for GG AA (more stable).[51] Metallointercalators and metalloinsertors can be combined with groove-binding, sequence-specific components in multifunctional assemblies to extend their recognition and properties. The first structurally characterized example was reported by Nordén in 2001.[72] Much elegant work has been done in this area in recent years but is beyond the scope of the current review. [44,47,48]

I. 2.2.2.2. Non-covalent binding by polynuclear platinum complexes (PPCs)

Enhanced DNA binding properties of the polynuclear platinum(II) chemotype led to the subsequent development of analogues with varying linker lengths and replacement of liable chloride groups with ammonia or dangling terminal amines. TriplatinNC, was therefore designed with 'dangling' terminal hexanediamine functionality and contains Pt(II) centres linked *via* bridging diam(m)ine groups (**Figure I-2C**). TriplatinNC forms non-covalent bonds with DNA, without any direct Pt-DNA coordination epitomised in cisplatin-type structures.[39] The architecture of the complex gave rise to a previously undiscovered mode of DNA binding called the 'phosphate clamp' that results from the selected affinity of symmetric am(m)ine-to-phosphate (N-H$\cdots$O=P) hydrogen bonding through cis-oriented NH_3 (ammine) and -RNH_2 (amine) ligands.[39] The discrete mechanism of phosphate clamping gives rise to two binding motifs: phosphate tracking and groove spanning (**Figure I-6A** and **B**). Triplatin-DNA coordination leads to a collapse in regular

helical structure[73] with subsequent enzymatic inhibition of topoisomerase I and type II restriction endonucleases.[74] Groove spanning is dependent on the local helical topology (localised to the minor groove) and base composition (specifically toward A-T content) and is discrete from classical intercalation and minor-groove binding.[75] Despite the highly positive charge of the molecule, cellular uptake is significantly enhanced in comparison to BBR3464.[76] Substitution of Cl^- ligands in BBR3464 with ammines groups lead to the derivative AH88—otherwise known as TriplatinNC-A—which similarly exhibits this non-covalent phosphate clamping association mode,[77] consequently inducing DNA condensation in the same manner to terminal Pt-dangling amine analogue TriplatinNC.[73] Note that the phosphate clamp formed by the spermine-bridged dinuclear $[\{Pt(NH_3)_3\}_2$-μ-spermine$]^{6+}$ is effected through a *cis*-$\{Pt(NH_3)_2\}$ group, suggesting also a model for initial interaction of cisplatin itself with DNA.[14]

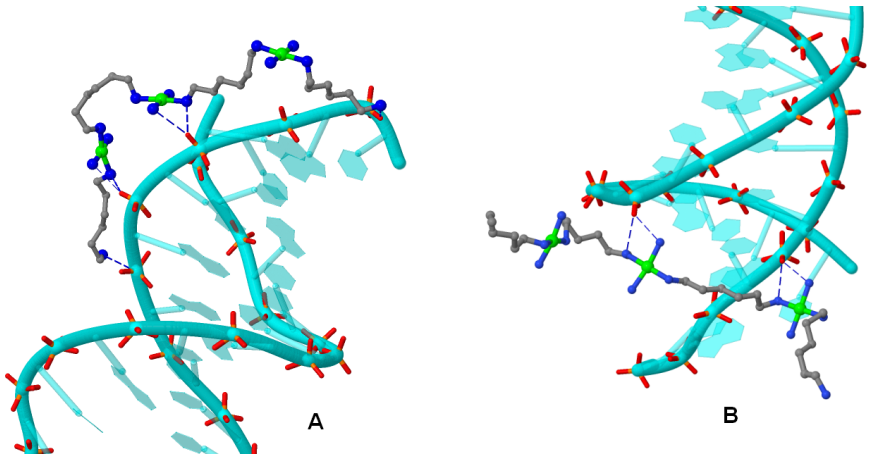

Figure I-6. TriplatinNC bound to Dickerson-Drew dodecamer (B-DNA) through backbone tracking (**A**) and groove spanning (**B**) interactions.[75] N-H·····O=P hydrogen bonds shown as dashed blue lines.

Extensive studies of the PPCs class have revealed a novel mechanism of incorporation and accumulation within cancer cells.[78] The polycationic properties of the complexes mimic polyarginine peptide sequences and glycosaminoglycans (GAG) important for protein transduction domains so they can be exploited for tumour selectivity and accumulation. A novel target of PPC is the heparan sulphate proteoglycan, HSPG, (**Figure I-3I**) verified through cellular uptake of classical platinum complex and polynuclear cationic species in differentially expressed Chinese hamster ovarian (CHO) cells with and without heparan sulphate and chondroitin sulphate deficiencies.[79] PPCs are competitive inhibitors of the polysaccharide degradation enzyme, heparinase, as co-incubation of the complexes with pentasaccharide GAG mimic fondaparinux significantly

reduced production of the cleavage products/pattern.[80] Indeed, the metalloshielding effect of PPCs has opened a novel area of platinum chemotherapeutic targets and interactions and has been coined ‘metalloglycomics’.

I. 3. Electrophoretic-based techniques

I. 3.1. DNA damage detection

DNA damage is known to play a major role in biological processes including ageing, mutagenesis and carcinogenesis as cellular DNA is susceptible to many forms of damage resulting from exposure to endogenous (spontaneous) and exogenous (environmental) sources. Examples of endogenous factors include enzymatic or spontaneous metabolic conversions, while exogenous sources include genotoxic agents such as ionizing radiation, redox metal ion overload, and therapeutic drug exposure. Such mutagens are capable of causing direct or indirect damage to nucleotides resulting in profound biological consequences including replication errors in genetic code and the production of free radical species.[81] Two major types of DNA damage mechanisms exist, hydrolytic and oxidative. Hydrolytic agents result in the cleavage of the phosphate backbone which can be enzymatically repaired by DNA ligases,[82] while oxidative mechanisms involve the production of diffusible free radicals—produced by mitochondria and also through exposure to physical agents such as oxidative nucleases—resulting in DNA cleavage by oxidative attack at a variety of C-H positions of the sugar moiety.[83]

Electrophoretic gel mobility shift assays are a well-established analytical technique used in molecular biology laboratories to analyze, separate and purify DNA samples. It is also a useful technique to probe DNA damage mechanisms. Gel electrophoresis facilitates the movement of DNA molecules based on both their size and conformation, through a solid-phase medium such as agarose or polyacrylamide, under the influence of an electric potential difference. Due to its inherent negative charge, DNA moves in the electric field as an anion, from the cathode to the anode. The rate of DNA migration through the gel is dependent on a number of factors including the length of the DNA sequence, the conformation of the DNA, whether the DNA is single stranded (ssDNA) or double stranded (dsDNA) and the presence of supercoiling. A number of external parameters can be controlled in order to maximize the resolution of a gel including the voltage applied, the physical length of the gel, running time and nature of stationary phase selected.

Plasmid DNA (FI, SC) is a supercoiled substrate widely used to probe drug-DNA interactions through the medium of agarose gel electrophoresis. scDNA cleavage induced by a small drug molecules—such as $[Cu_2(\mu\text{-terephthalate})(1,10\text{-phen})_4]^{2+}$ (Cu-Terph-Phen) (**Figure I-7**)—results in the formation of nicked open circular DNA (FII, OC),[84] while double stranded cleavage results in the formation of linear (FIII, L). Complete degradation of plasmid DNA, like that induced by copper phenanthrene complexes in the presence of added reductant, can be determined by fragmentation of DNA.[85]

I. 3.2. Antioxidant traps for oxidative cleavage detection

The cleavage efficiency of Cu^{2+} phenanthroline complexes are dependent on the presence of both a reductant (*L*-ascorbic acid) and an oxidant (O_2 or H_2O_2) resulting in a cascade of redox reactions initiated by the reduction of Cu^{2+} to Cu^{+} species.[86] The ROS species involved in chemical nuclease activity of [Cu(*o*-phthalate)(1,10-phenanthroline)], Cu-Ph-Phen (**Figure I-7**) were investigated on superhelical pUC19 DNA in the presence of ROS-specific quenchers and stabilisers; tiron for superoxide ($O_2^{\bullet-}$);[87] DMSO for the hydroxyl radical ($^{\bullet}OH$);[88] NaN_3 for singlet oxygen ($^1O_2$);[89] and KI for hydrogen peroxide (H_2O_2)[90] (**Figure I-8A**). The cleavage efficacy of Cu-Ph-Phen in the presence of scavengers identified the most prelevant species involved in strand scission as $O_2^{\bullet-}$. Co-incubation with 4,5-dihydroxy-1,3-benzenedisulfonic acid (tiron) significantly impeded the cleavage activity of the compound preventing double strand damage. The presence of DMSO diminished activity to a lesser extent while DNA damage was marginally altered by KI and NaN_3. Significantly, ovarian adenocarcinoma cancer cells (SKOV3) pretreated with tiron, then subsequently exposed to an LD_{50} concentration of Cu-Ph-Phen displayed enhanced survival by ~26%.[91] This method was also employed to probe the redox mechanism of the developmental copper phenazine series, $[Cu(DPQ)(phen)]^{2+}$ (Cu-DPQ-Phen), $[Cu(DPPZ)(phen)]^{2+}$ (Cu-DPPZ-Phen), and $[\{Cu(phen)_2\}_2(\mu\text{-terph})](terph)$ (Cu-Terph-Phen) (where DPQ = dipyridoquinoxaline and terph = terephthalate, **Figure I-7**) demonstrating the hydroxyl (or metal-hydroxyl) radical as the primary species involved in oxidative DNA degradation.[92]

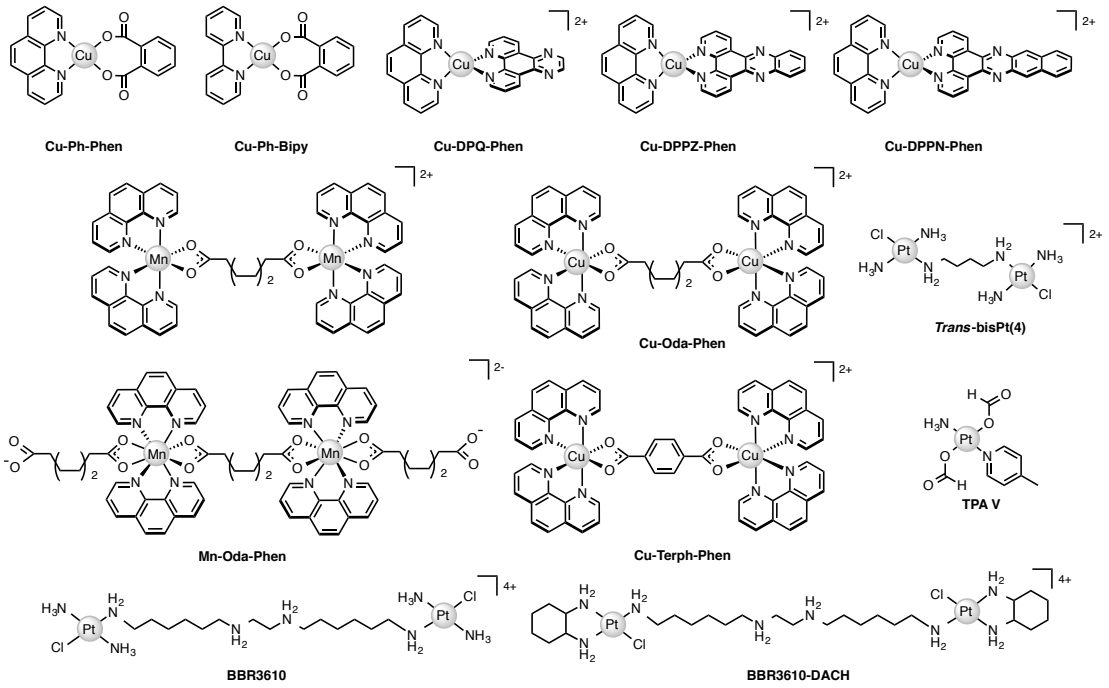

Figure I-7. Molecular structures of selected metal complexes discussed in this review.

I. 3.3. Intercalation: Topoisomerase I and II inhibition

Topoisomerases (Topo) are a specialised class of nuclear enzymes that catalyse the transient cleavage, passage and resealing of either a single strand (Topo I) or double strand (Topo II) of DNA in order to relax chain intertwinement, release superhelical tension and permit change in topology during replication, transcription, and DNA repair.[93] Topo I mediated relaxation is a robust assay to identify intercalative properties of DNA binding complexes.[94] Metal complexes with intercalating moieties, typically constructed from planar aromatic ligands, unwind and elongate the helical structure inhibiting topoisomerase enzymes from binding to DNA, or alternatively stabilising the enzyme-DNA complex. Topo I isolated from *E. coli* specifically relaxes negatively coiled superhelical plasmid DNA giving a distinct topological pattern of negative, or right handed, topoisomers. In the presence of intercalating agents, plasmid DNA reveals a migratory profile transitioning from this typical topology pattern to fully relaxed DNA or to positively (left-handed) sc plasmid. This is evident for intercalating molecule EtBr (**Figure I-10A**), which induces helical unwinding by 26°,[95] with positively wound topology of intact scDNA being observed after 0.5 μM (**Figure I-8B**). The treatment of established Topo II poison, doxorubicin (**Figure I-10A**) renders complete DNA degradation and shearing at higher concentrations (**Figure I-8C**) likely through ROS generation consequent to redox cycling of quinone moiety.[96,97]

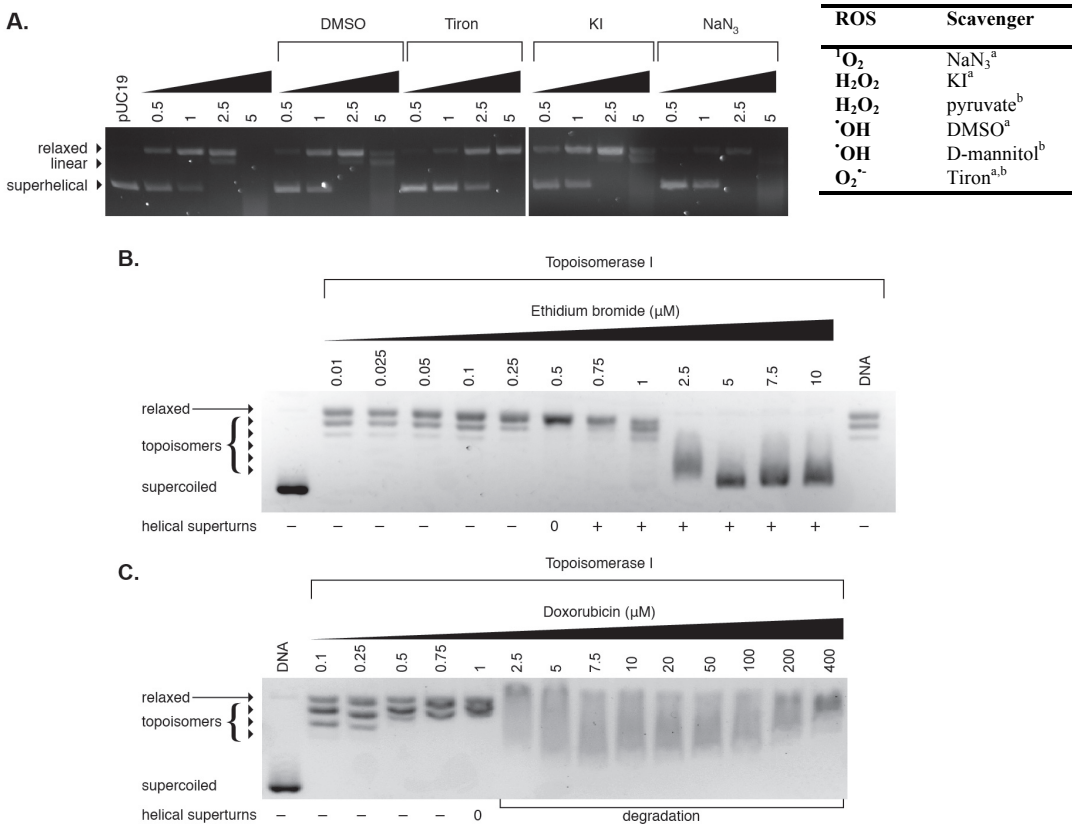

Figure I-8. A. Cleavage profile of Cu-Ph-Phen in the presence of radical-specific antioxidants and trapping agents. Table insert with scavengers[a] utilised in nuclease studies and intracellular antioxidants[b]. Electrophoretic gels of topoisomerase relaxation assay for intercalating agents, **B.** EtBr and **C.** known topoisomerase poison doxorubicin, Doxo (unpublished results)**.**

I. 3.4. DNA unwinding and bending

Distortion in helical structures and periodicity induced by metal-complexes leads to inhibition of protein-DNA recognition involved in transcriptional and replication processes. With this in mind, conformational modifications such as unwinding and bending can be identified through native gel electrophoresis.[98] Nucleotide monomers, typically 20-24 bp in length, are specifically designed to contain optimal platinum binding sites and a single nucleotide overhang that facilitates polymerisation through T4 mediated ligation. The polymerised constructs (100-200 bp in length) result in an overlapping laddering pattern when subjected to gel electrophoresis.[30] Upon platination of oligonucleotides, interplatinum distances are constant in the ligation product due to single orientation with constructive addition of bends facilitated by the non-complementary one nucleotide overhangs. Pt-distances in the plane of helical repeats assemble in the most constructively phased bend yielding the highest degree of anomalous migration.[30,99] Differential gel migration between unmodified and alkylated sequences can therefore be attributed to DNA unwinding where the natural repeat of B-DNA is 10.5 bp. Planar curvature is assessed

from relative mobility (K) values, based on the apparent length after electrophoretic migration relative to known sequence length, with higher values indicating a greater degree of bending. The curvature or retardation maxima gives the precise helical repeat and are obtained through plotting K values versus length of oligonucleotides. The unwinding angle can therefore be calculated on the basis that a helical repeat of 10.5 bp has a periodicity of 360° in B-DNA. The bend angle per helical turn or absolute curvature can be calculated from empirical equations based on sequence length, relative mobility and curvature relative to DNA bending induced by the tracts of A residues.[30,98,100] This procedure has been widely used to determine helical bending and local unwinding angles of site-specific platinated interstrand crosslinks (**Table I-1**).

Table I-1. Helical unwinding and bending angles for established platinum complexes.

	Interstrand crosslink	**Unwinding**	**Bending**
Cisplatin[100]	1,2-GG	79°	45°
Oxaliplatin[101,102]	1,2-GG	96°	55°
Trans-bisPt(4)[† 98]	1,4-GG 5′→5′	9°	10°
BBR3464[103]	1,4-GG 5′→5′	10°	21°
	1,4-GG 3′→3′	9°	15°

† *Trans*-bisPt(4) = [*trans*-{$PtCl(NH_3)_2$}$_2$-μ-$NH_2(CH_2)_4NH_2$]$^{2+}$

I. 3.5. Alkylation assays with melphalan

Melphalan is an aromatic nitrogen mustard with high alkylating affinity in the minor groove—inducing A•T→T•A transversions—and when heat-treated with piperidine DNA cleavage at guanine N7 adducts result (**Figure I-9A**).[104,105] Since thermolabile sites can be readily visualized by gel electrophoresis, the presence of high affinity minor groove binding agents—such as netropsin and distamycin—afford protection to DNA from alkylation.[106] Interestingly, the same protective effect can be seen in the case of PPCs, where melphalan is prevented from accessing A-rich regions, and this protective effect is illustrated in **figure I-9B**.[107]

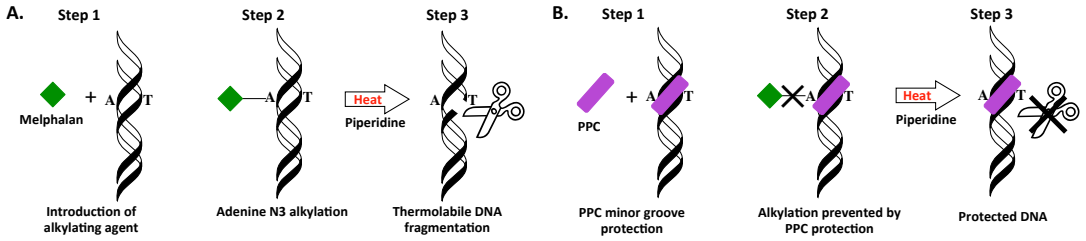

Figure I-9. Minor groove binding competition assay using polynuclear platinum complexes (PPC).

I. 3.6. On-chip microfluidic analysis

Lab on chip technology—such as that commercially available through the Agilent Bioanalyser 2100—has provided a platform to conduct high-throughput gel electrophoretic experiments on a microfluidic chip with up to 12 DNA, RNA or protein samples being analysed and processed sequentially.[108] Data can be processed and generated with output including electrograms, peak height, peak area and digital electropherograms. Many applications for nucleic acids have been found for this technique including determination of sample size, quality and concentration.[109-111]

Recently, we employed this technique to determine drug-DNA damage and selective binding interactions with double stranded DNA sequences. In the first case, an assay was devised to compare the oxidative degradation profiles of a family of structurally related bis-chelate Cu(II) phenanthroline-phenazine cationic complexes of Cu-DPQ-Phen, Cu-DPPZ-Phen, and Cu-DPPN-Phen (where DPPN = benzo[*i*]dipyridophenazine) on a linearized pUC19 sequence (2686 bp). We employed both peak height and peak area intensity in order to rank the activity of the complex series, revealing Cu-DPQ-Phen (**Figure I-7**) as the most active complex within the series.[85] In the second case, we employed the Agilent Bioanalyser 2100 to investigate whether cationic Triplatin complexes of varying linker length ($[\{Pt(NH_3)_3\}_2\text{-}\mu\text{-}\{trans\text{-}Pt(NH_3)_2(NH_2(CH_2)_6NH_2)_2\}]^{6+}$ (AH44, TriplatinNC-A) and $[\{trans\text{-}Pt(NH_3)_2(NH_2(CH_2)nNH_3)\}_2\text{-}\mu\text{-}(trans\text{-}Pt(NH_3)_2(NH_2(CH_2)nNH_2)_2\}]^{8+}$ cations where n = 5 (AH78P), 6 (AH78H, TriplatinNC) and 7 (AH78H) **Figure I-2C**) were capable of inhibiting site-selective excision by type II restriction endonucleases. Experiments were setup with pre-incubation of DNA using a variety of PPCs concentrations followed thereafter by exposure to a selection of endonucleases (BamHI, EcoRI, SalI). Concentration dependent endonuclease inhibition was identified in each case, with high intensities of the native pUC19 band visible (in linear form) indicative of protection.[75] Furthermore, a distinct dependency on linker chain length with the pentanediamine complex protecting or inhibiting linearized pUC19 DNA

from digestion in the nanomolar range, while a 10-fold concentration increase was required to block restriction activity in the hexane- and heptane- bridged Triplatin cations.

I. 3.7. Non-covalent recognition elements

Oxidative DNA damage is known to be dependent on a number of factors including and not limited to: DNA plasmid type and conformation, presence/absence of exogenous oxidant and reductant, presence of chelating agents and dependence on hydrogen peroxide.[85,112,113] Therefore, it was of interest to further probe the oxidation profiles of the copper(II) phenazine series and determine whether DNA cleavage site specificity could be enhanced or inhibited in the presence of non-covalent recognition elements such as minor groove (netropsin), major groove (methyl green) and electrostatic agents ($[Co(NH_3)_6]Cl_3$) (**Figure I-10B**). Pre-incubation of DNA with major groove binding agent methyl green resulted in enhanced chemical nuclease activity—most likely by directing drug-DNA interactions towards the minor groove—while the presence of the minor groove binding agent netropsin was found to significantly reduce the oxidative DNA damage profile of the Cu^{2+} phenazine complex series.[92]

I. 4. Fluorescence and absorbance based techniques

I. 4.1. Indirect fluorometric assays

Small organic molecules with high specificity and affinity for nucleic acids, becoming optically fluorescent upon binding, are invaluable tools in the molecular biology lab. In particular, when probing DNA binding affinity of metal complexes with low molar extinction coefficients (*e.g.* Cu(II) and Mn(II) metallodrugs), these techniques are valuable given the absence of direct electronic spectroscopic measurements. Examples of such dyes routinely used in fluorescence microscopy and flow cytometry include the blue fluorescent AT specific dye, DAPI (4′,6-diamidino-2-phenylindole), commonly used as a nuclear counterstain; intercalating Sybr Green I, used for the detection of double stranded DNA and also as a chromosomal stain, and red fluorescent nuclear and chromosome counterstain, propidium iodide (3,8-diamino-5-[3-(diethylmethylammonio)propyl]-6-phenylphenanthridinium diiodide) (**Figure I-10A**).[91,114-116] Fluorescent dyes, however, are not just limited to microscope imaging as they have also found use in high-throughput assays designed to indirectly assess the affinity at which a small drug molecule can bind to DNA (including fluorescence resonance energy transfer (FRET) assays extensively reviewed for metallodrug-stabilization and melting curves in G-quadruplex systems[19]).

Two such examples are the planar heterocyclic intercalator, ethidium bromide (3,8-diamino-5-ethyl-6-phenylphenanthridinium bromide; EtBr), and the crescent shaped minor groove binding agent, Hoechst 33258. Since these molecules have low fluorescence when free in solution and become highly fluorescent when bound to DNA,[117,118] their photophysical properties can be used to inversely determine the ability of a small molecules to bind DNA through fluorescence depletion.

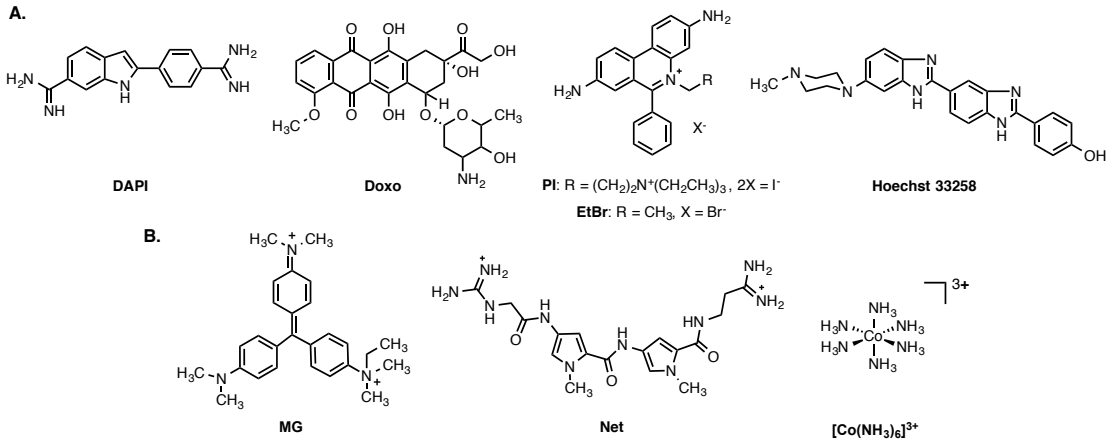

Figure I-10. A. Molecules with fluorescent DNA binding properties; DAPI, Doxo (doxorubicin), PI (propidium iodide), EtBr (ethidium bromide) and Hoechst 33258 and **B.** non-covalent DNA recognition elements; MG (methyl green, major groove binder), Net (netropsin, minor groove binder) and cobalt(III) hexammine ($[Co(NH_3)_6]^{3+,}$ electrostatic agent).

I. 4.2 Competitive fluorescent displacement

The competitive EtBr displacement assay is an indirect titration technique used to determine the apparent binding constants (K_{app}) of non-fluorescent DNA-binding ligands and complexes. This use of the intercalator EtBr to probe drug-DNA binding constants was originally proposed in 1979 by Morgan *et al.*[119] and conducted in rectangular quartz cuvettes, however in recent years Kellett *et al.* have modified this assay to take advantage of a 96 well fluorescence plate reader to allow for high throughput analysis.[113,120] This procedure involves treating DNA (10 μM) with an excess of the intercalating ethidium bromide molecule (12.6 μM)–saturating all available binding sites between the DNA base pairs–resulting in strong fluorescence. This quantitative titration method is used to determine the amount of test sample required to induce a 50% decrease in the fluorescence of the EtBr reporter molecule, referred to as the C_{50} value. Using this high-throughput approach, drug concentrations are measured in triplicate and the apparent binding constants are calculated using $K_{app} = K_e \times 12.6/C_{50}$ where $K_e = 8.8 \times 10^6$ $M(bp)^{-1}$.[75] This

reproducible displacement assay can be applied to rank the binding affinity of both individual and families of compounds over a defined concentration range.[75,85]

I. 4.3. Competitive fluorescence quenching

Fluorescence quenching assays under conditions of excess DNA (*e.g.* 25 μM $M(Bp)^{-1}$) treated with limited bound fluorescent EtBr (5 μM) allow for complexes to be characterised based on their ability to distinguish between modes of DNA interaction. Not only can fluorescent probe molecules be varied based on mode of interaction (*e.g.* EtBr – intercalator; Hoechst 33258 – minor groove binder) but so too can the %GC content of DNA.[85,113] Quenching (*Q*) values can be determined by the concentration of test sample required to induce 50% quenching of the drug-free control fluorescence giving rise to the identification of potentially novel intercalators or groove binders and their sequence dependence.

I. 4.4. Absorbance based techniques

I. 4.4.1. Overview

UV-visible spectroscopy of nucleic acids is dominated by base absorption since each nucleobase has low symmetry and several heteroatom lone pairs. Transitions for individual bases tend to overlap and produce a single broad strong absorption band for the whole nucleic acid polymer, with an absorbance maximum (A_{max}) between 250-280 nm. The maximal absorbance of a nucleic acid (λ_{max}) is dependent on its composition, AT content vs. GC content (**Figure I-11A**). Likewise, the molar extinction coefficient (ε_{max}) of the nucleic acid is dependent on composition and whether it is single stranded or double stranded (**Figure I-11B**).[111] A useful resource can be freely accessed on http://www.atdbio.com/tools/oligo-calculator, where the UV and thermodynamic properties of DNA sequences can be calculated.

A.

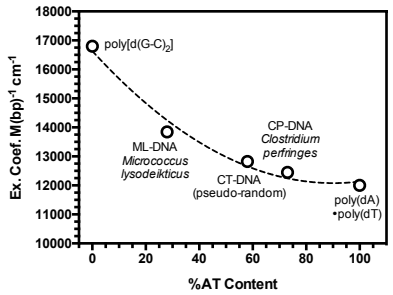

B.

DNA	ε_{max} ($M^{-1}cm^{-1}$)	λ_{max} (nm)
ctDNA	6600	260
Poly[d(A-T)$_2$]	6600	262
Poly[d(G-C)$_2$]	8400	256

Figure I-11. A. Determination of molar extinction coefficients for double stranded DNA and extinction coefficients and **B.** λ_{max} values for synthetic polymers of varying GC content.

I. 4.4.2. Thermal melting

Thermal melting (T_M) marks the midpoint in the melting process of DNA, when a 50:50 equilibrium exists between helical and single stranded states. Since AT regions contain fewer π-π stacking interactions, these hydrogen bonds melt first, promoting the initial unwinding of the DNA helix, followed by the melting of the remaining GC rich regions. The thermal melting process is based on the loss of both hydrophobic interactions and π-π stacking interactions from nearest neighbor interactions due to the denaturation of the double helix and ultimate loss of secondary structure when bases become unstacked.[121] This process is reversible and full renaturation of duplex DNA can occur approximately 25°C below the denaturation temperature.[122] This is a powerful technique that relies on the intrinsic extinction coefficients of nucleic acids, to probe the thermodynamic parameters involved in metallodrug-DNA binding interactions.

The differential stability of AT and GC rich regions and splitting of the duplex into single strands, is of paramount importance to many cellular processes such as transcription and recombination and is also critical in the molecular biology lab for techniques such as polymerase chain reaction (PCR). The thermal denaturation of DNA is also strongly influenced by duplex environment including salt and buffered solvent conditions. For example, the higher the salt concentration (≤1M), the higher the T_M, as increasing the salt concentration helps to diffuse the negative charge on the phosphate backbone (electrostatic stabilisation).[123] The relationship between T_M and ionic strength can be exploited in order to change a T_M to a more convenient experimental temperature.

The physical property of denaturation can be monitored easily using a UV-vis spectrophotometer by observing the change in absorbance as a function of temperature. The method offers a useful insight into the strength of a drug-DNA interaction as the more energy required to denature the stabilized secondary structure relative to the untreated polynucleotide, the stronger the drug interaction (ΔT_M) and *vice versa*.[85] Structural features of DNA dramatically impact the affinity of a drug molecule toward it. This influence can be clearly seen in **Table I-2**, as the intercalator actinomycin D substantially stabilized the thermal denaturation of poly[d(G-C)$_2$], while minor groove binding agent netropsin, was seen to have an equal magnitude of stabilisation on the thermal melting profile of poly[d(A-T)$_2$]. We have also used this method effectively in order to rank the activity of a triplatin complex series on both calf thymus DNA and alternating copolymers.[75,85]

Table I-2. Influence of standard agents and selected copper phenazine complexes on the thermal melting of synthetic alternating copolymers.[85]

	ΔT_M (°C)	
Agent	**Poly[d(A-T)$_2$]**	**Poly[d(G-C)$_2$]**
Netropsin	12.32 ± 0.79	02.83 ± 0.38
Actinomycin D	-0.32 ± 0.29	12.10 ± 0.95
Cu-DPQ-Phen	0.60 ± 0.18	11.39 ± 1.10
Cu-DPPZ-Phen	0.50 ± 0.10	10.44 ± 1.10

I. 4.4.3. Circular dichroism spectroscopy

Circular dichroism spectroscopy probes the absolute configuration and conformation of a system and is dependent on chirality. This UV based method is used extensively for the study of the secondary structure of chiral biomolecules and is particularly useful to determine conformational properties such as the α and β helix of proteins and the A, B and Z-forms of DNA. In the case of DNA, heterocyclic nitrogenous DNA bases are achiral themselves but when linked to a 5′ carbon sugar by a β-glycosidic linkage and placed within the phosphate framework in a stacked helical formation, the molecule as a whole becomes chiral, therefore the electronic transitions of bases are monitored in the UV range of 180-300 nm. DNA structures can be affected by environmental factors in solution—temperature, pH and ionic strength (Figure I-12A)—and also by drug-DNA interactions; inducing significant variations in the resulting spectra.[124]

Many DNA binding agents are achiral and optically inactive, however by observing changes at specific wavelengths in the UV spectrum where DNA typically absorbs (**Figure I-12B**), it is possible to determine the induced circular dichroism (ICD) of the drug-DNA interaction, through the coupling of electric transition moments of the ligand and the DNA bases.[125] Using this spectroscopic method it is possible to determine a molecules preferred binding mode (minor groove, major groove, intercalation) within the asymmetric DNA environment by observing the induced CD signal relative to untreated DNA at wavelengths of 210, 220, 246 and 268 nm.[126]

A.

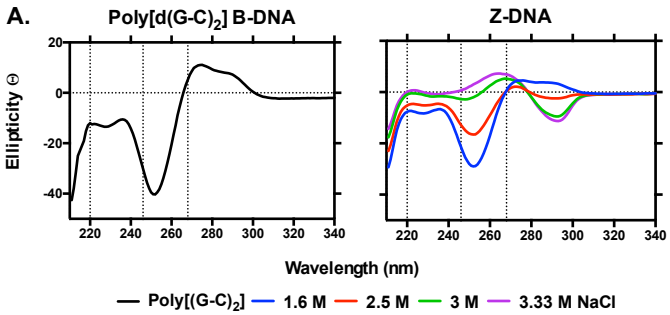

B.

Wavelength (nm)	Region of DNA
210	β-N-glycosidic linkages
220	Hydrogen bonding
246	Handedness / helicity
268	Base pair stacking interactions

Figure I-12. A. B → Z NaCl titration of alternating co-polymer poly[d(G-C)$_2$] with increasing amounts of salt (unpublished results) and **B.** and wavelengths of interest for CD DNA studies.

Intercalation typically leads to an increase in the elliptical signal of helicity and base pair stacking interactions of B-DNA, while groove binding agents typically cause an increase in the elliptical signal associated with hydrogen bonding interactions. CD has effectively been used to show a B→Z[127] and B→A[128] conformational changes when the alternating poly(dG-dC)•poly(dG-dC) co-polymer was treated with both monofunctional and bifunctional platinum complexes.

CD offers many advantages over NMR and X-ray crystallography in the analysis of structural interactions in biological systems as it is an inexpensive technique requiring small amounts of sample, allowing for rapid and highly sensitive analysis of oligonucleotides of both short and long base pair composition offering an alternative absorbance based technique to determine binding mode and affinity of drug-DNA interactions.[129] Linear dichroism—another powerful form of polarized-light spectroscopy complementing CD—has been successfully employed to deduce drug-DNA binding geometries and has been extensively reviewed elsewhere. [130,131]

I. 4.4.4. ELISA detection of 8-oxo-dG lesion formation

8-oxo-2′-deoxyguanosine (8-oxo-dG) is one of the most popular and well-studied biomarkers of oxidative stress since it can be readily detected indirectly in bodily fluids including urine, serum and plasma through the measurement of repaired adducts as the daily flux of repaired adducts should reflect the intracellular rate of oxidative DNA damage.[132] Several chromatography based methods can be employed to assess 8-oxo-dG as

a biomarker of oxidative stress including high pressure liquid chromatography with electrochemical detection (HPLC-EC), gas chromatography coupled to mass spectroscopy (GC-MS), and the standard stable isotope dilution liquid chromatography-MS/MS.[133,134] However, many debates still exist regarding the most suitable method to determine 8-oxo-dG, as nucleotides are prone to oxidation during both sample preparation and analysis. It has been reported in literature that GC-MS estimates of DNA oxidation have been shown to be higher than HPLC-EC estimates by a factor of ~10.[132]

We recently employed a Trevigen high throughput ELISA kit in order to quantify the extent of oxidative lesions induced by the copper phenazine complex series. Detection of oxidative lesions is conducted using a HRP conjugate and TACS Sapphire colorimetric substrate with lesions quantified using a fluorescence plate reader. It was determined that 8-oxo-dG liberation followed the overall trend Cu-DPQ-Phen > Cu-Phen > Cu-DPPZ-Phen (**Figure I-7**) with higher lesion numbers detected under heavily sheared plasmid conditions when DNA was treated with higher drug concentrations.[92]

I. 5. Viscosity

Unlike fluorescence and absorbance-based techniques, viscosity does not involve the study of new optical properties arising through metallodrug-nucleic acid binding. Rather, this is a method in which drug-DNA interactions can be studied as a function of the physical hydrodynamic changes induced by the addition of a drug molecule. Viscosity is a method in which drug-DNA interactions can be studied as a function of the hydrodynamic changes induced by the addition of a drug molecule. Experiments are conducted by introducing increasing ratios of drug into a solution containing a fixed concentration of DNA and observing how the velocity of DNA sedimentation influences a change in centipoise (cP). Relative viscosity data can be represented as (η/η_o) *versus* the [compound] / [DNA] ratio r, where η is the viscosity of complex treated DNA and η_o is the viscosity of untreated DNA.[86] This technique is sensitive to changes in the length of DNA chain and individual modes of binding can be distinguished effectively since covalent and non-covalent binding modes display different hydrodynamic characteristics.

Intercalating molecules induce extension and unwinding of the deoxyribose phosphate backbone due to separation of base pairs in order to accommodate the bound ligand ultimately resulting in the lengthening of the DNA molecule– these hydrodynamic changes can be monitored by viscometry as the length of the molecule is increased in

proportion to the amount of drug bound (**Figure I-13**).[42] Indeed the opposite effect can be noted for non-covalent major and minor groove binding agents since they cause little or no distortion to the phosphate backbone of DNA. In contrast, condensing agents –such as the triplatin series of complexes– are capable of compacting and precipitating sheared DNA, and ultimately decreasing the overall trend of viscosity.[75]

Compound	Mode of binding	η/η_o
EtBr[120]	Intercalation	1.16
Actinomycin D[75]	Threading intercalation	1.14
Netropsin[120]	Minor groove	1.00
Pentamidine[120]	Minor groove	0.99
$[Co(NH_3)_6]Cl_3$[85]	Electrostatic	0.82
TriplatinNC[75]	Phosphate clamp	0.39

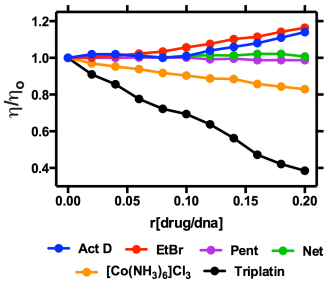

Figure I-13. Relative viscosity values of organic and inorganic compounds bound to duplex stDNA.

I. 6. Mass Spectrometry

Advances in technologies and ionization techniques now make Electrospray Ionization-Mass Spectrometry (ESI-MS) an indispensable tool for probing drug-nucleic acid interactions with several advantages including the need for only a small sample, speed of use, and ease of analysis.[135,136] Covalent binding with biomolecules in general is easily observed and with appropriate digestion can pinpoint stoichiometry and binding sites of metallodrugs. It is in the study of non-covalent interactions where most interest resides because, if strong enough, the canonical non-covalent binding modes of hydrogen-bonding, electrostatic interactions, and intercalation can be transferred to the gas phase without disruption. Single-stranded, double-stranded and G-quadruplex DNA have all been studied and primary spectra combined with MS-MS techniques can give information on strength and sites of binding.

DNA as a template affects kinetics of substitution reactions occurring within its domain. Mass spectrometric studies using 18-mers showed a kinetic preference for binding of BBR3464 to ssDNA over dsDNA.[137] In this case, electrospray ionization coupled with Fourier transform ion cyclotron resonance mass spectrometry (ESI-FTICR-MS) is sufficiently sensitive to observe the 'pre-association" of the covalently binding molecule prior to Pt-DNA bond formation. For single-stranded DNA, the site of binding of the substitution-inert TriplatinNC and AH44 on a 18-mer ssDNA (5'-

TCTCCCAGCGTGCGCCAT-3') was ascertained using Tandem MS-MS of the 1:1 adducts (**Figure I-14**).[40] The binding is sufficiently strong that the fragment ion pattern is distinctly different and upon MS-MS there is no drug-DNA dissociation, only cleavage of the oligonucleotide backbone.

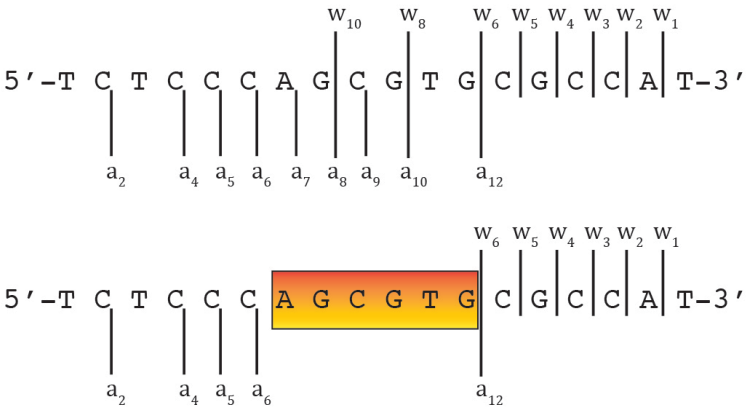

Figure I-14. ESI-MS/MS of free (top) and PPC (either TriplatinNC or AH44) adducted (bottom) 5'-d(TCTCCCAGCGTGCGCCAT) at 100 and 120V of collisional energy, respectively.[40] Fragmentation of the glycosidic bonds is prevalent throughout the free, with the region of enhanced stability in red. The associated fragment ions (w_8^{2-},w_9^{2-}, and a_9-a_{12} using standard McLuckey nomenclature[136,137]) are absent in the adduct indicating the area of PPC binding.

Full scan ESI-MS spectra of dsDNA AT duplex {5′-TAGCGCTTTTTCCGTA-3′} – {5′-TACGCGAAAAAGCGCTA-3′} complexed with substitution-inert PPCs also confirmed that the non-bonding interaction is strong enough to be transferred from solution to the gas phase.[14] The collision induced dissociation (CID) spectra showed duplex unzipping into single strands with again no loss of PPC-DNA binding and duplex stabilization correlates with increasing charge and hydrogen bonding character of the complex. The energy required to separate the PPC-DNA adducts is significantly more than that needed for the minor groove binding Hoechst dye 33258. Upon increasing the collisional energy the single-stranded DNA formed dissociates as above.

ESI-MS has also proven useful in probing relative binding affinities of metal complexes to duplex and quadruplex DNA.[140,141] Differences in binding within a series of octahedral metallointercalators based on $[Ru(phen)_3]^{2+}$ and $[Ru(phen)_2(dppz)]^{2+}$ and square-planar analogs such as $[Pt(en)(phen)]^{2+}$ demonstrated that the binding affinity in general towards quadruplex DNA is significantly less than that towards dsDNA.[140]

I. 7. NMR Spectroscopy

NMR spectroscopy, like mass spectrometry, has benefitted significantly from advances in field strength, magnetic shielding and cryogenic probes.[142,143] Spectral analysis of HPLC-purified site-specific oligonucleotide adducts with cisplatin have characterized the major conformational changes upon platination using essentially standard 2D-NMR techniques.[142,143] In the case of BBR3464 and congeners ([{*trans*-$PtCl(NH_3)_2$}$_2$μ-$H_2N(CH_2)_6NH_2$]$^{2+}$ adducted to the self-complementary DNA octamer 5′-d(ATG*TACAT)$_2$-3′, the formation of the novel 1,4-interstrand crosslinks was confirmed.[144,145] Strong H8/H1′ intraresidue crosspeaks observed for the A1 and A7 resonances are consistent with a *syn*-conformation for these bases as well as the platinated guanines. The structure suggests unusual cooperative effects unique to this class of anticancer drugs and the lack of severe DNA distortion such as a kink or directed bend may explain the inability of HMG-domain proteins to recognize these lesions, a biological consequence significantly different from that of mononuclear complexes such as cisplatin.[103] A unique feature of long-range {Pt,Pt} interstrand crosslinks is the occurrence of directional isomers–the existence of the unusual 3′ → 3′ linkage isomer in the sequence was also confirmed by 2D NMR specroscopy.[146]

The most useful isotopes for NMR studies are ^{1}H, ^{15}N and ^{195}Pt. The latter is extremely sensitive to the nature of the ligands attached and can be used for speciation and kinetic studies. The use of {^{1}H, ^{15}N} HMQC/HSQC NMR spectroscopy greatly enhances sensitivity and is especially useful in kinetic studies with biological molecules. The chemical shift and coupling constants (e.g. ^{1}J{^{15}N-^{195}Pt}) are sensitive to the nature of the *trans* ligands, and coupled to the fact that the only protons observed are those bound to the ^{15}N nucleus makes the technique of great practical use. Pre-association and strong non-covalent binding can be observed as well as kinetics of DNA binding.

Using fully ^{15}N-labelled TriplatinNC, the presence of the phosphate clamp in solution with the Dickerson-Drew Duplex (DDD) was confirmed by observation of large chemical shift differences of the δ(NH_3) and δ(-NH_2R) in both the ^{1}H and ^{15}N dimensions.[145] The 2D {^{1}H,^{15}N} HSQC NMR spectrum of ^{15}N-labeled TriplatinNC shows only two cross-peaks and a weak peak due to dangling amine (**Figure I-15**). In the presence of DDD at pH 6, dramatic downfield ^{15}N shifts of approximately 20 ppm are

observed. The coupling constant changes are also consistent with formation of the phosphate clamp.[147]

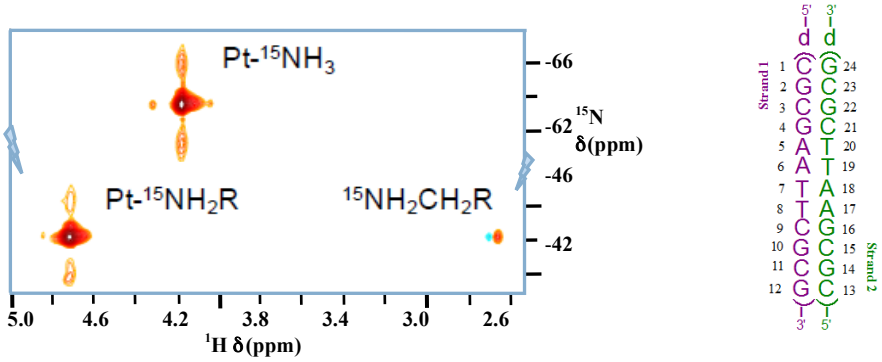

Figure I-15. {^{1}H,^{15}N} HSQC NMR of TriplatinNC (left) and Dickerson-Drew Duplex (DDD, right). Satellites from ^{1}J(^{15}N-^{195}Pt) are clearly visible. Adapted with permission from Qu *et al*.[145]

Pre-association may affect the final conformation of covalently-bound interstrand crosslinks and even the isomer directionality. These features have been studied by 2D {^{1}H,^{15}N} HSQC NMR.[148] A unique feature of DNA binding modes for PPCs is the kinetic preference for single-strand over dsDNA– as noted by ESI-MS studies. Mass spectrometric studies using 18-mers showed a kinetic preference for binding to ssDNA over dsDNA.[137] For BBR3464 the aquation rate constant is of the same order of magnitude to that of cisplatin, but the chloride anion rate constant is much higher so that the equilibrium favours the dichloro form.[149,150] A 3-fold slowing of the aquation of BBR3464 occurs in the presence of dsDNA but not ssDNA.[151] This feature may account for the kinetic binding preference and may also be relevant in stabilization of G-quartet quadruplex structures using BBR3464.[152] The results emphasize how the alteration of chemical properties of small molecules in the presence of large host interactions is dependent on the conformation and nature of that host and these examples show the utility of NMR techniques in probing these subtle interactions.

I. 8. *In cellulo* genotoxicity

I. 8.1. Intracellular ROS damage

The intracellular generation of endogeneous ROS can be monitored *via* the oxidation of the diacetate precursor to the highly fluorgenic 2′,7′-dichlorodihydroflorescin (DCFH).[153] Sequential time-course quantification can reveal time or concentration-dependent liberation of ROS from metal complexes. We have recently reported the Mn^{2+} bis-1,10-phenanthroline (phen) di-salt complex, bridged with octanedioate (oda) ([Mn_2(μ-

oda)(phen)$_4$(H_2O)$_2$][Mn_2(μ-oda)(phen)$_4$(oda)$_2$]·4H_2O (Mn-Oda-Phen) in conjunction with the cationic Cu^{2+} analogue, [Cu_2(μ-oda)(phen)$_4$]$^{2+}$ (Cu-Oda-Phen) (**Figure I-7**) as potent *in vitro* anticancer agents and ROS induction.[154] Mn-Oda elicited exceptional levels of endogenous ROS within cancer cells when examined with the intracellular ROS indicator at 15, 30, 60, 120 and 180 min intervals within a concentration range of 250 – 1000 nM with comparable activity at 12.5 μM equivalent to the positive control H_2O_2 (500 nM). Substitution of the metal centre notably altered redox properties as the copper analogue did not liberate significant levels when examined at higher concentrations (up to 100 μM).

I. 8.2. Intracellular ROS scavengers

Generation of intracellular ROS targets multiple biomolecules such as lipids, proteins and nucleic acids. Sequestering the species through the use of ROS specific antioxidants (similar to those described in section 2.2) can elucidate the redox chemistry and generation properties of metal-based anticancer drugs. Radical-selective antioxidants are treated within the cell at concentrations that do not alter cellular viability but are in excessive equivalent to the test complex and as such those previously mentioned in nuclease gel electrophoresis experiments are not suitable due to innate toxicity of DMSO and KI. The impact of ROS-specific scavengers (D-mannitol for $^{\bullet}OH$,[155] pyruvate for H_2O_2[156] and tiron for $O_2^{\bullet-}$,[87]) were examined for Cu-Ph-Phen treated SKOV3 cell survival where co-incubation of antioxidants were found to enhance viability by 12, 16, and 23%, respectively.[91] Results are in excellent agreement with the observed effects on plasmid DNA damage and it is particularly significant that the largest enhancement to viability occurred in the presence of the $O_2^{\bullet-}$ scavenger, tiron. Thus we resolved Cu-Ph-Phen exerts cytotoxicity through Haber-Weiss catalytic generation of the superoxide radical accelerating Fenton-like chemistry.

I. 8.3. Confocal microscopy: detection of DNA fragmentation and condensation

The use of confocal microscopy allows the evaluation of macromolecular structures in fine detail while revealing the intracellular molecular interactions and identification of morphorological changes associated with apoptotic cell death. Incorporating DNA specific fluorogenic dyes, such as propidium iodide, Hoechst, acridine orange and DAPI, can reveal alterations and distortions in genomic DNA and chromatin structure such as shrinking, condensations, fragmentation and disassembly of the nuclear envelope. This method was used to examine the pharmacological effects of TriplatinNC treated with 20

μM for 24h, stained with DAPI (4′,6-diamidino-2-phenylindole) (**Figure I-10A**), exhibited DNA condensation and compaction in colorectal cancer cell line, HCT116 (**Figure I-16A**).[157]

I. 8.4. Immunodetection of double strand breaks (DSBs) with γH2AX

A primary response to dsDNA damage is the site-selective phosphorylation of H2AX, a histone variant that is indiscriminately incorporated into the chromatin structure.[158,159] H2AX differs from other H2A histones through a carboxyl tail containing 139 serine residue that becomes phosphorylated in the presence of dsDNA damage and is denoted γH2AX.[160] The accumulation of phosphorylated H2AX creates a signaling beacon and focus for subsequent recruitment of DNA repair mechanisms. A proportional correlation is observed between the extent of DNA damage and formation of γH2AX foci thus rendering it as a pertinent method for dsDNA damage detection. Following the advent of phosphorylation, a recognition antibody for γH2AX can be utilised to visualise and quantify this process through either fluorogen conjugation to the primary or secondary antibodies. Using γH2AX, we have recently reported DNA damage induction by Cu-Ph-Phen and Cu-Ph-Bipy (**Figure I-7**).[86] In particular, the 1,10-phenanthroline analogue induced a large number of double strand breaks (DSBs) in comparison to the bipyridyl derivative and cisplatin, where DSBs observed in the latter is most likely due to DNA repair mechanisms and excision of platinated adducts (**Figure I-16B**). Quantification of H2AX was conducted through flow cytometry; by quantifying mean intensity fluorescence (MIF) and the trend Cu-Ph-Phen > cisplatin >> Cu-Ph-Bipy was identified and found to be in agreement with microscopic observations.

I. 8.5. COMET assay: neutral and alkaline

Single cell gel electrophoresis, otherwise known as the comet assay, is a useful method to evaluate the extent of DNA damage induced by genotoxic chemicals.[161] Various modifications to the COMET assay explores types of stand breaks and alkaline labile sites within the cell.[162] The severity of DNA degradation can be segregated based on the pH of electrophoretic buffer with the use of neutral buffers for DSBs while a more sensitive alkaline method can visualise both ds and ss breaks. Cells embedded onto agarose-coated slides are lysed of membrane and histone structure under high salt and detergent conditions leaving nucleoids of negatively supercoiled DNA. When subjected to electrophoresis, the migration of the DNA is dependent on the integrity and extent of damage. High levels of degradation result in patterns that are comet in shape, where intact DNA is localized to the

head, and increasingly damaged DNA results in retarded migration forming the tail shape. Based on the proportion of DNA in the head and tail, scoring a population of COMETs allows statistical comparison between treated and non-treated populations. This method can also be employed to measure the extent of interstrand cross-linking. Irradiation by γ-radiation induced double strand breaks, however in the presence of DNA platinating agents, the reduction in comet tail length is indicative of the extent of interstrand crosslinking.[163] This is observed for the mononuclear trans-platinum carboxylate complex with substituted pyridine (TPA V)[164] and polynuclear complexes BBR3610 and DACH analogue, (**Figure I-7**), capable of forming long-range inter and intrastrands (**Figure I-16C**).[163]

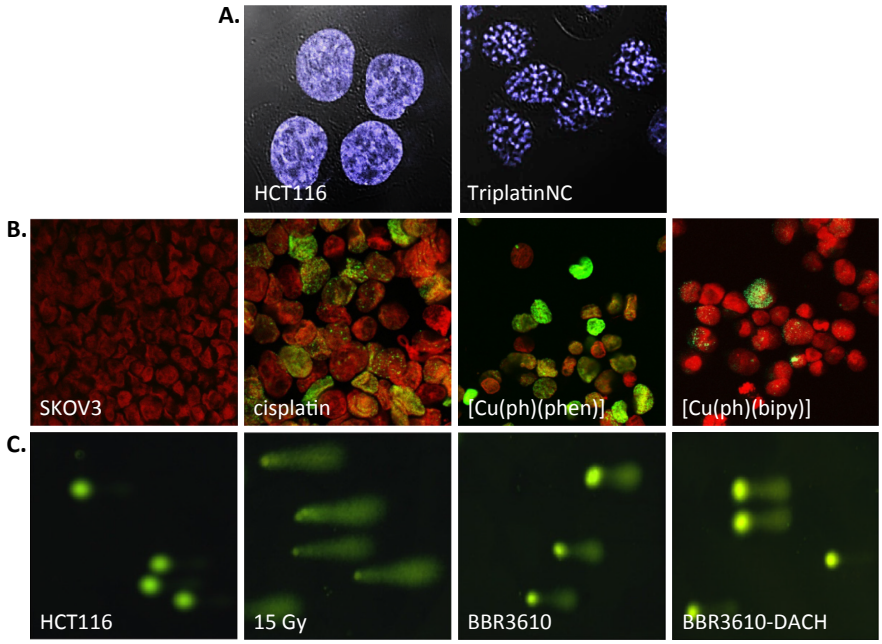

Figure I-16. A. Nuclear condensation observed in colorectal cancer cells, HTC116 when treated with TriplatinNC. **B.** Induction of double strand break detected *via* γH2AX foci (green) and nuclear counterstain (red) in ovarian cancer cells SKOV3. **C.** COMET assay evaluation of BBR3610 and DACH analogue interstrand crosslinks in irradiated HCT116 cells. Images reproduced with permission from original publications.[86,154,160]

I. 9. Conclusion

DNA is a well-established pharmacological target for metallodrugs and, as such, developmental anticancer complexes continue to be rationally designed for potential clinical use. The elucidation of covalent or non-covalent binding modes, along with helical and groove residency is therefore a crucial area of study in this field. As such, this review has focused on selected molecular and biophysical methods for determining metallodrug-DNA interactions using gel electrophoretic, electronic and fluorescent spectroscopic, immunohistochemical, NMR spectroscopic, and mass spectrometric techniques.

Significantly, when combinations of complementary molecular methods are employed, full elucidation of solution binding properties can be defined, which ultimately broaden our understanding of complex-DNA binding. The techniques for covalent binding as demonstrated for the platinum case can, and have been, easily applied to other classes of transition-metal cytotoxics such as those containing Ru(II) or Au(I/III).[165,166] Our recent work on probing the nucleic acid binding mode by 'phosphate clamping' Triplatin complexes elegantly reveals how these molecular techniques can function synergistically;[75] using a family of cationic tri-platinum(II) complexes of varying aliphatic linker length [{*trans*-$Pt(NH_3)_2(NH_2(CH_2)_nNH_3)\}_2$-$\mu$-(*trans*-$Pt(NH_3)_2(NH_2(CH_2)_nNH_2)_2\}$]$(NO_3)_8$, where n = 5 (AH78P), 6 (AH78; TriplatinNC) and 7 (AH78H), high-affinity PPC-DNA interactions were uncovered using ethidium bromide fluorescence quenching, while cooperative fluorescence binding of Hoechst 33258 was observed at the minor groove. Conformational changes on long DNA were then identified using viscosity, electrophoretic, and CD spectroscopic methods where aggregation/condensation of nucleic acids was evidenced in tandem with conversion from B → Z-DNA. 2D-^{1}H NMR experiments, in conjunction with several other molecular methods, then indicated two limiting modes of phosphate clamping—backbone tracking (GC dependent) and groove spanning (AT dependent)—could be distinguished and implied DNA condensation was driven, primarily, by minor-groove spanning. Further application of electrophoresis (including 'on-chip' microfluidics) showed Triplatin-DNA binding prevented endonuclease activity by type II restriction enzymes. Subsequent work by Farrell and co-workers identified nucleolar condensation in colorectal cancer cells using confocal microscopy[157] with atomic force microscopy (AFM) studies showing this class to condense both tRNA and dsDNA structures.[74] Other examples on the augmentation of molecular methods have been described in this review and, with this in mind, both the overlap and versatility of complementary techniques are further delineated.

I. 10. Acknowledgements

This work was supported by the Irish Research Council (IRC) grants GOIPG/2014/1182 and GOIPG/2013/826. AK acknowledges support from the Marie Skłodowska-Curie Innovative Training Network (ITN) ClickGene (H2020-MSCA-ITN-2014−642023). NF acknowledges support by NIH RO1CA78754.

I. 11. References

(1) Farrell, N. P. (2015) Multi-platinum anti-cancer agents. Substitution-inert compounds for tumor selectivity and new targets. *Chem. Soc. Rev. 44*, 8773–8785.
(2) Chen, J., and Stubbe, J. (2005) Bleomycins: towards better therapeutics. *Nat. Rev. Cancer 5*, 102–112.
(3) Johnstone, T. C., Suntharalingam, K., and Lippard, S. J. (2016) The Next Generation of Platinum Drugs: Targeted Pt(II) Agents, Nanoparticle Delivery, and Pt(IV) Prodrugs. *Chem. Rev. 116*, 3436–3486.
(4) Komor, A. C., and Barton, J. K. (2013) The path for metal complexes to a DNA target. *Chem. Commun. 49*, 3617–3630.
(5) Watson, J. D., and Crick, F. (1953) Molecular structure of nucleic acids. *Nature 171* 737–738.
(6) Rosenberg, B., van Camp, L., and Krigas, T. (1965) Inhibition of Cell Division in Escherichia coli by Electrolysis Products from a Platinum Electrode. *Nature 205*, 698–699.
(7) Chargaff, E. (1971) Preface to a grammar of biology. *Science 172*, 637–642.
(8) Wing, R., Drew, H., Takano, T., Broka, C., Tanaka, S., Itakura, K., and Dickerson, R. E. (1980) Crystal structure analysis of a complete turn of B-DNA. *Nature 287*, 755–758.
(9) Drew, H. R., Wing, R. M., Takano, T., Broka, C., Tanaka, S., Itakura, K., and Dickerson, R. E. (1981) Structure of a B-DNA dodecamer: conformation and dynamics. *Proc. Natl. Acad. Sci. U.S.A. 78*, 2179–2183.
(10) Harteis, S., and Schneider, S. (2014) Making the bend: DNA tertiary structure and protein-DNA interactions. *Int. J. Mol. Sci. 15*, 12335–12363.
(11) Önfelt, B., Lincoln, P., and Nordén, B. (2001) Enantioselective DNA Threading Dynamics by Phenazine-Linked [Ru(phen)2dppz]$^{2+}$ Dimers. *J. Am. Chem. Soc.*, *123*, 3630-3637.
(12) Rich, A., and Zhang, S. (2003) Z-DNA: the long road to biological function. *Nat. Rev. Genet. 4*, 566–572.
(13) Ussery, D. W. (2002) DNA Structure: A-, B- and Z-DNA Helix Families. John Wiley & Sons, Ltd., 0003122
(14) Komeda, S., Qu, Y., Mangrum, J. B., Hegmans, A., Williams, L. D., and Kelland, L. R. (2016) The phosphate clamp as recognition motif in platinum–DNA interactions. *Inorg. Chim. Acta*. *452*, 25-33.
(15) Georgiades, S. N., Abd Karim, N. H., Suntharalingam, K., and Vilar, R. (2010) Interaction of Metal Complexes with G-Quadruplex DNA. *Angew. Chem. Int. Ed. 49*, 4020–4034.
(16) Yu, Z., Han, M., and Cowan, J. A. (2015) Toward the Design of a Catalytic Metallodrug: Selective Cleavage of G-Quadruplex Telomeric DNA by an Anticancer Copper–Acridine–ATCUN Complex. *Angew. Chem. Int. Ed. 54*, 1901–1905.
(17) Phongtongpasuk, S., Paulus, S., Schnabl, J., Sigel, R. K. O., Spingler, B., Hannon, M. J., and Freisinger, E. (2013) Binding of a Designed Anti-Cancer Drug to the Central Cavity of an RNA Three-Way Junction. *Angew. Chem. Int. Ed. 52*, 11513–11516.
(18) Su, M., Tomás-Gamasa, M., and Carell, T. (2015) DNA based multi-copper ions assembly using combined pyrazole and salen ligandosides. *Chem. Sci. 6*, 632–638.

(19) Cao, Q., Li, Y., Freisinger, E., Qin, P. Z., Sigel, R. K. O., and Mao, Z.-W. (2016) G-quadruplex DNA targeted metal complexes acting as potential anticancer drugs. *Inorg. Chem. Front.* C6QI00300A.
(20) Kelland, L. R. (1999) Cisplatin-based Anticancer Agents, in *Uses of Inorganic Chemistry in Medicine*, pp 109–123. Royal Society of Chemistry, Cambridge.
(21) Wheate, N. J., Walker, S., Craig, G. E., and Oun, R. (2010) The status of platinum anticancer drugs in the clinic and in clinical trials. *Dalton Trans. 39*, 8113–8127.
(22) Dabrowiak, J. C. (2009) Cisplatin, in *Metals in Medicine*, pp 73–107. John Wiley & Sons, Ltd.
(23) Miller, S. E., and House, D. A. (1990) The hydrolysis products of cis-dichlorodiammineplatinum(II) 3. Hydrolysis kinetics at physiological pH. *Inorg. Chim. Acta 173*, 53–60.
(24) Cepeda, V., Fuertes, M. A., Castilla, J., Alonso, C., Quevedo, C., and Pérez, J. M. (2007) Biochemical Mechanisms of Cisplatin Cytotoxicity. *Anti-Cancer Agents Med. Chem. 7*, 3–18.
(25) Klein, A. V., and Hambley T. (2009) Platinum Drug Distribution in Cancer Cells and Tumors. *Chem. Rev. 109*, 4911–4920.
(26) Alberto, M. E., Butera, V., and Russo, N. (2011) Which One among the Pt-Containing Anticancer Drugs More Easily Forms Monoadducts with G and A DNA Bases? A Comparative Study among Oxaliplatin, Nedaplatin, and Carboplatin. *Inorg. Chem. 50*, 6965–6971.
(27) Dabrowiak, J. C. (2009) Cisplatin. *Metals in Medicine*, pp 73–107. John Wiley & Sons, Ltd, Chichester, UK.
(28) Jones, C. J., and Thornback, J. (2007) Chapter 4. Therapeutic Medicine, in *Medicinal Applications of Coordination Chemistry*, pp 201–323. Royal Society of Chemistry, Cambridge.
(29) Jamieson, E. R., and Lippard, S. J. (1999) Structure, Recognition, and Processing of Cisplatin-DNA Adducts. *Chem. Rev. 99*, 2467–2498.
(30) Bellon, S. F., Coleman, J. H., and Lippard, S. J. (1991) DNA unwinding produced by site-specific intrastrand cross-links of the antitumor drug cis-diamminedichloroplatinum(II). *Biochemistry 30*, 8026–8035.
(31) Chaney, S. G., Campbell, S. L., Temple, B., Bassett, E., Wu, Y., and Faldu, M. (2004) Protein interactions with platinum–DNA adducts: from structure to function. *J. Inorg. Biochem. 98*, 1551–1559.
(32) Tanida, S., Mizoshita, T., Ozeki, K., Tsukamoto, H., Kamiya, T., Kataoka, H., Sakamuro, D., and Joh, T. (2012) Mechanisms of Cisplatin-Induced Apoptosis and of Cisplatin Sensitivity: Potential of BIN1 to Act as a Potent Predictor of Cisplatin Sensitivity in Gastric Cancer Treatment. *Int. J. Surg. Oncol.* 862879.
(33) Chvalova, K., Brabec, V., and Kasparkova, J. (2007) Mechanism of the formation of DNA–protein cross-links by antitumor cisplatin. *Nucleic Acids Res. 35*, 1812–1821.
(34) El-Khateeb, M., Appleton, T. G., Gahan, L. R., Charles, B. G., Berners-Price, S. J., and Bolton, A.-M. (1999) Reactions of cisplatin hydrolytes with methionine, cysteine, and plasma ultrafiltrate studied by a combination of HPLC and NMR techniques. *J. Inorg. Biochem. 77*, 13–21.

(35) Bose, R. N., and Weaver, E. L. (1997) A long-lived ascorbate radical in the platinum(II) catalysedreductions of platinum(IV) antitumor drugs. *J. Chem. Soc., Dalton Trans.* 1797–1800.
(36) Kelley, S. L., Basu, A., Teicher, B. A., Hacker, M. P., Hamer, D. H., and Lazo, J. S. (1988) Overexpression of metallothionein confers resistance to anticancer drugs. *Science 241*, 1813–1815.
(37) Reißner, T., Schneider, S., Schorr, S., and Carell, T. (2010) Crystal structure of a cisplatin-(1,3-GTG) cross-link within DNA polymerase η. *Angew. Chem. Int. Ed. 49*, 3077–3080.
(38) Hegmans, A., Berners-Price, S. J., Davies, M. S., Thomas, D. S., Humphreys, A. S., and Farrell, N. (2004) Long Range 1,4 and 1,6-Interstrand Cross-Links Formed by a Trinuclear Platinum Complex. Minor Groove Preassociation Affects Kinetics and Mechanism of Cross-Link Formation as Well as Adduct Structure. *J. Am. Chem. Soc. 126*, 2166–2180.
(39) Komeda, S., Moulaei, T., Woods, K. K., Chikuma, M., Kelland, L. R., and Williams, L. D. (2006) A Third Mode of DNA Binding: Phosphate Clamps by a Polynuclear Platinum Complex. *J. Am. Chem. Soc. 128*, 16092–16103.
(40) Mangrum, J. B., and Kelland, L. R. (2010) Excursions in polynuclear platinum DNA binding. *Chem. Commun. 46*, 6640–6650.
(41) Jodrell, D. I., Evans, T. R. J., Steward, W., Cameron, D., Prendiville, J., Aschele, C., Noberasco, C., Lind, M., Carmichael, J., Dobbs, N., Camboni, G., Gatti, B., and De Braud, F. (2004) Phase II studies of BBR3464, a novel tri-nuclear platinum complex, in patients with gastric or gastro-oesophageal adenocarcinoma. *Eur. J. Cancer 40*, 1872–1877.
(42) Lerman, L. S. (1961) Structural considerations in the interaction of DNA and acridines. *J. Mol. Biol. 3*, 18–30.
(43) Rescifina, A., Zagni, C., Varrica, M. G., Pistarà, V., and Corsaro, A. (2014) Recent advances in small organic molecules as DNA intercalating agents: Synthesis, activity, and modeling. *Eur. J. Med. Chem. 74*, 95–115.
(44) Liu, H.-K., and Sadler, P. J. (2011) Metal Complexes as DNA Intercalators. *Acc. Chem. Res. 44*, 349–359.
(45) Jennette, K. W., Lippard, S. J., Vassiliades, G. A., and Bauer, W. R. (1974) Metallointercalation reagents. 2-hydroxyethanethiolato(2,2“,2-”terpyridine)-platinum(II) monocation binds strongly to DNA by intercalation. *Proc. Natl. Acad. Sci. U.S.A. 71*, 3839–3843.
(46) Bond, P. J., Langridge, R., Jennette, K. W., and Lippard, S. J. (1975) X-ray fiber diffraction evidence for neighbor exclusion binding of a platinum metallointercalation reagent to DNA. *Proc. Natl. Acad. Sci. U.S.A. 72*, 4825–4829.
(47) Zeglis, B. M., Pierre, V. C., and Barton, J. K. (2007) Metallo-intercalators and metallo-insertors. *Chem. Commun.* 4565–4579.
(48) Pages, B. J., Ang, D. L., Wright, E. P., and Aldrich-Wright, J. R. (2015) Metal complex interactions with DNA. *Dalton Trans. 44*, 3505–3526.
(49) Galindo-Murillo, R., García-Ramos, J. C., Ruiz-Azuara, L., Cheatham, T. E., and Cortés-Guzmán, F. (2015) Intercalation processes of copper complexes in DNA. *Nucleic Acids Res. 43*, 5364–5376.

(50) Li, G., Sun, L., Ji, L., and Chao, H. (2016) Ruthenium(ii) complexes with dppz: from molecular photoswitch to biological applications. *Dalton Trans. 45,* 13261-13276.
(51) Zhang, T.-B., Zhang, C.-L., Dong, Z.-L., and Guan, Y.-F. (2015) Determination of Base Binding Strength and Base Stacking Interaction of DNA Duplex Using Atomic Force Microscope. *Sci. Rep. 5*, 9143.
(52) Matta, C. F., Castillo, N., and Boyd, R. J. (2006) Extended weak bonding interactions in DNA: pi-stacking (base-base), base-backbone, and backbone-backbone interactions. *J. Phys. Chem. B 110*, 563–578.
(53) Hunter, C. A., and Sanders, J. K. M. (1990) The nature of π-π interactions. *J. Am. Chem. Soc. 112*, 5525–5534.
(54) Wheeler, S. E. (2011) Local Nature of Substituent Effects in Stacking Interactions. *J. Am. Chem. Soc. 133*, 10262–10274.
(55) Martinez, C. R., and Iverson, B. L. (2012) Rethinking the term "pi-stacking." *Chem. Sci. 3*, 2191–2201.
(56) Keck, M. V., and Lippard, S. J. (1992) Unwinding of supercoiled DNA by platinum-ethidium and related complexes. *J. Am. Chem. Soc. 114*, 3386–3390.
(57) Kielkopf, C. L., Erkkila, K. E., Hudson, B. P., Barton, J. K., and Rees, D. C. (2000) Structure of a photoactive rhodium complex intercalated into DNA. *Nat. Struct. Mol. Biol. 7*, 117–121.
(58) Rao, S. N., and Kollman, P. A. (1987) Molecular mechanical simulations on double intercalation of 9-amino acridine into d(CGCGCGC) X d(GCGCGCG): analysis of the physical basis for the neighbor-exclusion principle. *Proc. Natl. Acad. Sci. U.S.A. 84*, 5735–5739.
(59) Collins, J. G., Sleeman, A. D., Aldrich-Wright, J. R., Greguric, I., and Hambley T. (1998) A 1H NMR Study of the DNA Binding of Ruthenium(II) Polypyridyl Complexes. *Inorg. Chem. 37*, 3133–3141.
(60) Hall, J. P., Beer, H., Buchner, K., Cardin, D. J., and Cardin, C. J. (2013) Preferred orientation in an angled intercalation site of a chloro-substituted Λ-$[Ru(TAP)_2(dppz)]^{2+}$ complex bound to $d(TCGGCGCCGA)_2$. *Philos. Trans. A Math. Phys. Eng. Sci. 371*, 20120525–20120525.
(61) Niyazi, H., Hall, J. P., O'Sullivan, K., Winter, G., Sorensen, T., Kelly, J. M., and Cardin, C. J. (2012) Crystal structures of Λ-$[Ru(phen)2dppz]^{2+}$ with oligonucleotides containing TA/TA and AT/AT steps show two intercalation modes. *Nature Chem. 4*, 621–628.
(62) Franco, D., Vargiu, A. V., and Magistrato, A. (2014) $Ru[(bpy)_2(dppz)]^{2+}$ and $Rh[(bpy)_2(chrysi)]^{3+}$ Targeting Double Strand DNA: The Shape of the Intercalating Ligand Tunes the Free Energy Landscape of Deintercalation. *Inorg. Chem. 53*, 7999–8008.
(63) Yakovchuk, P., Protozanova, E., and Frank-Kamenetskii, M. D. (2006) Base-stacking and base-pairing contributions into thermal stability of the DNA double helix. *Nucleic Acids Res. 34*, 564–574.
(64) Howe-Grant, M., and Lippard, S. J. (1979) Binding of platinum(II) intercalation reagents to deoxyribonucleic acid. Dependence on base-pair composition, nature of the intercalator, and ionic strength. *Biochemistry 18*, 5762–5769.

(65) R Erik Holmlin, Eric D A Stemp, A., and Barton, J. K. (1998) $[Ru(phen)_2dppz]^{2+}$ Luminescence: Dependence on DNA Sequences and Groove-Binding Agents. *Inorg. Chem. 37*, 29–34.
(66) Krotz, A. H., Hudson, B. P., and Barton, J. K. (1993) Assembly of DNA recognition elements on an octahedral rhodium intercalator: predictive recognition of 5′-TGCA-3′ by .DELTA.-[Rh(R,R)-Me2trien]phi]3. *J. Am. Chem. Soc. 115*, 12577–12578.
(67) Pierre, V. C., Kaiser, J. T., and Barton, J. K. (2007) Insights into finding a mismatch through the structure of a mispaired DNA bound by a rhodium intercalator. *Proc. Natl. Acad. Sci. U.S.A. 104*, 429–434.
(68) Komor, A. C., and Barton, J. K. (2014) An Unusual Ligand Coordination Gives Rise to a New Family of Rhodium Metalloinsertors with Improved Selectivity and Potency. *J. Am. Chem. Soc. 136*, 14160–14172.
(69) Song, H., Kaiser, J. T., and Barton, J. K. (2012) Crystal structure of Δ-$[Ru(bpy)_2dppz]^{2+}$ bound to mismatched DNA reveals side-by-side metalloinsertion and intercalation. *Nature Chem. 4*, 615–620.
(70) Jackson, B. A., Alekseyev, V. Y., and Barton, J. K. (1999) A versatile mismatch recognition agent: specific cleavage of a plasmid DNA at a single base mispair. *Biochemistry 38*, 4655–4662.
(71) Boynton, A. N., Marcélis, L., and Barton, J. K. (2016) $[Ru(Me_4phen)_2dppz]^{2+}$, a Light Switch for DNA Mismatches. *J. Am. Chem. Soc. 138*, 5020–5023.
(72) Önfelt, B., Lincoln, P., and Nordén, B. (2001) Enantioselective DNA Threading Dynamics by Phenazine-Linked $[Ru(phen)_2dppz]^{2+}$ Dimers. *J. Am. Chem. Soc. 123*, 3630–3637.
(73) Malina, J., Kelland, L. R., and Brabec, V. (2014) DNA Condensing Effects and Sequence Selectivity of DNA Binding of Antitumor Noncovalent Polynuclear Platinum Complexes. *Inorg. Chem. 53*, 1662–1671.
(74) Malina, J., Kelland, L. R., and Brabec, V. (2014) Substitution-Inert Trinuclear Platinum Complexes Efficiently Condense/Aggregate Nucleic Acids and Inhibit Enzymatic Activity. *Angew. Chem. Int. Ed. 53*, 12812–12816.
(75) Prisecaru, A., Molphy, Z., Kipping, R. G., Peterson, E. J., Qu, Y., Kellett, A., and Farrell, N. P. (2014) The phosphate clamp: sequence selective nucleic acid binding profiles and conformational induction of endonuclease inhibition by cationic Triplatin complexes. *Nucleic Acids Res. 42*, 13474–13487.
(76) Harris, A. L., Ryan, J. J., and Farrell, N. (2006) Biological consequences of trinuclear platinum complexes: comparison of $[[trans\text{-}PtCl(NH_3)_2]_2\mu\text{-}(trans\text{-}Pt(NH_3)_2(H_2N(CH_2)_6\text{-}NH_2)_2)]^{4+}$ (BBR 3464) with its noncovalent congeners. *Mol. Pharmacol. 69*, 666–672.
(77) Komeda, S., Moulaei, T., Chikuma, M., Odani, A., Kipping, R., Kelland, L. R., and Williams, L. D. (2011) The phosphate clamp: a small and independent motif for nucleic acid backbone recognition. *Nucleic Acids Res. 39*, 325–336.
(78) Farrell, N. P. (2015) Multi-platinum anti-cancer agents. Substitution-inert compounds for tumor selectivity and new targets. *Chem. Soc. Rev. 44*, 8773–8785.
(79) Silva, H., Frézard, F., Peterson, E. J., Kabolizadeh, P., Ryan, J. J., and Kelland, L. R. (2012) Heparan Sulfate Proteoglycan-Mediated Entry Pathway for Charged Tri-Platinum

Compounds: Differential Cellular Accumulation Mechanisms for Platinum. *Mol. Pharmaceutics 9*, 1795–1802.
(80) Mangrum, J. B., Engelmann, B. J., Peterson, E. J., Ryan, J. J., Berners-Price, S. J., and Kelland, L. R. (2014) A new approach to glycan targeting: enzyme inhibition by oligosaccharide metalloshielding. *Chem. Commun. 50*, 4056–4058.
(81) Helleday, T., Eshtad, S., and Nik-Zainal, S. (2014) Mechanisms underlying mutational signatures in human cancers. *Nat. Rev. Genet. 15*, 585–598.
(82) Weiss, B., and Richardson, C. C. (1967) Enzymatic breakage and joining of deoxyribonucleic acid, I. Repair of single-strand breaks in DNA by an enzyme system from Escherichia coli infected with T4 bacteriophage. *Proc. Natl. Acad. Sci. U.S.A. 57*, 1021–1028.
(83) Pitié, M., and Pratviel, G. (2010) Activation of DNA Carbon−Hydrogen Bonds by Metal Complexes. *Chem. Rev. 110*, 1018–1059.
(84) Kellett, A., McCann, M., Howe, O., O'Connor, M., and Devereux, M. (2012) DNA cleavage reactions of the dinuclear chemotherapeutic agent copper(II) bis-1,10-phenanthroline terephthalate. *Int. J. Clin. Pharmacol. Ther. 50*, 79–81.
(85) Molphy, Z., Prisecaru, A., Slator, C., Barron, N., McCann, M., Colleran, J., Chandran, D., Gathergood, N., and Kellett, A. (2014) Copper phenanthrene oxidative chemical nucleases. *Inorg. Chem. 53*, 5392–5404.
(86) Kellett, A., Howe, O., O'Connor, M., McCann, M., Creaven, B. S., McClean, S., Foltyn-Arfa Kia, A., Casey, A., and Devereux, M. (2012) Radical-induced DNA damage by cytotoxic square-planar copper(II) complexes incorporating *o*-phthalate and 1,10-phenanthroline or 2,2′-dipyridyl. *Free Radic. Biol. Med. 53*, 564–576.
(87) Taiwo, F. A. (2008) Mechanism of tiron as scavenger of superoxide ions and free electrons. *J. Spectrosc. 22*, 491–498.
(88) Franco, R., Panayiotidis, M. I., and Cidlowski, J. A. (2007) Glutathione Depletion Is Necessary for Apoptosis in Lymphoid Cells Independent of Reactive Oxygen Species Formation. *J. Biol. Chem. 282*, 30452–30465.
(89) Miyoshi, N., Ueda, M., Fuke, K., Tanimoto, Y., and Itoh, M. (1982) Lifetime of singlet oxygen and quenching by NaN_3 in mixed solvents. *Z. Naturforsch. B Chem. Sci. 37*, 649–652.
(90) Dunand, C., Crèvecoeur, M., and Penel, C. (2007) Distribution of superoxide and hydrogen peroxide in Arabidopsis root and their influence on root development: possible interaction with peroxidases. *New Phytol. 174*, 332–341.
(91) Slator, C., Barron, N., Howe, O., and Kellett, A. (2016) [Cu(*o*-phthalate)(phenanthroline)] Exhibits Unique Superoxide-Mediated NCI-60 Chemotherapeutic Action through Genomic DNA Damage and Mitochondrial Dysfunction. *ACS Chem. Biol. 11*, 159–171.
(92) Molphy, Z., Slator, C., Chatgilialoglu, C., and Kellett, A. (2015) DNA oxidation profiles of copper phenanthrene chemical nucleases. *Front. Chem. 3*, 28, 1-9.
(93) Wang, J. C. (2002) Cellular roles of dna topoisomerases: a molecular perspective. *Nat. Rev. Mol. Cell Biol. 3*, 430–440.

(94) Peixoto, P., Bailly, C., and David-Cordonnier, M.-H. (2010) Topoisomerase I-mediated DNA relaxation as a tool to study intercalation of small molecules into supercoiled DNA. *Methods Mol. Biol. 613*, 235–256.
(95) Wang, J. G. (1974) The degree of unwinding of the DNA helix by ethidium: I. titration of twisted PM2 DNA molecules in alkaline cesium chloride density gradients. *J. Mol. Biol. 89*, 783–801.
(96) Bachur, N. R., Gordon, S. L., and Gee, M. V. (1977) Anthracycline antibiotic augmentation of microsomal electron transport and free radical formation. *Mol. Pharmacol. 13*, 901–910.
(97) Gewirtz, D. (1999) A critical evaluation of the mechanisms of action proposed for the antitumor effects of the anthracycline antibiotics adriamycin and daunorubicin. *Biochem. Pharmacol. 57*, 727–741.
(98) Kasparkova, J., Farrell, N., and Brabec, V. (2000) Sequence specificity, conformation, and recognition by HMG1 protein of major DNA interstrand cross-links of antitumor dinuclear platinum complexes. *J. Biol. Chem. 275*, 15789–15798.
(99) Rice, J. A., Crothers, D. M., Pinto, A. L., and Lippard, S. J. (1988) The major adduct of the antitumor drug cis-diamminedichloroplatinum(II) with DNA bends the duplex by approximately equal to 40 degrees toward the major groove. *Proc. Natl. Acad. Sci. U.S.A. 85*, 4158–4161.
(100) Malinge, J.-M., Pérez, C., and Leng, M. (1994) Base sequence-independent distortions induced by interstrand cross-links in cis-diamminedichloroplatinum(ll)-modified DNA. *Nucleic Acids Res. 22*, 3834–3839.
(101) Kasparkova, J., Vojtiskova, M., and Natile, G. (2008) Unique Properties of DNA Interstrand Cross-Links of Antitumor Oxaliplatin and the Effect of Chirality of the Carrier Ligand. *Chem. Eur. J. 14*, 1330–1341.
(102) Suchánková, T., Kubíček, K., Kasparkova, J., Brabec, V., and Kozelka, J. (2012) Platinum-DNA interstrand crosslinks: molecular determinants of bending and unwinding of the double helix. *J. Inorg. Biochem. 108*, 69–79.
(103) Kasparkova, J., Zehnulova, J., Farrell, N., and Brabec, V. (2002) DNA interstrand cross-links of the novel antitumor trinuclear platinum complex BBR3464. Conformation, recognition by high mobility group domain proteins, and nucleotide excision repair. *J. Biol. Chem. 277*, 48076–48086.
(104) Pieper, R. O., and Erickson, L. C. (1990) DNA adenine adducts induced by nitrogen mustards and their role in transcription termination in vitro. *Carcinogenesis 11*, 1739–1746.
(105) Wang, P., Bauer, G. B., Bennett, R. A. O., and Povirk, L. F. (1991) Thermolabile adenine adducts and A・T base pair substitutions induced by nitrogen mustard analogs in an SV40-based shuttle plasmid. *Biochemistry 30*, 11515–11521.
(106) Wang, P., Bauer, G. B., Kellogg, G. E., Abraham, D. J., and Povirk, L. F. (1994) Effect of distamycin on chlorambucil-induced mutagenesis in pZ189: evidence of a role for minor groove alkylation at adenine N-3. *Mutagenesis 9*, 133–139.
(107) Qu, Y., Moniodis, J. J., Harris, A. L., Yang, X., Hegmans, A., Povirk, L. F., Berners-Price, S. J., and Kelland, L. R. (2011) Non-Covalent Polynuclear Platinum Compounds as

Polyamine Analogs, in *Polyamine Drug Discovery*, pp 191–204. Royal Society of Chemistry, Cambridge.
(108) Goidin, D., and Thureau, C. (2002) Lab-on-chip technology. *Spectra Anal. 31*, 32–34.
(109) Lykidis, D., Van Noorden, S., Armstrong, A., Spencer-Dene, B., Li, J., Zhuang, Z., and Stamp, G. W. H. (2007) Novel zinc-based fixative for high quality DNA, RNA and protein analysis. *Nucleic Acids Res. 35*, e85.
(110) Brena, R. M., Auer, H., Kornacker, K., Hackanson, B., Raval, A., Byrd, J. C., and Plass, C. (2006) Accurate quantification of DNA methylation using combined bisulfite restriction analysis coupled with the Agilent 2100 Bioanalyzer platform. *Nucleic Acids Res. 34*, e17.
(111) Brisco, M. J., and Morley, A. A. (2012) Quantification of RNA integrity and its use for measurement of transcript number. *Nucleic Acids Res. 40*, e144.
(112) Prisecaru, A., Devereux, M., Barron, N., McCann, M., Colleran, J., Casey, A., McKee, V., and Kellett, A. (2012) Potent oxidative DNA cleavage by the di-copper cytotoxin: $[Cu2(\mu\text{-terephthalate})(1,10\text{-phen})_4]^2$. *Chem. Commun. 48*, 6906–6908.
(113) (2013) Regulating bioactivity of Cu^{2+} bis-1,10-phenanthroline artificial metallonucleases with sterically functionalized pendant carboxylates. *J. Med. Chem. 56*, 8599–8615.
(114) Tarnowski, B. I., Spinale, F. G., and Nicholson, J. H. (2009) DAPI as a Useful Stain for Nuclear Quantitation. *Biotech. Histochem. 66*, 296–302.
(115) Trantakis, I. A., Fakis, M., Tragoulias, S. S., Christopoulos, T. K., Persephonis, P., Giannetas, V., and Ioannou, P. (2010) Ultrafast fluorescence dynamics of Sybr Green I/DNA complexes. *Chem. Phys. Lett. 485*, 187–190.
(116) Krishan, A. (1975) Rapid flow cytofluorometric analysis of mammalian cell cycle by propidium iodide staining. *J. Cell Biol. 66*, 188–193.
(117) Olmsted, J., and Kearns, D. R. (1977) Mechanism of ethidium bromide fluorescence enhancement on binding to nucleic acids. *Biochemistry 16*, 3647–3654.
(118) Downs, T. R., and Wilfinger, W. W. (1983) Fluorometric quantification of DNA in cells and tissue. *Anal. Biochem. 131*, 538–547.
(119) Morgan, A. R., Lee, J. S., Pulleyblank, D. E., Murray, N. L., and Evans, D. H. (1979) Ethidium fluorescence assays. Part 1. Physicochemical studies. *Nucleic Acids Res. 7*, 547–565.
(120) McCann, M., McGinley, J., Ni, K., O'Connor, M., Kavanagh, K., McKee, V., Colleran, J., Devereux, M., Gathergood, N., Barron, N., Prisecaru, A., and Kellett, A. (2013) A new phenanthroline-oxazine ligand: synthesis, coordination chemistry and atypical DNA binding interaction. *Chem. Commun. 49*, 2341–2343.
(121) Breslauer, K. J., Frank, R., Blöcker, H., and Marky, L. A. (1986) Predicting DNA duplex stability from the base sequence. *Proc. Natl. Acad. Sci. U.S.A. 83*, 3746–3750.
(122) Marmur, J., and Doty, P. (1961) Thermal renaturation of deoxyribonucleic acids. *J. Mol. Biol. 3*, 585–594.
(123) Melchior, W. B., and Hippel, Von, P. H. (1973) Alteration of the relative stability of dA-dT and dG-dC base pairs in DNA. *Proc. Natl. Acad. Sci. U.S.A. 70*, 298–302.

(124) Bishop, G. R., and Chaires, J. B. (2002) Characterization of DNA Structures by Circular Dichroism, in *Current Protocols in Nucleic Acid Chemistry*, 7.11 pp 1-8. John Wiley & Sons, Inc.
(125) Garbett, N. C., Ragazzon, P. A., and Chaires, J. B. (2007) Circular dichroism to determine binding mode and affinity of ligand-DNA interactions. *Nat. Protoc. 2*, 3166–3172.
(126) Chang, Y.-M., Chen, C. K. M., and Hou, M.-H. (2012) Conformational Changes in DNA upon Ligand Binding Monitored by Circular Dichroism. *Int. J. Mol. Sci. 13*, 3394–3413.
(127) Wu, P. K., Qu, Y., Van Houten, B. and Farrell, N. (1994) Chemical reactivity and DNA sequence specificity of formally monofunctional and bifunctional bis(platinum) complexes. *J. Inorg. Biochem. 54*, 207–220.
(128) McGregor, T. D., Balcarová, Z., Qu, Y., Tran, M.-C., Zaludová, R., Brabec, V., and Farrell, N. (1999) Sequence-dependent conformational changes in DNA induced by polynuclear platinum complexes. *J. Inorg. Biochem. 77*, 43–46.
(129) Kypr, J., Kejnovská, I., Renčiuk, D., and Vorlíčková, M. (2009) Circular dichroism and conformational polymorphism of DNA. *Nucleic Acids Res. 37*, 1713–1725.
(130) Nordén, B., and Kurucsev, T. (1994) Analysing DNA complexes by circular and linear dichroism. *J. Mol. Recognit. 7*, 141–156.
(131) Bailly, C., Hénichart, J. P., Colson, P., and Houssier, C. (1992) Drug—DNA sequence-dependent interactions analysed by electric linear dichroism. *J. Mol. Recognit. 5*, 155–171.
(132) Beckman, K. B., and Ames, B. N. (1997) Oxidative decay of DNA. *J. Biol. Chem. 272*, 19633–19636.
(133) Nikitaki, Z., Hellweg, C. E., Georgakilas, A. G., and Ravanat, J.-L. (2015) Stress-induced DNA damage biomarkers: applications and limitations. *Front. Chem. 3*, 1–15.
(134) Cadet, J., Douki, T., and Ravanat, J.-L. (2010) Oxidatively generated base damage to cellular DNA. *Free Radic. Biol. Med. 49*, 9–21.
(135) Urathamakul, T., Waller, D. J., Beck, J. L., Aldrich-Wright, J. R., and Ralph, S. F. (2008) Comparison of Mass Spectrometry and Other Techniques for Probing Interactions Between Metal Complexes and DNA. *Inorg. Chem. 47*, 6621–6632.
(136) Beck, J. L., Colgrave, M. L., Ralph, S. F., and Sheil, M. M. (2001) Electrospray ionization mass spectrometry of oligonucleotide complexes with drugs, metals, and proteins. *Mass Spectrom. Rev. 20*, 61–87.
(137) Kloster, M. B. G., Hannis, J. C., Muddiman, D. C., and Farrell, N. (1999) Consequences of Nucleic Acid Conformation on the Binding of a Trinuclear Platinum Drug. *Biochemistry 38*, 14731–14737.
(138) McLuckey, S. A., Van Berker, G. J., and Glish, G. L. (1992) Tandem mass spectrometry of small, multiply charged oligonucleotides. *J. Am. Soc. Mass Spectrom. 3*, 60–70.
(139) Wu, J., and McLuckey, S. A. Gas-phase fragmentation of oligonucleotide ions. *Inter. J. Mass Spectrom. 237*, 197–241.

(140) Talib, J., Green, C., Davis, K. J., Urathamakul, T., Beck, J. L., Aldrich-Wright, J. R., and Ralph, S. F. (2008) A comparison of the binding of metal complexes to duplex and quadruplex DNA. *Dalton Trans.* 1018–1026.
(141) Pierce, S. E., Kieltyka, R., Sleiman, H. F., and Brodbelt, J. S. (2009) Evaluation of binding selectivities and affinities of platinum-based quadruplex interactive complexes by electrospray ionization mass spectrometry. *Biopolymers 91*, 233–243.
(142) Berners-Price, S. J., Ronconi, L., and Sadler, P. J. (2006) Insights into the mechanism of action of platinum anticancer drugs from multinuclear NMR spectroscopy. *Prog. Nucl. Magn. Reson. Spectrosc. 49*, 65–98.
(143) Vinje, J., and Sletten, E. (2007) NMR Spectroscopy of Anticancer Platinum Drugs. *Anti-Cancer Agents Med. Chem. 7*, 35–54.
(144) Qu, Y., Scarsdale, N. J., Tran, M.-C., and Kelland, L. R. (2003) Cooperative effects in long-range 1,4 DNA-DNA interstrand cross-links formed by polynuclear platinum complexes: an unexpected syn orientation of adenine bases outside the binding sites. *J. Biol. Inorg. Chem. 8*, 19–28.
(145) Qu, Y., Scarsdale, N. J., Tran, M.-C., and Farrell, N. (2004) Comparison of structural effects in 1,4 DNA–DNA interstrand cross-links formed by dinuclear and trinuclear platinum complexes. *J. Inorg. Biochem. 98*, 1585–1590.
(146) Qu, Y., Tran, M.-C., and Kelland, L. R. (2009) Structural consequences of a 3′ → 3′ DNA interstrand cross-link by a trinuclear platinum complex: unique formation of two such cross-links in a 10-mer duplex. *J. Biol. Inorg. Chem. 14*, 969–977.
(147) Qu, Y., Kipping, R. G., and Farrell, N. P. (2015) Solution studies on DNA interactions of substitution-inert platinum complexes mediated via the phosphate clamp. *Dalton Trans. 44*, 3563–3572.
(148) Ruhayel, R. A., Moniodis, J. J., Yang, X., Kasparkova, J., Brabec, V., Berners-Price, S. J., and Kelland, L. R. (2009) Factors affecting DNA-DNA interstrand cross-links in the antiparallel 3'-3' sense: a comparison with the 5′-5′ directional isomer. *Chem. Eur. J 15*, 9365–9374.
(149) Davies, M. S., Thomas, D. S., Hegmans, A., Berners-Price, S. J., and Farrell, N. (2002) Kinetic and Equilibria Studies of the Aquation of the Trinuclear Platinum Phase II Anticancer Agent $[\{trans\text{-}PtCl(NH_3)_2\}_2\{\mu\text{-}trans\text{-}Pt(NH_3)_2(NH_2(CH_2)_6NH_2)_2\}]^{4+}$ (BBR3464). *Inorg. Chem. 41*, 1101–1109.
(150) Hegmans, A., Berners-Price, S. J., Davies, M. S., Thomas, D. S., Humphreys, A. S., and Farrell, N. (2004) Long Range 1,4 and 1,6-Interstrand Cross-Links Formed by a Trinuclear Platinum Complex. Minor Groove Preassociation Affects Kinetics and Mechanism of Cross-Link Formation as Well as Adduct Structure. *J. Am. Chem. Soc. 126*, 2166–2180.
(151) Davies, M. S., Berners-Price, S. J., Cox, J. W., and Farrell, N. (2003) The nature of the DNA template (single- versus double-stranded) affects the rate of aquation of a dinuclear Pt anticancer drug. *Chem. Commun.* 122–123.
(152) Ourliac-Garnier, I., Elizondo-Riojas, M.-A., Redon, S., Kelland, L. R., and Bombard, S. (2005) Cross-links of quadruplex structures from human telomeric DNA by dinuclear platinum complexes show the flexibility of both structures. *Biochemistry 44*, 10620–10634.

(153) Bass, D. A., Parce, J. W., Dechatelet, L. R., Szejda, P., Seeds, M. C., and Thomas, M. (1983) Flow cytometric studies of oxidative product formation by neutrophils: a graded response to membrane stimulation. *J. Immunol 130*, 1910–1917.
(154) Kellett, A., O'Connor, M., McCann, M., Howe, O., Casey, A., McCarron, P., Kavanagh, K., McNamara, M., Kennedy, S., May, D. D., Skell, P. S., O'Shea, D., and Devereux, M. (2011) Water-soluble bis(1,10-phenanthroline) octanedioate Cu^{2+} and Mn^{2+} complexes with unprecedented nano and picomolar *in vitro* cytotoxicity: promising leads for chemotherapeutic drug development. *Med. Chem. Commun. 2*, 579–584.
(155) Goldstein, S., and Czapski, G. (1984) Mannitol as an $OH^{\bullet}$ scavenger in aqueous solutions and in biological systems. *Int. J. Radiat. Biol. 46*, 725–729.
(156) Giandomenico, A. R., Cerniglia, G. E., Biaglow, J. E., Stevens, C. W., and Koch, C. J. (1997) The importance of sodium pyruvate in assessing damage produced by hydrogen peroxide. *Free Radic. Biol. Med. 23*, 426–434.
(157) Peterson, E. J., Menon, V. R., Gatti, L., Kipping, R., Dewasinghe, D., Perego, P., Povirk, L. F., and Kelland, L. R. (2015) Nucleolar Targeting by Platinum: p53-Independent Apoptosis Follows rRNA Inhibition, Cell-Cycle Arrest, and DNA Compaction. *Mol. Pharmaceutics 12*, 287–297.
(158) Bonner, W. M., Redon, C. E., Dickey, J. S., Nakamura, A. J., Sedelnikova, O. A., Solier, S., and Pommier, Y. (2008) γH2AX and cancer. *Nat. Rev. Cancer 8*, 957–967.
(159) Paull, T. T., Rogakou, E. P., Yamazaki, V., Kirchgessner, C. U., Gellert, M., and Bonner, W. M. (2000) A critical role for histone H2AX in recruitment of repair factors to nuclear foci after DNA damage. *Curr. Biol. 10*, 886–895.
(160) Rogakou, E. P., Pilch, D. R., Orr, A. H., Ivanova, V. S., and Bonner, W. M. (1998) DNA Double-stranded Breaks Induce Histone H2AX Phosphorylation on Serine 139. *J. Biol. Chem. 273*, 5858–5868.
(161) Olive, P. L., and Banáth, J. P. (2006) The comet assay: a method to measure DNA damage in individual cells. *Nat. Protoc. 1*, 23–29.
(162) Collins, A. R., Oscoz, A. A., Brunborg, G., Gaivão, I., Giovannelli, L., Kruszewski, M., Smith, C. C., and Stetina, R. (2008) The comet assay: topical issues. *Mutagenesis 23*, 143–151.
(163) Menon, V. R., Peterson, E. J., Valerie, K., Kelland, L. R., and Povirk, L. F. (2013) Ligand modulation of a dinuclear platinum compound leads to mechanistic differences in cell cycle progression and arrest. *Biochem. Pharmacol. 86*, 1708–1720.
(164) Aris, S. M., Gewirtz, D. A., Ryan, J. J., Knott, K. M., and Kelland, L. R. (2007) Promotion of DNA strand breaks, interstrand cross-links and apoptotic cell death in A2780 human ovarian cancer cells by transplatinum planar amine complexes. *Biochem. Pharmacol. 73*, 1749–1757.
(165) Barry, N. P. E., and Sadler, P. J. (2013) Exploration of the medical periodic table: towards new targets. *Chem. Commun. 49*, 5106–5131.
(166) Berners-Price, S. J., and Filipovska, A. (2011) Gold compounds as therapeutic agents for human diseases. *Metallomics 3*, 863–873.

CHAPTER II.

Copper Phenanthrene Oxidative Chemical Nucleases

This paper was published in *Inorganic Chemistry*, 2014, 53, 5392-5404.

Zara Molphy, Andreea Prisecaru, Creina Slator, Niall Barron, Malachy McCann, John Colleran, Deepak Chandran, Nicholas Gathergood, and Andrew Kellett.

My contribution to this paper was to synthesise and characterise the series of copper(II) phenanthrene complexes. I then proceeded to investigate the DNA-binding affinity of the complexes to DNA of varying GC content using a number of high-throughput assays and also to investigate the oxidative profile of the complexes using gel electrophoresis and on-chip analysis-in collaboration with Dr. Andreea Prisecaru. During this project, I also established a protocol for thermal melting and investigated the SOD mimetic properties of the complex series.

II. 1. Abstract

Here we report the synthesis and isolation of a series of bis-chelate Cu^{2+} phenanthroline−phenazine cationic complexes of $[Cu(DPQ)(Phen)]^{2+}$, $[Cu(DPPZ)(Phen)]^{2+}$, and $[Cu(DPPN)(Phen)]^{2+}$ (where Phen = 1,10-phenanthroline, DPQ = dipyridoquinoxaline, DPPZ = dipyridophenazine, and DPPN = benzo[i]dipyridophenazine). These compounds have enhanced DNA recognition relative to the well-studied chemical nuclease, $[Cu(Phen)_2]^{2+}$ (bis-Phen), with calf thymus DNA binding constants of DPQ and DPPZ agents ($\sim 10^7$ $M(bp)^{-1}$) being the highest currently known for Cu^{2+} phenanthrene compounds. Complex DNA binding follows DPQ ≈ DPPZ > DPPN > bis-Phen, with fluorescence quenching and thermal melting experiments on poly[d(A-T)$_2$] and poly[d(G-C)$_2$] supporting intercalation at both the minor and major groove. Phenazine complexes, however, show enhanced targeting and oxidative cleavage on cytosine-phosphate-guanine-rich DNA and have comparable in vitro cytotoxicity toward the cisplatin-resistant ovarian cancer line, SKOV3, as the clinical oxidative DNA-damaging drug doxorubicin (Adriamycin). In this study we also describe how a novel "on-chip" method devised for the Bioanalyser 2100 was employed to quantify double- stranded DNA damage, with high precision, by the complex series on pUC19 DNA (49% A-T, 51% G-C). Both DPQ and bis-phen complexes are highly efficient oxidizers of pUC19, with DPQ being the most active of the overall series. It is apparent, therefore, that oxidative chemical nuclease activity on homogeneous canonical DNA is not entirely dependent on dynamic nucleotide binding affinity or intercalation, and this observation is corroborated through catalytic interactions with the superoxide anion radical and Fenton breakdown of hydrogen peroxide.

II. 2. Introduction

The advent of coordinating phenanthrene-based intercalators to transition-metal cations has unveiled a new frontier for DNA-targeted metallodrug development.[1] While the application of cis-diamminedichloroplatinum(II) (cisplatin) continues to be a cornerstone of modern cancer chemotherapy,[2] the functionalization of this agent with intercalating ligands[3] and the construction of nonplatinum metallo-intercalators with bis- and tris-phenanthrene chelated symmetry[4] has revealed unique but structurally interrelated chemotypes of promising biological utility. Significant examples of these cationic agents (see **Scheme II-1**) include cis-$[Pt(NH_3)_2(phenanthridine)Cl]^+$ (phenanthriplatin),[5] which

exhibits a unique spectrum of activity within the National Cancer Institute 60-cell tumoral panel and enhanced cellular uptake relative to cisplatin; Δ-[Ru(DPPZ)-$(Phen)_2]^{2+}$, which has excellent DNA recognition properties and is widely known as a "light switch" complex due to photoluminescent enhancement upon nucleotide binding;[6] and $[Cu(Phen)_2]^{2+}$, which is an effective chemical nuclease that induces DNA degradation through free-radical oxidation of deoxyribose.[7–9] Thus, by varying both the metal center and coordinated phenanthrene base, unique interactions on DNA and within human-derived cancer cells can be achieved. The chemical nuclease $[Cu(Phen)_2]^{2+}$ is capable of abstracting hydrogen ($^{\bullet}H$) from the pentose ring of DNA in the presence of both exogenous reductant ($Cu^{2+} \rightarrow Cu^{+}$) and oxidant ($O_2$ or H_2O_2), under a quasi-reversible electrochemical process,[7,8] and has served as an important template for cytotoxic metallodrug design.[10] The mechanism of abstraction is sequential and is dependent on both Cu^{+} and hydrogen peroxide (H_2O_2).[11] Furthermore, the production of H_2O_2 in the reaction is believed to result from superoxide dismutase (SOD) mimetic activity,[12] post electron-transfer from Cu^{+} to O_2. $[Cu(Phen)_2]^{2+}$ oxidizes DNA without specificity, predominately at the minor groove, and in an effort to improve this lack of specificity, chimeric $[Cu(Phen)_2]^{2+}$ molecules have been generated using target-specific, DNA-recognition vectors of single-stranded DNA[13,14] and also with the adenine−thymine (A-T) specific minor-groove binder distamycin.[15,16]

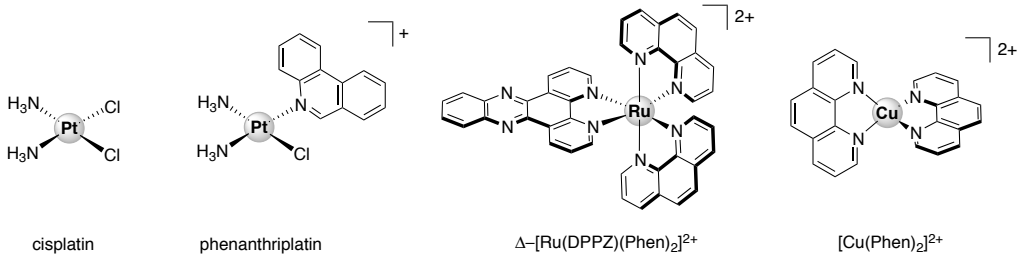

Scheme II-1. Molecular Structures of Cytotoxic Platinum(II) Complexes Cisplatin and Phenanthriplatin, the Ruthenium(II) DNA Light Switch Complex, Δ-$[Ru(DPPZ)(Phen)_2]^{2+}$, and the Copper(II) Chemical Nuclease, $[Cu(Phen)_2]^{2+}$.

In this study we report the synthesis and isolation of a series of bis-chelate Cu^{2+} phenanthroline−phenazine cationic complexes of $[Cu(DPQ)(Phen)]^{2+}$, $[Cu(DPPZ)(Phen)]^{2+}$, and $[Cu(DPPN)(Phen)]^{2+}$ (where DPQ = dipyrido[3,2-f:2′,3′-h]quinoxaline, DPPZ = dipyrido[3,2-a:2′,3′-c]phenazine, and DPPN = benzo[i]dipyrido[3,2-a:2′,3′-c]phenazine) (Scheme II-2). Since designer metal-chelating phenazine ligands have shown interesting potential within Ru^{2+} DNA-selective binding probes,[17−20] a question remains unanswered regarding their application within Cu^{2+} complexes toward (i) nucleotide equilibrium binding affinity, base-specific targeting and intercalation, (ii) oxidative chemical nuclease activity, (iii) redox behavior including interactions with superoxide and hydrogen peroxide, and (iv) cytotoxicity toward platinum- resistant human-derived cancer cells. Our aim here was to investigate how systematic extension of the ligated phenazine ligand influences DNA recognition and oxidative degradation, and how this study can ultimately supply basic information toward the design of enhanced artificial chemical nucleases of biological utility. To identify and compare the DNA degradation profiles in this family of structurally related compounds, we proposed the development of a capillary electrophoresis microfluidic chip assay for the Bioanalyzer 2100 (Agilent Technologies), which is capable of high-resolution sizing and quantitation of dsDNA (ds = double-stranded) fragments based on normalization to internal markers and a standard DNA ladder.[21−23]

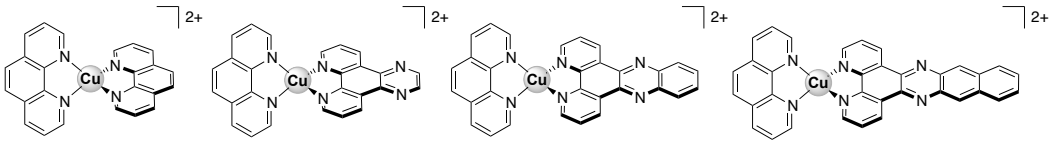

Scheme II-2. Molecular Structures of the Cu^{2+} Coordination Complexes 1-4.

II. 3. Results

II. 3.1. Preparation of the Complexes

The quinoxaline and phenazine ligands (DPQ, DPPZ, and DPPN) were generated through Schiff-base condensation reactions of 1,10-phenanthroline-5,6-dione with either ethylenediamine, o-phenylenediamine, or 2,3-diaminonaphthalene, with some modification to previously reported methods.[24−26] The bis-phenanthroline complex $[Cu(Phen)_2](NO_3)_2$ (Cu-Phen, **1**) was prepared by aqueous−ethanol reflux of 1,10-phenathroline with copper(II) nitrate (2:1).[27] The complexes $[Cu(DPQ)(Phen)](NO_3)_2$ (Cu-DPQ-Phen, **2**),

[Cu(DPPZ)(Phen)]$(NO_3)_2$ (Cu-DPPZ-Phen, **3**), and [Cu(DPPN)(Phen)]$(NO_3)_2$ (Cu-DPPN-Phen, **4**) (**Scheme II-2**) were generated by first isolating the mono- phenanthroline complex [Cu(Phen)]$(NO_3)_2$ and subsequently treating this with 1 equiv of the corresponding phenazine ligand.

II. 3.2. Binding Affinity to Calf Thymus and Salmon Testes DNA

The DNA binding affinity of the complex series was determined using calf-thymus DNA (ctDNA, Ultra-Pure, Invitrogen) and salmon testes dsDNA (Sigma) by ethidium bromide and Hoechst 33258 fluorescence quenching and competition studies[28] and also through viscosity analysis (**Figure II-1** and **Table II-1**). The presence of phenazine ligands in the complex cation function to significantly enhance ctDNA binding affinity with K_{app} (apparent DNA binding constant) values for Cu-DPQ-Phen and Cu-DPPZ-Phen reagents being at the order of ~3×10^7 $M(bp)^{-1}$ and of similar magnitude as the intercalating polypeptide antibiotic, Actinomycin D. The DPPN-containing complex, although binding by an order of magnitude over Cu-Phen, was the lowest ctDNA-binding phenazine complex, at ~6×10^6 $M(bp)^{-1}$. Fluorescence quenching (Q) of limited bound Hoechst 33258 (minor-groove binder) and ethidium bromide (intercalator) bound ctDNA were examined to identify potential binding specificity. Unlike the classical intercalator Actinomycin D and minor-groove binding agent netropsin, the complex series did not display a large degree of discrimination for quenching either of the selected fluorophores. The quenching effects of the DPQ and DPPZ complexes are stronger, overall, than Cu-Phen; however, this trend is reversed as the phenazine agents displace bound Hoechst with slightly more efficiency than ethidium bromide compared with Cu-Phen. Viscosity analysis on salmon testes dsDNA fibers revealed Cu-DPQ-Phen as having a significant intercalating (hydrodynamic) binding effect, followed thereafter by Cu-DPPZ-Phen, Cu-Phen, and finally Cu-DPPN-Phen. In nearly all experiments conducted, the Cu^{2+} complexes exhibited distinctive behavior compared to the simple $[Co(NH_3)_6]^{3+}$ complex, which is known only to have electrostatic binding affinity to the surface of DNA. Indeed this effect was confirmed by our analysis of its inability to displace intercalated ethidium, enhanced ability to displace minor-groove, surface-bound Hoechst 33258, and an overall decrease in relative viscosity.

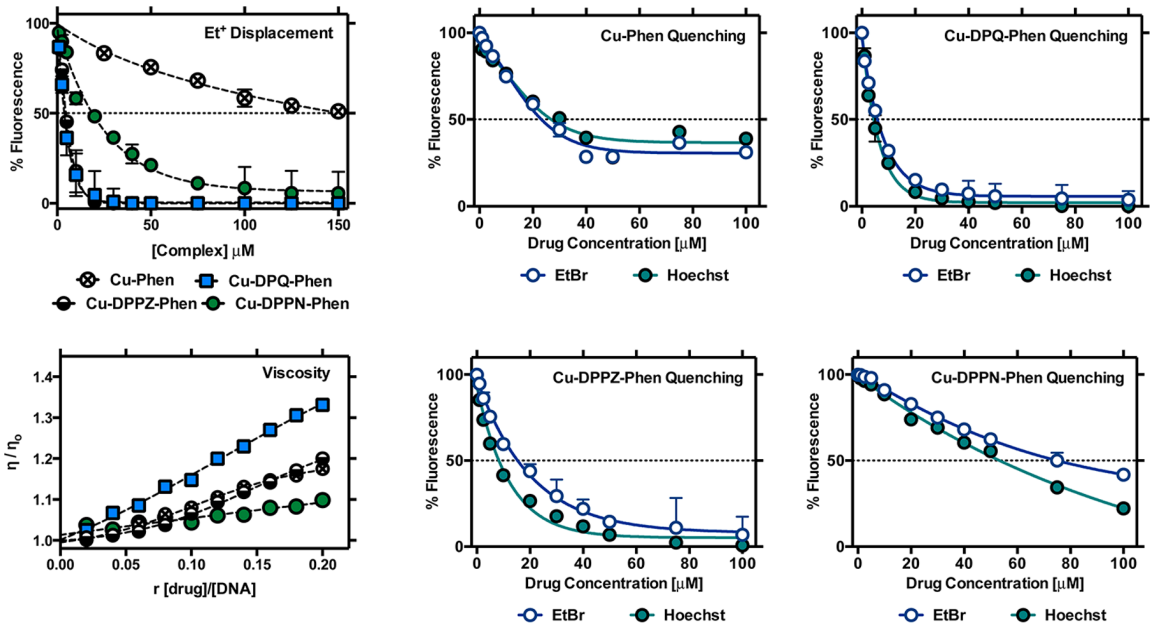

Figure II-1. Binding of Cu^{2+} complexes 1−4 to ethidium-saturated solutions of dsDNA (ctDNA), fluorescence quenching of limited ethidium bromide or Hoechst 33258 bound dsDNA (ctDNA) upon titration of complex, and viscosity properties of complex treated salmon testes dsDNA. (Data points presented as an average of triplicate fluorescence measurement ± standard deviation (S.D.))

Table II-1. DNA binding properties

Compound	C_{50}[a]	K_{app} M(bp)$^{-1}$ [b]	Q Hoechst[c]	Q Ethidium[c]	η / η_o[d]
Netropsin	46.27	2.50 x 10^6	02.40	20.04	1.00
Actinomycin D	04.10	2.92 x 10^7	26.34	04.78	1.14
$[Co(NH_3)_6]Cl_3$	>300	N/A	23.18	273.62	0.82
Cu-Phen[27]	179.21	6.67 x 10^5	34.96	20.38	1.17
Cu-DPQ-Phen	03.93	3.04 x 10^7	04.33	06.10	1.33
Cu-DPPZ-Phen	04.63	2.58 x 10^7	07.69	16.12	1.20
Cu-DPPN-Phen	18.72	6.40 x 10^6	56.57	75.10	1.10

[a] C_{50} = concentration required to reduce fluorescence by 50% [b] $K_{app} = K_e$ x 12.6/C_{50} where K_e = 9.5 x 10^6 M(bp)$^{-1}$ [c] reduction of 50% initial fluorescence from DNA-bound dye by tested compound (μM) [d] relative viscosity value at r = 0.20.

II. 3.3. Binding Affinity to Double-Stranded Synthetic Co-polymers of Adenine−Thymine (A-T) and Guanine− Cytosine (G-C)

To explore base-specific nucleotide binding by this series, synthetic alternating copolymers of adenine−thymine, poly[d(A-T)$_2$], and guanine−cytosine, poly[d(G-C)$_2$], were examined through fluorescence quenching and thermal melting analysis. Fluorescence quenching was conducted by first introducing a limited concentration (5 μM) of ethidium bromide with synthetic polynucleotide (25 μM). The complex series, along with the classical intercalator Actinomycin D and minor-groove binder netropsin, was also examined across the concentration range of 1−200 μM (**Figure II-2** and **Table II-2**). The standard agents, as predicted, were highly specific in their quenching of either poly[d(A-T)$_2$] (netropsin) or poly[d(G-C)$_2$] (Actinomycin D). A-T-rich polymers are known to have "T-tract structure", which features a compressed minor groove and a shorter helical repeat of 10 bp per turn, compared to 10.5 bp per turn determined for canonical B- DNA. As such, these polymers are excellent substrates for minor-groove binding drugs, and this interaction was evident in these experiments with netropsin. G-C-rich polymers, conversely, can have up to 12 bp per helical turn and are known to form left-handed "Z-DNA" conformations with a helical rise per base pair dimer of ~7.4 Å. These polymers, therefore, are highly suited for intercalative binding by agents such as Actinomycin D. It was also evident that both netropsin and Actinomycin D were selective in their binding interactions and thus did not quench fluorescence (up to 200 μM) on disfavored DNA polymers of poly[d(G-C)$_2$] and poly[d(A-T)$_2$], respectively. The Cu^{2+} complexes displayed effective quenching on both A-T and G-C polymers and so could not be characterized by either classical binding mode alone. Each complex was found to have a slight preference for ethidium quenching on poly[d(G-C)$_2$], with Cu-DPQ-Phen displaying the highest overall activity in the series, followed thereafter by Cu-DPPZ-Phen, Cu-Phen, and finally Cu-DPPN-Phen.

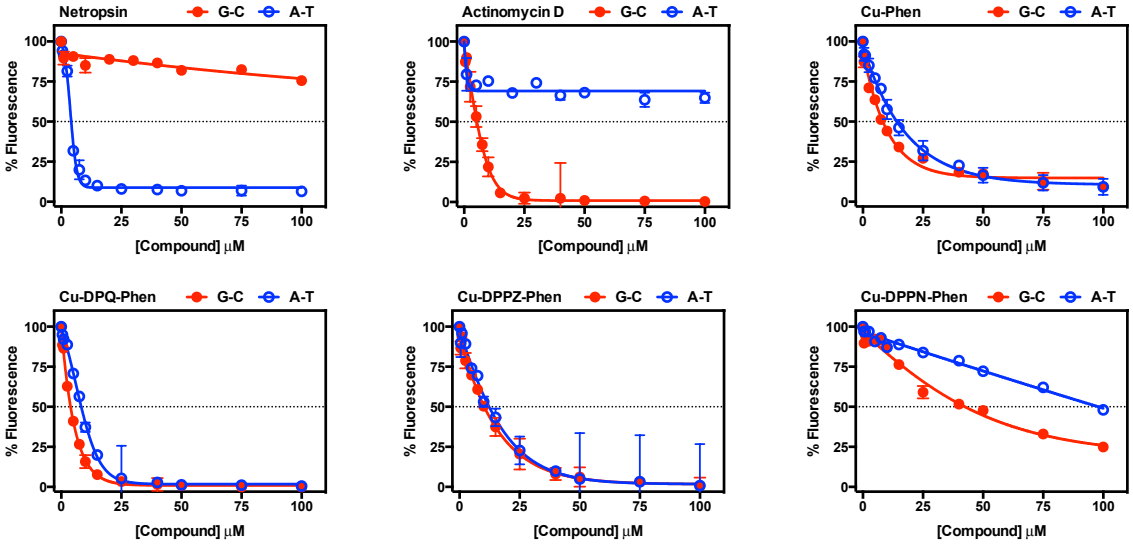

Figure II-2. Fluorescence quenching of limited bound intercalator (ethidium bromide) to poly[d(G-C)$_2$] and poly[d(A-T)$_2$] upon titration of netropsin, actinomycin D and Cu^{2+} complexes. (data points presented as an average of duplicate fluorescence measurement, ± S.D.).

Table II-2. Fluorescence quenching *(Q)* of limited ethidium bromide (5 µM) bound poly[d(G-C)$_2$] and poly[d(A-T)$_2$] (25 µM) by standard agents netropsin, actinomycin D and Cu^{2+} complexes.

Compound	***Q* (µM) poly[d(A-T)$_2$]**	***Q* (µM) poly[d(G-C)$_2$]**
Netropsin	4.08	>>200
Actinomycin D	>>200	5.47
Cu-Phen	13.34	7.96
Cu-DPQ-Phen	8.34	3.97
Cu-DPPZ-Phen	11.60	10.12
Cu-DPPN-Phen	96.56	44.18

Table II-3. Influence of Standard Agents (Netropsin, Actinomycin D) and Copper Phenazine Complexes on the Thermal Denaturation of Poly[d(G-C)$_2$] and Poly[d(A-T)$_2$] Alternating Copolymers.

Compound	**ΔT_M (°C) poly[d(A-T)$_2$]**	**ΔT_M (°C) poly[d(G-C)$_2$]**
Netropsin	12.32 ± 0.79	2.83 ± 0.38
Actinomycin D	-0.32 ± 0.29	12.10 ± 0.95
Cu-Phen	-0.02 ± 0.29	6.64 ± 1.58
Cu-DPQ-Phen	0.60 ± 0.18	11.39 ± 1.10
Cu-DPPZ-Phen	0.50 ± 0.10	10.44 ± 1.10
Cu-DPPN-Phen	-0.39 ± 0.21	2.10 ± 1.03

ΔT_M = difference in thermal melting (T_M) of drug treated nucleotide at $r = 0.1$ compared with drug untreated nucleotide.

Thermal melting studies were also conducted on poly[d(G-C)$_2$] and poly[d(A-T)$_2$] synthetic nucleotides exposed to the complex series, netropsin, and Actinomycin D (**Table II-3**) (Appendix A-2) Thermal melting (T_M) marks the midpoint in the melting process of DNA when a 50:50 equilibrium exists between the helical and single-stranded state. This method of analysis offers a useful insight into the strength of interaction between a drug and nucleic acid; the stronger this interaction, the more energy required to denature the stabilized secondary structure relative to the untreated polynucleotide (ΔT_M). As expected, Actinomycin D substantially stabilized the thermal denaturation of poly[d(G-C)$_2$] (ΔT_M + 12.10 ± 0.95°C). Similarly, the minor- groove binding drug netropsin gave an almost equal magnitude of stabilization on the thermal melting of poly[d(A-T)$_2$] (ΔT_M + 12.32 ± 0.79°C). Further, these classical agents had either low or no stabilization effects on disfavored nucleotide polymers, again highlighting their nucleotide binding specificity. The Cu^{2+} complexes all stabilized the thermal melting temperature of poly[d(G-C)$_2$] to varying extents and more closely demonstrated thermochemical behavior in line with intercalator Actinomycin D. Cu-DPQ-Phen had the strongest stabilizing effect (ΔT_M + 11.39 ± 1.10°C) on G-C, and this was followed closely by the Cu-DPPZ-Phen complex (ΔT_M + 10.44 ± 1.10°C). To a lesser extent, Cu-Phen also enhanced the melting temperature of G-C (ΔT_M + 6.64 ± 1.58°C), while the DPPN agent was only weakly stabilizing (ΔT_M + 2.10 ± 1.03°C). In contrast to G-C polynucleotides, all complexes had negligible or negative effects on the thermal stabilization of poly[d(A-T)$_2$], thus reflecting similarity with Actinomycin D in this regard.

II. 3.4 Chemical Nuclease Activity

The oxidative chemical nuclease activity of the complex series was identified using a novel "on-chip" method devised for the Agilent 2100 Bioanalyzer, which is outlined in **Figure II-3**. The DNA 7500 "On-Chip" protocol for examining artificial metallonuclease activity using the Bioanalyzer 2100. microfluidic chip was employed as it can detect and quantify linear dsDNA fragments sized between 100 and 7500 bp by capillary electrophoresis. Superhelical plasmid DNA (pUC19, 2686 bp) was generated by Escherichia coli and subsequently linearized by the type II endonuclease HindIII, which has one recognition sequence on this vector. Linear pUC19 (400 ng) was then purified on an anion-exchange column (Qiagen) and incubated with 500 nM of complex, under standard atmospheric conditions, in the presence of 1 mM reductant (sodium L-ascorbate). At successive time periods, between 1 and 30 min, aliquots were removed from each reaction and quenched

with 100 μM of both 2,9-dimethyl-1,10-phenanthroline (neocuproine) and ethylenediaminetetraacetic acid (EDTA). Complex-treated and untreated linear DNA samples (1 μL) were then loaded onto the Agilent DNA 7500 microfluidic chip. Further, sample wells were also loaded with standard DNA markers sized at 50 and 10,380 bp, which are evident in each electrogram. Untreated pUC19 produced a single high-resolution peak located at ~2870 bp (**Figure II-4A**, time = 0), which was within the experimental error margin for nucleotide sizing accuracy (±10% coefficient of variation). Degradation of pUC19 by each complex was followed by a reduction in peak area and peak height intensity and was accompanied by asymmetric tailing, which is indicative of smaller fragments being sheared off through chemical nuclease activity. Typical electrograms generated are shown in **Figure II-4A**, which details the untreated control DNA (time = 0) and each copper complex kinetically exposed to pUC19 at specific time points indicated. Further, typical electropherograms generated by each complex are shown in **Figure II-4D**, which details the standard DNA ladder (L), untreated control pUC19 (lane 1), and complex-treated DNA between either 1−15 min (for Cu-Phen and Cu-DPQ-Phen complexes) or 1−30 min (for Cu-DPPZ-Phen and Cu-DPPN-Phen complexes) (lanes 2−12). In our preliminary experiments we discovered that bis- phen and DPQ complexes were much more efficient in degrading pUC19; hence, our analysis on the Bioanalyzer was conducted on a shorter time frame for both these agents. Quantification of pUC19 damage was achieved (**Figure II-4**, center) using peak height reduction and peak area reduction analysis from triplicate electrograms, and comparisons of cleavage efficiency were made based on the time taken to degrade 50% (D_{50}) of pUC19, with 100% being taken as the normalized intensity of triplicate-untreated pUC19 DNA. Both Cu-Phen and Cu-DPQ-Phen are remarkably efficient in degrading dsDNA and are similar, in terms of both their D_{50} values and overall profile. Analysis by pUC19 peak height reduction shows that both agents similarly reduce intensity, by 50%, after ~2 min; however, Cu-Phen has a marked enhancement over DPQ-Phen between 4.0 and 7.5 min on comparison of peak area degradation. Nonetheless, the DPQ agent totally degrades the plasmid by 7.5 min under both analyses, whereas it is ~10 min before this is achieved by Cu-Phen. The DPPZ and DPPN reagents are less efficient in their chemical nuclease activity, with Cu-DPPZ-Phen displaying rapid degradation between 5 and 12.5 min ($D_{50} \approx 7.5$ min by peak height), while Cu-DPPN-Phen delivers a somewhat linear profile over the complete time frame ($D_{50} \approx$ 12.5 min by peak height). Further evidence the DPPZ agent is a more efficient chemical

nuclease compared with Cu-DPPN-Phen can be gleaned from peak area analysis. DPPZ completely digests the plasmid by ~20 min, while at the end of our analysis (30 min) a small concentration of nucleotide remained within the DPPN- treated sample.

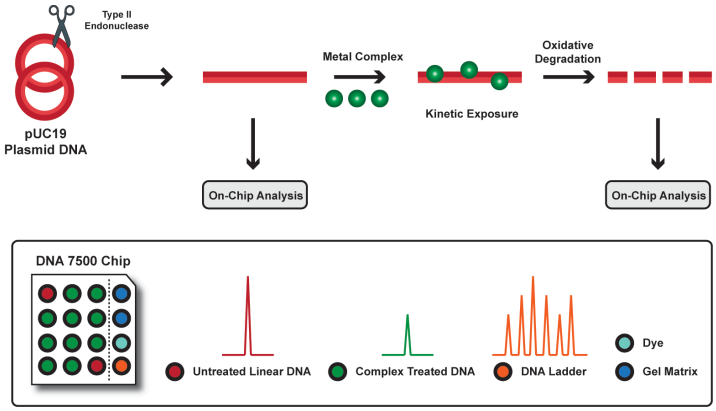

Figure II-3. 'On-Chip' protocol for examining artificial metallonuclease activity using the Bioanalyzer 2100.

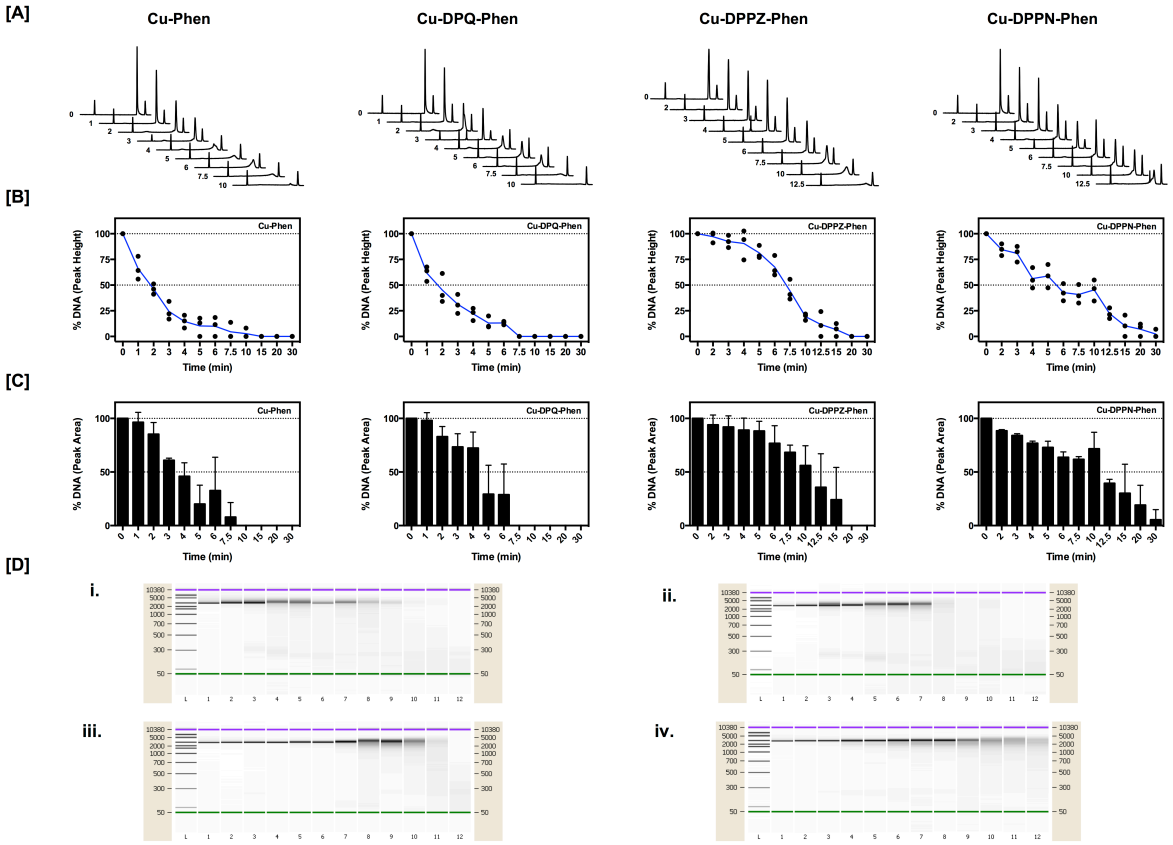

Figure II-4. (**A**) Electrograms of linearized pUC19 (400 ng) exposed to metal complex (500 nM) between 0 and 12.5 min on the Bioanalyzer 2100 with DNA 7500 microfluidic chips, (**B**) %DNA degradation (from peak height analysis of triplicate experiments) of pUC19 exposed to Cu^{2+} complexes between 0 and 30 min, (**C**) %DNA degradation (from peak area analysis of triplicate experiments, error bars ± S.D.) of pUC19 exposed to Cu^{2+} complexes between 0 and 30 min, and (**D**) typical electropherograms generated by the Bioanalyzer 2100, L = ladder, lane 1 = pUC19 control, lanes 2−12 = pUC19 + complex exposed between 1 and 15 min for bis-Phen (i) and DPQ-Phen (ii) samples, and between 1 and 30 min for DPPZ-Phen (iii) and DPPN-Phen (iv) samples.

II. 3.5. Interactions with Superhelical pUC19

The interaction of purified superhelical pUC19 (generated using E. coli as described above) with the complex series was studied under similar conditions (500 nM [complex] with 1 mM reductant) (**Figure II-5**) using standard agarose gel electrophoresis. All complexes induced complete degradation of the superhelix with the exception of Cu-DPPN-Phen, where evidence of nicked (Form I) and linear (Form II) tertiary conformations remained after 30 min. The importance of Cu^{+} and hydrogen peroxide in the cleavage mechanism was demonstrated by the complete inhibition of nuclease activity upon addition of 1000 U of bovine liver catalase (**Figure II-5B**) and 100 μM neocuproine (**Figure II-5C**). Further trapping studies revealed that bovine superoxide dismutase (1000 U, **Figure II-5D**) could strongly inhibit Cu-DPPN-Phen from plasmid digestion, and this complex, along with Cu-DPPZ-Phen, was also impeded by the hydroxyl radical scavenger dimethyl sulfoxide (DMSO) (10% v/v, **Figure II-5E**).

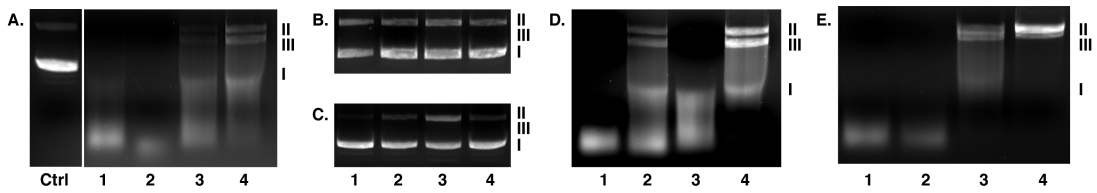

Figure II-5. Agarose gel electrophoresis of purified (EDTA free) supercoiled pUC19 (400 ng) with 1 mM Na-L-ascorbate incubated for 30 min with 500 nM of metal complexes (**A**), and in the presence of 1000 units of bovine liver catalase (**B**), 100 μM neocuproine (**C**), 1000 units of bovine SOD (**D**) and 10% v/v DMSO (**E**). Ctrl = pUC19 complex untreated control, Lanes 1-4 = 500 nM Cu-Phen, Cu-DPQ-Phen, Cu-DPPZ-Phen and Cu-DPPN-Phen, respectively.

II. 3.6. Comparison Study of pUC19 and pBC4 Cleavage Efficacy

To determine the chemical nuclease on DNA of different guanine−cytosine (G-C) compositions, commercially available pUC19 (2686 bp, 51% G-C, NEB, N3033L), and pBC4 (10673 bp, 59% G-C, donated by NEB) were analyzed using gel electrophoresis in the presence of 1 mM solution of added reductant (Na-L-ascorbate). Note that both plasmids are supplied in EDTA-buffered solution, and, thus, chemical nuclease activity was examined at higher complex concentration. Further, the pBC4 plasmid was amplified in a recA+ E. *coli* host and so does not have dimer deficiency usually associated with commercially available strains used for plasmid production. As a consequence, pBC4 migrates as two bands: the plasmid monomer followed by the dimer, and so this plasmid is not suitable to identify conversion among super- helical (Form I), nicked (Form II), or linear (Form III) conformations due to the overlapping nature of the dimer and Form II or

Form III bands. This plasmid, however, can be exploited for artificial metallonuclease activity in its linearized form, and we employed the type II endonuclease AgeIto generate Form III of the plasmid. For comparison purposes, pUC19 was also required in a linearized form, and this was completed using the type II endonuclease ScaI. Both pBC4 and pUC19 (400 ng) were then exposed, over 30 min, to between 2.5 and 10.0 μM solution of the complex series, in the presence of 1 mM exogenous ascorbate, with each reaction containing the same amount of EDTA (40.0 μM) (**Figure II-6**). The chemical nuclease activity of Cu-DPQ-Phen and Cu-DPPZ- Phen were found to be independent of %G-C content, with the DPQ complex being the most effective cleaving agent, overall, inducing complete digestion of both pUC19 and pBC4 upon 5 μM exposure. Cu-DPPN-Phen was found to have a remarkably low effect on pUC19 oxidation but was more reactive toward pBC4. In contrast to the observed activities of the phenazine reagents, Cu-Phen was selectively reactive toward the plasmid of lower %G-C content, and this was evidenced through complete disappearance of pUC19 at a 5 μM, while the majority of pBC4 remained unaffected under identical conditions. The final aspect of this study involved the characterization of nuclease activity on commercial (EDTA buffered) supercoiled pUC19 plasmid. In this experiment a fixed concentration of metal complex (10 μM) was exposed to 400 ng of superhelical DNA over 30 min in the presence of 1 mM added reductant (**Figure II-7**), and reactions all contained a final EDTA concentration of 56 μM. Surprisingly, Cu-Phen was found to only partially nick (Form I → Form II) pUC19, while Cu- DPPN-Phen had little or no oxidative affect. Cu-DPQ-Phen and Cu-DPPZ-Phen, however, facilitated complete conversion to the nicked form (Form II) of pUC19, and this observation supports the enhanced stability of these chemical nucleases within a competing, EDTA-chelated, environment.

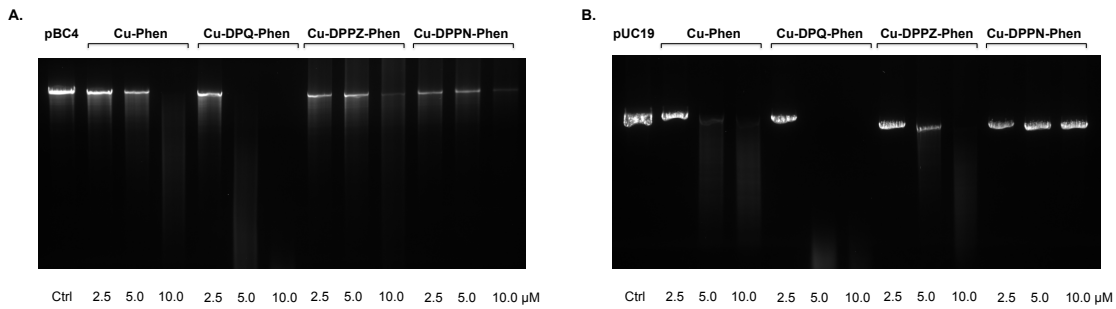

Figure II-6. Degradation of 400 ng of linearised plasmid pBC4 (**A**) and pUC19 (**B**) DNA with 2.5, 5.0, and 10.0 μM of tested metal complex in the presence of 1 mM of added reductant for 30 min at 37^{o}C; A. pBC4 (59% G-C); B. pUC19 (51% G-C).

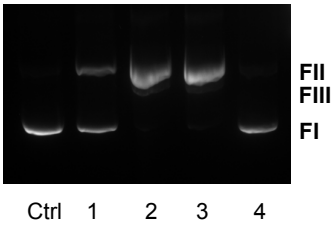

Figure II-7. DNA cleavage reactions with 10 μM of Cu-Phen, Cu-DPQ-Phen, Cu-DPPZ-Phen, and Cu-DPPN-Phen (lanes 1 – 4, respectively) with 400 ng of commercial (EDTA buffered) superhelical pUC19. Reactions were carried out with 1 mM of added Na-L-ascorbate over 30 min at 37°C.

II. 3.7. In vitro Cytotoxicity toward SKOV3 Cancer Cells

Flow cytometric analysis using Guava ViaCount reagent was used to examine the cytotoxic properties of the complex series and the clinical antitumor agent doxorubicin on human SKOV3 ovarian cancer cells. This cell line was selected as it possesses both a mutant p53 gene and is intrinsically resistant to cisplatin.[29,30] The ViaCount reagent determines viability of a cell population based upon differential membrane permeability of two fluorescent DNA intercalators that classify live and dead cell ratios. SKOV3 cells were incubated with drug concentrations ranging from 100 to 0.10 μM over 24 h (**Figure II-8**). Cytotoxicity data used to calculate the IC_{50} values (at the 95% confidence interval) were derived from sigmoidal, nonlinear regression curves (Appendix, **Figure A-5**). The IC_{50} complex trend follows Cu-DPPZ-Phen > Cu-DPQ-Phen > Cu-Phen > Cu-DPPN-Phen, with all compounds exhibiting significant 24 h *in vitro* cytotoxicity values of 0.59, 1.34, 1.40, and 3.55 μM, respectively. The most active complex, Cu-DPPZ-Phen, is comparable to that of the clinically used chemotherapeutic drug doxorubicin, with both agents exhibiting potent inhibitory values in the nanomolar region. Indeed, doxorubicin (Adriamycin) was specifically selected for this study due to its clinical DNA-damaging properties related to intercalation and topoisomerase II inhibition.[31−33]

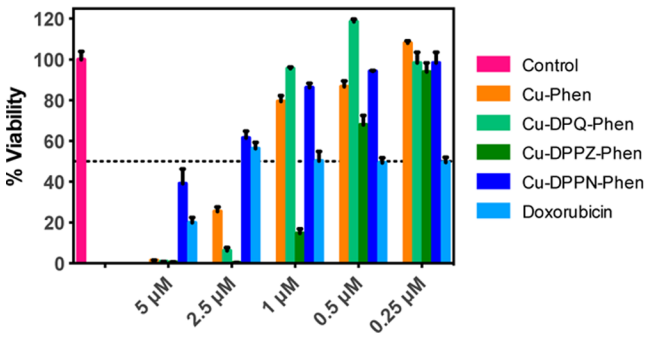

Compound	IC_{50} (μM)
Cu-Phen	1.40
Cu-DPQ-Phen	1.34
Cu-DPPZ-Phen	0.59
Cu-DPPN-Phen	3.55
Doxorubicin	0.52

Figure II-8. Dose-response inhibition and IC_{50} values (at the 95% confidence interval) of Cu^{2+} complexes and the clinical agent, doxorubicin, within SKOV3 human cancer cells over 24 h of drug exposure.

II. 3.8. Electrochemistry and Redox Interactions with the Superoxide Radical Anion and Hydrogen Peroxide

The electrochemical behaviour of each complex was investigated in the absence and presence of an excess of Na-L-ascorbate and hydrogen peroxide (**Figure II-9**). All complexes exhibit well defined, quasi-reversible redox profiles, with added oxidant or reductant having little effect on the reversibility of electron transfer reactions for each complex. Added reductant does shift the redox potentials anodically, while added oxidant shifts the complex redox potentials to more cathodic values. Interestingly, added reductant does increase the concentration of Cu(I) species in solution; this is reflected in the observed enhancement of complex oxidation peak currents. Conversely, on addition of peroxide, the expected increase in reduction peak currents for each complex, corresponding to a solution-phase increase in Cu(II) species, is not observed. Thus, a kinetic constraint exists in the electrochemical regeneration of Cu(I) in the presence of oxidant and may be indicative of the presence of copper-hydroperoxo species being generated in solution.

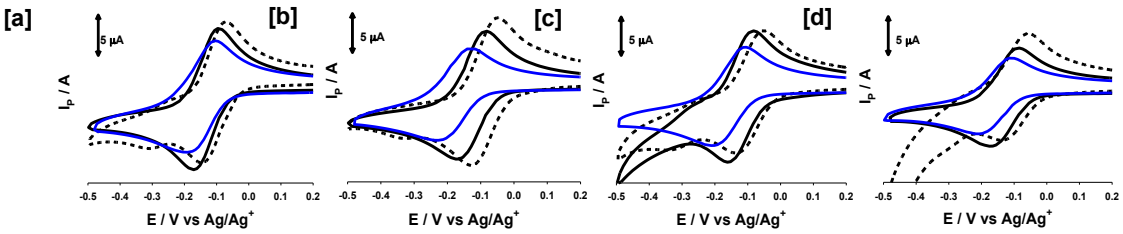

		[i]			[ii]			[iii]	
Entry	**Complex**	E_{Pa}	E_{Pc}	ΔE_P	E_{Pa}	E_{Pc}	ΔE_P	E_{Pa}	E_{Pc}	ΔE_P
[a]	**1**	-0.096	-0.171	0.075	0.074	-0.137	0.069	-0.104	0.190	0.086
[b]	**2**	-0.081	-0.175	0.094	-0. 51	-0 129	0. 78	-0.124	-0.211	0.087
[c]	**3**	0.082	-0.162	0.080	-0.057	-0.131	0.074	-0.105	-0.211	0. 06
[d]	**4**	-0.100	-0.181	0.081	-0.060	-0.144	0 084	-0.100	-0.190	0. 90

Figure II-9. Cyclic voltammograms describing the redox behavior of 1 mM of complex, at a scan rate of 100 mV s^{-1}, (solid black trace), and in the presence of 2 mM Na-L-ascorbate (dashed black trace), and 2 mM H_2O_2 (solid blue trace), (**A**) Cu-Phen, (**B**) Cu-DPQ-Phen, (**C**) Cu-DPPZ-Phen and, (**D**) Cu-DPPN-Phen, and, electrochemical parameters (V) for complexes, and in the presence of added Na-L-ascorbate, and H_2O_2 (bottom). Analysis conducted in 10% v/v DMF; [i] complex without exogenous treatment (V) [ii] complex with added Na-L-ascorbate (V) [iii] complex with added H_2O_2 (V).

The superoxide dismutase mimetic (SODm) properties of the group were investigated using the nitro blue tetrazolium (NBT) assay, where a xanthine/xanthine oxidase system served as the source of superoxide radical anion ($O_2^{\bullet -}$).[34] All complexes displayed similar, concentration-dependent, SODm activity (**Figure II-10b**) and have notable catalytic rates with K_{cat} values ranging between 9.80×10^6 M^{-1} s^{-1} (Cu-DPPZ-Phen) and 7.64×10^6 M^{-1} s^{-1} (Cu-DPPN-Phen). Complexes were then examined for their Fenton-like activity using the Amplex Red hydrogen peroxide assay (Invitrogen). None of the compounds were found to degrade H_2O_2 (5 μM) in the absence of reductant (results not shown); however, in the presence of Na-L- ascorbate (100 μM) all four chemical nucleases displayed one-phase exponential decay of peroxide (**Figure II-10a** and **Table II-4**). The rate of degradation, overall, is kinetically sluggish, with the rate constants for Cu-Phen and Cu-DPQ-Phen being 3.22 and 3.54 s^{-1}, respectively, and being more than twice that of Cu-DPPZ-Phen (1.56 s^{-1}) and Cu-DPPN-Phen (1.26 s^{-1}) complexes. Significantly, there was overlap between Fenton behavior and chemical nuclease activity with the most efficient reagents, $[Cu(DPQ)(Phen)]^{2+}$ and $[Cu(Phen)_2]^{2+}$, ablating H_2O_2 fluorescence at twice the rate of the DPPZ and DPPN complexes. Furthermore, given the series significant SODm activity and redox electrochemical profiles, it seems the rate limiting factor in the chemical nuclease activity is, predominately, due to the subsequent metallo-hydroperoxo reaction.

Table II-4. Kinetic properties of the complex series under Fenton-like and SODm conditions and catalytic cycle of Cu^+/Cu^{2+} ions with molecular oxygen, superoxide and hydrogen peroxide.

	H_2O_2 (Fenton)	SODm
Compound	K (s^{-1}) [a]	K_{cat} (M^{-1} s^{-1}) [b]
Cu-Phen	3.22	8.97×10^6
Cu-DPQ-Phen	3.54	7.82×10^6
Cu-DPPZ-Phen	1.56	9.80×10^6
Cu-DPPN-Phen	1.26	7.64×10^6

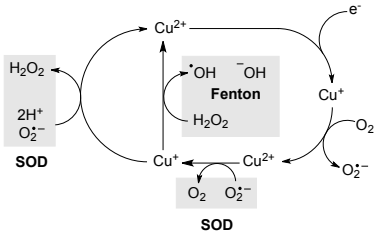

[a] Fenton degradation of 5 μM hydrogen peroxide in the presence of 5 μM complex and 100 μM Na-L-ascorbate. [b] Superoxide dismutase mimetic (SODm) activity determined by the xanthine/xanthine-oxidase system.

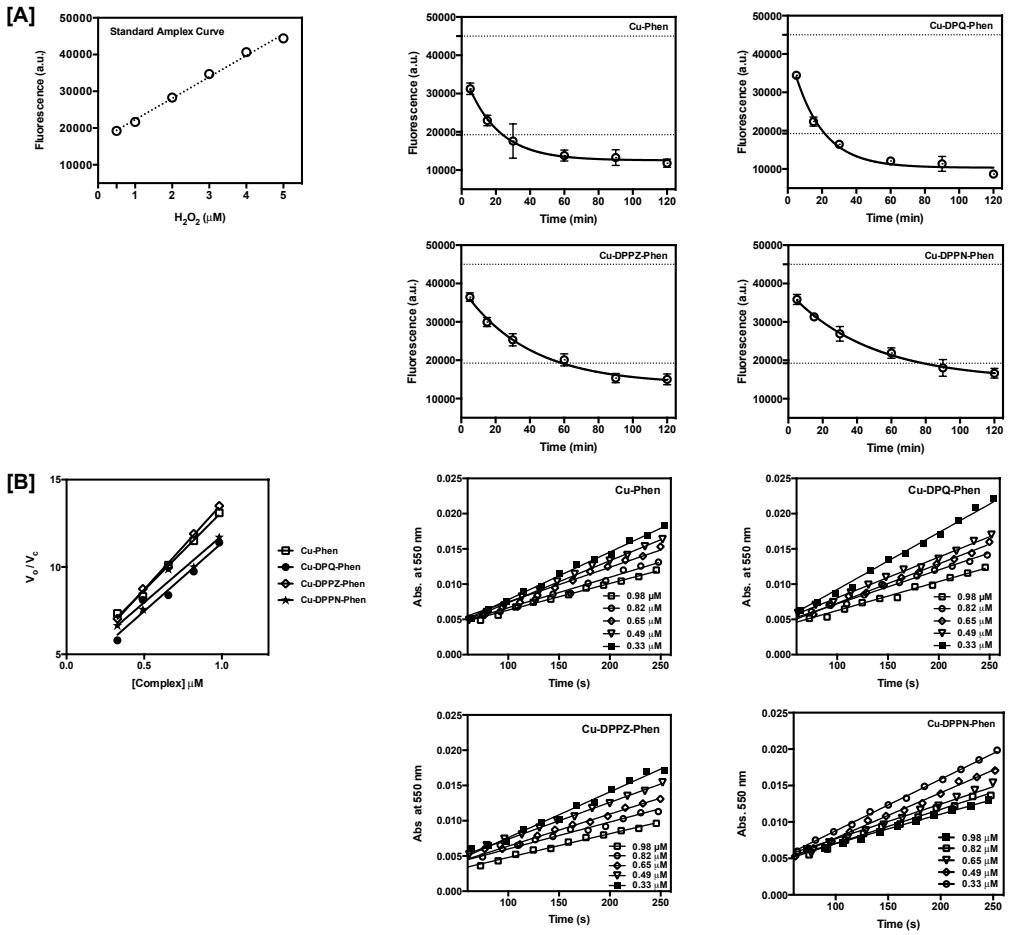

Figure II-10. (**A**) Fenton-like degradation of hydrogen peroxide (5 μM) in the presence of 5 μM of metal complex and 100 μM Na-L-ascorbate determined using the Amplex Red hydrogen peroxide assay kit (Invitrogen) (replicate experiments conducted on four separate occasions), a calibration curve is also shown which details the linear (r^2 >0.99) fluorescent response achieved from hydrogen peroxide detection in the assay, (**B**) superoxide dismutase mimetic (SODm) activity determined by the xanthine/xanthine-oxidase system, metal complexes were examined between 0.98 – 0.33 μM at 25°C under constant enzymatic production of superoxide (~1 μM / min) using the detector molecule, nitrobluetetrazolium chloride and this data was plotted as a function of V_0/V_c (catalytic rate in the absence / presence of catalyst) as a function of [complex] to yield the catalytic rate K_{cat} in units, M^{-1} s^{-1}.

II. 4. Discussion

The incorporation of designer phenazine ligands in the "bis- phen" $[Cu(Phen)_2]^{2+}$ chemical nuclease model pronounces DNA recognition and intercalation with significant enhancement to the dynamic binding constant for dipyrido[3,2-f:2′,3′-h]quinoxaline (DPQ) and dipyrido[3,2-a:2′,3′-c]phenazine (DPPZ) containing complexes; $[Cu(DPQ)(Phen)]^{2+}$ and $[Cu(DPPZ)(Phen)]^{2+}$. To our knowledge these binding constants ($K_{app} \approx 3 \times 10^7$ $M(bp)^{-1}$) are the highest reported to date for any existing copper(II) phenanthrene complex and surpass the $[Cu(Phen)_2]^{2+}$ cation by ~60-fold. Additionally, these values compare favorably with the binding constants of Actinomycin D, identified in this study as 2.92×10^7 $M(bp)^{-1}$, and rhodium(III) complexes rac-$[Rh(phi)(phen)_2]^{3+}$ and rac-$[Rh(phi)2(bipy)]^{3+}$ ($K_b \approx 10^6$–10^7 M^{-1})[35] (where phi = 9,10- phenanthrene-quinone-diimine and bpy = 2,2′-bipyridine) but do not match the ctDNA binding affinity of ruthenium(II) DPPZ complexes Δ-$[Ru(DPPZ)(Phen)_2]^{2+}$ or Λ-$[Ru(DPPZ)(Phen)_2]^{2+}$ ($K_{eff} \approx 10^8$ M^{-1}).[6] Indeed, the lowest binding constant among the three phenazine complexes generated ($K_{app} \approx 6 \times 10^6$ $M(bp)^{-1}$), observed for the $[Cu(DPPN)(Phen)]^{2+}$ complex, is on par with many high-affinity copper(II) binding constants in the literature.[36] Interestingly, copper(II) DPQ and DPPZ compounds have shown only mediocre DNA binding constants ($K_b = 10^4$–10^3 M^{-1}) when complexed with amino acid chelators L-leucine, L-tryptophan, and L-tyrosine which, surprisingly, have far lower binding constants than the amino acid complex $[Cu(glycine)(DPPZ)]^+$ ($K_b \approx 10^6$ M^{-1}), along with $[Cu(L\text{-arginine})(DPQ)]^+$ and [Cu(L-arginine)(DPPZ)] ($K_b \approx 10^5$ M^{-1} and $K_{app} \approx 10^6$ M^{-1}).[37–41] Enhanced binding constants ($K_{app} \approx 5 \times 10^6$ M^{-1}) were observed, however, for binuclear complexes $[\{Cu(DPQ)(DMF)\}_2(\mu\text{-}OH)_2]^{2+}$ (DMF= dimethylformamide) and $[\{Cu(DPPZ)(DMF)\}_2(\mu\text{-}OH)_2]^{2+}$, which feature two phenazine ligands spanning opposite directions along the hydroxide-bridged Cu–Cu axis.[42] Thus, in addition to the influence of an extended phenazine π- framework, our results suggest a prominent role for the ancillary chelated phenanthroline in nucleotide binding affinity. These ligands are presumably involved in secondary interactions with DNA bases or at the surface of the minor groove and may function to optimize complex binding geometry.[17,18,43]

The complex series has distinctive nucleotide binding specificity compared with netropsin and Actinomycin D. Their ability to similarly quench Hoechst 33258 and ethidium bromide-bound ctDNA fluorogenic dyes, along with their broadly analogous displacement of limited bound ethidium to poly[d(G-C)$_2$] and poly[d(A-T)$_2$], departs

substantially from the observed binding specificity of these classical minor-groove binding or intercalating agents. Thermal melting analysis, however, reveals that both DPQ and DPPZ complexes extensively stabilize poly[d(G-C)$_2$] denaturation, comparable to Actinomycin D, and that the overall complex series has a large degree of similarity with this intercalator given their negligible stabilization on poly[d(A-T)$_2$]. Taken together, it appears likely that the complexes intercalate DNA at both the minor and major grooves, and these interactions are appreciably enhanced by the presence of coordinated phenazine ligands, in particular DPQ and DPPZ.

We reported a novel on-chip microfluidic method for the Agilent Bioanalyzer 2100 for examining, with high precision, chemical nuclease activity. In our view, this technique offers advantages over existing methodologies (e.g., band densitometry) in the quantitation of dsDNA damage and undoubtedly has application in quantifying the activity of cytotoxic DNA damaging drugs, in particular those from families of structurally related agents. Further, this technique is suited for detecting sequence-specific metallodrug DNA interactions as in our laboratory we have observed the effects of introducing a second endonuclease (SalI) with single site-recognition specificity on this sequence. The analysis methods we have employed on the Bioanalyzer 2100 to detect DNA degradation involve both peak height and peak area intensity reduction. Our motivation for applying both techniques stems from the observation that the Cu^{2+} complexes induced random damage, and thus asymmetric peak tailing on the pUC19 fragments (due to shearing chemical nuclease effects) were evident in each electrogram. This factor had an influence on peak area intensity, and so we found that peak height analysis was suitable to employ as a tandem method to enhance the overall accuracy of the technique. Our work revealed the $[Cu(DPQ)(Phen)]^{2+}$ complex as the most active chemical nuclease within this series; however, the degradation kinetics of this reagent is closely followed by $[Cu(Phen)_2]^{2+}$. The interaction of the phenazine complexes with pBC4 (59% G-C) and pUC19 (51% G-C) plasmid DNA, however, reveal significant differences compared with the $[Cu(Phen)_2]^{2+}$ cation in terms of chemical nuclease efficacy. $[Cu(Phen)_2]^{2+}$ had enhanced activity toward the lower G-C containing plasmid (pUC19), while each of the phenazine complexes maintained, or enhanced, their activity toward the higher G-C-content plasmid (pBC4). These data suggest Cu^{2+} phenazine compounds may have targeting properties toward cytosine-phosphate-guanine (CpG) islands, which are found in the promoter regions of many mammalian genes.[44,45] Thus, it is of significant future importance to examine the

DNA-targeting properties of these phenazine complexes within cisplatin- resistant cancer cell models such as SKOV3. While these complexes, in particular Cu-DPPZ-Phen, display interesting in vitro chemotherapeutic potential compared with doxorubicin on SKOV3, their targeted DNA-damaging effects have yet to be identified. Indeed, we recently reported that, although Cu-Phen has significant cytotoxic properties toward SKOV3, this agent non-selectively induces DNA damage and can be classified as a "promiscuous" cytotoxin.[27]

All complexes in this study have excellent superoxide dismutase mimetic activities (K_{cat} 7.6 − 9.8 × 10^6 M^{-1} s^{-1}) but are slow, kinetically, within the Fenton reaction (Cu^+ + H_2O_2 → Cu^{2+} + $^{\bullet}OH$ + OH^-). Significantly, however, Fenton breakdown follows linearized pUC19 chemical nuclease efficiency in the overall series (Cu-DPQ-Phen > Cu-Phen ≫ Cu-DPPZ-Phen > Cu-DPPN-Phen) with DPQ and the bis-phen complex consuming peroxide at twice the rate constant of DPPZ and DPPN reagents.

In summary, we showed that phenazine-functionalized Cu^{2+} phenanthroline complexes offer a clear enhancement toward DNA binding affinity relative to the well-studied $[Cu(Phen)_2]^{2+}$ cation and possess the highest ctDNA binding affinities currently known for Cu^{2+} phenanthrene complexes. We reported a new on-chip methodology for determining dsDNA degradation, and it is our opinion that both this technique and these Cu^{2+} phenazine reagents will have an important future role to play in the development of site-directed, gene-silencing, artificial metallonucleases for use as targeted chemotherapeutics for human disease.

II. 5. Materials And Methods

II. 5.1. Preparation of Ligands and Metal Complexes

Chemicals and reagents of analytical grade for the preparation of organic ligands and metal complexes were purchased from Sigma-Aldrich (Ireland) and used without further purification.

II. 5.1.1. Preparation of 1,10-Phenanthroline-5,6-dione (Phendio)

Phendio was prepared according to the literature method reported by Dickeson and Summers, with slight modification.[24] 1,10- Phenanthroline (4.00 g, 22.19 mmol) and potassium bromide (4.00 g, 33.6 mmol) were thoroughly mixed and slowly added to an ice-cold mixture of H_2SO_4 (40 mL) and HNO_3 (20 mL). The solution was refluxed for 3 h

at 100°C, then cooled to room temperature, poured onto crushed ice (~400 mL), and neutralized with an aqueous NaOH solution (80.0 g per 400 mL) to a pH between 4 and 5, yielding a yellow solution. The solution was extracted with $CHCl_3$ (in 8 × 100 mL portions). The organic phase was combined and dried with anhydrous magnesium sulfate and then filtered before being evaporated to dryness, whereupon a bright yellow solid (4.03 g) was obtained. The product could be further purified by recrystallization from high-performance liquid chromatography (HPLC)-grade methanol but was sufficiently pure to use in subsequent reactions. Yield: 4.03 g (86%). ^{1}H NMR (400 MHz, $CDCl_3$): 9.05 (dd, J = 4.6, 1.8 Hz, 2H), 8.44 (dd, J = 7.9, 1.8 Hz, 2H), 7.52 (dd, J = 7.9, 4.6 Hz, 2H). IR (ATR, cm^{-1}): 3348, 3061, 1678, 1559, 1458, 1412, 1290, 1204, 1114, 1009, 924, 806, 734. Solubility: DMF, EtOH, DMSO (partially), melting point (mp) 258−260°C.

II. 5.1.2. Preparation of Dipyrido[3,2-f:2′,3′-h]quinoxaline (DPQ)

DPQ was prepared according to the literature method reported by Hambley et al., with some modification.[26] To a solution of phendio (0.510 g, 2.44 mmol) in water (35 mL) was added ethylenediamine (0.70 mL, 10.47 mmol), and the resultant suspension was refluxed for 12 h at 60°C. The resulting product was washed with water (10 mL) and minimum volume of diethyl ether. Yield: 0.372 g (66%). ^{1}H NMR (400 MHz, $CDCl_3$): 9.47 (dd, J = 8.2, 1.8 Hz, 2H), 9.24 (dd, J = 4.3, 1.8 Hz, 2H), 9.19 (s, 2H), 7.96 (dd, J = 8.2, 4.3 Hz, 2H). IR (ATR, cm^{-1}): 2990, 1570, 1472, 1466, 1206, 1073, 1077, 825, 803, 739. Solubility: DMF, EtOH, DMSO (partially). mp 330−335°C.

II. 5.1.3. Preparation of Dipyrido[3,2-a:2′,3′-c]phenazine (DPPZ)

DPPZ was prepared according to literature, with slight changes made to the method.[24] A methanolic solution (20 mL) of 1,2-phenylenediamine dihydrochloride (0.640 g, 3.53 mmol) was refluxed until it was dissolved. A warm ethanolic solution of phendio (0.500 g, 2.38 mmol) was prepared (20 mL), added over the methanolic solution, and refluxed with constant stirring for 3 h. The resulting solution was vacuum-filtered and recrystallized from EtOH, producing metallic-like orange filaments. Yield: 0.521 g (78%). ^{1}H NMR (400 MHz, $CDCl_3$): 9.58 (dd, J = 8.1, 1.7 Hz, 2H), 9.20 (dd, J = 4.5, 1.7 Hz, 2H), 8.29 (dd, J = 6.5, 3.4 Hz, 2H), 7.86 (dd, J = 6.5, 3.4 Hz, 2H), 7.73 (dd, J = 8.1, 4.5 Hz, 2H). IR (ATR, cm^{-1}): 3040, 1615, 1570, 1486, 1412, 1336, 1077, 1072, 808, 739. Solubility: DMF, EtOH, DMSO (partially). mp 248−253°C.

II. 5.1.4. Preparation of Benzo[I]dipyrido[3,2-a:2′,3′-c]phenazine (DPPN)

DPPN was prepared according to literature, with slight changes made to the method.[25] To a solution of phendio (0.300 g, 1.422 mmol) in EtOH (45 mL) was added 2,3-diaminonaphthalene (0.339 g, 2.136 mmol), and the resulting suspension was refluxed for 3 h, during which time an orange precipitate formed. The precipitate was vacuum-filtered, washed with cold ethanol, and allowed to dry. Yield: 0.443 g (93%). ^{1}H NMR (400 MHz, $CDCl_3$): 9.49 (dd, J = 8.1, 1.8 Hz, 2H), 9.16 (dd, J = 4.4, 1.8 Hz, 2H), 8.80 (s, 2H), 8.09 (dd, J = 6.5, 3.1 Hz, 2H), 7.68 (dd, J = 8.1, 4.4 Hz, 2H), 7.53 (dd, J = 6.5, 3.1 Hz, 2H). IR (ATR, cm^{-1}): 3362, 1628, 1583, 1565, 1409, 1360, 1274, 1128, 1070, 1033, 892, 871, 850, 817. Solubility: DMF (partially). mp 283−285°C.

II. 5.1.5. Preparation of $[Cu(Phen)](NO_3)_2$

To a solution of copper(II) nitrate hemipentahydrate (1 g, 4.3 mmol) in EtOH (75 mL) was added Phen (0.78 g, 4.3 mmol), and the resulting suspension was refluxed for 2 h. The solution was left to stand for 12 h, vacuum- filtered, and washed with a minimum volume of cold EtOH. Yield: 1.43 g (90%). Anal. Calc. for $C_{12}H_8CuN_4O_6$: C, 39.19; H, 2.19; N, 15.23. %Found: C, 39.65; H, 2.06; N, 14.92. IR (ATR, cm^{-1}): 3068, 1583, 1451, 1426, 1270, 1151, 1110, 1011, 972, 847, 807, 739, 719. Solubility: DMF, EtOH. Preparation of $[Cu(Phen)_2](NO_3)_2$ (Cu-Phen). This complex was prepared according to the method reported by Prisecaru et al.[27]

II. 5.1.6. General Procedure for Preparing $[Cu(N,N')(Phen)](NO_3)_2$ Complexes (where N,N' = DPPZ, DPPN, and DPQ)

To a solution of $[Cu(phen)(NO_3)_2]$ (0.1 g, 0.27 mmol) in EtOH (30 mL) was added 0.27 mmol of either DPQ (0.063 g), DPPZ (0.076 g), or DPPN (0.090 g), and the resulting suspension was stirred for 12 h at 50°C. The solution was vacuum-filtered and washed with a minimum volume of cold EtOH.

II. 5.1.6.1. $[Cu(DPQ)(Phen)](NO_3)_2 \cdot 0.5H_2O$ (Cu-DPQ-Phen)

Yield: 0.1207 g (73%). Anal. Calc. for $C_{26}H_{17}CuN_8O_{6.5}$: C, 51.28; H, 2.81; N, 18.40. %Found: C, 51.15; H, 2.29; N, 18.68. IR (ATR, cm^{-1}): 3034, 1581, 1472, 1360, 1288, 1210, 1081, 818, 718. Solubility: EtOH, MeOH, DMF, DMSO (partially).

II. 5.1.6.2. [Cu(DPPZ)(Phen)]$(NO_3)_2$ (Cu-DPPZ-Phen)

Yield: 0.0709 g (41%). Anal. Calc. for $C_{30}H_{18}CuN_8O_6$: C, 55.43; H, 2.79; N, 17.24. %Found: C, 56.38; H, 2.88; N, 17.83. IR (ATR, cm^{-1}): 3023, 1578, 1451, 1376, 1292, 1076, 819, 718, 729. Solubility: DMF, DMSO (partially).

II. 5.1.6.3. [Cu(DPPN)(Phen)]$(NO_3)_2 \cdot 2H_2O$ (Cu-DPPN-Phen)

Yield: 0.1341 g (67%). Anal. Calc. for $C_{34}H_{24}CuN_8O_8$: C, 55.47; H, 3.29; N, 15.22. %Found: C, 55.42; H, 2.76; N, 15.38. IR (ATR, cm^{-1}): 3020, 1578, 1518, 1375, 1358, 1290, 1046, 868, 719. Solubility: DMF, DMSO (partially).

II. 5.2. DNA Binding Studies

The fluorescence-quenching assay, the competitive ethidium bromide displacement assay, and the viscosity measurements we all conducted according to the method reported by Kellett et al.[28]

II. 5.3. Fluorescence Quenching for poly[d(A-T)$_2$] and poly[d(G-C)$_2$]

Solutions of double-stranded alternating copolymers poly[d(A-T)·d(A-T)] (Sigma PO883, ε_{260} = 13 100 M $(bp)^{-1}$ cm^{-1}) and poly[d(G-C)·d(G-C)] (Sigma P9389, ε_{260} = 16 800 $M(bp)^{-1}$ cm^{-1}) were prepared in nuclease-free water and quantified on a Cary 100 UV−visible spectrophotometer. A working solution of 50 μM poly[d(A- T)$_2$] (or poly[d(G-C)$_2$]) along with 10 μM ethidium bromide (EtBr) in *N*-(2-hydroxyethyl)piperazine-*N*′-ethanesulfonic acid (HEPES) buffer (80 mM, pH = 7.2) and NaCl (40 mM) was prepared. Stock solutions of metal complexes, metal salts, and groove-binding drugs were prepared at ∼4 mM in DMF and were further diluted to 80 mM in HEPES buffer. 50 μL of the poly[d(A-T)$_2$] (or (poly[d(G-C)$_2$]) EtBr working solution was placed in each well of a 96-well microplate with the exception of the blanks, which contained 95 μL of 80mM HEPES and 5 μM EtBr. Serial aliquots of the tested compound were added to the working solutions, and the volume was adjusted to 100 μL in each well such that the final concentrations of nucleotide and EtBr were 25 μM and 5 μM, respectively. The plate was then allowed to incubate at room temperature for 5 min before being analyzed using a Bio-Tek synergy HT multimode microplate reader with excitation and emission wavelengths being set to 530 and 590 nm for EtBr detection. Concentrations of the tested compounds were optimized such that fluorescence was 30−40% of the initial control at their highest reading. Each drug concentration was measured in duplicate. From a plot of fluorescence

versus added drug concentration, the Q value is given by the concentration required to effect 50% removal of the initial fluorescence of the bound dye.

II. 5.4. Thermal Melting Experiments

Analysis was carried out on an Agilent Cary 100 dual beam spectrophotometer equipped with a 6 × 6 Peltier multicell system with temperature controller. For poly[d(G-C)$_2$]; in a final volume of 1 mL using Starna black-walled quartz cuvettes with tight-fitting seals, 2 mM NaOAc buffer (pH = 5.0), 1 mM NaCl and poly[d(G-C)$_2$] (Sigma, P9389) were added to give a final absorbance of between 0.18 and 0.20 absorbance units at 260 nm (ε_{max} = 8400 M^{-1} cm^{-1}). For poly[d(A-T)$_2$]; in a final volume of 1 mL using Starna black-walled quartz cuvettes with tight-fitting seals, 50 mM NaOAc buffer (pH = 5.0), 250 mM NaCl and poly[d(A-T)$_2$] (Sigma, PO883) were added to give a final absorbance of between 0.18 and 0.20 absorbance units at 260 nm (ε_{max} = 6600 M^{-1} cm^{-1}). Stock solutions of metal complexes, netropsin, and Actinomycin D, prepared beforehand in DMF, were dissolved in 80 mM HEPES (pH 7.2). An aliquot of test reagent was then added to each cuvette such that an r value of 0.1 was achieved (*r* = [compound]/[nucleotide]). The test reagent and respective alternating copolymer were then incubated for 10 min at 20°C prior to commencing the temperature ramp. Thermal melting measurements were recorded at 260 nm at 0.25 s intervals. Temperature was ramped at 3°C/min over the range of 20.0−97.0°C. The spectral bandwidth (SBW) was set to 1. Temperature was calibrated, for each measurement, using a temperature probe placed in an identical black-walled cuvette containing equivalent buffer and NaCl. Samples were run in triplicate, and the melting temperature T_M (°C) was calculated using the built-in derivative method on the instrument.

II. 5.6. Artificial Metallonuclease Activity

Generation of pUC19 DNA

The vector pUC19 was generated following the transformation of E. coli using an LB ampicillin-resistant media protocol, extracted using a maxi-prep kit protocol (NucleoBond Xtra Midi Plus, EF-Macherey-Nagel), and then quantified using the NanoDrop (ND-1000 Spectrophotometer).

II. 5.7. Gel Electrophoresis Experiments on pUC19 DNA

Reactions were carried out according to the literature procedure by Kellett et al.[46] Briefly, in a total volume of 20 μL using 80 mM HEPES buffer (Fisher) at pH 7.2 with 25 mM NaCl, an aliquot of the stock complex (prepared in DMF) was mixed with 400 ng of

supercoiled pUC19 and 1 μL of 20 mM Na-L-ascorbate. Samples were incubated for 30 min at 37°C before being quenched with 6X loading dye (Fermentas), containing 10 mM tris(hydroxymethyl)aminomethane-HCl (pH 7.6), 0.03% bromophenol blue, 0.03% xylene cyanol, 60% glycerol, and 60 mM EDTA, then loaded onto agarose gel (1%) containing 2.0 μL of GelRed (10 000X). Electrophoresis was completed at 80 V for 1.5 h using a wide mini-sub cell (BioRad) in 1X Tris−acetate−EDTA buffer (Millipore). Trapping experiments with 100 μM neocuprione (Sigma, N1501), 10% v/v DMSO, 1000 units of bovine SOD enzyme (Sigma, S7571), and 1000 units of catalase enzyme from bovine liver (Sigma, C1345) were also examined using this procedure.

II. 5.8. Linearization of Supercoiled pUC19

In a total volume of 20 μL, using 5 μg of supercoiled pUC19, 5 μL of 10X HEPES buffer, 2.5 μL of 20 000 U/mL HindIII (NEB), 5 μL of NEBuffer 2 (NEB), 1 μL of bovine serum albumin (BSA) (NEB) and nuclease-free water were added. This mixture was allowed to incubate at 37°C for 2.5 h, after which 1 μL of this mixture was loaded onto an agarose gel to confirm linearization. Linear DNA from the mixture was then purified from the enzymatic reaction, using a QIAquick Purification column (QIAGEN). Linearized DNA was quantified using the NanoDrop (ND-1000 Spectrophotometer).

II. 5.9. Microfluidic Chip Analysis of DNA Degradation on the Agilent Bioanalyzer 2100

In a total volume of 20 μL, using 80 mM HEPES buffer (Fisher) at pH 7.2 with 25 mM NaCl, the complex (500 nM) was mixed with 400 ng of linear pUC19 and 1 mM Na-L-ascorbate. Samples were incubated at 37°C for between 1 and 30 min and quenched with both neocuproine (100 μM) and EDTA (100 μM) before being loaded onto a DNA 7500 microfluidic chip as per the manufacturer's protocol.[23] Data was then collected using Agilent 2100 Bioanalyzer. Electrograms generated by the Bioanalyzer 2100 for all complexes are available in the Supporting Information.

II. 5.10. Chemical Nuclease of Linearized pUC19

In a total volume of 20 μL, using 400 ng of supercoiled pUC19 (2686 bp), 1 μL of SalI (20 000 U/mL, NEB, cleaving the plasmid at one site located at 429 bp), 2 μL of 10X HEPES buffer, 2 μL of NEBuffer 3.1, and nuclease- free water were added. The reaction mixture was allowed to incubate at 37°C for 1.5 h, after which the endonuclease was heat-inactivated at 65°C for 20 min. After the mixture was cooled, an aliquot of the stock

complex and 1 mM Na-L-ascorbate were added to the reaction mixture, and the final concentration of EDTA was adjusted (where appropriate) to ensure a final concentration 40.0 μM before incubation at 37°C for 30 min was completed. The reaction was then quenched with 6X loading dye (Fermentas), and DNA fragments were subjected to gel electrophoresis (prepared and stained as previously described).

II. 5.11. Chemical Nuclease of Linearized pBC4

In a total volume of 20 μL, using 400 ng of supercoiled pBC4 (10 673 bp), 1 μL of AgeI (20 000 U/mL, NEB, cleaving the plasmid at one site located at 5037 bp), 2 μL of 10X HEPES buffer, 2 μL of NEBuffer 1, 0.2 μL of BSA and nuclease-free water were added. Reaction mixture was allowed to incubate at 37°C for 1.5 h, after which the endonuclease was heat inactivated at 65°C for 20 min. After the mixture was cooled, an aliquot of the stock complex and 1 mM Na-L-ascorbate were added to the reaction mixture, and the final concentration of EDTA was adjusted (where appropriate) to ensure a final concentration 40.0 μM before incubation at 37°C for 30 min was completed. The reaction was then quenched with 6X loading dye (Fermentas), and DNA fragments were subjected to gel electrophoresis (prepared and stained as previously described).

II. 5.12. Cell Culture Experiments

SKOV-3 cells were grown in RPMI 1640 supplemented with 10% fetal calf serum (FCS) at 37°C in a humidified atmosphere with 5% CO_2. Compound viability was tested using Guava Viacount (Millipore) reagent following 24 h exposure. Positive control, doxorubicin, was purchased from Sigma-Aldrich as a European Pharmacopoeia reference standard. DMSO stocks for the complexes Cu-Phen, Cu-DPQ-Phen, Cu-DPPZ-Phen, Cu-DPPN-Phen, and doxorubicin were prepared in 1 mL, ranging from 11 to 34 mM.

II. 5.13. ViaCount Assay

SKOV3 cells were seeded at an initial density of 4 × 104 cell/mL in 96-well plates and incubated overnight prior to drug addition. DMSO stocks of the complexes and controls were diluted in RPMI 1640 containing 10% FCS, to give the following final concentrations in 200 μL wells: 5.0, 2.5, 1.0, 0.5, and 0.25 μM. A DMSO control of the highest incubation concentration was also included. Cells were incubated for 24 h at 37°C in a humidified atmosphere with 5% CO_2. After 24 h of exposure, spent media was removed, and cells were washed once with 200 μL of phosphate- buffered saline and detached using 50 μL of 1X trypsin, with the subsequent addition of 50 μL of media. Cells were transferred to 96-

well round-bottom plates with 100 µL of ViaCount reagent incubated at room temperature in the dark for 10 min. Viability data was collected on Guava EasyCyte HT flow cytometer using Guava Viacount software.

II. 5.14. Electrochemistry

Electrochemical measurements were performed on a Solartron 1825 potentiostat, and data were analyzed using CorrView software. Electrochemistry was performed in 1 mM solutions of each complex, made up in 0.1 M tetrabutylammonium hexafluorophosphate (TBAPF6) in 10% v/v DMF as the supporting electrolyte. Concentrations of added reductant and oxidant were 2 mM to ensure an excess was present in solution (ratio 1:2, complex/ (reductant/oxidant)). Electrochemical cell setup: Glassy Carbon working electrode (2 mm diameter), platinum wire counter electrode, nonaqueous Ag/Ag^{+} reference electrode ($E_{1/2}$ = 0.075 V versus Fc/ Fc^{+}). Glassy carbon electrodes were polished using alumina oxide powder (0.05 µm) on a microcloth (Buehler). Cyclic voltammetric data presented were obtained after steady-state was attained, at a scan rate of 100 mV s^{-1}, with scans initiating in the cathodic direction.

II. 5.15. Superoxide Dismutase Mimetic Activity

The SOD mimetic activities of the complexes were determined using a nitro blue tetrazolium (NBT) assay,[34] in which the xanthine/xanthine oxidase system serves as the source of superoxide radicals. The quantitative reduction of NBT to blue formazan by $O_2^{\bullet-}$ was followed spectrophotometrically using a thermostatically controlled Agilent Cary 100 dual-beam spectrophotometer at 550 nm at 25°C. Reagents were obtained from Sigma−Aldrich, and the assays were run in a total volume of 3 mL. Tabulated results were derived from linear regression analyses and are reported as rate in the absence of catalyst/rate in the presence (V_o/V_c) versus catalyst concentration, which yielded the catalytic rate (K_{cat} M^{-1} s^{-1}).

II. 5.16. H_2O_2 Breakdown Assay

A 5 mL stock solution of 100 µM Amplex Red containing 10 mM Amplex Red reagent and 10 U/ml horseradish peroxidase (HRP) was prepared in 1X buffer as per Amplex Red hydrogen Peroxide/Peroxidase assay kit instruction (Invitrogen Cat. A22188). A standard fluorescence response curve from H_2O_2 was obtained by adding a series of aliquots (0.5−5 µM) of H_2O_2 and the Amplex Red stock solution, and the volume was adjusted to 100 µL with 1X buffer in each sample well. An aliquot containing 5 µM of tested compounds, 5

μM H_2O_2, and 100 μM Na-L-ascorbate that were previously incubated between 0−120 min was added to 50 μL of Amplex Red solution, and again the volume was adjusted to 100 μL using 1X buffer. The fluorescence intensity of the Article reaction mixture was measured with a Bio-Tek synergy HT multimode microplate reader equipped with excitation and emission filters at 530 and 590 nm.[47]

II. 6. Acknowledgments

This work was supported by the Dublin City University Career Start fund, Irish Research Council (IRC) grants, GOIPG/2013/826 and GOIPG/2013/937, Dublin City University Distinguished Scholars Studentship award and EU COST Action CM1201: Biomimetic Radical Chemistry.

II. 7. References

(1) Liu, H.-K.; Sadler, P. J. Acc. Chem. Res. 2011, 44, 349.
(2) Jamieson, E. R.; Lippard, S. J. Chem. Rev. 1999, 99, 2467.
(3) Lippard, S.; Bond, P.; WU, K.; Bauer, W. Science 1976, 194, 726.
(4) Zeglis, B. M.; Pierre, V. C.; Barton, J. K. Chem. Commun. 2007, 4565.
(5) Park, G. Y.; Wilson, J. J.; Song, Y.; Lippard, S. J. Proc. Natl. Acad. Sci. U.S.A. 2012, 109, 11987.
(6) Hiort, C.; Lincoln, P.; Norden, B. J. Am. Chem. Soc. 1993, 115, 3448.
(7) Sigman, D. S.; Graham, D. R.; D'Aurora, V.; Stern, A. M. J. Biol. Chem. 1979, 254, 12269.
(8) Sigman, D. S.; Mazumder, A.; Perrin, D. M. Chem. Rev. 1993, 93, 2295.
(9) Chen, C.-h. B.; Milne, L.; Landgraf, R.; Perrin, D. M.; Sigman, D. S. ChemBioChem. 2001, 2, 735.
(10) Santini, C.; Pellei, M.; Gandin, V.; Porchia, M.; Tisato, F.; Marzano, C. Chem. Rev. 2013.
(11) Gutteridge, J. M. C.; Halliwell, B. Biochem. Pharmacol. 1982, 31, 2801.
(12) Goldstein, S.; Michel, C.; Bors, W.; Saran, M.; Czapski, G. Free Radical Biol. Med. 1988, 4, 295.
(13) Sigman, D. S.; Bruice, T. W.; Mazumder, A.; Sutton, C. L. Acc. Chem. Res. 1993, 26, 98.
(14) Chen, C. H.; Sigman, D. S. Proc. Natl. Acad. Sci. U.S.A. 1986, 83, 7147.
(15) Bales, B. C.; Kodama, T.; Weledji, Y. N.; Pitié, M.; Meunier, B.; Greenberg, M. M. Nucleic Acids Res. 2005, 33, 5371.
(16) Pitié, M.; Burrows, C. J.; Meunier, B. Nucleic Acids Res. 2000, 28, 4856.
(17) Niyazi, H.; Hall, J. P.; O'Sullivan, K.; Winter, G.; Sorensen, T.; Kelly, J. M.; Cardin, C. J. Nat. Chem. 2012, 4, 621.
(18) Song, H.; Kaiser, J. T.; Barton, J. K. Nat. Chem. 2012, 4, 615.
(19) Holmlin, R. E.; Dandliker, P. J.; Barton, J. K. Angew. Chem., Int. Ed. Engl. 1997, 36, 2714.
(20) Hall, J. P.; Cook, D.; Morte, S. R.; McIntyre, P.; Buchner, K.; Beer, H.; Cardin, D. J.; Brazier, J. A.; Winter, G.; Kelly, J. M.; Cardin, C. J. J. Am. Chem. Soc. 2013, 135, 12652. 5403
(21) Wang, J. Nucleic Acids Res. 2000, 28, 3011.
(22) Agilent Technologies. http://www.agilent.com/ (accessed January, 2013).
(23) Agilent Technologies Genomics. http://www.genomics.agilent. com/en/Bioanalyzer-DNA-RNA-Kits/DNA-Analysis-Kits/?cid=AG- PT-105&tabId=AG-PR-1040 (accessed January, 2013).
(24) Dickeson, J.; Summers, L. Aust. J. Chem. 1970, 23, 1023.
(25) Yam, V. W.-W.; Lo, K. K.-W.; Cheung, K.-K.; Kong, R. Y.-C. Chem. Commun. 1995, 1191.
(26) Collins, J. G.; Sleeman, A. D.; Aldrich-Wright, J. R.; Greguric, I.; Hambley, T. W. Inorg. Chem. 1998, 37, 3133.

(27) Prisecaru, A.; McKee, V.; Howe, O.; Rochford, G.; McCann, M.; Colleran, J.; Pour, M.; Barron, N.; Gathergood, N.; Kellett, A. J. Med. Chem. 2013, 56, 8599.
(28) McCann, M.; McGinley, J.; Ni, K.; O'Connor, M.; Kavanagh, K.; McKee, V.; Colleran, J.; Devereux, M.; Gathergood, N.; Barron, N.; Prisecaru, A.; Kellett, A. Chem. Commun. 2013, 49, 2341.
(29) O'Connor, P. M.; Jackman, J.; Bae, I.; Myers, T. G.; Fan, S.; Mutoh, M.; Scudiero, D. A.; Monks, A.; Sausville, E. A.; Weinstein, J. N.; Friend, S.; Fornace, A. J., Jr.; Kohn, K. W. Cancer Res. 1997, 57, 4285.
(30) O'Neill, C. F.; Koberle, B.; Masters, J. R. W.; Kelland, L. R. Br. J. Cancer. 1999, 81, 1294.
(31) Momparler, R. L.; Karon, M.; Siegel, S. E.; Avila, F. Cancer Res. 1976, 36, 2891.
(32) Capranico, G.; Kohn, K. W.; Pommier, Y. Nucleic Acids Res. 1990, 18, 6611. (33) Pang, B.; Qiao, X.; Janssen, L.; Velds, A.; Groothuis, T.; Kerkhoven, R.; Nieuwland, M.; Ovaa, H.; Rottenberg, S.; van Tellingen, O.; Janssen, J.; Huijgens, P.; Zwart, W.; Neefjes, J. Nat. Commun. 2013, 4, 1908.
(34) Goldstein, S.; Czapski, G. Free Radicals: A Practical Approach; IRL Press at Oxford University Press: New York, 1996.
(35) Arkin, M. R.; Stemp, E. D. A.; Turro, C.; Turro, N. J.; Barton, J. K. J. Am. Chem. Soc. 1996, 118, 2267.
(36) Liu, Z.-C.; Wang, B.-D.; Yang, Z.-Y.; Li, Y.; Qin, D.-D.; Li, T.-R. Eur. J. Med. Chem. 2009, 44, 4477.
(37) Chen, J.; Ren, X.; Le, X.; Feng, X. Chin. J. Chem. 2010, 28, 2179.
(38) Le, X. Y.; Gu, Q.; Song, Z. J.; Zhuang, C. X.; Feng, X. L. J. Coord. Chem. 2007, 60, 1359.
(39) Rao, R.; Patra, A. K.; Chetana, P. R. Polyhedron 2008, 27, 1343.
(40) Terenzi, A.; Tomasello, L.; Spinello, A.; Bruno, G.; Giordano, C.; Barone, G. J. Inorg. Biochem. 2012, 117, 103.
(41) Patra, A. K.; Bhowmick, T.; Roy, S.; Ramakumar, S.; Chakravarty, A. R. Inorg. Chem. 2009, 48, 2932.
(42) Thomas, A. M.; Nethaji, M.; Chakravarty, A. R. J. Inorg. Biochem. 2004, 98, 1087.
(43) Liu, J.-G.; Zhang, Q.-L.; Shi, X.-F.; Ji, L.-N. Inorg. Chem. 2001, 40, 5045.
(44) Jaenisch, R.; Bird, A. Nat. Genet. 2003, 33, 245.
(45) Spruijt, Cornelia G.; Gnerlich, F.; Smits, Arne H.; Pfaffeneder, T.; Jansen, Pascal W. T. C.; Bauer, C.; Münzel, M.; Wagner, M.; Müller, M.; Khan, F.; Eberl, H. C.; Mensinga, A.; Brinkman, Arie B.; Lephikov, K.; Müller, U.; Walter, J.; Boelens, R.; van Ingen, H.; Leonhardt, H.; Carell, T.; Vermeulen, M. Cell 2013, 152, 1146.
(46) Prisecaru, A.; Devereux, M.; Barron, N.; McCann, M.; Colleran, J.; Casey, A.; McKee, V.; Kellett, A. Chem. Commun. 2012, 48, 6906.
(47) Rhee, S.; Chang, T.-S.; Jeong, W.; Kang, D. Mol. Cells 2010, 29, 539. Article 5404.

Appendix A.

Copper Phenanthrene Oxidative Chemical Nucleases

A-1: Electrogram and electropherogram data from the Bioanalyzer 2100

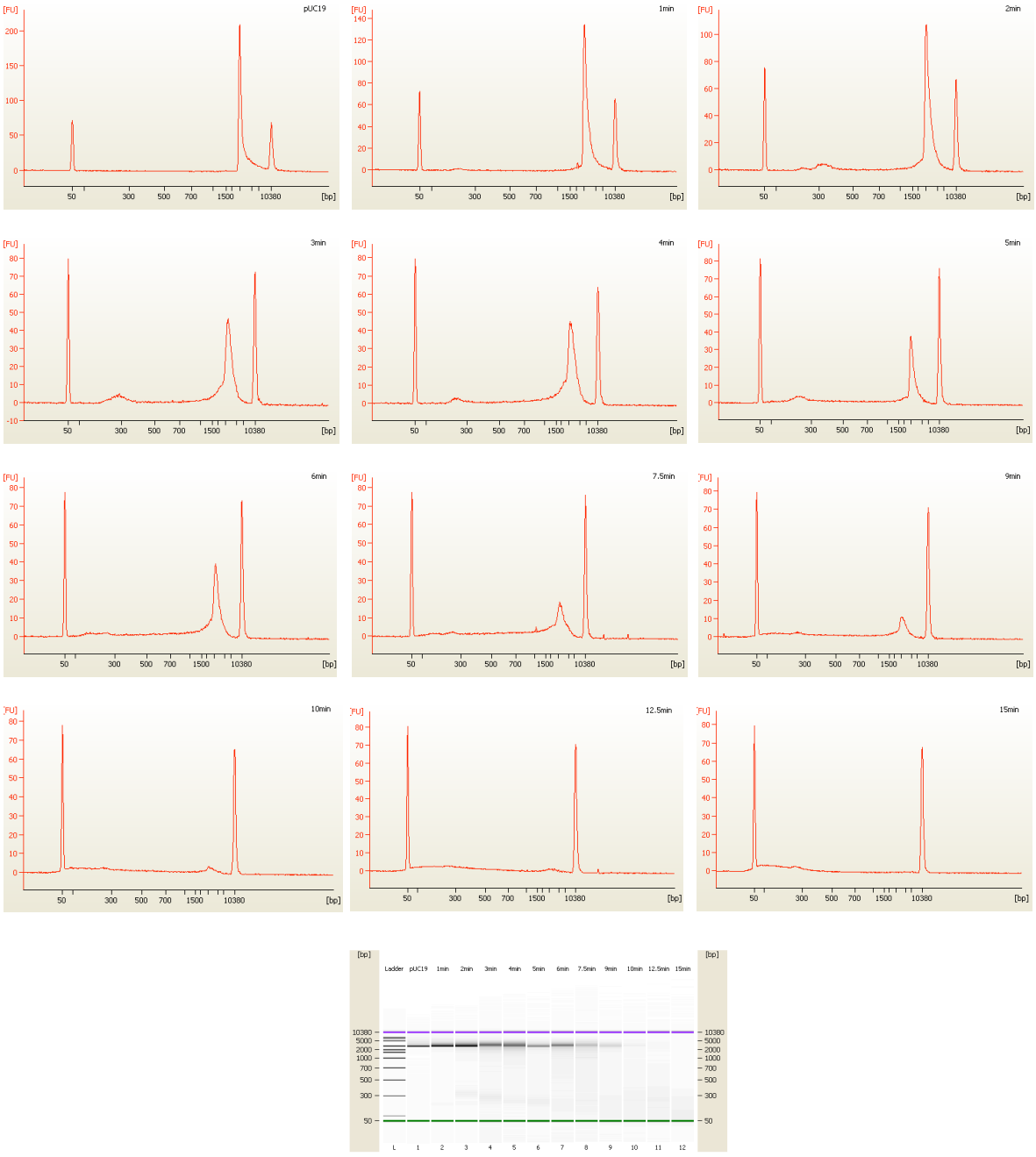

Figure A-1. Individual electrograms and electropherogram of linearized pUC19 (400 ng) exposed to Cu-Phen (500 nM) in the presence of 1 mM Na-L-ascorbate between 0-15 min generated by a single micofluidic chip. Triplcate microfluidic chips (DNA 7500) were run for each sample.

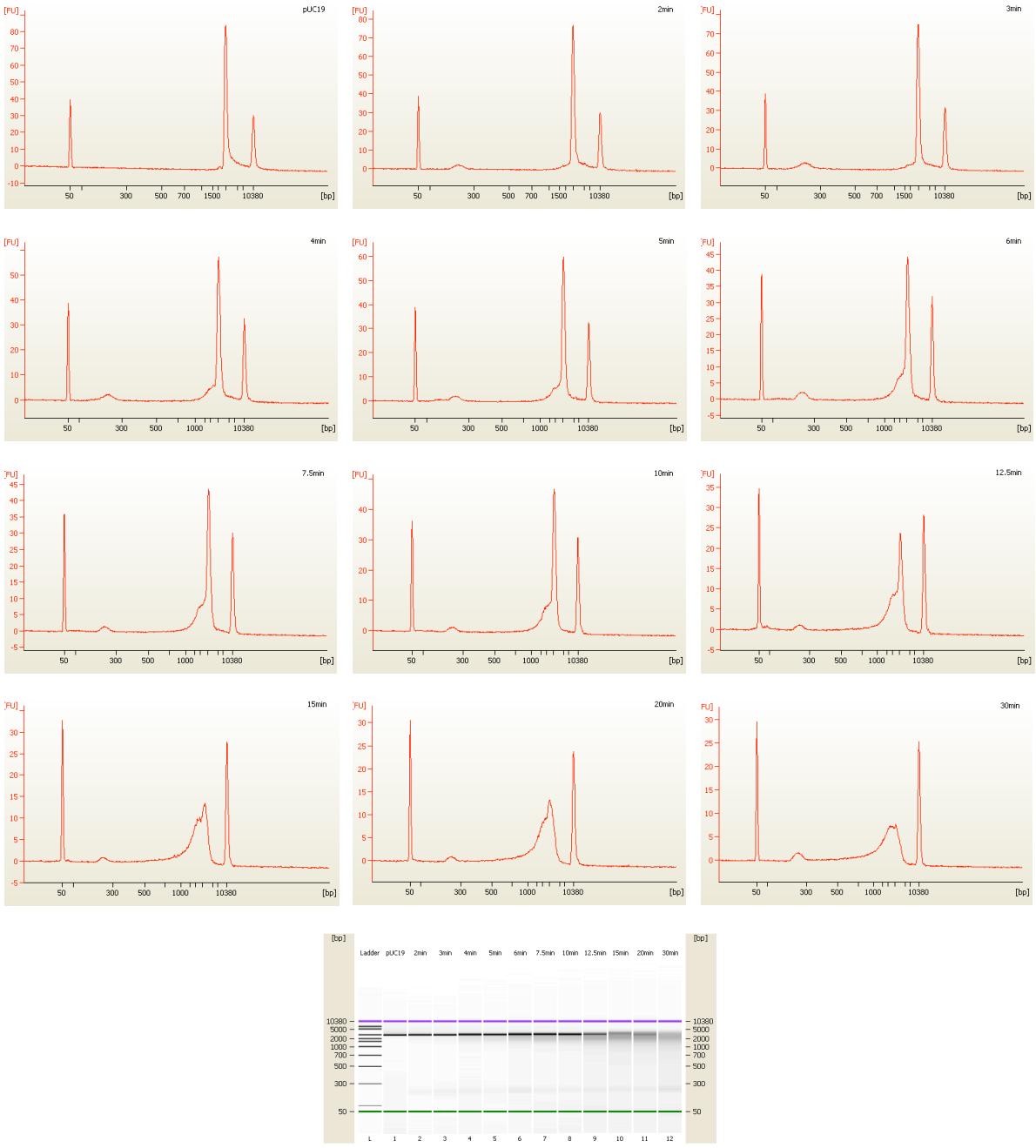

Figure A-2. Individual electrograms and electropherogram of linearized pUC19 (400 ng) exposed to Cu-DPQ-Phen (500 nM) in the presence of 1 mM Na-L-ascorbate between 0-15 min generated by a single micofluidic chip. Triplcate microfluidic chips (DNA 7500) were run for each sample.

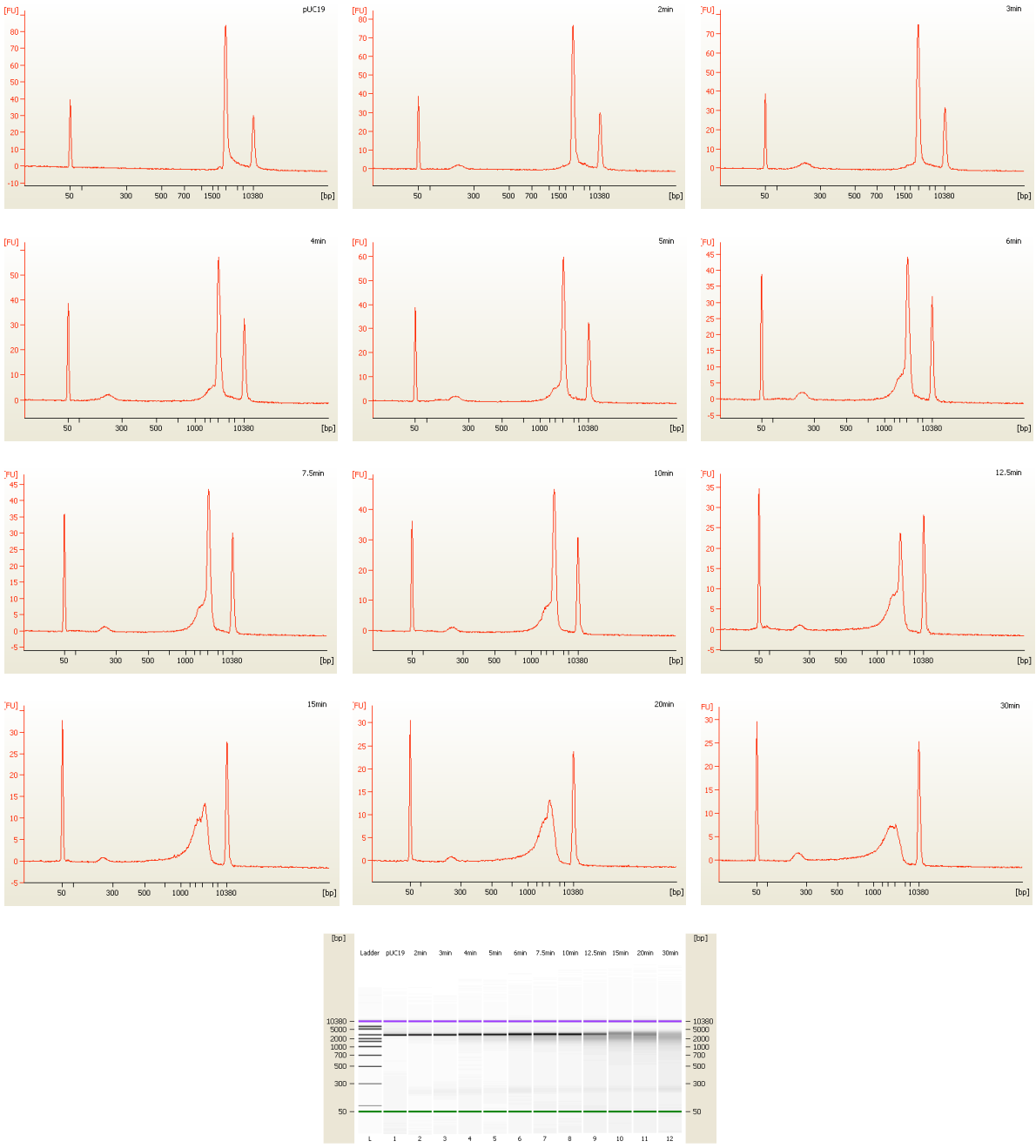

Figure A-3. Individual electrograms and electropherogram of linearized pUC19 (400 ng) exposed to Cu-DPPZ-Phen (500 nM) in the presence of 1 mM Na-L-ascorbate between 0-30 min generated by a single micofluidic chip. Triplcate microfluidic chips (DNA 7500) were run for each sample.

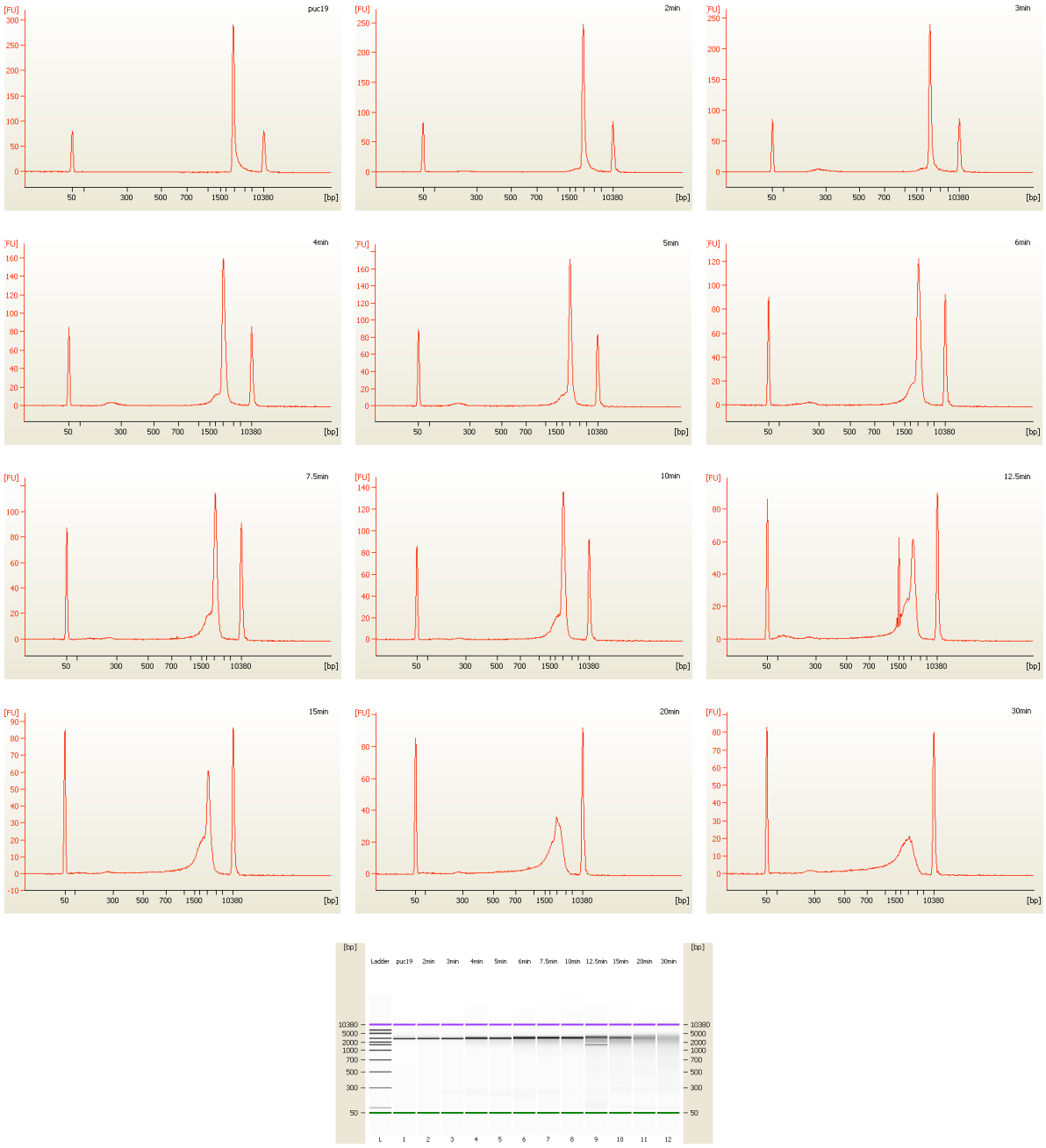

Figure A-4. Individual electrograms and electropherogram of linearized pUC19 (400 ng) exposed to **Cu-DPPN-Phen** (500 nM) in the presence of 1 mM Na-L-ascorbate between 0-30 min generated by a single micofluidic chip. Triplcate microfluidic chips (DNA 7500) were run for each sample.

A-2: Optimization of thermal melting on poly[d(A-T)$_2$] and poly[d(G-C)$_2$]

Overview. In order to examine the stabilization effects on poly[d(G-C)$_2$] and poly[d(A-T)$_2$], a series of optimisation experiments were conducted to identify the most suitable pH and ionic buffer strength required (ESI). Previous reports on drug binding effects to G-C polynucleotides, where strands are bound through three hydrogen bonds at each base pair, could not be identified owing to polymer stabilization beyond the limit of detection (>110°C). In our experiments, suitable conditions for the melting of poly[d(G-C)$_2$] (T_M = 80.74°C) were found at pH 5.0 in 2.0 mM sodium acetate buffer containing 1.0 mM NaCl. In order to maintain similar experimental conditions for the thermal melting on poly[d(A-T)$_2$], where strands are bound through two hydrogen bonds between each base pair only, pH 5.0 sodium acetate buffered (50 mM) solutions containing 250 mM of NaCl were employed for the thermal melting of this polynucleotide (T_M = 69.32°C).

poly[d(G-C)$_2$]. It was necessary to carry out experimental optimisation before commencing thermal melting analysis as it was noted in literature previously published, the T_M for poly(dG-dC)•poly(dC-dG) could not be determined as it was beyond the level of detection, in some cases >110°C.[1,2] Thermal melting analysis was initially investigated in potassium phosphate buffer at pH 7.2 with varying NaCl concentrations of 0.1 mM, 1 mM and 2 mM generating T_M values of 90.60°C, 89.57°C and 91.52°C for the untreated polymer, respectively. It was therefore necessary to identify conditions where the T_M of poly[d(G-C)$_2$] would be lower prior to the addition of any stabilizing test compound. Varying concentrations (2.0 – 5.0 mM) of sodium acetate buffer (NaOAc) at pH 5.0 were then investigated in the presence and absence of added NaCl (Table A-1). 2.0 mM NaOAc buffer with 1.0 mM of added NaCl gave a favourable T_M value of 80.74°C which was used in all thermal denaturation studies.

Table A-1. Thermal melting analysis of poly[d(G-C)$_2$] under alternating buffer, pH and ionic strength.

Buffer	Buffer (mM)	Added NaCl (mM)	T_M (°C)
Phosphate (pH 7)	50	0.1	90.60
	50	1.0	89.57
	50	2.0	91.52
NaOAc (pH 5)	2	0.0	73.02
	2	1.0	80.74
	2.5	0.0	89.02
	5	0.0	86.02

poly[d(A-T)$_2$]. The thermal melting was also investigated in both potassium phosphate (pH 7.0) and NaOAc (pH 5.0) buffers with varying ionic strength. At pH 7.0 the T_M of poly[d(A-T)2] in both the presence and absence of additional NaCl was 59°C and 59.27°C respectively (Table A-2). As experimental conditions for poly[d(G-C)$_2$] were carried out in pH 5.0 sodium acetate buffer, it was necessary to optimise similar conditions for this nucleotide for comparative reasons. The T_M of poly[d(A-T)$_2$] in NaOAc buffer over the concentration range of 100 mM to and 1.0 M NaCl produced an upward trend in T_M, confirming thermal stabilization is directly related to the logarithm of the salt concentration up to ~1 M NaCl.[3,4] poly[d(A-T)$_2$] thermal melting experiments were selected to be carried out in 50 mM NaOAc buffer at pH 5.0 with 250 mM of added NaCl.

Table A-2. Thermal melting analysis of poly[d(A-T)$_2$] under alternating buffer, pH and ionic strength.

Buffer	Buffer (mM)	Added NaCl (mM)	T_M (°C)
Phosphate (pH 7)	50	0.0	59.00
	50	2.0	59.27
NaOAc (pH 5)	2.0	0.0	25.52
	50	100	64.01
	50	250	69.32
	50	500	73.02
	50	750	75.22
	50	1000	76.47

A-3: Non-linear regression dose-response curves for cytotoxicity on SKOV3

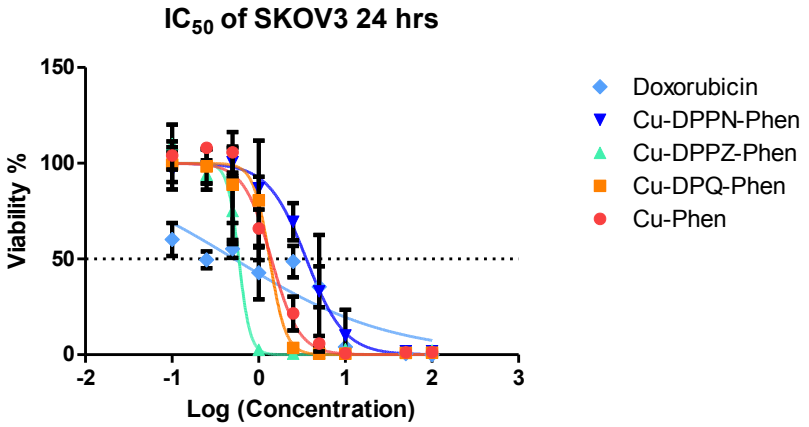

Figure A-5. Non-linear regression dose-response curves for **Cu-Phen** (red), **Cu-DPQ- Phen** (orange), **Cu-DPPZ-Phen** (green) and **Cu-DPPN-Phen** (light blue) and doxorubicin (dark blue). IC50 values were calculated from log concentrations equivalent to 0.1 - 100 μM.

A-4: References

(1) García, B.; Leal, J. M.; Ruiz, R.; Biver, T.; Secco, F.; Venturini, M. *J. Phys. Chem. B.,* **2010**, *114*, 8555.

(2) Saha, I.; Hossain, M.; Suresh Kumar, G. *J. Phys. Chem. B.,* **2010**, *114*, 15278.

(3) Wilson, D.; Tanious, F. A.; Fernandez-Saiz, M.; Rigl, C. T. In *Drug-DNA Interaction Protocols*; 1997; pp. 219–240.

(4) Doktycz, M. J. In *Encyclopedia of Life Sciences*; John Wiley & Sons, Ltd, 1997

CHAPTER III.

DNA oxidation profiles of copper phenanthrene chemical nucleases

---

This paper was published in *Frontiers in Chemistry*, 2015, 28, 1-9.

Zara Molphy, Creina Slator, Chryssostomos Chatgilialoglu and Andrew Kellett.

My contribution to this paper was to design and conduct DNA cleavage experiments including developing non-covalent recognition and polymerase chain reaction (PCR) inhibition assays. I also contributed toward the optimisation and examination of 8-oxo-dG through an ELISA assay with my co-worker Dr. Creina Slator.

III. 1. Abstract

The deleterious effects of metal-catalyzed reactive oxygen species (ROS) in biological systems can be seen in a wide variety of pathological conditions including cancer, cardiovascular disease, ageing, and neurodegenerative disorder. On the other hand however, targeted ROS production in the vicinity of nucleic acids – as demonstrated by metal-activated bleomycin – has paved the way for ROS-active chemotherapeutic drug development. Herein we report mechanistic investigations into the oxidative nuclease activity and redox properties of copper(II) developmental therapeutics $[Cu(DPQ)(phen)]^{2+}$ (Cu-DPQ-Phen), $[Cu(DPPZ)(phen)]^{2+}$ (Cu-DPPZ-Phen), and $[\{Cu(phen)_2\}_2(\mu$-terph)](terph) (Cu-Terph), with results being compared directly to Sigman's reagent $[Cu(phen)_2]^{2+}$ throughout (phen = 1,10-phenanthroline; DPQ = dipyridoquinoxaline; DPPZ = dipyridophenazine). Oxidative DNA damage was identified at the minor groove through use of surface bound recognition elements of methyl green, netropsin, and $[Co(NH_3)_6]Cl_3$ that functioned to control complex accessibility at selected regions. ROS-specific scavengers and stabilisers were employed to identify the cleavage process, the results of which infer hydrogen peroxide produced metal-hydroxo or free hydroxyl radicals ($^{\bullet}OH$) as the predominant species. The extent of DNA damage owing to these radicals was then quantified through 8-oxo-2'-deoxyguanosine (8-oxo-dG) lesion detection under ELISA protocol with the overall trend following Cu-DPQ-Phen > Cu-Terph > Cu-Phen > Cu-DPPZ. Finally, the effects of oxidative damage on DNA replication processes were investigated using the polymerase chain reaction (PCR) where amplification of 120 base pair DNA sequences of varying base content were inhibited – particularly along A-T rich chains – through oxidative damage of the template strands.

III. 2. Introduction

Oxygen radical generation is an inevitable consequence of aerobic existence and has been implicated in a wide variety of pathological conditions including cancer, cardiovascular disease, ageing, and neurodegenerative disease (Cooke & Evans, 2007). Reactive oxygen species (ROS) are created in a variety of endogenous chemical and biological processes in the human body – predominantly through oxygen metabolism. The sequential reduction of molecular oxygen can generate reactive intermediates such as superoxide ($O_2^{\bullet-}$) and hydrogen peroxide (H_2O_2) that initiate a cascade of redox reactions toward the production of hydroxyl radicals ($^{\bullet}OH$) and related metal-oxo species (Kellett et al., 2012). Molecular targets of ROS include proteins, lipids, and nucleic acids – the deleterious effects of which

include base and deoxyribose modifications that ultimately precipitate single or double strand breaks. To counteract this, the majority of cells possess defence mechanisms such as base excision repair (BER) – *e.g.* 8-oxoguanine glycosylase (OGG1) (Xu et al., 2014) – and nucleotide excision repair (NER) pathways that prevents genome instability to ultimately limit cytotoxicity, the accumulation of deleterious mutations, and maintain genome integrity. Two major $^{\bullet}$OH induced DNA lesions are 8-oxoguanine (8-oxo-dG), a mutagenic lesion which induces G → T transversions widely seen in mutated oncogenes and tumour suppressor genes, and the poorly mutagenic thymine glycol (Basu, Loechler, Leadon, & Essigmann, 1989; Chatgilialoglu & O'Neill, 2001). Recent evidence suggests $^{\bullet}$OH attacks occur primarily at base moieties and account for the majority of total hydrogen atom abstraction on DNA alone (Chatgilialoglu, Ferreri, & Terzidis, 2011). Thus, 8-oxo-dG has been subjected to intensive investigation due to its prominence as a biomarker within ROS-mediated disease pathology, and its ease of detection in bodily fluids and tissue samples has allowed a variety of detection methods to accurately assess 8-oxo-dG lesions including high-pressure liquid chromatography (HPLC), gas chromatography (GC), mass spectrometry (MS), and the enzyme linked immunosorbent assay (ELISA).

In addition to the induction of endogenous DNA damage, exogenous sources including UV light, ionizing radiation, environmental agents, pharmaceuticals, and industrial chemicals can also initiate ROS production (Klaunig, Kamendulis, & Hocevar, 2010). Indeed the clinical antineoplastic agent bleomycin (BLM) is a redox active agent capable of DNA oxidative cleavage in the presence of Fe(II) (and Cu(I)), molecular oxygen, and endogenous one electron reductants (Burger, 1998; Stubbe and Kozarich, 1987; Chen et al., 2008). Bleomycin can abstract hydrogen atoms from deoxyribose in the DNA backbone, specifically from C4' position (Breen and Murphy, 1995). The active form of Fe(II)-BLM is a ternary, high-valence Fe(III)-O$^{\bullet}$ species (Rodriguez and Hecht, 1982; Gajewski et al., 1991; Pratviel and Bernadou, 1989) that undergoes an electron reduction by endogenous reductants (*e.g. L*-ascorbate) or by another molecule of Fe(II)-BLM (Burger et al., 1981; Natrajan et al., 1990). Fe(II)-BLM can form 8-oxo-dG and other base propenals, however these are known to occur in small amounts; the formation of such DNA degradation products results from $^{\bullet}$OH oxidative damage – a side product only of the ferryl-oxo species – that does not functionally contribute to biological systems or participate in the nuclease activity of activated Fe(II)-BLM (Rodriguez and Hecht, 1982).

Our group have recently investigated a range of $[Cu(phen)_2]^{2+}$ (Cu-Phen) (Phen = 1,10-phenanthroline) type systems as potential lead compounds for therapeutic and biochemical application (Kellett et al., 2011; Prisecaru et al., 2012; 2013; Molphy et al., 2014). $[Cu(phen)_2]^{2+}$, originally reported by Sigman *et al.* (Sigman, Graham, Aurora, & Stern, 1979), is believed to cleave DNA through a variety of copper bound oxidants including Cu^{3+}-OH and Cu^{+}-OOH with the possibility of free $^{\bullet}OH$ playing a role in the overall process (Johnson & Nazhat, 1987; Marshall, Graham, Reich, & Sigman, 1981). Recent work on the development of bis-chelate Cu^{2+} phenanthroline-phenazine cationic complexes of $[Cu(DPQ)(phen)]^{2+}$ (Cu-DPQ-Phen) and $[Cu(DPPZ)(phen)]^{2+}$ (Cu-DPPZ-Phen) (DPQ = dipyridoquinoxaline; DPPZ = dipyridophenazine) have demonstrated how extension of the ligated phenazine ligand influences DNA recognition and oxidative degradation (Molphy et al., 2014). Indeed, when designer phenazine ligands (DPQ and DPPZ) are incorporated into the 'copper bis-phen' chemical nuclease model, these agents display enhanced DNA recognition and intercalation among the highest reported on ctDNA (**Table III-1**, $K_{app} \approx 3 \times 10^7$ $M(bp)^{-1}$). Since nuclearity is also established as an important factor in oxidative DNA cleavage (van der Steen et al., 2010; Li et al., 2005), we also reported the dinuclear complex, $[\{Cu(phen)_2\}_2(\mu\text{-terph})](terph)$ (Cu-Terph) (terph = terephtalate), which is capable of inducing oxidative DNA strand breaks in the absence of exogenous reductant (Kellett et al., 2011). Cu-Terph has promising *in vitro* cytoxicity toward human derived breast, prostate, colon, ovarian, and lung human cance cell lines, with comparable activity to mitoxantrone – a clinincal anthracene topoisomerase II inhibitor (Kellett et al., 2011; Prisecaru et al., 2012).

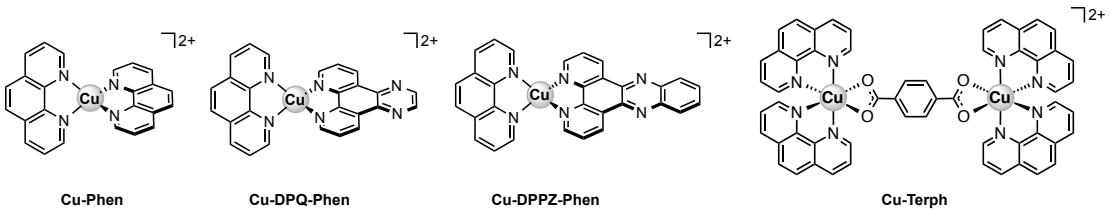

Scheme III-1. Molecule structures of the copper(II) complex cations examined in this study.

Table III-1. Summary of DNA binding properties of tested complexes toward calf thymus DNA (ctDNA) along with synthetic nucleic acid polymers poly[d(A-T)$_2$] and poly[d(G-C)$_2$].

Compound	C_{50} [a]	K_{app} M(bp)$^{-1}$ [b]	*Q* (μM) poly[d(A-T)$_2$][c]	*Q* (μM) poly[d(G-C)$_2$][c]	ΔT_M (°C) poly[d(A-T)$_2$][d]	ΔT_M [a] (°C) poly[d(G-C)$_2$][d]
Cu-Phen	179.21	0.67×10^6	13.34	7.96	-0.02 ± 0.29	06.64 ± 1.58
Cu-DPQ-Phen	3.93	30.45×10^6	8.34	3.97	0.60 ± 0.18	11.39 ± 1.10
Cu-DPPZ-Phen	4.63	25.85×10^6	11.60	10.12	0.50 ± 0.10	10.44 ± 1.10
Cu-Terph	39.36	0.30×10^6	8.6	10.3	NT	NT

[a] C_{50} = concentration required to reduce 50% fluorescence of saturated bound ethidium bromide (12.6 μM) on ctDNA (10 μM).
[b] $K_{app} = K_e \times 12.6/C_{50}$ where $K_e = 9.5 \times 10^6$ M(bp)$^{-1}$ (apparent binding constant on ctDNA).
[c] Fluorescence Quenching (*Q*) of limited bound Ethidium Bromide (5 μM) bound poly[d(A-T)$_2$] and poly[d(G-C)$_2$] by Cu^{2+} complexes.
[d] ΔT_M = difference in thermal melting (T_M) of drug-treated nucleotide at $r = 0.1$ compared with drug-untreated nucleotide.
NT = not tested.

In this contribution we identify, using head-to-head analysis, the comparative oxidative DNA cleavage properties of DNA binding Cu^{2+} complexes Cu-Phen, Cu-DPQ-Phen, Cu-DPPZ-Phen, and Cu-Terph (**Scheme III-1**) through a variety of biophysical and molecular biological methods. Additionally, we report these agents inhibit DNA polymerase activity—particularly at A-T rich sites—through oxidative degradation of template strands. To that end, we report *i.*) oxidative DNA profiles in the presence of DNA recognition agents of netropsin, methyl green, and $[Co(NH_3)_6]Cl_3$, *ii.*) DNA cleavage profiles in the presence of radical trapping and stabilising co-factors, *iii.*) quantitation of 8-oxo-dG lesions arising from complex treated superhelical plasmid DNA, and *iv.*) DNA polymerase inhibition on DNA templates of differential A-T content. The DNA binding profiles for this series have previous been reported and are summarised in Table 1 (McCann et al., 2013; Molphy et al., 2014; Kellett et al., 2011; Prisecaru et al., 2013); simple phenanthroline containing complexes (Cu-Phen and Cu-Terph) have moderate binding constants toward ctDNA while phenazine compounds (Cu-DPQ-Phen and Cu-DPPZ-Phen) can be considered as high-affinity dsDNA intercalators. Further, ethidium bromide fluorescence quenching on alternating duplex polymers—poly[d(A-T)$_2$] and poly[d(G-C)$_2$]—has shown complexes bind at both minor and major grooves. It has not been established, as yet, if chemical nuclease activity occurs preferentially at either or both recognition sites.

III. 3. Materials and Methods

III. 3.1. Preparation of the complexes

Chemicals were purchased from Sigma-Aldrich Ireland and used without further purification.

DPQ and DPPZ ligands were initially generated through the Schiff base condensation reactions of 1,10-phenanthroline-5,6-dione with ethylenediamine and *o*-phenylenediamine respectively. The bis-phenanthroline complex $[Cu(phen)_2](NO_3)_2$ (Cu-Phen) was prepared by refluxing 1,10-phenanthroline with copper(II) nitrate in a 2:1 molar ratio in aqueous-ethanol (Prisecaru et al., 2013). The phenazine complexes $[Cu(DPQ)(Phen)](NO_3)_2$ (Cu-DPQ-Phen) and $[Cu(DPPZ)(Phen)](NO_3)_2$ (Cu-DPPZ-Phen) were prepared by treating the mono-phenanthroline complex $[Cu(Phen)](NO_3)_2$ with 1 molar equivalent of the corresponding phenazine ligand in ethanol (Molphy et al., 2014). The $[Cu_2(\mu\text{-terephthalate})(1,10\text{-phen})_4]^{2+}$ was prepared by ethanolic reflux of copper(II) terephthalate hydrate and 1,10-phenanthroline in a 1:2 ratio according to the reported method (Kellett et al., 2011).

III. 3.2. DNA cleavage studies

III. 3.2.1. DNA cleavage in the presence of added reductant

The ability of the complexes to oxidatively damage DNA in the presence of added reductant was determined using a method previously published by this laboratory with minor changes (Molphy et al., 2014). Reactions were carried out according to the following general procedure: in a total volume of 20 µL using 80 mM HEPES buffer (pH 7.2) with 25 mM NaCl, 1 mM Na-L-ascorbate, 400 ng superhelical pUC19 (NEB, N3041) and varying concentrations of test complex (250 nM, 500 nM, 1 µM and 2.5 µM). Complexes were initially prepared in DMF and further diluted in HEPES buffer (Fisher). Samples were incubated at 37°C for 30 minutes. Reactions were quenched by adding 6× loading buffer (Fermentas) containing 10 mM Tris-HCl, 0.03 % bromophenol blue, 0.03 % xylene cyanole FF, 60 % glycerol, 60 mM EDTA and samples were loaded onto an agarose gel (1.2 %) containing 8 µL EtBr. Electrophoresis was completed at 70 V for 2 hours in 1× TAE buffer.

III. 3.2.2. DNA cleavage in the presence of non-covalently bound recognition elements

This protocol was adapted from a previously reported procedure (Tabassum *et al.,* 2012). Briefly, 400 ng pUC19 was incubated with 25 mM NaCl, 1 mM Na-L-ascorbate, and 8, or 16 μM of either methyl green, netropsin or hexamine cobalt(III) chloride in 80 mM HEPES buffer (pH 7.2) for 45 minutes at 37°C. Sample tubes were then vortexed and varying concentrations of test complex were added (250 nM, 500 nM, 1 μM and 2.5 μM). The reaction mixture was further incubated at 37°C for 30 minutes. The reaction was then quenched with 6× loading buffer and subjected to gel electrophoresis (prepared and stained as previously described).

III. 3.2.3. DNA oxidation with ROS scavengers and stabilisers

The presence of ROS specific scavengers was used to determine the effect on the DNA cleavage abilities of each copper complex. The procedure was adapted to the previously reported method (Zhou et al., 2014). Briefly, to a final volume of 20 μL, 80 mM HEPES (pH = 7.2), 25 mM NaCl, 1 mM Na-L-ascorbate, and 400 ng of pUC19 DNA were treated with drug concentrations of 250 nM, 500 nM, 1 μM and 2.5 μM in the presence ROS scavengers / stablilisers; KI (10 mM), NaN_3 (10 mM), DMSO (10 %), and D_2O (77 %). Reactions were incubated for 30 min at 37^{o}C, quenched with DNA loading dye and loaded onto 1.2 % agarose gel and run under conditions previously described.

III. 3.3. HT quantitation of 8-oxo-dG

Quantitation of 8-oxo-dG lesions present in 3000 ng pUC19 plasmid DNA pre-incubated with test complexes (10 and 20 μM) at 37°C for 30 minutes was achieved utilising a high throughput 8-oxo-dG ELISA kit (Trevigen) and performed as per manufacturers guidelines. Samples of damaged DNA were examined in triplicate using a 96 well plate, pre-coated with 8-oxo-dG along with varying concentrations of a standard 8-oxo-dG (200, 100, 50, 25, 12.5, 6.25 and 3.13 nM). An 8-oxo-dG monoclonal antibody, which competitively binds to 8-oxo-dG immobilized to each well, was added to the plate with excess antibody being washed with PBST (1× PBS, 0.1% Tween 20). The concentration of 8-oxo-dG was determined based on antibody retention in each well using goat anti-mouse IgG-HRP conjugated antibody and colorimetric detection substrate TACS-Sapphire. Product formation was inversely proportional to 8-oxo-dG present in the DNA sample. Samples were determined using a Bio-Tek synergy HT multimode microplate reader at 450 nm and quantitation of 8-oxo-dG was extrapolated from the standard curve.

III. 3.4. PCR inhibition studies

This protocol was adapted from a previously reported procedure (Sanchez-Cano et al., 2010). 400 ng pUC19 DNA was initially exposed to each test complex in the presence and absence of 1 mM added reductant at 37°C for 30 minutes (**Figure B-2** and **B-3**). 20 ng of damaged DNA template was removed and PCR reactions (35 cycles) were carried out with each varying G-C content primer set (**Figure B-4**) at optimum annealing temperatures and analysed using gel electrophoresis. This investigation was replicated in the absence of added reductant (Figure B-5) and also at lower drug loading (250 nM, 500 nM, 1 μM and 2.5 μM) with 1 mM reductant (Figure B-6).

III. 4. Results and Discussion

III. 4.1. DNA cleavage in the presence of non-covalently bound recognition elements

We have previously shown that DNA oxidative cleavage by copper complexes is dependent on a range of factors including (but not limited to): plasmid DNA conformation and type, presence of competing metal chelating agents (*e.g.* EDTA), reaction / exposure time, and presence / concentration of exogenous reductant or oxidant. In the current work we examine chemical nuclease activity of supercoiled pUC19 plasmid DNA in the presence of 1 mM reductant (Na-L-ascorbate) using agarose gel electrophoresis. In order to ensure the copper(I) active species (i.e. the nuclease) was fully generated, each complex was initially reduced with 1 mM of added reductant prior to pUC19 titration. Relaxation of supercoiled (SC, FI) pUC19 DNA into open circular (OC, FII) and linear (LC, FIII) conformations was employed to qualitatively measure the cleavage efficiency of complexes over a concentration range of 250 nM, 500 nM, 1.0 μM and 2.5 μM for 30 minutes at 37 °C (Figure III-1 A-D, lanes 1-4). Complexes show concentration-dependent relaxation of FI (superhelical) to FII (open circular / nicked), while FIII (linear conformation) is evident at 2.5 μM Cu-DPQ-Phen exposure and with 500 nM of the dinuclear agent Cu-Terph. Complete digestion of SC DNA occurs only with the maximum tested concentration (2.5 μM) of Cu-Terph. The overall trend in chemical nuclease activity is Cu-Terph > Cu-DPQ-Phen > Cu-Phen > Cu-DPPZ-Phen. The activity profiles observed here are in good agreement with those previously reported by this group; Cu-Terph has previously displayed nicking at 1.0 μM on the plasmid pBR322 with complete digestion occurring thereafter (Prisecaru et al., 2012). We also established that both 2.5 and 5.0 μM of Cu-Phen induced nicking (OC) on both pBR322 (McCann et al., 2013; Prisecaru et al., 2012) with activity being impeded in the presence of EDTA (Prisecaru et al., 2013). The

nuclease activity of both Cu-DPQ-Phen and Cu-DPPZ-Phen has been identified previously (Molphy et al., 2014), however, direct analysis with the current conditions cannot be made.

In an attempt to determine DNA cleavage site specificity, minor groove (netropsin, Net) and major groove (methyl green, MG) binders, along a surface electrostatic binding and condensing agent ($[Co(NH_3)_6]Cl_3$, Co(III)) were pre-incubated with pUC19 DNA prior to the addition of test complex (Figure III-1 A-D, lanes 5-16). In all cases, presence of the major groove binder MG enhanced chemical nuclease activity with greater nicking (OC) and linearisation (LC) frequency compared with control experiments. Conversely, the minor groove binder Net impedes chemical nuclease activity as pUC19 is clearly protected from both OC and LC damage across all experiments. The cationic surface binding agent $[Co(NH_3)_6]^{3+}$ had no major impact on the chemical nuclease activity of Cu-Phen and Cu-DPPZ-Phen but did reduce nicking by Cu-DPQ-Phen at 1 μM and was also effective in protecting pUC19 damage by Cu-Terph. Taken together, evidence here points toward the minor groove as the major site of DNA oxidation by this complex series; MG bound pUC19 primes the minor groove for chemical nuclease activity while titrated Net clearly diminishes this damage. Indeed this observation of minor groove targeting is consistent with previous analysis on the rapid cleavage of poly(dA-dT) by 2:1 phenanthroline-Cu^+ mixtures (Sigman et al., 1979).

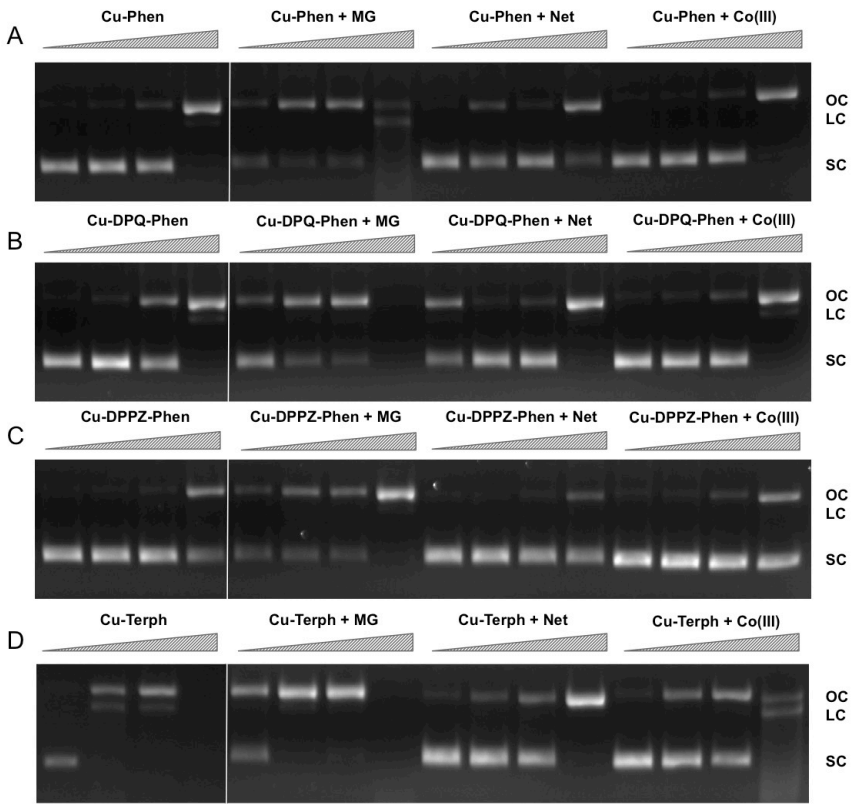

Figure III-1. Lane 1-4 (A-D) DNA cleavage reactions with 250 nM, 500 nM, 1.0 μM and 2.5 μM test complex (**A**: Cu-Phen, **B**: Cu-DPQ-Phen, **C**: Cu-DPPZ-Phen and **D**: Cu-Terph), 400 ng superhelical pUC19 and 1 mM added Na-L-ascorbate incubated at 37°C for 30 minutes. Lanes 5-16 (A-D) DNA cleavage reactions in the presence of recognition elements, methyl green (MG), netropsin (Net) and $[Co(NH_3)_6]Cl_3$ (Co(III)), where 400 ng pUC19 was initially pre-treated with 8 μM of respective non-covalent binding control at 37°C for 45 minutes and then with 250 nM, 500 nM, 1 μM and 2.5 μM test complex in the presence of 1 mM added Na-L-ascorbate at 37°C for 30 minutes.

III. 4.2. DNA oxidation with ROS scavengers and stabilisers.

In order to examine ROS species involved in DNA oxidation, activity was investigated in the presence of radical-specific scavengers and stabilisers (Table 2) with results shown in Figure III-2. Before complex analysis, scavengers were confirmed to have no impact on pUC19 conformation (data not shown). Control experiments are in excellent agreement with those observed in **Figure III-1** (lanes 1-4), however, a fraction of superhelical (FI) pUC19 was found to remain upon 2.5 μM exposure of Cu-Phen. Results here suggest that $^{\bullet}OH$ is the most prevalent radical species involved in strand scission as the presence of DMSO considerably impedes cleavage activity of all complexes. It is noteworthy DMSO had a major impact on cleavage activity of Cu-Terph as only the maximum tested concentrations (1.0 and 2.5 μM) contained nicked cleavage products. The presence of the H_2O_2 scavenger, KI, was also found to inhibit chemical nuclease activity of tested complexes—again most notably within Cu-Terph reactions—and this observation is consistent with previous trapping studies conducted on these model systems (Johnson & Nazhat, 1987; Prisecaru et al., 2013). It is interesting to note the catalase enzyme is a more effective scavenger of H_2O_2 compared with KI as previous work revealed complete inhibition of DNA oxidation by Cu-Phen, Cu-DPQ-Phen, and Cu-DPPZ-Phen complexes (Molphy et al., 2014).

The role of $^1O_2$ was next examined utilising the NaN_3 scavenger (Franco et al., 2007) and D_2O as a $^1O_2$ stabiliser (Merkel et al., 1972; Xia et al., 2006). Nuclease activity by Cu-Phen, Cu-DPQ-Phen, and Cu-DPPZ-Phen complexes was only marginally inhibited by NaN_3 while no change in activity (relative to control) was observed in D_2O thus suggesting a limited role in DNA oxidation by $^1O_2$. NaN_3 did, however, impede activity by Cu-Terph but the role of $^1O_2$ in the scission process could not be verified as D_2O was also found to remove activity.

Table III-2. Scavengers and stabilisers utilised within this study.

Scavenger [a] / Stabiliser [b]	ROS	References
NaN_3 [a]	$^1O_2$	(Franco et al., 2007)
KI [a]	H_2O_2	(Dunand et al., 2007; Steffens et al., 2012)
DMSO [a]	$^{\bullet}OH$	(Franco et al., 2007; Mazzer et al., 2007)
D_2O [b]	$^1O_2$	(Merkel et al., 1972; Xia et al., 2006)

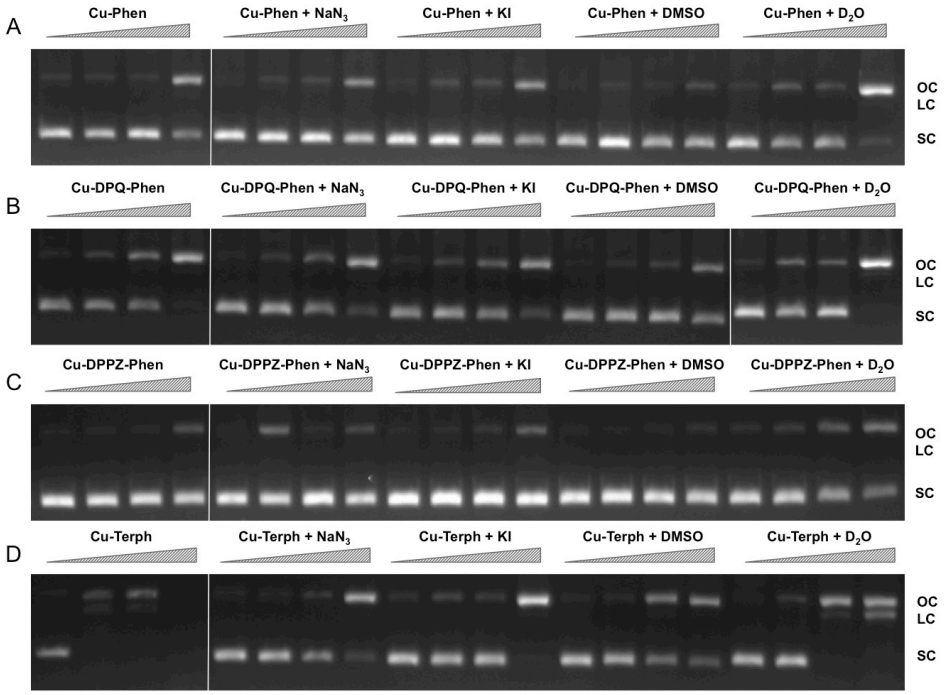

Figure III-2. DNA cleavage reactions in the presence of ROS scavengers. 400 ng of SC pUC19 was incubated for for 30 min at 37°C with 250 nM, 500 nM, 1 µM and 2.5 µM of test complex (**A**: Cu-Phen, **B**: Cu-DPQ-Phen, **C**: Cu-DPPZ-Phen and **D**: Cu-Terph) in the presence of 1 mM added Na-L-ascorbate for 30 minutes. Lanes 1-4 metal complex only, lanes 5-8: complex + 10 mM NaN_3, lanes 9-12: complex + 10 mM KI, lanes 13-16: complex + 10% DMSO, and lanes 17-20: complex + 77% D_2O.

III. 4.3. Quantitation of 8-oxo-dG

To examine if the oxidative DNA lesion, 8-oxo-dG, is formed during complex reactions with DNA, an HT 8-oxo-dG ELISA kit was employed for immunological detection and quantification. The complex series was investigated at 10 and 20 μM with 3000 ng of SC pUC19, with 8-oxo-dG being quantified in both nM and ng/mL (**Figure III-3**). Nuclease activity was firstly confirmed at 10 μM and 20 μM (**Figure B-1**). Low numbers of lesions were detected in the untreated control (3.92 ± 0.79 nM) and the exposure of pUC19 to each of the complexes at 10 μM resulted in detectable increases in 8-oxo-dG (between 35.24 – 5.05 nM) with the trend following Cu-Terph > Cu-DPPZ-Phen > Cu-DPQ-Phen > Cu-Phen. Upon 20 μM complex exposure significant levels of 8-oxo-dG (between 129.22 – 17.77 nM) were produced with the trend changing toward Cu-DPQ-Phen > Cu-Terph > Cu-Phen > Cu-DPPZ-Phen. Given the $^{\bullet}$OH radical is fundamental in the production of 8-oxo-dG, results here demonstrate DNA oxidation by copper phenanthrene complexes, particularly under extensive shearing conditions (**Figure B-1**), drive formation of 8-oxo-dG lesions.

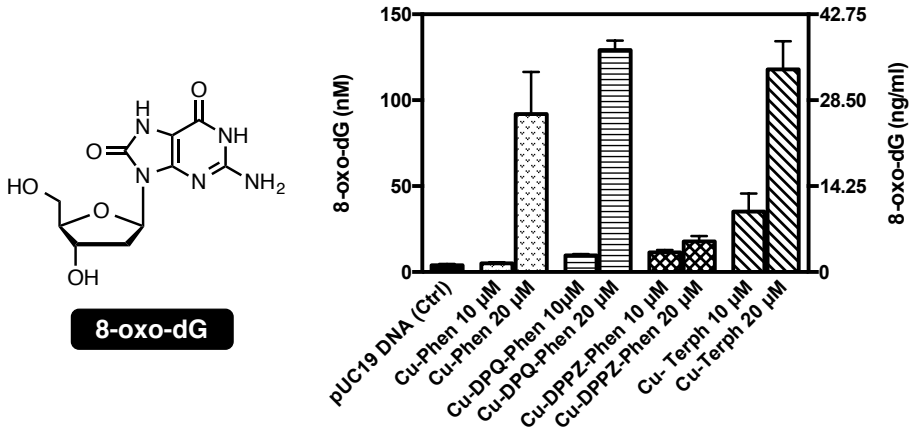

Figure III-3. Structure and quantification of 8-oxo-dG. Graph represents level of generated 8-oxo-dG as nM (left axis) and ng/mL (right axis). 3000 ng of SC pUC19 with 10 and 20 μM of test complexes Cu-Phen, Cu-DPQ-Phen, Cu-DPPZ-Phen and Cu-Terph with 1 mM Na-L-ascorbate were incubated at 37 °C for 30 minutes and followed by ELISA protocol.

III. 4.4. PCR inhibition studies

Our next aim was to investigate how oxidative lesions – induced through complex exposure – can ultimately impact on *in vitro* DNA processing by the polymerase chain reaction (PCR) (**Figure III-4**). During the normal PCR process, a DNA template is initially denatured through heating to more than 90°C to separate double stranded DNA into constituent single strands. The second step involves lowering the temperature (40 – 60°C) to allow specifically designed forward and reverse primers to anneal at targeted regions (for selective amplification) through complementary base pairing. At this point the temperature is increased again to allow Taq polymerase to attach at each priming site and extend to synthesise a new DNA strand. This thermal cycling process allows for a chain reaction to occur in which the selected DNA template is exponentially amplified creating millions of copies of the targeted sequence (**Figure III-4A**). In our study 400 ng of pUC19 plasmid DNA was initially exposed to increasing concentrations (2.5, 5, 10, 20, 30, 40 and 50 μM) of test complexes in the absence and presence of exogenous reductant at 37°C for 30 minutes and used as a substrate for the PCR reaction along with specific primer sets to generate three 120 bp sequences of varying G·C content (35%, 50% and 63%). PCR inhibition (up to 50 μM) was not achieved by any tested agent (Figure B-5) in the absence of added reductant indicating physical blocking of the PCR process (**Figure III-4B**) does not occur. With added reductant, however, the pattern emerges as described in **Figure III-4C**. In the high A·T amplification set (35% G·C), PCR was inhibited by 5.0 μM of the mono-nuclear complexes (Cu-Phen, Cu-DPQ-Phen and Cu-DPPZ-Phen). In the case of the di-nuclear agent (Cu-Terph), complete inhibition of template amplification was observed at all exposure levels (**Figure III-5A**). Within the 50% and 63% G·C templates (**Figure III-5 B** and **C** respectively), the PCR reaction was impeded at 5.0 μM for both Cu-DPQ-Phen and Cu-Terph complexes whereas template DNA, oxidatively damaged by 5.0 μM of Cu-Phen and Cu-DPPZ-Phen, was still suitable for amplifying 120 base pair DNA sequences.

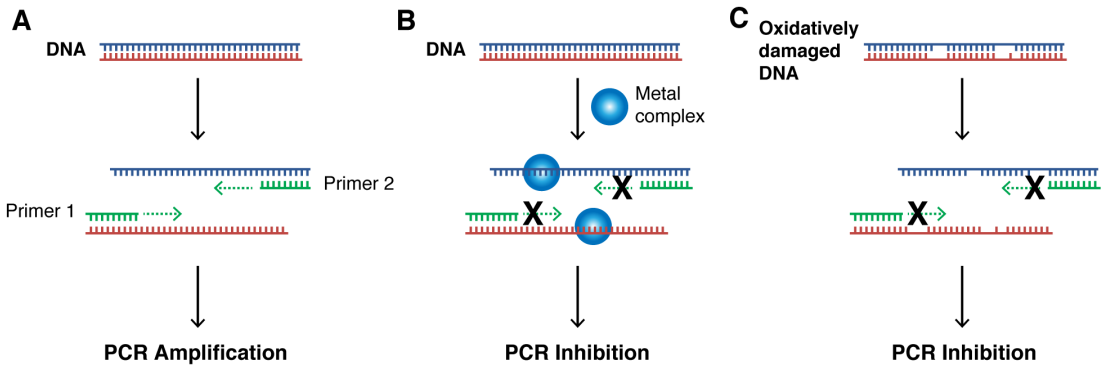

Figure III-4. A. Illustration of steps involved in a successful PCR reaction (denaturation, primer annealing, primer extension and template amplification), **B.** the impact of a bound metal complex as physical block of the primer extension step, **C.** inhibition of DNA amplification in the PCR cycle through the oxidative damage of template strand.

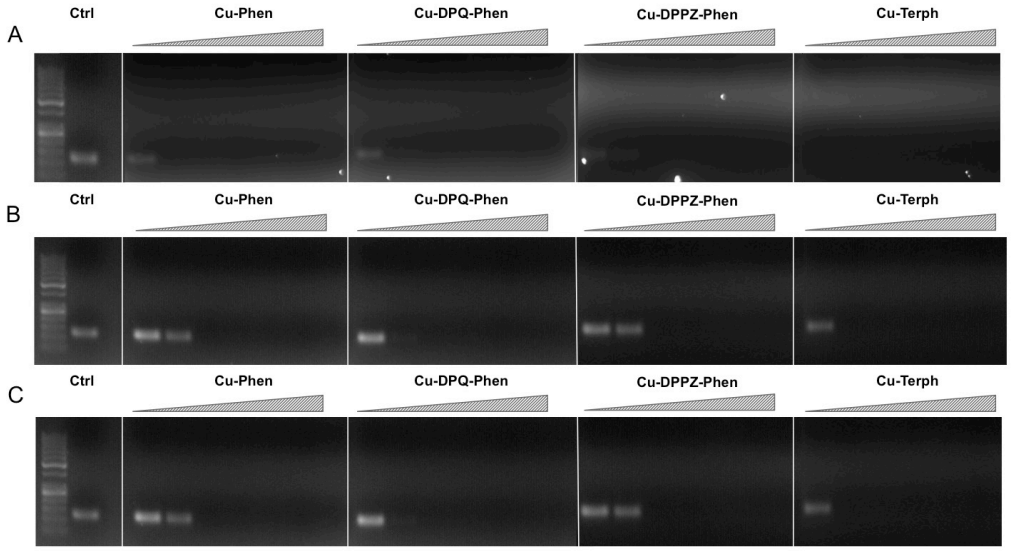

Figure III-5. 400 ng pUC19 DNA was initially exposed to 2.5, 5, 10, 20, 30, 40 and 50 µM of each test complex in the presence of 1 mM added reductant at 37°C for 30 minutes. 20 ng of damaged DNA template was removed and PCR reaction was carried out with each varying GC content primer set at optimum annealing temperatures and analysed using gel electrophoresis. Fig. **A** Lane 1: 35% GC control, lane 2-8 35% GC + Cu-Phen, lane 9-15 35% GC + Cu-DPQ-Phen and lane 15-21: 35% GC + Cu-Terph. Fig. **B** 50% GC and Fig. **C** 63% GC respectively. All sequences generated were 120 base pairs.

III. 5. Conclusions

Mechanistic investigations into oxidative cleavage properties of the copper(II) complex series $[Cu(phen)_2]^{2+}$ (Cu-Phen) $[Cu(DPQ)(phen)]^{2+}$ (Cu-DPQ-Phen), $[Cu(DPPZ)(phen)]^{2+}$ (Cu-DPPZ-Phen), and $[\{Cu(phen)_2\}_2(\mu\text{-terph})](terph)$ (Cu-Terph) reveal chemical nuclease activity occurs primarily at the minor groove; titration of the major groove binder, methyl green, enhances DNA degradation – most likely by directing (priming) complex-DNA interactions to the minor groove – while the presence of the minor grove binder, netropsin, was found to significantly reduce oxidative damage on pUC19. It is also interesting to note that no correlation exists between chemical nuclease activity (**Figure III-1**) and apparent DNA binding constant (Table III-1). Instead, nuclearity has a more dramatic effect as evidenced by Cu-Terph mediated DNA damage. ROS-specific scavengers employed to identify the cleavage mechanism revealed metal-hydroxo or free hydroxyl radicals ($^{\bullet}OH$), and not $^1O_2$, as the predominant species generated; DMSO was found to limit DNA oxidation – most likely through the trapping of hydroxyl radicals ($(CH_3)_2SO + {}^{\bullet}OH \rightarrow CH_3SO_2H + {}^{\bullet}CH_3$) (Burkitt and Mason, 1991) – with sodium azide (NaN_3) having neglibile influence on all complexes except Cu-Terph. It is also likely that hydrogen peroxide (H_2O_2) is the key intermediary in $^{\bullet}OH$ production as the peroxide scavenger KI (Dunand et al., 2007; Steffens et al., 2012) was refractory to oxidative damage by tested agents. The generation of hydroxyl-based radicals was corroborated through identification of 8-oxo-2'-deoxyguanosine (8-oxo-dG) DNA lesions quantified under an ELISA protocol. 8-oxo-dG liberation followed the overall trend Cu-DPQ-Phen > Cu-Terph > Cu-Phen > Cu-DPPZ with higher lesion numbers detected under heavily sheared (damaged) plasmid conditions. Finally, oxidative damage by the complex series was found to inhibit the DNA replication process; polymerase chain reaction (PRC) reactions were impeded – particularly along A-T rich chains – through oxidative damage of template strands with the di-nuclear Cu-Terph, and mono-nuclear Cu-DPQ-Phen, being particularly potent oxidants to this process.

III. 6. Acknowledgement

This work was supported by Irish Research Council (IRC) grants GOIPG/2013/826 and GOIPG/2014/1182. Sponsorship from COST Action CM1201: “Biomimetic Radical Chemistry” is gratefully acknowledged.

III. 7. References

Basu, A. K., Loechler, E. L., Leadon, S. A., and Essigmann, J. M. (1989). Genetic effects of thymine glycol: Site-specific mutagenesis and molecular modeling studies. *Proc. Natl. Acad. Sci. United States* 86, 7677–7681.

Breen, A. P., and Murphy, J. A. (1995). Reactions of oxyl radicals with DNA. *Free Radic. Biol. and Med.* 18, 1033–1077. doi:10.1016/0891-5849(94)00209-3.

Burger, R. M. (1998). Cleavage of nucleic acids by Bleomycin. *Chem. Rev.* 98, 1153–1169. doi:10.1021/cr960438a.

Burger, R. M., Peisach, J., and Horwitz, S. B. (1981). Activated bleomycin. A transient complex of drug, iron, and oxygen that degrades DNA. *J. Biol. Chem.* 256, 11636–11644.

Burkitt, M. J., and Mason, R. P. (1991). Direct evidence for in vivo hydroxyl-radical generation in experimental iron overload: an ESR spin-trapping investigation. *Proc. Natl. Acad. Sci. U. S. A.* 88, 8440–8444. doi:10.1073/pnas.88.19.8440.

Chatgilialoglu, C., Ferreri, C., and Terzidis, M. A. (2011). Purine 5',8-cyclonucleoside lesions: chemistry and biology. *Chem. Soc. Rev.* 40, 1368–82. doi:10.1039/c0cs00061b.

Chatgilialoglu, C., and O'Neill, P. (2001). Free radicals associated with DNA damage. *Exp. Gerontol.* 36, 1459–71. doi:10.1016/S0531-5565(01)00132-2.

Chen, J., Ghorai, M. K., Kenney, G., and Stubbe, J. (2008). Mechanistic studies on bleomycin-mediated DNA damage: multiple binding modes can result in double-stranded DNA cleavage. *Nucleic Acids Res.* 36, 3781–3790. doi:10.1093/nar/gkn302.

Cooke, M. S., and Evans, M. D. (2007). 8-Oxo-deoxyguanosine: Reduce, reuse, recycle? *Proc. Natl. Acad. Sci. United States* 104, 13535–13536. doi:10.1073/pnas.0706878104.

Douki, T., Martini, R., Ravanat, J. L., Turesky, R. J., and Cadet, J. (1997). Measurement of 2,6-diamino-4-hydroxy-5-formamidopyrimidine and 8-oxo-7,8-dihydroguanine in isolated DNA exposed to gamma radiation in aqueous solution. *Carcinogenesis* 18, 2385–2391. doi: 10.1093/carcin/18.12.2385

Dunand, C., Crèvecoeur, M., and Penel, C. (2007). Distribution of superoxide and hydrogen peroxide in Arabidopsis root and their influence on root development: possible interaction with peroxidases. *New Phytol.* 174, 332–341. doi:10.1111/j.1469-8137.2007.01995.x.

Franco, R., Panayiotidis, M. I., and Cidlowski, J. A. (2007). Glutathione depletion Is necessary for apoptosis in lymphoid cells independent of reactive oxygen species formation. *J. Biol. Chem.* 282, 30452–30465. doi:10.1074/jbc.M703091200.

Gajewski, E., Aruoma, O. I., Dizdaroglu, M., and Halliwell, B. (1991). Bleomycin-dependent damage to the bases in DNA is a minor side reaction. *Biochemistry* 30, 2444–2448. doi:10.1021/bi00223a021.

Johnson, G. R. A., and Nazhat, N. B. (1987). Kinetics and Mechanism of the Reaction of the Bis(1,10-phenanthroline)copper(I) Ion with Hydrogen Peroxide in Aqueous Solution. *J. Am. Chem. Soc.* 109, 1990–1994. doi:10.1021/ja00241a015.

Kellett, A., Howe, O., O'Connor, M., McCann, M., Creaven, B. S., McClean, S., Foltyn-Arfa Kia, A., Casey, A., and Devereux, M. (2012). Radical-induced DNA damage by cytotoxic square-planar copper(II) complexes incorporating o-phthalate and 1,10-phenanthroline or 2,2'-dipyridyl. *Free Radic. Biol. Med.* 53, 564–76. doi:10.1016/j.freeradbiomed.2012.05.034.

Kpricf P., Rosair, G., McKee, V., Creaven, B., Walsh, M., McClean, S., et al. (2011). Bis-phenanthroline copper(II) phthalate complexes are potent in vitro antitumour agents with "self-activating" metallo-nuclease and DNA binding properties. *Dalton Trans.* 40, 1024–7. doi:10.1039/c0dt01607a.

Klaunig, J. E., Kamendulis, L. M., and Hocevar, B. a (2010). Oxidative stress and oxidative damage in carcinogenesis. *Toxicol. Pathol.* 38, 96–109. doi:10.1177/0192623309356453.

Li, L., Karlin, K. D., and Rokita, S. E. (2005). Changing selectivity of DNA oxidation from deoxyribose to guanine by ligand design and a new binuclear copper complex. *J. Am. Chem. Soc.* 127, 520–521. doi:10.1021/ja044209e.

Marshall, L. E., Graham, D. R., Reich, K. A., and Sigman, D. S. (1981). Cleavage of Deoxyribonucleic Acid by the 1,10-Phenanthroline-Cuprous Complex. Hydrogen Peroxide Requirement and Primary and Secondary Structure Specificity. *Biochemistry* 20, 244–250. doi:10.1021/bi00505a003.

Mazzer, P. A., Maurmann, L., and Bose, R. N. (2007). Mechanisms of DNA damage and insight into mutations by chromium(VI) in the presence of glutathione. *J. Inorg. Biochem.*101, 44–55. doi:10.1016/j.jinorgbio.2006.08.008.

McCann, M., McGinley, J., Ni, K., O'Connor, M., Kavanagh, K., McKee, V., Colleran, J., Devereux, M., Gathergood, N., Barron, N., et al. (2013). A new phenanthroline-oxazine ligand: synthesis, coordination chemistry and atypical DNA binding interaction. *Chem. Comm.* 49, 2341–2343. doi:10.1039/c3cc38710k.

Merkel, P. B., Nilsson, R., and Kearns, D. R. (1972). Deuterium effects on singlet oxygen lifetimes in solutions. New test of singlet oxygen reactions. *J. Am. Chem. Soc.* 94, 1030–1031. doi:10.1021/ja00758a072.

Molphy, Z., Prisecaru, A., Slator, C., Barron, N., McCann, M., Colleran, J., Chandran, D., Gathergood, N., and Kellett, A. (2014). Copper phenanthrene oxidative chemical nucleases. *Inorg. Chem.* 53, 5392–5404. doi:10.1021/ic500914j.

Natrajan, A., Hecht, S. M., and Van der Marel, G. A. (1990). A study of oxygen-versus hydrogen peroxide-supported activation of iron. cntdot. bleomycin. *J. Am. Chem. Soc.* 112, 3997–4002. doi:10.1021/ja00166a042.

Pflaum, M., Will, O., and Epe, B. (1997). Determination of steady-state levels of oxidative DNA base modifications in mammalian cells by means of repair endonucleases. *Carcinogenesis* 18, 2225–2231.

Pouget, J. P., Douki, T., Richard, M. J., and Cadet, J. (2000). DNA Damage Induced in Cells by γ and UVA Radiation As Measured by HPLC/GC−MS and HPLC−EC and Comet Assay. *Chem. Res. Toxicol.* 13, 541–549. doi:10.1021/tx000020e.

Pratviel, G., and Bernadou, J. (1989). Evidence for high-valent iron-oxo species active in the DNA breaks mediated by iron-bleomycin. *Biochem. Pharmacol.* 38, 133–140. doi: 10.1093/carcin/18.12.2385

Prisecaru, A., Devereux, M., Barron, N., McCann, M., Colleran, J., Casey, A., McKee, V., and Kellett, A. (2012). Potent oxidative DNA cleavage by the di-copper cytotoxin: $[Cu_2(\mu$-terephthalate)$(1,10\text{-phen})_4]^{2+}$. *Chem. Commun.* 48, 6906–6908. doi:10.1039/c2cc31023f.

Prisecaru, A., McKee, V., Howe, O., Rochford, G., Mccann, M., Colleran, J., Pour, M., Barron, N., Gathergood, N., and Kellett, A. (2013). Regulating Bioactivity of Cu2+ Bis-1,10-phenanthroline Artificial Metallonucleases with Sterically Functionalized Pendant Carboxylates. *J. Med. Chem.* 56, 8599–8615. doi:10.1021/jm401465m.

Rodriguez, L. O., and Hecht, S. M. (1982). Iron(II)-bleomycin. Biochemical and spectral properties in the presence of radical scavengers. *Biochem. Biophys. Res. Commun.* 164, 1470–1476. doi:10.1016/0006-291X(82)91416-4

Sanchez-Cano, C., Huxley, M., Ducani, C., Hamad, A. E., Browning, M. J., Navarro-Ranninger, C., Quiroga, A. G., Rodger, A., and Hannon, M. J. (2010). Conjugation of testosterone modifies the interaction of mono-functional cationic platinum(II) complexes with DNA, causing significant alterations to the DNA helix. *Dalton Trans.* 39, 11365–74. doi:10.1039/c0dt00839g.

Sigman, D. S., Graham, D. R., Aurora, V. D., and Stern, A. M. (1979). Oxygen-dependent cleavage of DNA by the 1,10-phenathroline cuporous complex. Inhibition of Escherichia coli DNA polymerase I. *J. Biol. Chem.* 254, 12269–12272.

Steffens, B., Kovalev, A., Gorb, S. N., and Sauter, M. (2012). Emerging Roots Alter Epidermal Cell Fate through Mechanical and Reactive Oxygen Species Signaling. *The Plant Cell* 24, 3296–3306. doi:10.1105/tpc.112.101790.

Stubbe, J. A., and Kozarich, J. W. (1987). Mechanisms of bleomycin-induced DNA degradation. *Chem. Rev.* 87, 1107–1136. doi:10.1021/cr00081a011.

Tyrrell, R. M., and Keyse, S. M. (1990). New trends in photobiology. The interactions of UVA radiation with cultured cells. *J. Photochem. Photobiol., B* 4, 349–361. doi:10.1016/1011-1344(90)85014-N

Tabassum, S., Al-Asbahy, W. M., Afzal, M., Arjmand, F., and Bagchi, V. (2012). Molecular drug design, synthesis and structure elucidation of a new specific target peptide based metallo drug for cancer chemotherapy as topoisomerase I inhibitor. *Dalton Trans.* 41, 4955–64. doi:10.1039/c2dt12044e.

van der Steen, S., de Hoog, P., van der Schilden, K., Gamez, P., Pitié, M., Kiss, R., and Reedijk, J. (2010). Novel heteronuclear ruthenium–copper coordination compounds as efficient DNA-cleaving agents. *Chem. Commun.* 46, 3568. doi:10.1039/c000077a.

Xia, Q., Chou, M. W., Yin, J. J., Howard, P. C., Yu, H., and Fu, P. P. (2006). Photoirradiation of representative polycyclic aromatic hydrocarbons and twelve isomeric methylbenz[α]anthracene with UVA light: formation of lipid peroxidation. *Toxicol. Ind. Health* 22, 147–156. doi:10.1191/0748233706th259oa.

Xu, M., Lai, Y., Jiang, Z., Terzidis, M. A., Masi, A., Chatgilialoglu, C., and Liu, Y. (2014). A 5', 8-cyclo-2'-deoxypurine lesion induces trinucleotide repeat deletion via a unique lesion bypass by DNA polymerase β. *Nucleic Acids Res.* 42, 13749–63. doi:10.1093/nar/gku1239.

Zhou, W., Wang, X., Hu, M., Zhu, C., and Guo, Z. (2014). A mitochondrion-targeting copper complex exhibits potent cytotoxicity against cisplatin-resistant tumor cells through multiple mechanisms of action. *Chem. Sci.* 5, 2761–2770. doi:10.1039/c4sc00384e.

Appendix B.

DNA oxidation profiles of copper phenanthrene chemical nucleases

B-1: Corresponding nuclease activity for 8-oxo-dG conditions

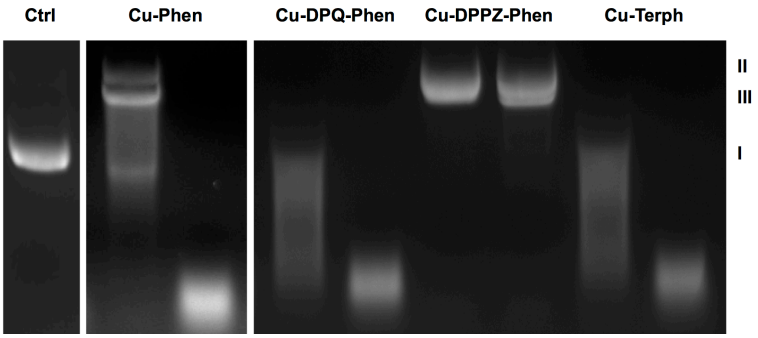

Figure B-1. DNA cleavage reactions with 10 and 20 μM test complex, 3000 ng superhelical pUC19 and 1 mM added Na-L-Ascorbate incubated at 37°C for 30 minutes. Lane 1: pUC19 only, lane 2,3: 10 and 20 μM Bis-Phen, lane 4,5: 10 and 20 μM Cu-DPQ-Phen, lane 6, 7: 10 and 20 μM Cu-DPPZ-Phen, lane 8-9: 10 and 20 μM Cu-Terph.

B-2: DNA cleavage optimisation (high concentration range with added reductant) for PCR amplification studies

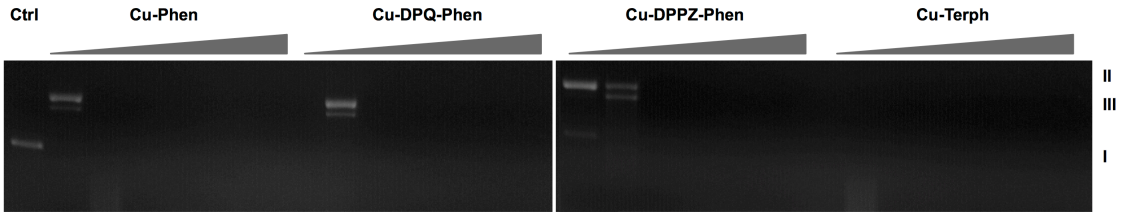

Figure B-2. DNA cleavage reactions with 2.5, 5, 10, 20, 30, 40 and 50 μM test complex, 400 ng superhelical pUC19 and 1 mM added Na-L-Ascorbate incubated at 37°C for 30 minutes. Lane 1: pUC19 only, lane 2-8: Bis-Phen and lane 9-15: Cu-DPQ-Phen, lane 16-22: Cu-DPPZ-Phen and lane 23-29: Cu-Terph.

B-3: DNA cleavage optimisation (high concentration range without added reductant) for PCR amplification studies

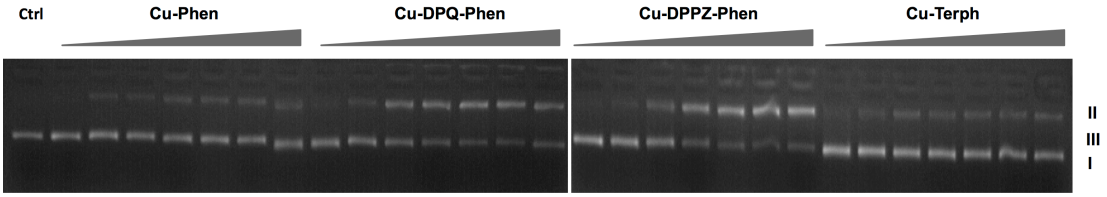

Figure B-3. DNA cleavage reactions with 2.5, 5, 10, 20, 30, 40 and 50 μM test complex, 400 ng superhelical pUC19 without added Na-L-Ascorbate incubated at 37°C for 30 minutes. Lane 1: pUC19 only, lane 2-8: Bis-Phen and lane 9-15: Cu-DPQ-Phen, lane 16-22: Cu-DPPZ-Phen and lane 23-29: Cu-Terph.

B-4: PCR Primer Design

The pUC19 vector (2686 bp) was studied in detail and 3 sets of primers were designed such that it was possible to generate 120 bp long sequences of varying G·C content (35%, 50% and 63%). The lengths of the short nucleotide sequences were verified by carrying out PCR reactions (35 cycles) with 1 ng pUC19 plasmid using 2× MyTaq Red Mix (Bioline) at suitable annealing temperatures for respective primer pairs and comparing the band generated by gel electrophoresis to a 50 bp DNA ladder (Fermentas).

35% forward: `5′-gatcttttctacggggtctg-3′`
35% reverse: `5′-gatttaaaacttcattttta-3′`
50% forward: `5′-ttatcgccactggcagcagc-3′`
50% reverse: `5′-accaaatactgttcttctag-3′`
63% forward: `5′-tcgcgcgtttcggtgatgacg-3′`
63% reverse: `5′-cacccgctgacgcgccctgacg-3′`

B-5: PCR amplification studies without reductant (high concentration range)

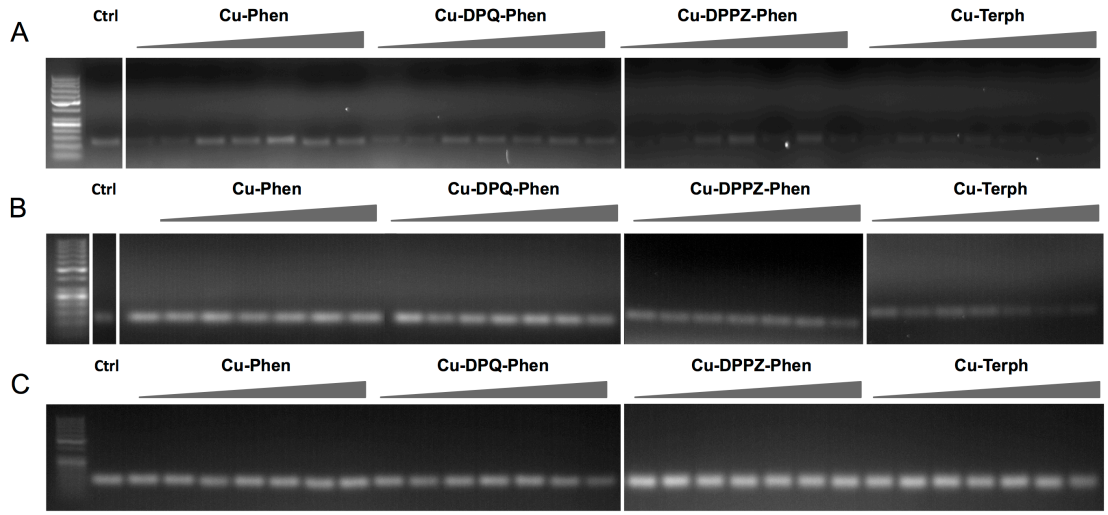

Figure B-5. 400 ng pUC19 DNA was initially exposed to 2.5, 5, 10, 20, 30, 40 and 50 μM of each test complex in the absence of added reductant at 37°C for 30 minutes. 20 ng of complex exposed DNA template was removed from the reaction and PCR reaction was carried out as previously described with each varying G·C content primer set at optimum annealing temperatures and analysed using gel electrophoresis. Fig. **A.** Lane 1: 35% G·C control, lane 2-8 35% G·C + Cu-Phen, lane 9-15: 35% G·C + Cu-DPQ-Phen and lane 16-22: 35% G·C + Cu-Terph, **B.** 50% G·C and **C.** 63% G·C respectively. All sequences generated were 120 base pairs.

B-6: PCR amplification studies with reductant (low concentration range)

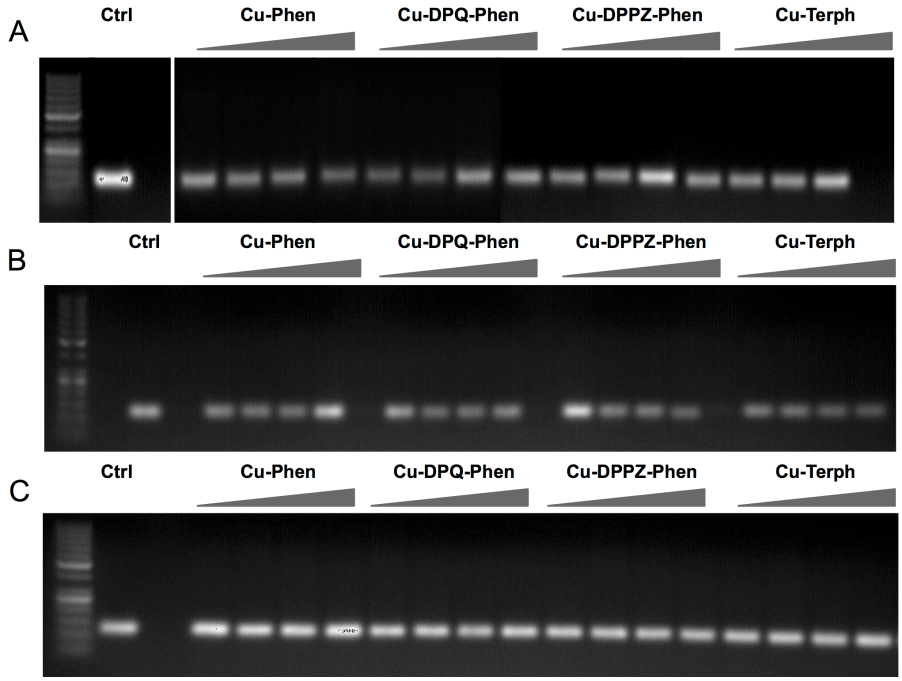

Figure B-6. 400 ng pUC19 DNA was initially exposed to 250 nM, 500 nM, 1 µM and 2.5 µM of each test complex in the presence of 1 mM added reductant at 37°C for 30 minutes. 20 ng of complex exposed DNA template was removed from the reaction and PCR reaction was carried out as previously described with each varying G·C content primer set at optimum annealing temperatures and analysed using gel electrophoresis. Fig. **A.** Lane 1: 35% G·C control, lane 2-5 35% G·C + Cu-Phen, lane 6-9 35% G·C + Cu-DPQ-Phen and lane 10-13: 35% G·C + Cu-Terph, **B**. 50% G·C and **C**. 63% G·C respectively. All sequences generated were 120 base pairs.

CHAPTER IV.

$[Cu_2$(*tetra*-(2-pyridyl)-naphthalene)$Cl_4]$ Displays Non-Intercalative Major Groove Binding and Self-Activating Oxidative DNA Damage

---

This manuscript is in preparation for submission to *Nucleic Acids Research*, 2017.

Zara Molphy, Diego Montagner, Satish S. Bhat, Creina Slator, Andrea Erxleben and Andrew Kellett.

My contribution to this paper involved conducting DNA binding and cleavage experiments. Due to the unique DNA binding characteristics of this novel *di*-nuclear molecule, a number of new experiments were developed during this project in order to elucidate the molecules interaction with nucleic acids. Examples include gel electrophoretic-based assays such as topoisomerase I-mediated DNA relaxation, melphalan alkylation and the absorbance based spectroscopy technique, circular dichroism.

IV. 1. Abstract

Oxygen radical generation is an inevitable consequence of an aerobic existence and is implicated in a wide variety of pathological conditions including cancer, cardiovascular disease, ageing and neurodegenerative disorder. However, oxygen radicals can also be used to our advantage since they are generated from synthetic artificial metallonucleases carrying designer ligands that selectively induce oxidative DNA scission. Reported here is the rational design, DNA binding activity, and antitumoural potential of a novel di-nuclear Cu^{2+} complex [Cu_2(tetra-(2-pyridyl)-naphthalene)Cl_4] (Cu_2TPNap). Cu_2TPNap binds DNA non-intercalatively at the major groove (K_{app} ~1 x 10^7 $M(bp)^{-1}$) inducing guanine-cytosine specific deformation and condensation. The complex oxidatively damages DNA producing strand breakage in the absence of co-activating exogenous species.

IV. 2. Introduction

The production of reactive oxygen species (ROS) in biological systems has a major impact on human health and disease progression. ROS, many of which are 'free radicals', are produced endogenously in biological systems through oxygen metabolism in the mitochondria. However, several well recognised exogenous factors such as exposure to ionising radiation, redox metal ion overload, and therapeutic drug exposure can all trigger their production to directly impact human health. Genetic content in the form of DNA is particularly susceptible to oxidative stress as ROS are known to damage both the nucleobase, leading to the formation of mutagenic lesions (*e.g.* 8-oxo-7,8-dihydro-2′-deoxyguanosine (8-oxo-dG)), and carbon-hydrogen (C-H) bond abstraction located on 2-deoxyribose producing nucleic acid strand breakages.(1-3) Since the integrity of genomic structure is crucial for cell survival, medicinal chemists have uncovered small molecules, natural products, and ionising radiation sources as powerful oxidants that damage DNA, leading to cell death. The application of these agents provides a vital first-line defence against almost all forms of human cancer in our society today.

Accordingly, there has been considerable interest toward the discovery of novel nucleic acid targeting metallodrug candidates based on the clinical success of the antitumoural antibiotic bleomycin. This natural product is capable of inducing double strand cleavage of duplex DNA through hydrogen atom abstraction at C-4′ sites in the presence of molecular oxygen and a suitable one-electron reductant (activated metallo-bleomycin).(4) Damage induced by this agent is likely responsible for its therapeutic

efficacy since double strand breaks are less readily repaired by *in vivo* repair mechanisms. Another biologically ROS-active class of molecule are Cu^{2+} phenanthroline (phen) agents (*e.g.* $[Cu(phen)_2]^{2+}$)(5) along with mixed chelate derivatives $[Cu(N\text{-}N')(A\text{-}A')]^{+}$, where N-N′ represent neutral aromatic diimine donors (*e.g.* phen or bipyridine) and A-A′ stands for uninegative N-O or O-O′ donor ligands (*e.g.* aminoacidates, acetylacetonate and dicarboxylates). Some of these ternary agents have recently entered phase I clinical trials and it is generally accepted they exert their biological effect within cancer cells by binding to DNA and subsequently degrading the nucleic acid backbone by C-1′ sugar oxidation at the minor groove.(6-8)

Within the field of nucleic acid targeting metallodrug development, a recent trend has emerged in polynuclear metal complex design. As such, the introduction of two (*di*-) or three (*tri*-) metal centres into complex scaffolds has transformed not only metallodrug transport and cellular accumulation properties, but has also uncovered binding interactions not possible through the use of simple univalent compounds. Examples of this trend include: the *tri*-platinum^{2+} (Triplatin, **Figure C-1A**) series(9) that utilise bridging aliphatic diamine linkers to coordinate successive Pt^{2+} ions that engage DNA *via* discrete 'phosphate-clamping' interactions; the di-nuclear Ce^{4+}-EDTP (**Figure C-1B**) complex recruited to the 5′ end of an oligonucleotide sequence that binds to human telomere DNA by G-quadruplex formation and subsequently induces site-selective hydrolytic strand breakage;(10) and the bi-metallic Zn^{2+} *tetra*-2-amino-pyridine complex (**Figure C-1C**) that achieves both tight phosphate binding, remarkable phosphodiester catalytic cleavage, and catalyses isomerization of the RNA dinucleotide uridyl(3′-5′)uridine (UpU).(11) In conjunction with these promising discoveries, the development of *di*-nuclear Cu^{2+} complexes has received attention due to their ability to mediate oxygen binding and activation through highly accessible—and biologically accessible—redox states.(12) In the context of redox chemistry at the DNA interface, it was recently demonstrated that linking *bis*-$[Cu(phen)_2]^{2+}$ units *via* bridging aromatic ($[Cu_2(\mu\text{-octanedioate})(phen)_4]^{2+}$), or aliphatic carboxylate ligands ($[Cu_2(\mu\text{-terephthalate})(phen)_4]^{2+}$) (Cu-Terph) gives rise to potent 'self-activating' DNA oxidants with promising cytotoxic potential.(13-15) In the case of the Cu-Terph species, the influence of nuclearity was later shown to play a role in the liberation of 8-oxo-dG lesions during the DNA damage process.(16)

Our strategy here for designing a new *di*-Cu^{2+} cytotoxic agent capable of tightly binding and oxidising duplex DNA stems from observations on *i.*) the utility of the *tetra*-2-pyridine ligand scaffold for efficient nucleic acid catalytic cleavage within di-Zn^{2+} systems,(11) and *ii.*) the introduction of an aromatic DNA binding moiety(17) that could potentially enhance both nucleic acid targeting and binding affinity. With this rational design in mind, herein we report the isolation, nucleic acid interactions and antitumoural potential of the di-nuclear Cu^{2+} complex [Cu_2(*tetra*-(2-pyridyl)-naphthalene)Cl_4] (Cu_2TPNap).

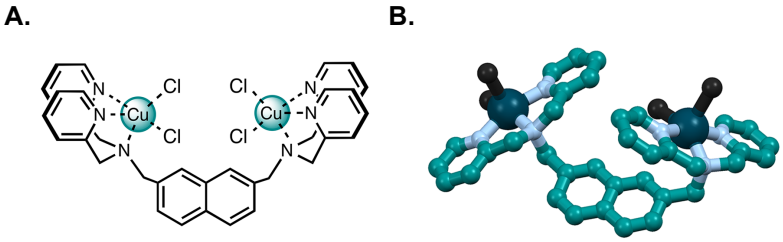

Figure IV-1. A. Molecular structure of the di-Cu^{2+} complex Cu_2TPNap and **B.** perspective, space-filling view of **Cu_2TPNap**, the copper ions are bridged by the naphthalene-diamine group. (Colour scheme: copper, teal; nitrogen, blue; carbon, turquoise; chlorine, black).

IV. 3. Materials and Methods

IV. 3.1. Materials synthesis and characterisation

$CuCl_2$, 2,7-bis(bromomethyl)naphthalene, and potassium carbonate were purchased from TCI Europe and used without further purification. Bis(2-pyridylmethyl)amine was synthesised as previously reported.(18) Deuterated chloroform was obtained from Apollo Scientific. ^{1}H NMR spectra were recorded on Jeol ECX-400 and Varian 500 AR spectrometers at room temperature and all chemical shifts are relative to the residual solvent peak. ESI Mass Spectra were recorded on a Waters LCT Premier XE Spectrometer in positive mode. Microanalysis (C, H, and N) was carried out using a Perkin Elmer 2400 series II analyzer. UV-Vis spectra were recorded on a Jasco UV-Vis spectrophotometer in phosphate buffer (pH = 6.8). Emission experiments were conducted on a Shimadzu RF-5301 spectrofluorometer at room temperature. Calf thymus DNA was purchased from Invitrogen (15633019) while DNA from salmon testes (D1626), *Micrococcus luteus* (D8259) and synthetic alternating co-polymers (poly[d(A-T)$_2$] (P0883) and poly[d(G-C)$_2$] (P9389)) were obtained from Sigma Aldrich Ireland.

IV. 3.1.1. ***2,7-Di(aminomethyl)-N,N,N',N'-tetra-(2-pyridylmethyl)naphthalene*** **(TPNap)**

2,7-bis(bromomethyl)naphthalene (0.300 g, 0.955 mmol) was dissolved in acetonitrile and added to an acetonitrile solution containing bis(2-pyridylmethyl)amine (0.380 g, 1.9 mmol) and potassium carbonate (0.395 g, 2.86 mmol). The solution was stirred at room temperature for 3 days and filtered. The acetonitrile solution was then evapourated to dryness, the residue was dissolved in ethyl acetate and washed with water and brine. The organic layer was dried over anhydrous sodium sulphate. Evaporation under vacuum gave a white solid that was purified by column chromatography (silica gel, chloroform/methanol). Yield: 0.361 g (68.7%). ^{1}H-NMR ($CDCl_3$, 400 MHz). 8.51-8.53 (m, 4H), 7.76 (br, s, 2H), 7.52-7.79 (m, 12H), 7.11-7.16 (m, 4H), 3.86 (s, 4H), 3.84 (s, 8H). ^{13}C-NMR ($CDCl_3$, 400 MHz): 159.87, 149.1, 136.85, 136.66, 136.52, 129.21, 127.8, 127.54, 126.94, 122.92, 122.03, 60.00, 58.73.

IV. 3.1.2. ***[Cu$_2$(tetra-(2-pyridyl)-naphthalene)Cl$_4$]*** **(Cu$_2$TPNap)**

A 10 mL methanolic solution of $CuCl_2$ (0.067 g, 0.50 mmol) was added to a methanolic solution of TPNap (0.138 g, 0.25 mmol) and stirred for 4 hours at room temperature. The complex Cu_2TPNap was precipitated by the addition of diethyl ether. Yield: 0.140 g (63%). Elem. Anal. Calcd. (%) for $C_{36}H_{34}N_6Cl_4Cu_2 \cdot 2H_2O$: C, 50.53; H, 4.48; N, 9.82; found: C, 50.29; H, 4.23; N, 9.75. ESI MS: m/z calcd. for [**1**-Cl]$^+$ 783.04, found 783.05 (100%).

IV. 3.2 DNA Binding experiments

IV. 3.2.1. Competitive Ethidium Bromide Displacement Assay

The DNA binding affinity of the title complex was studied on synthetic alternating copolymers (poly[d(A-T)$_2$] and poly[d(G-C)$_2$]) and conducted according to the literature procedure previously reported by Molphy *et al*.(5)

IV. 3.2.2. Thermal Melting Studies

Briefly, the concentrations of varying kinds of DNA were determined by measuring the absorption intensity at 260 nm using suitable molar extinction coefficients and salt buffered concentrations.(9, 16) Prior to commencing the thermal melting study, Cu_2TPNap (r = 0.1) was incubated with DNA for 10 minutes at 25°C to allow for drug-DNA binding to occur. Melting curves were recorded by tracking changes in absorbance at 260 nm as a function of temperature from 25 - 95°C. The study was conducted in triplicate and T_M values were determined from the midpoint of the melting curve or in the case of poly[d(G-

$C)_2$], by the maxima of the first derivative. Average thermal melting values and changes in drug treated DNA with respect to untreated nucleotide can be found in table IV-1.

IV. 3.3.3. Circular Dichroism Spectroscopy

Complex-DNA interactions were analysed using Starna quartz cuvettes in 10 mM PBS solution (pH 7) in the presence of 25 mM NaCl. Solutions of salmon testes DNA (stDNA, Sigma Aldrich, D1626, ε_{260} = 12824 $M(bp)^{-1}$ cm^{-1}), Poly[$(d(A\text{-}T)_2$] (Sigma Aldrich, PO883, ε_{260} = 13100 $M(bp)^{-1}$ cm^{-1}) and Poly[$(d(G\text{-}C)_2$] (Sigma Aldrich, P9389, ε_{260} = 16800 $M(bp)^{-1}$ cm^{-1}) were initially heat treated and allowed to renature prior to quantification using an Agilent Cary 100 dual beam spectrophotometer equipped with a 6×6 peltier multicell system with temperature controller to give a working solution with final DNA concentration of ~100 μM. The CD investigation was conducted on an Applied Photophysics Chirascan qCD instrument in the range of 200-400 nm and measurements were recorded at a rate of 1 nm per second. DNA solutions were incubated for 30 minute periods at 37°C with Cu_2TPNap at varing r ([drug] / [DNA]) values where r = 0.1 and 0.2 (r being the ratio of complex per μM DNA) with data being recorded in mdeg.

IV. 3.2.4. Topoisomerase I-mediated DNA relaxation assay

400 ng of pUC19 plasmid DNA (NEB, N3041) was exposed to varying concentrations of Cu_2TPNap (0.1 - 400 μM) for 15 min at room temperature in a final volume of 20 μL containing 80 mM HEPES buffer (pH 7.2), CutSmart® buffer (NEB, B7204), and 100× BSA (NEB, B9000). 1 unit of topoisomerase I (*E. coli*) (NEB, M0301) was added to the mixture and incubated for 15 min at 37°C to ensure relaxation of plasmid DNA. The reaction was stopped through the addition of SDS and protein kinase (Sigma Aldrich), to a final concentration of 0.25% and 250 μg/mL respectively. To remove protein from the DNA, samples were then incubated for 30 minutes at 50°C. Samples were then loaded onto a 1.2% agarose gel in the absence of ethidium bromide. Topoisomers of DNA were separated by electrophoresis in 1× TBE buffer at room temperature for 270 min at 50 V. The agarose gel was post-stained using a 25 μM EtBr bath for 20 min at room temperature. Finally, the gel was soaked for 24 hours in 300 mL of deionized water and photographed using a UV transilluminator.

IV. 3.3. DNA Cleavage Studies

IV. 3.3.1. DNA cleavage studies in the absence of added reductant

Reactions were carried out according to the literature procedure reported by Kellett *et al* with minor changes.(15) DNA-complex incubation was carried out at 37°C over 5 hours. Samples were loaded onto an agarose gel (1.2%) and electrophoresis was completed at 70 V for 2 hours in 1× TAE buffer.

IV. 3.3.2. DNA cleavage in the presence of non-covalently bound recognition elements

Reactions were carried out according to the literature procedure reported by Molphy *et al.* with minor changes.(16) Briefly, 400 ng pUC19 was preincubated with 25 mM NaCl, and 20 μM of minor groove binding agent, netropsin, in 80 mM HEPES buffer (pH 7.2) for 45 minutes at 37°C. Sample tubes were then vortexed and varying concentrations of Cu_2TPNap were added (2.5 μM, 10 μM, 20 μM and 40 μM) and further incubated at 37°C for 4 hours. In parallel, a 4 hour incubation of Cu_2TPNap (from 2.5-40 μM) with pUC19 was prepared for control purposes and subjected to gel electrophoresis (prepared and stained as previously described). Cu_2TPNap only treated pUC19 was then directly compared to pUC19 pre-treated with netropsin prior to the addition of test complex.

IV. 3.3.3. Hydrolytic DNA damage investigation using T4 ligase

Reactions were adapted from the literature procedure reported by Prisecaru *et al*.(15) 800 ng pUC19 was initially treated with 60 μM of Cu_2TPNap in the presence of 25 mM NaCl for 7 hours at 37°C. Control linear (LC) DNA was obtained through the treatment of 400 ng of pUC19 with EcoRI restriction endonuclease (NEB, R0101S) for 1 hour at 37°C followed by heat denaturation for 20 minutes at 65°C. Gel electrophoresis was carried out and linear DNA (LC) bands were cut, purified and eluted in 30 μL nuclease free H_2O using QIAquick PCR purification kit (Qiagen, 28104). Purified DNA was then incubated with 2 μL T4 DNA Ligase (NEB, M0202S) and 3 μL of T4 DNA Ligase Reaction Buffer (10×) in an ice bath overnight and slowly allowed to reach room temperature.

IV. 3.3.4. DNA alkylation inhibition investigation – Melphalan assay

This assay was adapted from the literature procedures reported by Wang *et al.* and Farrell *et al*.(19, 20) The pBR322 vector (4361 bp) was studied in detail and a set of primers (Forward: 5'-gctgcaaaacgtctgcgacc-3' and reverse: 5'-cgcatcaggcgctcttccgc-3') were designed such that it was possible to generate a sequence of DNA 798 base pairs long containing 4 CpG islands by PCR (54% GC content). The length of the nucleotide

sequence was verified by carrying out PCR reactions (35 cycles) with 1 ng pUC19 plasmid using 2× MyTaq Red Mix (Bioline) at suitable annealing temperatures for the primer pair and comparing the band generated by gel electrophoresis to a 1 Kb DNA ladder (Fermentas).

400 ng of 798 bp sequence was incubated with 100, 250, 500, 1000 and 2500 μM Cu_2TPNap for 30 minutes at 37°C. The complex-DNA solution was then exposed to 5 μM of melphalan for 30 minutes at 37°C followed by DNA heat denaturation for 15 minutes at 90°C. 2 μL of a 1 M piperidine solution was then added and incubated for 1 hour at 90°C. Netropsin was used as a control agent in this assay, as its minor groove binding properties protect DNA from the alkylating properties of melphalan. 400 ng of 798 bp DNA was initially exposed to 50, 100, 250 and 500 μM netropsin for 30 minutes at 37°C and treated with melphalan and piperidine as previously stated and subjected to gel electrophoresis (prepared and stained as previously described).

IV. 3.3.5. DNA cleavage of single stranded M13mp18 plasmid DNA (7,248 bp)

Briefly, cleavage reactions were conducted on 400 ng single stranded M13mp18 plasmid DNA (7249 bp) in the presence of 25 mM NaCl and exposed to increasing concentrations of Cu_2TPNap (5, 10, 20, 40 μM) for 30 minutes at 37°C and subjected to gel electrophoresis on a 0.8% agarose gel at 60V for 70 minutes.

IV. 3.3.6. DNA cleavage in the presence of ROS scavengers and stabilizers.

Reactions were adapted from a literature procedure recently reported by this group.(16) To a final volume of 20 μL, 80 mM HEPES (pH 7.2), 25 mM NaCl and 400 ng pUC19 DNA were treated with Cu_2TPNap concentrations of 5, 10, 20 and 40 μM in the presence ROS scavengers; DMSO (10%), Tiron (10 mM), pyruvate (10 mM), EDTA (100 μM) and neocuproine (100 μM). Reactions were incubated for 1 hour at 37°C and loaded onto 1.5% agarose gel and electrophoresis was completed at 70 V for 80 minutes in 1× TAE buffer.

IV. 4. Results and Discussion

IV. 4.1. Synthesis and characterisation

Tetra-(2-pyridyl)-naphthalene was generated by the addition of two equivalents of bis-(2-pyridylmethyl)-amine to a solution of 2,7-bis-(bromomethyl)-naphthalene in acetonitrile containing excess potassium carbonate (Appendix C-2). Subsequent treatment by $CuCl_2$ in methanol generated Cu_2TPNap (**Figure IV-1A**), from which crystals suitable for X-ray

analysis were grown upon slow evaporation of acetonitrile at room temperature (**Figure IV-1B**, **Tables C1-2**). Each copper atom in Cu_2TPNap is five-coordinate with an N_3Cl_2 donor set. The coordination geometry is best described as distorted square pyramidal with chloride occupying the apical position. The N-Cu-N and Cl-Cu-Cl bite angles are 80.80 (9)° and 105.71 (3)° respectively, with the naphthalene scaffold holding the two metal centres 8.9 Å apart. The complex is fluorescent (**Figure C-3**: absorption, emission spectra; **Table C-3**: photophysical parameters) with an emission maxima at 370 nm.

IV. 4.2. DNA binding and cleavage studies

DNA binding constants of Cu_2TPNap were determined using high-throughput saturation binding analysis with the fluorogenic intercalator, ethidium bromide (EtBr) (Fig. IV-2A, Table IV-1).(5) The complex can be described as a high-affinity DNA binder with K_{app} (apparent binding constant) values of ca. 1×10^7 $M(bp)^{-1}$ on both calf thymus DNA (ctDNA) and poly[d(G-C)$_2$], while slightly lower equilibrium constants were observed on poly[d(A-T)$_2$]. Interestingly, these K_{app} binding values are amongst the highest reported in literature and are in line with Cu^{2+} phenazine complexes previously reported by some of us.(5) Cu_2TPNap was found to quench saturated EtBr bound duplex polymers without adenine-thymine (A-T) specificity and was observed to displace both limited bound EtBr (intercalator) and Hoechst 33258 (minor groove binder) from ctDNA with similar affinity (Data not shown). The title complex was further identified to compact DNA with a significant reduction—unlike aromatic intercalator EtBr—in the hydrodynamic viscosity profile of salmon testes dsDNA (**Figure IV-2B**). The binding interaction of the di-Cu^{2+} complex may conceivably result in deformation of the B-helical structure, giving rise to the observed DNA condensation effect and thus ejecting both bound intercalating and minor groove binding fluorescent dyes. The technique of thermal melting (T_M) was then employed as it provides a valuble insight into the relative strength and nature of drug-DNA binding interactions.(5) Thermal melting analysis, however, revealed the agent to selectively destabilise poly[d(G-C)$_2$]. Here, a biphasic thermal melting profile was observed with the first derivative (d1) melting at the highly negative value of -18.47 ± 1.18°C, and the second (d2) at -1.47 ± 1.18°C (**Figure IV-2C**, **Table IV-1**). These results depart substantially from previously reported non-covalent minor groove and intercalating binding agents netropsin and actinomycin-D.[5] Furthermore, we conducted a parallel study using poly[d(G-C)$_2$] with the major groove binder methyl green (**Figure C-4**). Here, a thermal stabilization of 5°C was observed on the synthetic alternating poly[d(G-C)$_2$] co-

polymer in identical experimental conditions (Appendix C-3).

Circular dichroism (CD) was then employed to probe drug-induced conformational changes to a variety of duplex DNA polymers. The CD profile of classical right-handed B-DNA is composed of two positive (220 and 276 nm) and two negative (210 and 246 nm) elliptical signals with slight spectral variations observed when the base pair composition of DNA is altered (**Figure C-5A**). Salmon testes DNA (stDNA; 41% G-C content) was monitored at wavelengths of interest including 220 nm (hydrogen bonding), 246 nm (handedness/helicity) and 276 nm (base pair stacking) in the presence of Cu_2TPNap and directly compared to non-covalent binding agents: methyl green (MG; major groove binder), netropsin (Net; minor groove binding) and EtBr (intercalator) (**Figure IV-3A**). Cu_2TPNap induced similar concentration-dependent effects to the major groove binding agent MG at both 220 and 276 nm signifying an increase in the distance between hydrogen bonds linking individual base pairs along with a limited effect on base pair stacking interactions, respectively. It was therefore of interest to investigate the CD profile of the complex in the presence of poly[d(G-C)$_2$]—an alternating co-polymer that has up to 12 bp per helical turn and a helical rise per base pair dimer of ~7.4 Å. The complex again displayed CD changes on poly[d(G-C)$_2$] in line with that of MG with an increase in ellipticity noted at 210 nm and no appreciable spectral changes observed at 246 and 276 nm (**Figure IV-3C**). As expected, EtBr was found to alter the spectra with changes in ellipticity associated with its propensity to intercalate (**Figure IV-3C**). The binding interaction of Net with duplex polymers was also different to Cu_2TPNap, particularly on stDNA and poly[d(A-T)$_2$] when monitored at 276 nm where base stacking reductions are evident due to Net-induced minor groove H-bonding contraction (**Figure C-6**). Although base stacking interactions by Cu_2TPNap were not evidenced by CD spectroscopy, significant changes to the handedness (helicity) of stDNA are visible at 246 nm (**Figure IV-3B**).

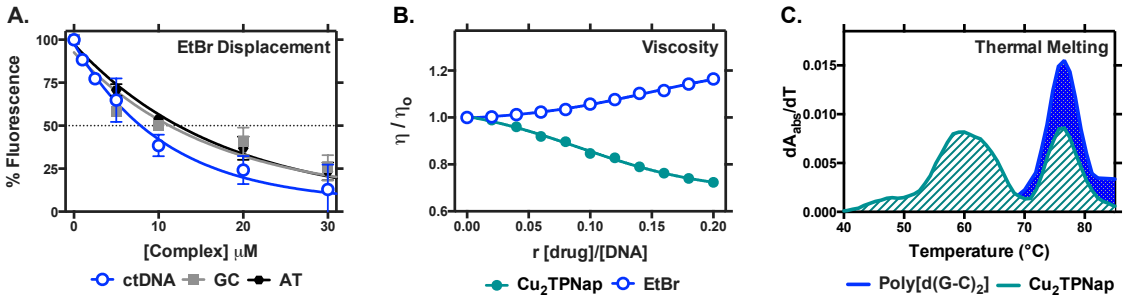

Figure IV-2. A. Binding of Cu_2TPNap complex to ethidium-saturated solutions of dsDNA (ctDNA, poly[d(A-T)$_2$] and poly[d(G-C)$_2$]); **B.** viscosity profile of complex treated and EtBr treated salmon testes dsDNA; **C.** thermal melting profile of untreated poly[d(G-C)$_2$] nucleotide and complex treated nucleotide at r = 0.1.

Table IV-1. Apparent DNA binding constants (K_{app}) and influence on thermal denaturation of Cu_2TPNap.

DNA	%AT content	C_{50}[a]	K_{app}[b]	ΔT_M[c]
poly[d(G-C)$_2$]	0	10.35	1.07×10^7	-18.97± 1.18 [d1] -0.31 ± 1.18 [d2]
ctDNA	58	7.81	1.42×10^7	-0.38 ± 0.93
poly[d(A-T)$_2$]	100	12.30	9.01×10^6	0.04 ± 0.17

[a] C_{50} = μM concentration required to reduce fluorescence by 50%; [b] $K_{app} = K_b \times 12.6/C_{50}$ where $K_b = 8.8 \times 10^6$ M(bp)$^{-1}$ and [c] ΔT_M = difference in thermal melting (°C) of drug treated nucleotide at r = 0.1 compared with drug-untreated nucleotide (where d1= phase 1 and d2 = phase 2).

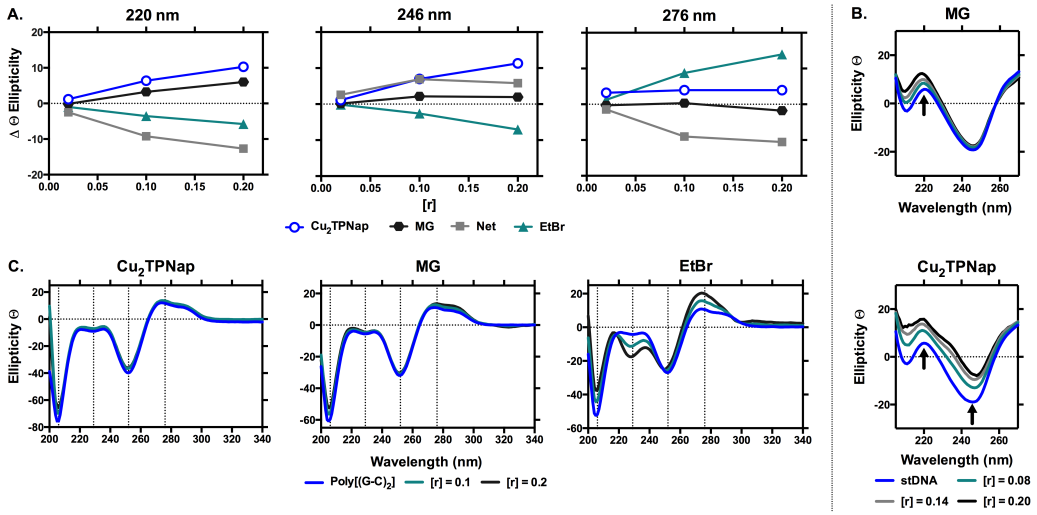

Figure IV-3. A. Change in ellipticity of Cu_2TPNap and classical major groove (MG), minor groove (Net) and intercalating agents (EtBr) with respect to classical B-form stDNA at r = 0.1 and 0.2 loading ratios at 220 nm; 246 nm; and 276 nm; **B,** increasing ratios of MG and Cu_2TPNap on stDNA and **C.** interactions of Cu_2TPNap, MG and EtBr on alternating copolymer poly[d(G-C)$_2$] (Θ =mdeg).

To confirm this effect within duplex DNA, topoisomerase-I mediated relaxation of supercoiled (sc) pUC19 plasmid DNA was investigated (**Figure IV-4D**). In the presence of increasing concentrations of Cu_2TPNap, the complex was found to induce complete unwinding of scDNA at 50 μM with a fraction of oxidatively nicked open circular (oc) DNA remaining at concentrations >50 μM along with positively supercoiled plasmid DNA. Since Cu_2TPNap-mediated strand scission was identified within topo-I unwinding, further studies with pUC19 in the absence of topo-I were undertaken. Cu_2TPNap was found to promote single-strand nicking, in a concentration dependent manner over 30 min exposure without exogenous factors (i.e. in the absence of added peroxide or reductant) and double stranded (l) DNA damage over a 5 h period (**Figure IV-4A**). Furthermore, Cu_2TPNap was found to induce complete degradation of single stranded M13mp18 plasmid DNA at 40 μM complex exposure, in the absence of added reductant, over a 30 min period (**Figure C-8**). These results markedly contrast with the well-studied chemical nuclease $[Cu(phen)_2]^{2+}$ that displays a dependence on exogenous reductant and/or oxidant and is known to oxidise duplex DNA primarily at the minor groove.(21) Since Cu_2TPNap displayed self-activating cleavage properties, it was of importance to determine the nature of this scission mechanism. Hydrolytic and oxidative DNA damage can be distinguished through the use of the T4 DNA ligase enzyme—an enzyme that catalyses the relegation of hydrolytically cleaved DNA duplexes *via* phosphodiester bond formation.(22) Prolonged exposure of pUC19 to Cu_2TPNap resulted in the formation of double stranded DNA damage that could not undergo religation when treated with the T4 ligase enzyme, indicating the molecule participates in oxidative DNA cleavage mechanisms (**Figure IV-4B**). This result was in direct contrast to that of EcoRI trandformed pUC19, which can be seen to form concatamers, indicative of DNA religation only possible through hydrolytic DNA excision.

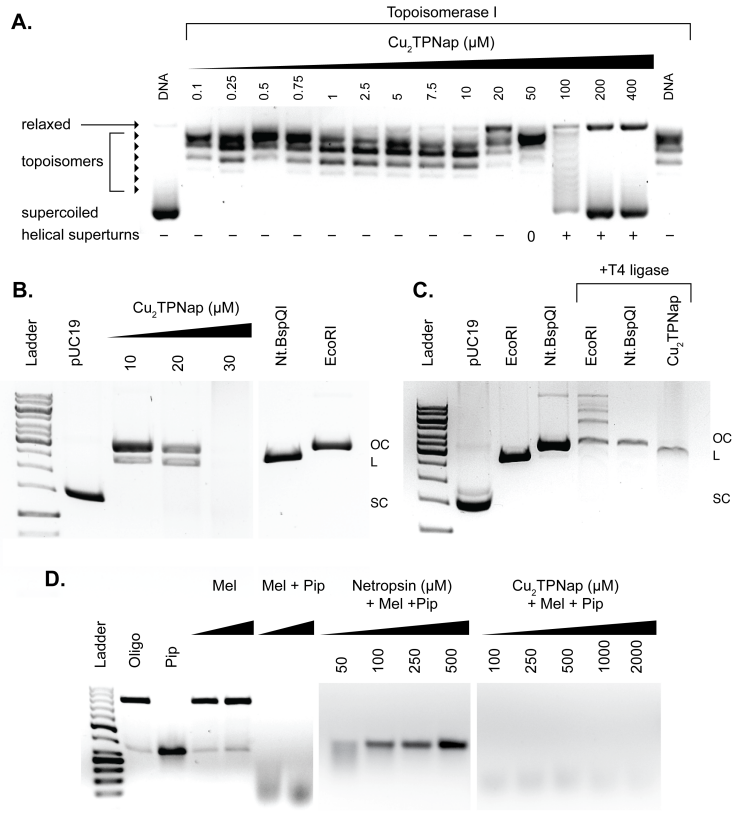

Figure IV-4. A. Topoisomerase I-mediated relaxation in the presence of Cu_2TPNap; **B.** DNA cleavage reactions by Cu_2TPNap on pUC19 (in the absence of exogenous oxidant or reductant); **C.** T4 DNA ligase experiments with Cu_2TPNap and restriction enzymes EcoRI and Nt.BspQI; and; **D.** Melphalan alkylation assay using Cu_2TPNap and minor groove binder netropsin.

In order to delineate ROS species involved in the oxidation process, Cu_2TPNap activity was investigated with a variety of free radical scavengers (**Figure C-9**). Results show the oxidation mechanism is dependent on superoxide ($O_2^{\bullet-}$) as DNA damage was completely inhibited in the presence of 4,5-dihydroxy-1,3-benzenedisulfonic acid disodium salt (tiron). Hydrogen peroxide (H_2O_2) is also involved in the cleavage process as pyruvate substantially impeded DNA oxidation. Interestingly, the metal chelating agent EDTA was found to fully sequester the active copper species and inhibit DNA damage across all concentration ranges, while the presence of neocuproine did not display the same level of inhibition—a further departure from the chemical nuclease action of $[Cu(phen)_2]^{2+}$ and Cu-Terph. Since the hydroxyl radical was involved only to a minor extent in the degradation pathway of Cu_2TPNap (**Figure IV-5A**), the oxidative DNA lesion 8-oxo-dG was quantified and compared to $[Cu(phen)_2]^{2+}$—a known producer of hydroxyl or metal-hydroxo radicals—using an ELISA protocol. As anticipated, minimal 8-oxo-dG lesions (<13 nM) were found upon exposure of pUC19 to Cu_2TPNap (**Figure IV-5B**) thus corroborating an alternative metal-dioxygen (superoxo) promoted pathway. Previously, we

identified ~100 nM of 8-oxo-dG lesions produced by both $[Cu(phen)_2]^{2+}$ and Cu-Terph at lower complex loading.(16)

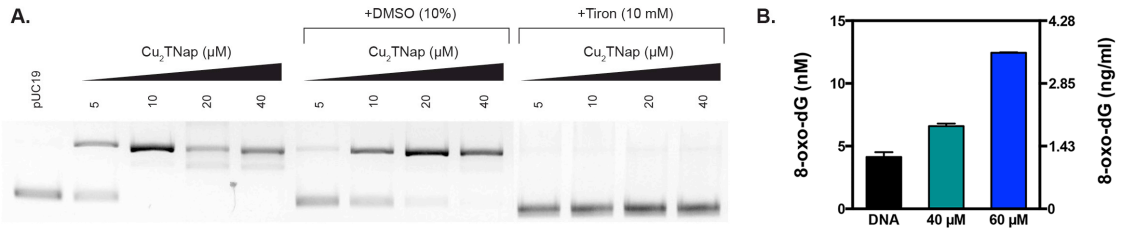

Figure IV-5. A. Cu_2TPNap DNA cleavage experiments in the absence and presence of hydroxyl radical scavenger DMSO and superoxide radical scavenger tiron and **B.** quantification of 8-oxo-dG lesions in 3000 ng of pUC19 DNA treated with 40 and 60 μM of Cu_2TPNap for 4 h at 37°C.

Of further relevance, we observed no inhibition of DNA damage by Cu_2TPNap toward pUC19 pre-saturated with the minor groove-binding agent, netropsin (**Figure C-7**); this result is again in direct contrast to Cu-phen type systems that are known to induce DNA scission in this region (due to the exposed nature of deoxyribose C1′)(16) thus supporting cleavage by Cu_2TPNap at the major groove. To further corroborate the major groove as the Cu_2TPNap recognition site, we employed a melphalan protection assay (**Figure IV-4D**).(20) Melphalan is an aromatic nitrogen mustard with high affinity for alkylating the minor groove—inducing A•T→T•A transversions—and when heat-treated with piperidine, DNA cleavage at guanine N-7 adducts result.[19] An oligonucleotide fragment of 798 bp generated by polymerase chain reaction (PCR), was exposed to melphalan and heat-treated with piperidine in order to generate thermolabile DNA fragmentation. Pre-exposure of this oligonucleotide to netropsin (50 – 500 μM) results, as expected, in protection of the minor groove. Cu_2TPNap however, was found to offer no protection of the minor groove across an extended concentration range (0.1 – 2.5 mM).

IV. 5. Conclusions

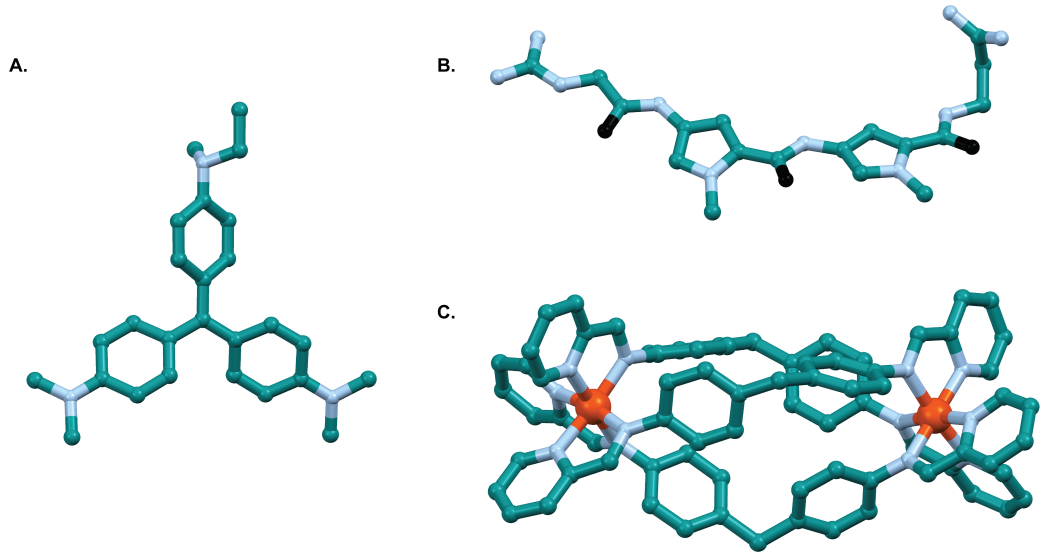

Figure IV-6. Perspective, space-filling view of **A.** major groove binding methyl green, **B.** minor groove binding netropsin, and **C.** *di*-iron(II) supramolecular helicate $[Fe_2L_3]Cl_4$ where L = $C_{25}H_{20}N_4$.(23, 24) (Colour scheme: carbon, turquoise; nitrogen, blue; oxygen, black; iron, orange).

Taken together, evidence here suggests the complex tightly binds and oxidises double stranded DNA through the major groove using a superoxide-mediated process without involving co-activating species. We suggest Cu_2TPNap is selectively incorporated, non-intercalatively, into the major groove and this interaction results in deformation of the B-DNA helical structure, giving rise to the observed condensation and unwinding effects. Circular dichroism analysis supports this interaction as the binding profile is similar to methyl green (MG), a known major groove binding agent (**Figure IV-6A**). The major groove binding agent methyl green is composed of three phenyl rings arranged in a propeller like conformation and has been shown to be excluded from binding to triple helical poly(dA)•2poly(dT) DNA, unlike minor groove binders DAPI, Hoechst 33258 and netropsin (**Figure IV-6B**) that primarily interact with the walls and floor of the narrow minor groove. Indeed, there are structurally analogous aspects between MG and Cu_2TPNap as both molecules contain non-coplanar aromatic conformation(25, 26) rendering classical intercalation difficult to conceive. Binding by metal complexes exclusively at the major groove is rare with the exception of *di*-iron(II) supramolecular helicates developed by Hannon and co-workers.(23, 24) These helicates contain the general formula $[Fe_2L_3]Cl_4$ (**Figure IV-6C**) and bind the major groove of B-DNA due to their matching optimum conformation and enhanced DNA binding arising from their 4+ charge and induce intramolecular coiling of negatively supercoiled plasmid DNA at low micromolar loading.

The current work demonstrates Cu_2TPNap is a unique major groove-binding small molecule with distinct features compared with both methyl green and *di*-Fe(II) helicates; these interactions result in DNA helical perturbment and this unwinding effect is amplified, and directly observable, within thermal melting experiments with poly[d(G-C)$_2$] and within topoisomerase-I mediated relaxation. In summary, this work represents a significant advancement toward the development of catalytic metallodrugs targeting the major groove of duplex DNA.

IV. 6. Funding

This work was supported by the Irish Research Council (IRC) grants GOIPG/2013/826 and GOIPG/2014/1182, and the European Commission (Marie Curie FP7-IEF). AK acknowledges funding from the Marie Skłodowska-Curie Innovative Training Network (ITN) ClickGene (H2020-MSCA-ITN-2014-642023) and the European Cooperation in Science Engineering and Technology (COST) CM1201.

IV. 7. References

1. Cadet,J., Douki,T. and Ravanat,J.L. (2010) Oxidatively generated base damage to cellular DNA. *Free Radic. Biol. Med.*, **49**, 9–21.
2. Gimisis,T. and Chatgilialoglu,C. (2012) Oxidatively Formed Sugar Radicals in Nucleic Acids. In *Encyclopedia of Radicals in Chemistry, Biology and Materials*. John Wiley & Sons, Ltd., pp. 1–26.
3. Pitié,M. and Pratviel,G. (2010) Activation of DNA carbon-hydrogen bonds by metal complexes. *Chem. Rev.*, **110**, 1018–1059.
4. Stubbe,J. and Kozarich,J.W. (1987) Mechanisms of Bleomycin-Induced DNA degradation. *Chem. Rev.*, **87**, 1107–1136.
5. Molphy,Z., Prisecaru,A., Slator,C., Barron,N., McCann,M., Colleran,J., Chandran,D., Gathergood,N. and Kellett,A. (2014) Copper Phenanthrene Oxidative Chemical Nucleases. *Inorg. Chem.*, **53**, 5392–5404.
6. Galindo-Murillo,R., Garcia-Ramos,J.C., Ruiz-Azuara,L., Cheatham,T.E. and Cortes-Guzman,F. (2015) Intercalation processes of copper complexes in DNA. *Nucleic Acids Res.*, **43**, 5364–5376.
7. Rivero-Müller,A., De Vizcaya-Ruiz,A., Plant,N., Ruiz,L. and Dobrota,M. (2007) Mixed chelate copper complex, Casiopeina IIgly, binds and degrades nucleic acids: a mechanism of cytotoxicity. *Chem. Biol. Interact.*, **165**, 189–199.
8. Alemón-Medina,R., Breña-Valle,M., Muñoz-Sánchez,J.L., Gracia-Mora,M.I. and Ruiz-Azuara,L. (2007) Induction of oxidative damage by copper-based antineoplastic drugs (Casiopeínas). *Cancer Chemother. Pharmacol.*, **60**, 219–228.
9. Prisecaru,A., Molphy,Z., Kipping,R.G., Peterson,E.J., Qu,Y., Kellett,A. and Farrell,N.P. (2014) The phosphate clamp: sequence selective nucleic acid binding profiles and conformational induction of endonuclease inhibition by cationic Triplatin complexes. *Nucleic Acids Res.*, **42**, 13474–13487.
10. Xu,Y., Suzuki,Y., Lönnberg,T. and Komiyama,M. (2009) Human telomeric DNA sequence-specific cleaving by G-quadruplex formation. *J. Am. Chem. Soc.*, **131**, 2871–2874.
11. Feng,G., Natale,D., Prabaharan,R., Mareque-Rivas,J.C. and Williams,N.H. (2006) Efficient phosphodiester binding and cleavage by a ZnII complex combining hydrogen-bonding interactions and double lewis acid activation. *Angew. Chemie Int. Ed.*, **45**, 7056–7059.

12. Kieber-Emmons,M.T., Ginsbach,J.W., Wick,P.K., Lucas,H.R., Helton,M.E., Lucchese,B., Suzuki,M., Zuberbuhler,A.D., Karlin,K.D. and Solomon,E.I. (2014) Observation of a $Cu(II)_2(\mu\text{-}1,2\text{-peroxo})/Cu(III)_2(\mu\text{-oxo})_2$ Equilibrium and its Implications for Copper-Dioxygen Reactivity. *Angew. Chemie Int. Ed.*, **2**, 4935–4939.
13. Kellett,A., O'Connor,M., McCann,M., Howe,O., Casey,A., McCarron,P., Kavanagh,K., McNamara,M., Kennedy,S., May,D.D., *et al.* (2011) Water-soluble bis(1,10-phenanthroline) octanedioate Cu2+ and Mn2+ complexes with unprecedented nano and picomolar in vitro cytotoxicity: promising leads for chemotherapeutic drug development. *Med. Chem. Commun.*, **2**, 579–584.
14. Kellett,A., O'Connor,M., McCann,M., McNamara,M., Lynch,P., Rosair,G., McKee,V., Creaven,B., Walsh,M., McClean,S., *et al.* (2011) Bis-phenanthroline copper(II) phthalate complexes are potent in vitro antitumour agents with 'self-activating' metallo-nuclease and DNA binding properties. *Dalt. Trans.*, **40**, 1024–1027.
15. Prisecaru,A., Devereux,M., Barron,N., McCann,M., Colleran,J., Casey,A., McKee,V. and Kellett,A. (2012) Potent oxidative DNA cleavage by the di-copper cytotoxin: $[Cu2([\mu\text{-terephthalate})(1,10\text{-phen})4]^{2+}$. *Chem. Commun.*, **48**, 6906–6908.
16. Molphy,Z., Slator,C., Chatgilialoglu,C. and Kellett,A. (2015) DNA oxidation profiles of copper phenanthrene chemical nucleases. *Front. Chem.*, **3**, 1–9.
17. Liu,H.-K. and Sadler,P.J. (2011) Metal complexes as DNA intercalators. *Acc. Chem. Res.*, **44**, 349–359.
18. Hamann,J.N., Rolff,M. and Tuczek,F. (2015) Monooxygenation of an appended phenol in a model system of tyrosinase: implications on the enzymatic reaction mechanism. *Dalt. Trans.*, **44**, 3251–3258.
19. Wang,P., Bauer,G.B., Bennett,R.A.O. and Povirk,L.F. (1991) Thermolabile adenine adducts and A-T base pair substitutions induced by nitrogen mustard analogues in an SV40-based shuttle plasmid. *Biochemistry*, **30**, 11515–11521.
20. Qu,Y., Moniodis,J.J., Harris,A.L., Yang,X., Hegmans,A., Povirk,L.F., Berners-Price,S.J. and Farrell,N.P. (2011) Non-Covalent Polynuclear Platinum Compounds as Polyamine Analogs. In *RSC Drug Discovery Series No. 17 Polyamine Drug Discovery*.pp. 191–204.
21. Sigman,D.S., Mazumder,A. and Perrin,D.M. (1993) Chemical Nucleases. *Chem. Rev.*, **93**, 2295–2316.
22. Ferretti,L. and Sgaramella,V. (1981) Specific and reversible inhibition of the blunt end joining activity of the T4 DNA ligase. *Nucleic Acids Res.*, **9**, 3695–3705.

23. Hannon,M.J., Moreno,V., Prieto,M.J., Moldrheim,E., Sletten,E., Meistermann,I., Isaac,C.J., Sanders,K.J. and Rodger,A. (2001) Intramolecular DNA Coiling Mediated by a Metallo-Supramolecular Cylinder. *Angew. Chemie Int. Ed.*, **40**, 879–884.
24. Malina,J., Hannon,M.J. and Brabec,V. (2015) Iron(II) Supramolecular Helicates Condense Plasmid DNA and Inhibit Vital DNA-Related Enzymatic Activities. *Chem. - A Eur. J.*, **21**, 11189–11195.
25. Bailly,C., Hénichart,J.-P., Colson,J.-P., Colson,P. and Houssier,C. (1992) Drug-DNA Sequence-Dependent Interactions Analysed by Electric Linear Dichroism. *J. Mol. Recognit.*, **5**, 155–171.
26. Kim,S.K. and Nordén,B. (1993) Methyl green. A DNA major-groove binding drug. *Fed. Eur. Biochem. Soc. Lett.*, **315**, 61–64.

Appendix C.

$[Cu_2$(*tetra*-(2-pyridyl)-naphthalene)$Cl_4]$ Displays Non-Intercalative Major Groove Binding and Self-Activating Oxidative DNA Damage

---

C-1: Structures from paper

A.

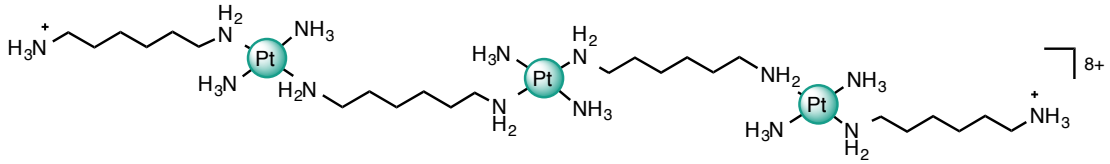

B.

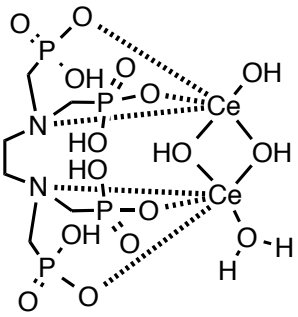

C.

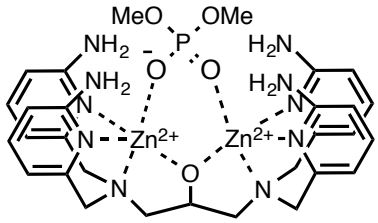

Figure C-1. (A) Molecular structure of TriplatinNC [{*trans*-$Pt(NH_3)_2(NH_2(CH_2)_6\text{-}NH_3)$}$_2$-μ-{*trans*-$Pt(NH_3)_2(NH_2(CH_2)_6NH_2)_2$}]$^{8+}$, **(B)** Ce^{4+}-EDTP (EDTP = ethylenediamine-tetramethylene-phosphonic acid and **(C)** Zn^{2+} *tetra*-2-amino-pyridine complex.(1-3)

C-2: Characterisation of [Cu_2(*tetra*-(2-pyridyl)-naphthalene)Cl_4] (Cu_2TPNap)

Crystallography

Single crystals of Cu_2TPNap suitable for single crystal X-ray diffraction were grown by slow evaporation of a solution of the complex in CH_3CN at room temperature. Crystal data were collected at room temperature on an Agilent (formerly OxfordDiffraction) Xcalibur CCD diffractometer using graphite-monochromated Mo-K_α radiation (λ= 0.71069 Å).(4) The structure was solved by direct methods and subsequent Fourier syntheses and refined by full-matrix least squares on F^2 using using SHELXS-97 and SHELXL-97(5, 6) within the Oscail package.[7] The scattering factors were those given in the SHELXL program. Hydrogen atoms were generated geometrically and refined as riding atoms with isotropic displacement factors equivalent to 1.2 times those of the atom to which they were attached. Graphics were produced with ORTEX.(7)

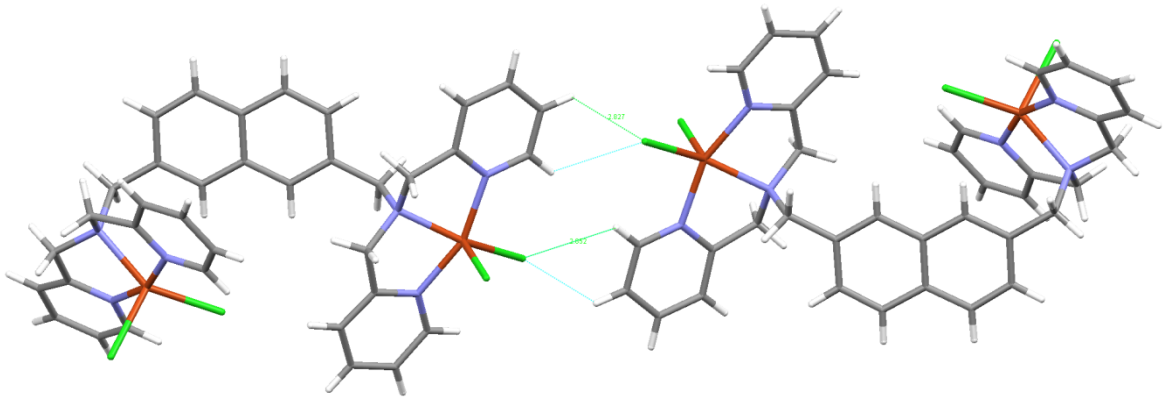

Figure C-2. Packing diagram of Cu_2TPNap·H_2O showing inter-molecular hydrogen bonding interactions. For the sake of clarity, water molecules of crystallization are not shown.

Crystallographic data are given in **Table C-1**, and a list of selected bond lengths and angles can be found in **Table C-2**.

Table C-1. Crystal data and structure refinement parameters for $Cu_2TPNap \cdot H_2O$.

Chemical formula	$C_{36}H_{36}Cl_4Cu_2N_6O$
Formula weight	837.59
Crystal system, space group	Triclinic, *P*-1
Temperature (K)	293
Unit cell dimensions	a=9.5092 (3) Å, α=83.693 (3)° b=14.282 (6) Å, β=71.530 (3)° c=14.982 (5) Å, γ=74.327 (3)°
V (Å^3)	1857.62 (12)
Z	2
F(000)	856
Density (Mg m^{-3})	1.497
No. of reflections for cell measurement	7595
ɵ range (°) for cell measurement	3.0–26.4
μ (mm^{-1})	1.47
Crystal shape	Prism
Colour	Blue
Crystal size (mm)	0.40 × 0.35 × 0.20
No. of measured, independent and observed [$I > 2\sigma(I)$] reflections	14030, 7595, 5992
θ values (°)	θ_{max} = 26.4, θ_{min} = 3.0
$(\sin \theta/\lambda)_{max}$ (Å^{-1})	0.625
No. of reflections	7595
No. of parameters	442
No. of restraints	0
R_{int}	0.026
$R[F^2 > 2\sigma(F^2)]$, $wR(F^2)$, S	0.037, 0.102, 1.05

Table C-2. Selected bond lengths [Å] and angles [°] for complex $Cu_2TPNap{\cdot}H_2O$.

Bond lengths			
Cu1—N3	2.000 (2)	Cu2—N6	2.006 (2)
Cu1—N2	2.001 (2)	Cu2—N5	2.023 (2)
Cu1—N1	2.086 (2)	Cu2—N4	2.078 (2)
Cu1—Cl2	2.3020 (7)	Cu2—Cl4	2.2496 (8)
Cu1—Cl1	2.4632 (9)	Cu2—Cl3	2.4483 (8)
Bond angles			
N3—Cu1—N1	81.77 (9)	N5—Cu2—N4	80.61 (9)
N2—Cu1—N1	80.73 (9)	N6—Cu2—Cl4	97.08 (7)
N3—Cu1—Cl2	98.09 (7)	N5—Cu2—Cl4	97.54 (7)
N2—Cu1—Cl2	96.64 (7)	N4—Cu2—Cl4	154.34 (7)
N3—Cu1—Cl1	91.55 (7)	N6—Cu2—Cl3	96.10 (8)
N2—Cu1—Cl1	93.53 (7)	N5—Cu2—Cl3	93.44 (7)
N1—Cu1—Cl1	109.07 (7)	N4—Cu2—Cl3	99.95 (7)
Cl2—Cu1—Cl1	105.72 (3)	Cl4—Cu2—Cl3	105.71 (3)
N6—Cu2—N4	80.10 (9)		

Absorption and emission spectra

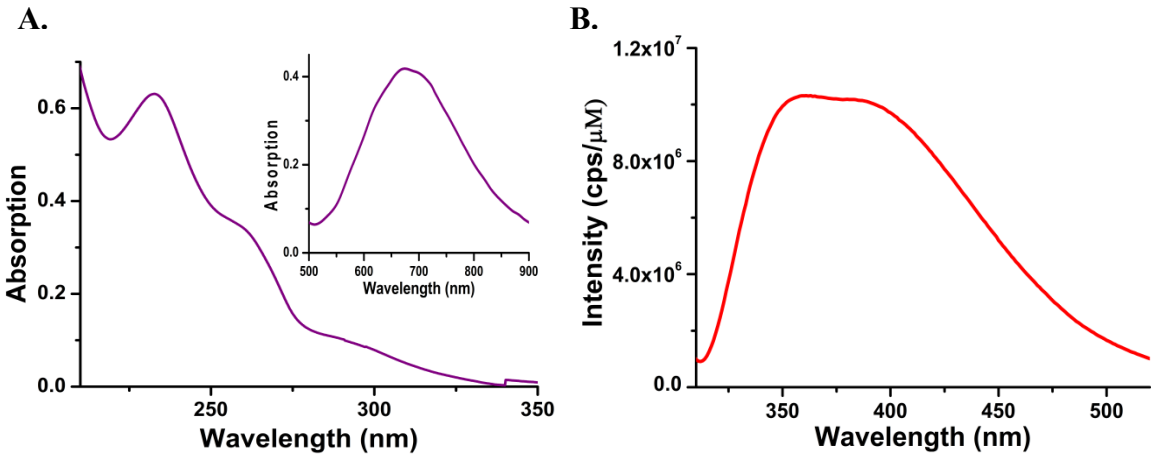

Figure C-3. Absorption **(A)** and emission **(B)** spectra of complex Cu_2TPNap (20 μM) in methanol at room temperature. (**(A)** Inset corresponds to absorption spectra of Cu_2TPNap in visible region at 2 mM concentration).

Table C-3. Photophysical properties of complex **Cu_2TPNap** at room temperature.

Absorption, λ_{max} (nm), (ε ($M^{-1}cm^{-1}$) Ligand Transitions (MLCT)	Emission λ_{em} (nm)
232 (31658), 260 (17174), 676 (209), 294 (4672)	370

C-3: DNA binding studies

Materials

Calf thymus DNA was purchased from Invitrogen (15633019) while DNA from salmon testes (D1626), *Micrococcus luteus* (D8259) and synthetic alternating co-polymers (poly[d(A-T)$_2$] (P0883) and poly[d(G-C)$_2$] (P9389)) were obtained from Sigma Aldrich Ireland.

Table C-4. % GC content of DNA used in biological studies

DNA	%GC content
ctDNA	42
Salmon Testes	41.2
Micrococcus luteus	72
poly[d(A-T)$_2$]	0
poly[d(G-C)$_2$]	100

Thermal melting studies

Methyl Green (MG) was used as a major groove binding control agent in this study and it was determined from the 1st derivative of the melting curve that the average ΔT_M with respect to untreated nucleotide was found to be +5.19°C.

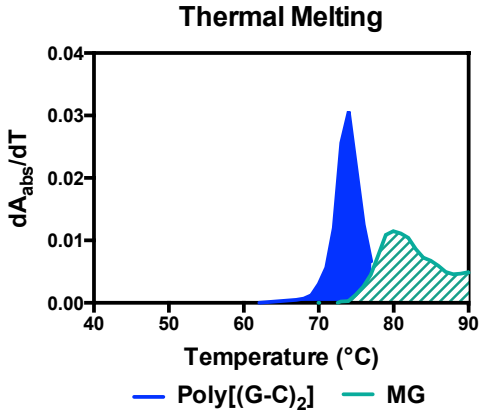

Figure C-4. Thermal melting profile of untreated poly[d(G-C)$_2$] nucleotide and methyl green (MG) treated nucleotide at r = 0.1.

Circular dichroism spectroscopy

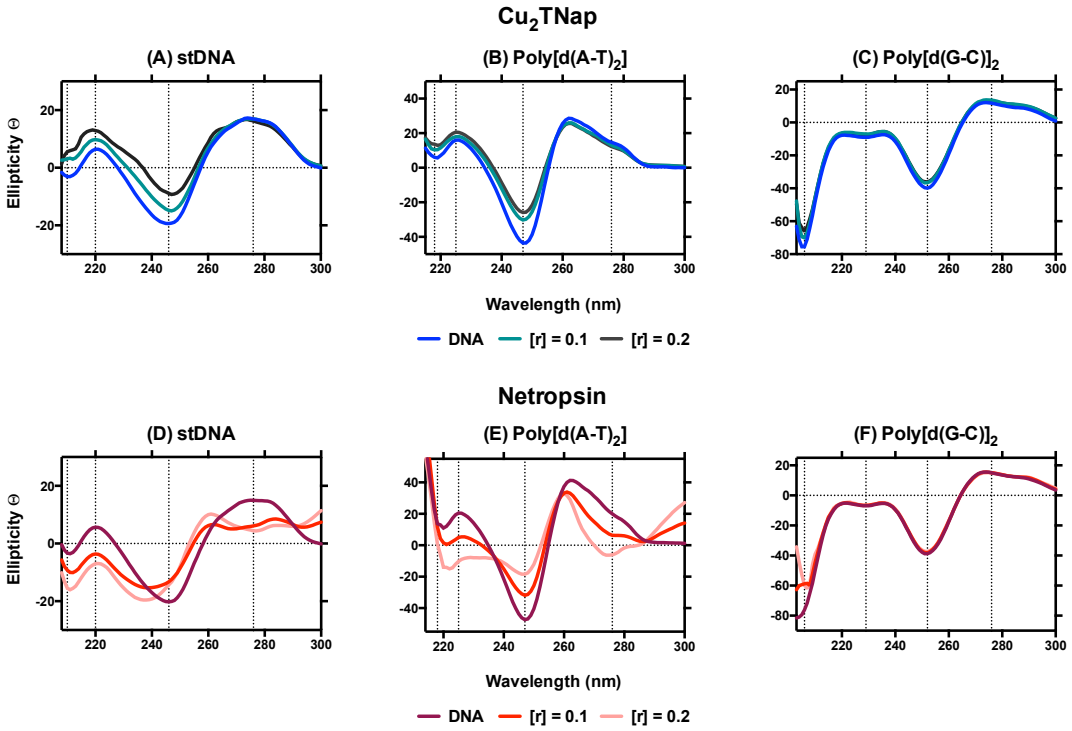

Figure S-5. CD profile of Cu_2TPNap **(A-C)** and netropsin **(D-F)** with stDNA and alternating co-polymers poly[d(A-T)$_2$] and poly[d(G-C)$_2$] at r = 0.1 and r = 0.2 drug loading.

Topoisomerase I-mediated DNA relaxation assay

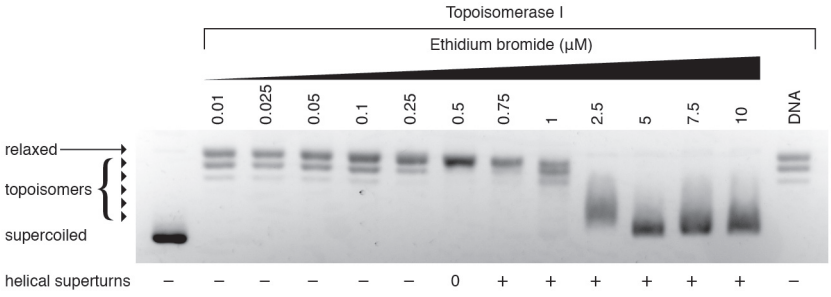

Figure C-6. Topoisomerase I-induced DNA relaxation in the presence of intercalator ethidium bromide.

DNA cleavage in the presence of non-covalently bound recognition elements

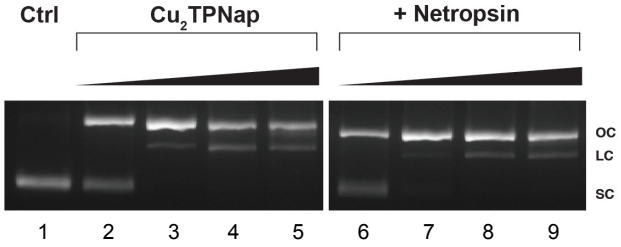

Figure C-7. 400 ng supercoiled pUC19 (lane 1), DNA cleavage of increasing concentrations of Cu_2TPNap (2.5 μM, 10 μM, 20 μM and 40 μM) (lanes 2-5) and DNA cleavage reactions pretreated with 20 μM of netropsin prior to Cu_2TPNap exposure (lanes 6-9).

DNA cleavage of single stranded M13mp18 plasmid DNA

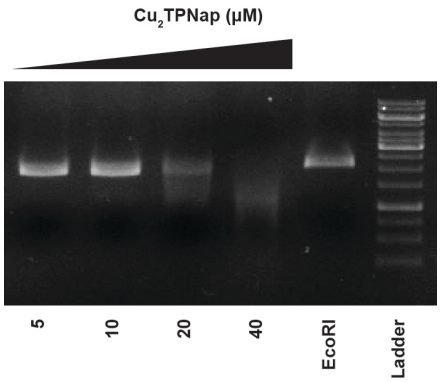

Figure C-8. 400 ng M13mp18 incubated with increasing concentrations of Cu_2TPNap over 30 minutes at 37°C.

DNA cleavage in the presence of ROS scavengers and stabilizers

Table C-5. Radical specific scavengers and stabilizers.

Scavanger[a]/Stabilizer[b]	Species
DMSO[a]	$^{\bullet}OH$
Tiron[a]	$O_2^{\bullet-}$
Pyruvate	H_2O_2
EDTA/Neocuproine	Copper

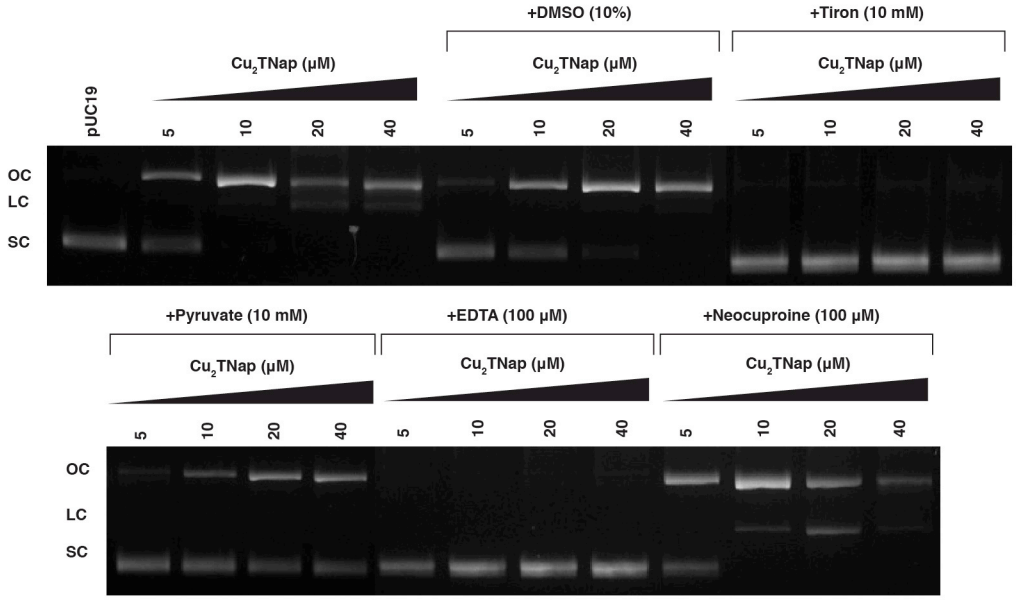

Figure C-9. DNA cleavage experiment in the absence and presence of radical scavangers; DMSO, tiron, pyruvate, EDTA and neocuproine.

C-6: References

1. Malina,J., Farrell,N.P. and Brabec,V. (2014) Substitution-Inert Trinuclear Platinum Complexes Efficiently Condense/Aggregate Nucleic Acids and Inhibit Enzymatic Activity. *Angew. Chemie Int. Ed.*, **53**, 12812–12816.
2. Xu,Y., Suzuki,Y., Lönnberg,T. and Komiyama,M. (2009) Human telomeric DNA sequence-specific cleaving by G-quadruplex formation. *J. Am. Chem. Soc.*, **131**, 2871–2874.
3. Feng,G., Natale,D., Prabaharan,R., Mareque-Rivas,J.C. and Williams,N.H. (2006) Efficient phosphodiester binding and cleavage by a ZnII complex combining hydrogen-bonding interactions and double lewis acid activation. *Angew. Chemie Int. Ed.*, **45**, 7056–7059.
4. CrysAlisPro, Oxford Diffraction Ltd., Version 1.171.33.31 (release 08-01-2009 CrysAlis171.NET).
5. Sheldrick,G.M. (2015) SHELXT. *Acta Crystallogr.*, **A71**, 3–8.
6. Sheldrick,G.M. (2015) SHELXL. *Acta Crystallogr.*, **C71**, 3–8.
7. McArdle,P., Gilligan,K., Cunningham,D., Dark,R. and Mahon,M. (2004) A method for the prediction of the crystal structure of ionic organic compounds - the crystal structures of o-toluidinium chloride and bromide and polymorphism of bicifadine hydrochloride. *CrystEngComm*, **6**, 303–309.

CHAPTER V.

C_3-Symmetric Opioid Scaffolds are pH-Responsive DNA Condensation Agents

---

This paper was accepted for publication in *Nucleic Acids Research*, 2017, DOI: 10.1093/nar/gkw1097.

Natasha McStay, Zara Molphy, Alan Coughlan, Attilio Cafolla, Vickie McKee, Nicholas Gathergood and Andrew Kellett.

My contibution to this paper was to design and conduct condensation studies on a series of mono-substituted (C_1-symmetric), di-substitued (C_2-symmetric) and tri-substituted (C_3-symmetric) mesitylene-linked opioid scaffolds. Assays carried during this project include; condensation studies on both linear and double stranded DNA and endonuclease enzyme inhibition assays using both molecular biology and absorbance based techniques. The effects of methylation of each *N*-piperidine moiety in MC3 were also investigated. DNA binding studies were carried out in collaboration with my co-worker Miss. Natasha McStay.

V. 1. Abstract

Herein we report the synthesis of tripodal C_3-symmetric opioid scaffolds as high-affinity condensation agents of duplex DNA. Condensation was achieved on both supercoiled and canonical B-DNA structures and identified by agarose electrophoresis, viscosity, turbidity, and atomic force microscopy (AFM) measurements. Structurally, the requirement of a *tris*-opioid scaffold for condensation is demonstrated as both di- (C_2-symmetric) and mono-substituted (C_1-symmetric) mesitylene-linked opioid derivatives poorly coordinate dsDNA. Condensation, observed by toroidal and globule AFM aggregation, arises from surface-binding ionic interactions between protonated, cationic, tertiary amine groups on the opioid skeleton and the phosphate nucleic acid backbone. Indeed, by converting the 6-hydroxyl group of C_3-morphine (**MC3**) to methoxy substituents in C_3-heterocodeine (**HC3**) and C_3-oripavine (**OC3**) molecules, dsDNA compaction is retained thus negating the possibility of phosphate—hydroxyl surface-binding. Tripodal opioid condensation was identified as pH dependent and strongly influenced by ionic strength with further evidence of cationic amine-phosphate backbone coordination arising from thermal melting analysis and circular dichroism spectroscopy, with compaction also witnessed on synthetic dsDNA co-polymers poly[d(A-T)$_2$] and poly[d(G-C)$_2$]. On-chip microfluidic analysis of DNA condensed by C_3-agents provided concentration-dependent protection (inhibition) to site-selective excision by type II restriction enzymes: BamHI, HindIII, SalI, and EcoRI, but not to the endonuclease DNase I.

V. 2. Introduction

The search for new synthetic DNA recognition agents is an area of considerable research importance. These agents can be categorised, broadly, into two main areas: *i.*) those that covalently bind nucleic acids at electron rich sites on the nucleobase (1–3), and *ii.*) those that bind in non-covalent fashion through hydrogen (H)-bonding, ionic, or π-stacking interactions (4–6). Accordingly, non-covalent recognition scaffolds may be further classified to the area of DNA where recognition occurs thus giving rise to groove binders (7–9), intercalators (9–12) (including threading intercalators(13)) and surface-binding compounds (14). Within this last category, surface interacting compounds have been designed, and compared, to naturally occurring protein binding domains containing, for example, cationic arginine (arginine fork(15)) or lysine (poly-*L*-lysine(16)) amino acid residues that facilitate their complexation to nucleic acids. Indeed, a commonality between synthetic and naturally occurring surface binders is their ability to efficiently bind electron-

rich phosphate atoms located at the nucleic acid backbone, principally through H-bonding and electrostatic interactions. Furthermore, electrostatic binding by polycationic molecules can directly lead to a collapse in the B-DNA conformation with resultant condensation or aggregation of tertiary DNA helical structures (17). Condensation agents have, in-turn, found widespread utility in molecular biology as transfection agents capable of mediating cellular delivery of nucleic acids for ubiquitous therapeutic and bioprocessing applications (18). Thus, an important consideration in the development of new DNA condensation agents is their relative inertness toward chemical reactivity (*e.g*. artificial nuclease) or secondary interactions (*e.g*. intercalation) that may interrupt or block efficient transport and incorporation of target nucleic acids into mammalian cells.

While nucleic acid condensation can be achieved through mechanisms of neutral crowding, antisolvent precipitation and liposomal packaging (amongst others), significant attention focuses on the condensation properties of multivalent cationic compounds including cationic polymers. Although DNA condensation has been reviewed by Bloomfield (17) and others including theoretical descriptions into the dynamics of polymer collapse (19, 20), it is worth considering some examples of multivalent cations currently accessible to this field. Cationic charge density—essential for the neutralisation of anionic phosphate charge and the reorganisation of water dipoles adjacent to DNA surfaces—plays a critical role in driving condensation and the majority of cationic agents carry a formal charge of 3+ or higher. Prominent examples here include the naturally occurring polyamines spermine^{4+} and spermidine^{3+} that are abundantly found in living organisms and aid in the packaging of cellular DNA by lowering the free energy of transition required for condensation (21). Within the polyamine class, it was demonstrated that DNA collapse occurs once ~90% of phosphate charge neutralisation has occurred (22) and that polyamine structure, allied with charge, plays a role within condensation transitions (21). Polyamines of varying aliphatic linker length have recently been incorporated into substitution inert tri-platinum(II) complexes (Triplatin) and these highly cationic agents are capable of aggregating nucleic acids (both RNA and DNA) through clamping interactions along the phosphate backbone and across the minor groove of DNA (23–25). Evidence of condensation by Triplatin agents was identified by turbidity and AFM analysis with DNA (24), particularly poly[d(A-T)$_2$] (23), undergoing a B $\longrightarrow$ ψ transition during the collapse. Another substitutionally inert complex cation, cobalt(III) hexammine $[Co(NH_3)_6]^{3+}$, has undergone extensive study for its ionic surface-binding, condensation and dehydration

properties with DNA (26, 27). Although $[Co(NH_3)_6]^{3+}$ can also induce a B ⟶ ψ transitions in short oligonucleotide sequences, aggregation of long DNA polymers occurs without modification to the secondary B-DNA conformation (28). Furthermore, while the morphology of DNA condensates with $[Co(NH_3)_6]^{3+}$ are commonly toroidal in structure, non-toroidal (rod-like) structures are observed in the presence of alcohol solvents. A further example of metal complex-promoted DNA condensation was recently identified by *di*-Fe^{2+} supramolecular helicates; these 4+ cationic agents bind DNA non-covalently and are capable of inhibiting DNA-processing enzymes including RNA polymerase, DNA topoisomerase I, deoxyribonuclease I, along with a variety of restriction endonucleases (29). Polycations can also induce alternative changes in B-DNA configuration; a reversible B ⟶ A transition, regulated by dehydration, was recently evidenced in short G-C rich oligonucleotide sequences exposed to a poly(allylamine)-*graft*-dextran synthetic cationic polymer (16). Finally, although exceptions to the ≥3+ cationic valence requirement for DNA collapse are rare, both Mn^{2+} and the putrescine^{2+} cations are known to aggregate DNA but only at high (millimolar) concentration (30).

In this study we report the synthesis of a new class of DNA binding scaffold incorporating opioid derivatives. Opioids are naturally derived alkaloids from the opium poppy, *Papaver somniferum*, and serve as one of the major drug classes within pharmaceutical chemistry widely known for their potent analgesic properties (31). Morphine was the first opioid isolated from the poppy and is the most abundant opioid interacting with three principal opioid receptors located in the central nervous system (CNS): mu (μ, MOR), kappa (κ, KOR) and delta (δ, DOR). The interaction of opioids with CNS receptors has led toward the development of synthetic analogues (including heterocodeine, buprenorphine, and naltrexone) and to more heavily modified structures containing multiple opiate substituents. Morphine congeners can also be extracted from the poppy (e.g. codeine, thebaine and oripavane) and offer a range of bio-renewable derivatives to support proposed SAR studies. Our group has recently developed a high-throughput ethidium bromide displacement screen to identify potentially new DNA binding molecules (32) and, as such, identified a synthetic C_3-symmetric morphine molecule (**MC3**), containing a mesitylene bridging ligand, as a lead compound that was subsequently found to induce DNA condensation at low micromolar concentration. Our motivation for developing heterocodeine (**HC3**) and oripavine (**OC3**) analogues stemmed from structural analysis of **MC3** that focused on the 6′-OH group in the morphine C ring as

a possible hydrogen(H)-bonding site for phosphate coordination at the nucleic acid backbone. If this were the case, masking this H-bond through the introduction of methyl groups in the form of methoxy substituents present in heterocodeine (**H**) and oripavine (**O**) should render the DNA binding properties negligible. In addition, as oripavine is a natural product, and commercially available, a short and direct synthesis of the C_3-symmetry target was envisaged. Surprisingly however, enhanced EtBr displacement was observed for both **HC3** and **OC3** agents, thus implying only a limited role for 6′-OH phosphate interaction in the binding mechanism. Consequently, the DNA binding mode and condensation properties of this class of molecule were elucidated using an array of biophysical techniques including turbidity, viscosity, thermal melting, circular dichroism spectroscopy, electrophoresis and AFM analysis, and are reported herein.

V. 3. Materials and Methods

V. 3.1. Materials synthesis and characterisation

Chemicals and reagents were sourced from Sigma-Aldrich and were used without any further purification required. HPLC grade chloroform, methanol, and acetonitrile were used with no futher purification. All other solvents were used as supplied. Morphine and oripavine were provided from Johnson Matthey MacFarlan Smith Ltd. Thin layer chromatography was performed on Fluka Silica gel (60 F254) coated on aluminium plates. The TLC plates were visualised using UV light. Davisil 60 Å silica gel was used for column chromatography. ^{1}H and ^{13}C NMR spectra were obtained on a Bruker AC 400 MHz NMR spectrometer. The pH was monitored by a Mettler Toledo InLab Expert Pro-ISM pH probe. Electrospray ionisation mass spectra (ESI-MS) were recorded using a Thermo Fisher Exactive Orbitrap mass spectrometer coupled to an Advion TriVersa Nanomate injection system with samples being prepared in 100% HPLC-grade acetonitrile prior to ESI-MS analysis. Circular dichroism spectrometry was conducted on an Applied Photophysics Chirascan plus qCD spectrometer with samples being prepared in acetonitrile.

V. 3. 1. 1. *Morphine-C_3 (MC3)*

Morphine (0.573 g, 2.01 mmol) and potassium carbonate (1.110 g, 8.03 mmol) were suspended in ACN (30 ml) and heated to reflux. 2,4,6-*Tris*-(bromomethyl)-mesitylene (0.268 g, 0.66 mmol) was added in small aliquots to the reaction mixture and vigorously stirred overnight (18 h) under reflux conditions. After allowing the reaction mixture to cool

to rt, the reaction solvent was removed by rotary evaporation and crude product dissolved in DCM (50 ml). The organic layer was washed with d.H_2O (40 ml) and the aqueous layer extracted with DCM (3 x 20 ml). All organic layers were combined, then washed with d.H_2O (3 x 20 ml) and with a saturated brine solution (20 ml). The organic layer was dried over magnesium sulphate, filtered and solvents removed by rotary evaporation. The crude product was purified by column chromatography (SiO_2, 95:1:1 to 92:8:1 CH_2Cl_2:MeOH:NH_4OH). The title compound **MC3** was isolated as a white solid in 50% yield (0.338 g, 0.33 mmol). mp. 187-189°C. ^{1}H NMR (600 MHz, $CDCl_3$) δ 6.80 (d, J = 8.2 Hz, 3H); 6.58 (d, J = 8.2 Hz, 3H); 5.69 (ddt, *J* = 9.9, 3.2, 1.4 Hz, 3H); 5.30 – 5.27 (m, 3H); 5.21 (d, J = 10.5 Hz, 3H); 5.05 (d, J = 10.4 Hz, 3H); 4.85 (dd, J = 6.5, 1.1 Hz, 3H); 4.17 – 4.13 (m, 3H); 3.35 (s, 3H); 3.05 (d, J = 18.7 Hz, 3H); 2.66 (s, 3H); 2.61 – 2.56 (m, 3H); 2.48 (s, 9H); 2.44 (s, 9H); 2.41 – 2.37 (m, 3H); 2.31 (dd, J = 18.7, 6.2 Hz, 3H); 2.05 (td, *J* = 12.4, 5.0 Hz, 3H); 1.88 (d, J = 11.3 Hz, 3H). ^{13}C NMR (151 MHz, $CDCl_3$) δ 147.59, 141.43, 139.43, 133.41, 131.82, 131.44, 128.19, 119.61, 116.36, 91.27, 77.22, 77.00, 76.79, 67.32, 66.46, 58.93, 46.47, 43.09, 42.96, 40.81, 35.78, 20.64, 15.98. IR (ATR, cm^1): 2907, 1632, 1602, 1492, 1443, 1247, 1200, 1157, 1118, 1099, 1034, 983, 940, 833, 784, 766, 731. ESI-MS: [**MC3**] 1012 m/z. $[\alpha]_D = -85°$ (c = 0.154, $CHCl_3$, 589nm, 25°C).

V. 3.1.2. *Oripavine-C_3 (OC3)*

A flask was charged with oripavine (0.595 g, 2.00 mmol), tetrabutylammonium hydroxide (40% aqueous solution, 18 ml) and DCM (6 ml) and stirred under nitrogen for 30 mins. A solution of 2,4,6-*tris*-(bromomethyl)-mesitylene (0.269 g, 0.66 mmol) in DCM (4 ml) was added and the biphasic reaction mixture was stirred for 6 h at rt. The reaction solution was transferred into d.H_2O (150 ml) and washed with DCM (4 x 10 ml). Organic layers were combined and washed with aqueous NaOH solution (0.1 M, 2 x 20 ml) followed by d.H_2O (3 x 20 ml) then saturated brine solution (20 ml). The organic layer was dried over magnesium sulphate, filtered and solvents removed by rotary evaporation. The crude product was purified by column chromatography (SiO_2, 95:1:1 to 92:8:1 CH_2Cl_2:MeOH:NH_4OH), The title compound **OC3** was isolated as a golden yellow solid in 47% yield (0.329 g, 0.31 mmol). mp 174-176°C. ^{1}H NMR (600 MHz, $CDCl_3$) δ 6.73 (d, J = 8.1 Hz, 3H); 6.58 (d, J = 8.1 Hz, 3H); 5.56 (d, J = 6.4 Hz, 3H); 5.28 (s, 3H); 5.25 (d, J = 10.7 Hz, 3H); 5.17 (d, J = 10.7 Hz, 3H); 5.03 (d, J = 6.4 Hz, 3H); 3.62 (d, J = 6.6 Hz, 3H); 3.59 (s, 9H); 3.32 (d, J = 18.0 Hz, 3H); 2.83 (td, J = 12.7, 3.3 Hz, 3H); 2.68 (dd, J = 18.1, 7.0 Hz, 3H); 2.63 (dd, J = 12.7, 4.6 Hz, 3H); 2.47 (s, 9H); 2.46 (s, 9H); 2.20 (td, *J* = 12.6,

5.1 Hz, 3H); 1.78 – 1.75 (m, 3H). ^{13}C NMR (151 MHz, $CDCl_3$) δ: 152.96, 146.07, 142.13, 139.65, 133.99, 132.59, 132.06, 128.73, 119.46, 117.48, 111.73, 96.09, 89.16, 89.11, 77.37, 77.16, 76.95, 67.74, 61.07, 55.04, 46.25, 46.16, 42.57, 37.11, 29.93, 16.02. IR (ATR, cm^{-1}): 2908, 1605, 1491, 1437, 1368, 1331, 1302, 1231, 1143, 1105, 1066, 1021, 987, 914, 867, 812, 767, 748, 698. ESI-MS: [**OC3**]$^+$ 1048 m/z. $[\alpha]_D$ = − 88° (c = 0.12, $CHCl_3$, 589nm, 25°C).

V. 3.1.3. *Heterocodeine* (33, 34)

Reaction carried out on parallel synthesiser. Potassium hydride (4.421 g, 110.23 mmol) was prepared in the reaction vessel under nitrogen flux and washed with dry hexane, suspended in dry THF (150 ml) over ice. A solution of morphine (2.862 g, 10.03 mmol) in THF (30 ml) was added slowly over 30 min to the reaction under a nitrogen atmosphere and the resulting solution was allowed to stir at rt for 16 h. Methyl Iodide (1.710 g, 0.75 ml, 12.05 mmol) was added to the reaction slowly over 15 mins and reaction left stirring for 4 h. The reaction was quenched with a mixture of 10:1 THF/H_2O over ice. The reaction was quenched slowly with a mixture of THF/H_2O (10:1) at 0°C. The solution was neutralised to pH 7.0 with 2 M HCl and volatiles were then removed by rotary evaporation. The pH was adjusted to 8.0 by the addition of 1M NaOH and the aqueous layer extracted with chloroform/isopropanol (3:1, 3 x 25 ml). The resulting organic layer was washed with H_2O (4 x 30 ml) and a final wash with saturated brine solution (20 ml). The organic layer was dried over magnesium sulphate, filtered and solvents removed by rotary evaporation. The crude product was purified by column chromatography (SiO_2, 95:1:1 to 92:8:1 CH_2Cl_2:MeOH:NH_4OH), heterocodeine was isolated as a white solid in 25% yield (756 mg, 2.53 mmol). ^{1}H NMR (600 MHz, $CDCl_3$,): δ 6.57 (d, *J* = 8.1 Hz, 1H); 6.41 (d, *J* = 8.1 Hz, 1H); 5.64 (ddt, *J* = 9.9, 3.2, 1.5 Hz, 1H); 5.26 (dt, *J* = 9.8, 2.7 Hz, 2H); 4.91 (dd, *J* = 5.8, 1.3 Hz, 1H); 3.72 (td, *J* = 5.5, 2.3 Hz, 1H); 3.45 (s, 3H); 3.32 (dd, *J* = 6.3, 3.2 Hz, 1H); 2.97 (d, *J* = 18.6 Hz, 1H); 2.63 – 2.49 (m, 2H); 2.43 – 2.31 (m, 4H); 2.23 (dd, *J* = 18.7, 6.4 Hz, 1H); 1.99 (td, *J* = 12.4, 5.1 Hz, 1H); 1.88 – 1.79 (m, 2H).

V. 3.1.4. *Heterocodeine-C_3* (HC3)

A flask was charged with heterocodeine (0.700 g, 2.34 mmol), tetrabutylammonium hydroxide (40% aqueous solution, 20 ml) and DCM (8 ml) and stirred under nitrogen for 30 mins. A solution of 2,4,6-*tris*-(bromomethyl)-mesitylene (0.269 g, 0.66 mmol) in DCM (4 ml) was added and the mixture was stirred for 6 h at rt. The reaction solution was

transferred into d.H_2O (150 ml) and washed with DCM (4 x 10 ml). Organic layers were combined and washed with aqueous NaOH solution (0.1 M, 2 x 20 ml) followed by d.H_2O (3 x 20 ml) then a saturated brine solution (20 ml). The organic layer was dried over magnesium sulphate, filtered and solvents removed by rotary evaporation. The crude product was purified by column chromatography (SiO_2, 95:1:1 to 92:8:1 CH_2Cl_2:MeOH:NH_4OH), **HC3** was isolated by column chromatography as a white solid in 13% yield (95 mg 0.09 mmol). mp. 164-166°C. ^{1}H NMR (400 MHz, $CDCl_3$) δ: 6.73 (d, J = 8.1 Hz, 3H); 6.49 (d, J = 8.1 Hz, 3H); 5.71 (d, J = 9.9 Hz, 3H); 5.32 (dt, J = 10.0, 2.7 Hz, 3H); 5.27 – 5.16 (m, 6H); 5.00 (d, J = 5.1 Hz, 3H); 3.80 (dd, J = 5.4, 2.7 Hz, 3H); 3.51 (s, 9H); 3.36 (dd, J = 5.9, 3.1 Hz, 3H); 3.04 (d, J = 18.7 Hz, 3H); 2.69 – 2.65 (m, 3H); 2.61 – 2.56 (m, 3H); 2.52 (s, 9H); 2.44 (s, 9H); 2.40 (d, J = 3.4 Hz, 3H); 2.31 (dd, J = 18.7, 6.3 Hz, 3H); 2.04 (td, J = 12.4, 5.0 Hz, 3H); 1.93 (d, J = 11.0 Hz, 3H).^{13}C NMR (101 MHz, $CDCl_3$) δ: 148.88, 141.35, 139.66, 132.09, 131.46, 131.01, 128.56, 128.18, 119.02, 118.34, 89.14, 77.48, 77.36, 77.16, 76.84, 75.67, 68.01, 59.06, 56.92, 53.58, 46.68, 43.61, 43.26, 43.19, 41.23, 36.06, 29.82, 20.66, 16.10. IR (ATR, cm^{-1}): 2905, 2798, 1632, 1601, 1492, 1442, 1247, 1199,1104, 984, 941, 831, 787, 768, 727, 679. $[\alpha]_D = -185°$ (c = 0.08, $CHCl_3$, 589 nm, 25°C).

V. 3.2. DNA binding experiments

V. 3.2.1. Competitive Ethidium Bromide Displacement Assay

The DNA binding affinity of the tripodal series was determined over a five hour time period using calf-thymus DNA (ctDNA, Ultra-Pure Invitrogen, 15633019) and synthetic alternating co-polymers poly[d(A-T)$_2$)] (Sigma Aldrich, P0883) and poly[d(G-C)$_2$] (Sigma Aldrich, P9389) by ethidium bromide fluorescence quenching in a similar manner to the high-throughput method previously reported by Kellett *et al* (35). Each drug concentration was measured in triplicate, on at least two separate occasions, and the apparent binding constants were calculated using $K_{app} = K_b$ x 12.6/C_{50} where $K_b = 8.80 \times 10^6$ M(bp)$^{-1}$ (K_{app} = apparent binding constant).

V. 3.2.2. Viscosity studies

Experiments were conducted in a similar manner to the method reported previously using DV-II-Programmable Digital Viscometer equipped with Enhanced Brookfield UL Adapter at room temperature by gradually increasing the [compound/DNA] ratios from 0.02-0.20 (36).

V. 3.2.3. Thermal Melting Studies

The thermal melting of DNA of varying %AT content was conducted using an Agilent Cary 100 dual beam spectrophotometer equipped with a 6 × 6 Peltier multicell system with temperature controller. The protocol was previously developed within the Kellett group and reported elsewhere (6, 7).

V. 3.3. DNA condensation studies (dsDNA)

V. 3.3.1. Turbidity Investigation (ctDNA)

This method was adapted from the Brabec laboratory (24). Absorption spectra were initially measured at 260 nm in order to give a final absorbance of ~0.5 units and the concentration of ctDNA was determined using the extinction coefficient ε_{260} = 12824 $M(bp)^{-1}$ cm^{-1}. The turbidity of the ctDNA solution was determined spectrophotometrically by monitoring the absorbance of DNA at both 350 nm and 260 nm at 25°C using an Agilent Cary 100 dual beam spectrophotometer equipped with a 6×6 Peltier multicell system with temperature controller and stirring mechanism. In a final volume of 3 ml containing ~40 μM ctDNA, 1 mM PBS buffer (pH 7.0) and 25 mM NaCl, varying concentrations of **MC3**, **OC3** and **HC3** (2.5, 5, 7.5, 10, 12.5, 15, 20, 25, 30, 35, 45, 50, 65, 75, 80, 90, 100 μM) were titrated into quartz cuvettes. Between each aliquot, solutions were mixed thoroughly and allowed to incubate at 25°C until the absorbance equilibrated and values obtained remained constant.

V. 3.3.2. DNA condensation investigation (pUC19 scDNA)

The ability of the organic compounds to condense supercoiled plasmid DNA was determined using a method previously published by this laboratory with minor changes being made (23). Tripodal opiates were initially prepared in DMF and further diluted in 80 mM HEPES buffer (Fisher). Reactions were carried out according to the following general procedure: in a total volume of 20 μl using 80 mM HEPES buffer (pH 7.2) with 25 mM NaCl, 400 ng pUC19 (NEB, N3041) and varying concentrations of test compound (5, 10, 20 and 30 μM), samples were incubated at 37°C for both 5 and 12 h. Reactions were quenched by adding 6× loading buffer (Fermentas) containing 10 mM Tris-HCl, 0.03% bromophenol blue, 0.03% xylene cyanole FF, 60% glycerol, 60 mM EDTA and samples were loaded onto an agarose gel (1.2%) containing 3 μl EtBr. Electrophoresis was completed at 60 V for 1 h in 1× TAE buffer.

V. 3.3.3. DNA condensation investigation in the presence of non-covalently bound recognition elements (pUC19 scDNA)

This protocol was carried out as previously reported by this group with minor changes made (37). Briefly, 400 ng pUC19 was incubated with 25 mM NaCl, and 20 μM of either methyl green, netropsin or hexamine cobalt(III) chloride in 80 mM HEPES buffer (pH 7.2) for 30 min at 37°C. Sample tubes were then vortexed and varying concentrations of test compound were added (5, 10, 20 and 30 μM). The reaction mixture was further incubated at 37°C for 5 h. The reaction was then quenched and subjected to gel electrophoresis as previously described.

V.3.3.4. Investigation of DNase I inhibition by DNA condensation (pUC19 scDNA)

400 ng of pUC19 DNA was initially exposed to 75, 100, 200 and 300 μM of test compounds with 25 mM NaCl in a total volume of 20 μl using 80 mM HEPES buffer (pH 7.2) for 5 h at 37°C. The condensed DNA was then treated with the endonuclease, DNase I (NEB, M0303S), for 10 min at 37°C and heat inactivated at 75°C for 10 min. Samples were then loaded onto an agarose gel (1.5%) containing 3 μl EtBr and electrophoresis was completed at 50 V for 40 min in 1× TAE buffer.

V. 3.3.5. Circular Dichroism Spectrometry.

Opioid profiles (**MC3** and **OC3**) and opioid-DNA interactions were analysed using Starna quartz cuvettes in 10 mM PBS solution (pH 7.0) in the presence of 25 mM NaCl. Salmon testes DNA (stDNA, Sigma Aldrich, D1626) was initially quantified using the extinction co-efficient ε_{260} = 12824 $M(bp)^{-1}$ cm^{-1} to give a working solution with final stDNA concentration of ~100 μM. The investigation was conducted in the range of 200-400 nm and measurements were recorded at a rate of 1 nm per second. 100 μM stDNA solution was incubated with **MC3**, **OC3** and control agents hexammine cobalt(III) chloride and spermine at r = 0.1 (r being the ratio [drug] / [DNA]) over a 7 h period at 37°C. The DNA free CD spectra for **MC3** and **OC3** are shown in appendix D-2.

V. 3.4. DNA condensation studies (linear dsDNA)

V. 3.4.1. PCR Primer Design

Primers were designed (Eurofins Genomics) such that it was possible to generate a 742 bp long sequence of linear dsDNA from the pUC19 vector encompassing the lacZα gene. The short nucleotide sequence was generated through PCR (35 cycles) with 1 ng pUC19

plasmid using 2× MyTaq Red Mix (Bioline) at an annealing temperature of 66°C and the band generated was compared to a 50 bp DNA ladder (Invitrogen, 10416014).

Forward: `5'-TCGCGCGTTTCGGTGATGACGG-3'`

Reverse: `5'-CCGCTCGCCGCAGCCGAACG-3'`

V. 3.4.2. DNA condensation investigation.

400 ng of the 742 bp transcript was then treated under identical conditions as described (5 h incubation at 5, 10, 20 and 30 μM) and samples were loaded onto an agarose gel (1.2%) containing EtBr. Electrophoresis was completed at 70 V for 40 min in 1× TAE buffer.

V. 3.5. Endonuclease enzyme Inhibition

V. 3.5.1. Endonuclease Optimisation on linear DNA sequence

400 ng of linear dsDNA was treated with 1 μL of EcoRI (NEB, R0101S), BamHI (NEB, R0136S), SalI (NEB, R0138S) and HindIII (NEB, R0104S) respectively at 37°C overnight to verify the presence of their recognition sites within the short 742 bp sequence. All enzymes induced double stranded nicks to this sequence as evidenced by agarose gel electrophoresis.

V. 3.5.2. Microfluidic analysis of endonuclease inhibition assay using Agilent BioAnalyser DNA 1000 chip

This assay was conducted as previously described by the Kellett Group with small changes being made (23). 400 ng of the PCR fragment was pre-treated with 10, 25, 50, 100 and 200 μM of either **MC3, HC3** or **OC3**. Subsequent digestion experiments were performed by incubating drug treated and un-treated DNA with 1 μL of EcoRI, BamHI, SalI and HindIII overnight and heat deactivated as per NEB guidelines. The reactions of EcoRI, BamHI, SalI and HindIII, in the presence and absence of tripodal scaffolds, were then examined using the Agilent DNA 1000 microfluidic chip (Agilent 5067-1504) with data being collected on the Agilent Bioanalyser 2100 platform.

V. 3.6. Atomic Force Microscopy

AFM was used to determine the morphology of the DNA condensates induced by morphine C_3 opiate to support the effects of condensation at low concentrations. AFM samples were prepared according to the following general procedure: in a total volume of 10 μl final concentrations of 3 ng/μl of pUC19 (NEB, N3041) or linearised pUC19, 5 mM MgCl, and varying concentrations of test compound, were incubated at 37°C for 1 h. 10 μl

of each sample was pipetted directly on to freshly cleaved mica and allowed to incubate for 5 min followed by rinsing with 500 μl of water. The samples were dried under compressed air for a period of 1 h. AFM examinations were performed in ambient air with a commercial microscope (Dimension 3100 controlled by a Nanoscope IIIa controller, Digital Instruments), in tapping-mode, using standard unmodified silicon cantilevers (BudgetSensors, Bulgaria) with a 40 N/m force constant. Topographic images are recorded at a scanning rate of 1–2 Hz, and a resonance frequency of about 300 kHz (nominal value). Images were processed using the WSxM software (38) to remove the background slope and normalise the z-scale across all images, no additional filtering was performed.

V. 3.7. Influence of pH and ionic strength on condensation

V. 3.7.1. Influence of pH on condensation

Absorption spectra were initially measured at 260 nm in order to give a final absorbance of ~0.4 units and the concentration of ctDNA was determined using the extinction co-efficient ε_{260} = 12824 $M(bp)^{-1}$ cm^{-1}. The condensation aggregates of the ctDNA solution was determined spectrophotometrically by monitoring the absorbance of DNA at both 350 nm and 260 nm at 25°C using an Agilent Cary 100 dual beam spectrophotometer equipped with a 6 × 6 Peltier multicell system with temperature controller. In a final volume of 5 mL containing ~30μM ctDNA, nuclease free water (pH 7) and 25 mM NaCl, containing 35 μM **OC3**, the pH of solution was adjusted with 1 M HCl and 1 M NaOH to basic and acidic conditions as required using a Mettler Toledo SevenExcellence pH meter equipped with a Mettler Toledo Inlab expert Pro-ISM pH probe. 100 μl aliquots were titrated into quartz cuvettes and between each pH adjustment the solution were mixed thoroughly and allowed to incubate at 25°C until the absorbance equilibrated and values obtained remained constant.

V. 3.7.2. DNA condensation in acidic and basic buffers

400 ng of pUC19 DNA was treated as previously stated with slight modifications (5 h incubation at 5, 10, 20, 30, and 50 μM). Samples were incubated in acidic and basic buffers at pH 4.0 and 8.0 respectively. NaOAc and Tris buffers were prepared and adjusted with HCl and NaOH accordingly to achieve the desired pH. Samples were loaded onto an agarose gel (1.2%) containing 3 μl EtBr. Electrophoresis was completed at 70 V for 40 min in 1× TAE buffer.

V. 4. Results and Discussion

V. 4.1. Synthesis of opioid scaffolds

Morphine scaffolds **MC3**, **HC3**, and **OC3** were generated and their molecular structures are shown in Figure V-1. Treating 1 equivalent of 2,4,6-*tris*-(bromomethyl)-mesitylene with 3 equivalents of either morphine (**M**), heterocodeine (**H**) or oripavine (**O**) yielded the respective C_3-symmetric opioid compounds **MC3**, **HC3**, and **OC3**. These were isolated as yellow or white solids after purification by column chromatography. A satisfactory yield for both **MC3** (50%) and **OC3** (48%) was obtained, however **HC3** could only be isolated in a low yield (13%). Indeed, generation of the **HC3** opioid was restricted due to the poor synthetic conversion of morphine to heterocodeine with yields <25% (39), which leads to a low overall yield for **HC3** from morphine. C_1 and C_2 opiate analogues (**MC1**, **MC2**, **OC1** and **OC2**) were synthesised in a similar manner to the C_3 congeners using α-2-chloroisodurene (**MC1** and **OC1**) and 2,4-bis(chloromethyl)-1,3,5-trimethylbenzene (**MC2** and **OC2**), respectively, of each opioid derivative (Appendix S-7). The series of compounds for this study were all prepared in either a one- or two-step synthesis and enable rapid access to samples for evaluation in biological investigations. All compounds were characterised by ^{1}H and ^{13}C nuclear magnetic resonance (NMR, Appendix S-1) and attenuated total reflectance (ATR) Fourier transform infrared (FTIR) spectroscopies, and by electrospray ionisation mass spectrometry (ESI-MS). Solution-based NMR studies in deuterated chloroform were performed to elucidate whether all three opiate units were on the same face of the molecule (C_3) or whether rotation of one opiate 'arm' was rapidly occurring at room temperature. To test the latter, a temperature study was conducted. This confirmed a C_3-symmetric opioid compound was formed for each of the *tris* target compounds; a single set of peaks in the ^{1}H NMR was observed for the opioid substructure for **MC3**, **HC3** and **OC3** in both 1D and 2D NMR studies. As the probe temperature was decreased from 293 K to 243 K no changes in the proton NMR were detected, supporting the C_3 symmetry of the compounds as a stable configuration.

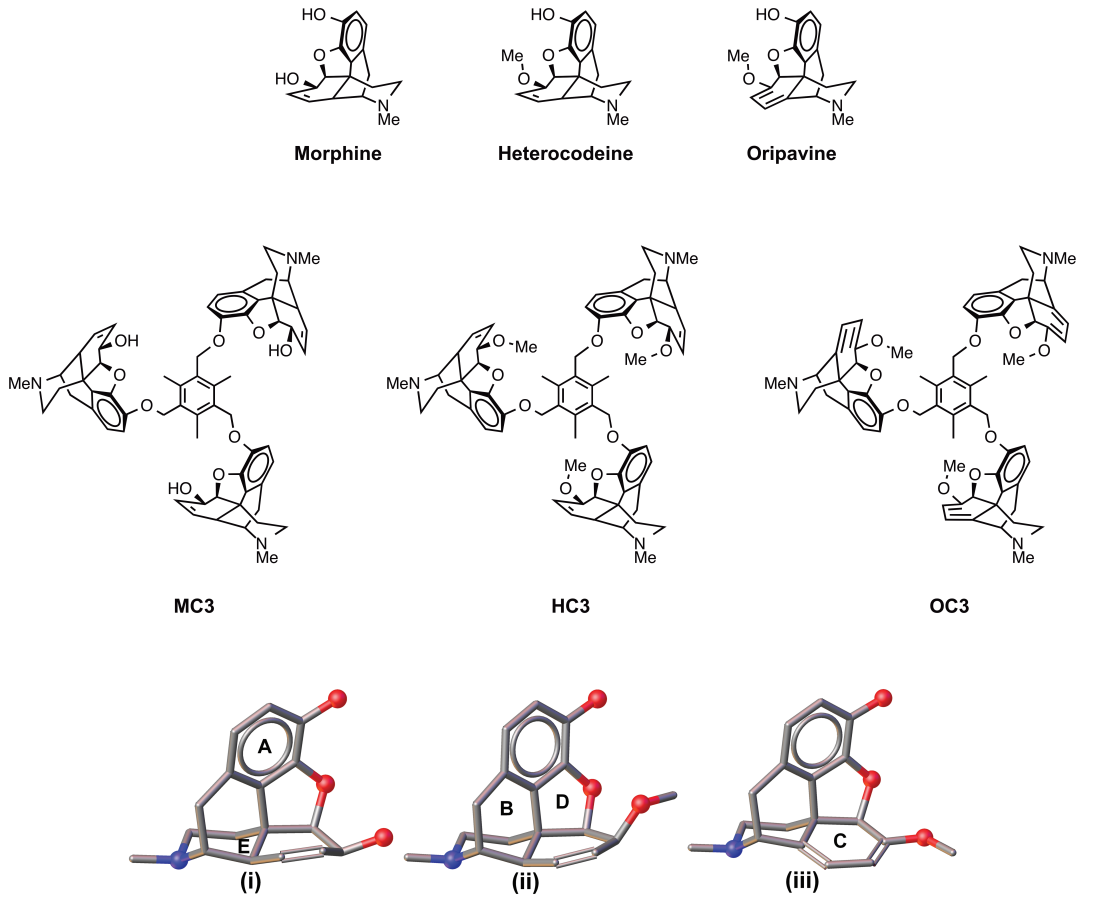

Figure V-1. Molecular structures of, heterocodeine, and oripavine along with C_3-symmetic opioids molecules developed in this study: morphine (**MC3**), heterocodeine (**HC3**), and oripavine (**OC3**). Left to right, morphine, heterocodeine and oripavine scaffolds. Structures **(i)**, **(ii)** and **(iii)** show the geometries of each scaffold (morphine, heterocodeine and oripavine respectively), with labeled ring substituents **A-E**, modified from X-ray structures reported in the CSD.

V. 4.2. Condensation of duplex DNA

C_3 opiate binding interactions with duplex DNA were first identified using a saturated ethidium bromide (EtBr) fluorescence quenching study with calf thymus DNA (CT-DNA) (Figure V-2). In our initial high-throughput screen, which involved a series of novel opioid scaffolds, **MC3** was identified as a potentially new DNA binding molecule. Our motivation for developing **HC3** and **OC3** isomers stemmed from structural analysis on **MC3** that focused on the 6′-OH group in the morphine C ring as a possible H-bonding site for phosphate coordination. Since this group is masked by methylation in heterocodeine (**H**) and oripavine (**O**), we anticipated **HC3** and **OC3** analogues would have negligible DNA binding properties. Unexpectedly, however, enhanced EtBr displacement was observed (Table V-1), particularly on poly[d(G-C)$_2$] and poly[d(A-T)$_2$] co-polymers with apparent binding constants (K_{app}) of ~10^6 M(bp^{-1}) and ~10^7 M(bp^{-1}), respectively.

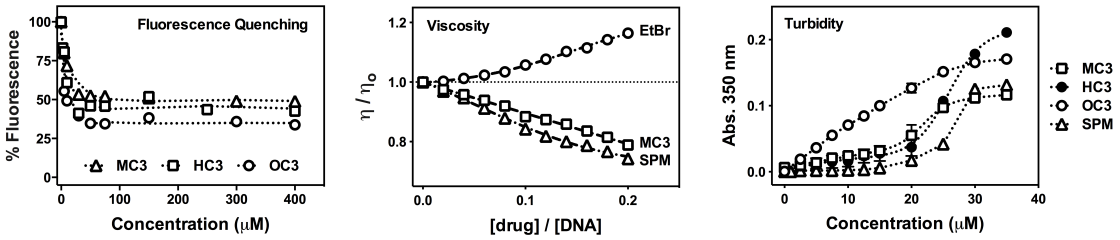

Figure V-2. Competitive fluorescence quenching of ethidium bromide bound to CT-DNA by opioid drugs **MC3**, **HC3**, and **OC3**, viscosity properties of **MC3**, ethidium bromide (EtBr) and spermine (SPM) exposed to salmon testes dsDNA, and turbidity profiles of CT-DNA in the presence of titrated C_3 opioids and spermine. Data points being displayed as an average of triplicate measurement for fluorescence quenching and turbidity measurements.

Table V-1. Apparent binding constants of opioid C_3 compounds to dsDNA polymers. (N.D. = not detected)

	K_{app} M(bp^{-1})			ΔT_M °C (± S.D.)	
	Poly A-T (100% A-T)	CT-DNA (58% A-T)	Poly G-C (0% A-T)	Poly A-T (100% A-T)	Poly G-C (0% A-T)
Actinomycin D (35)	N.D.	2.92×10^7	5.35×10^7	-0.32 ± 0.29	12.10 ± 0.95
Netropsin (35)	5.75×10^7	2.5×10^6	N.D.	12.32 ± 0.79	2.83 ± 0.38
MC3	3.03×10^5	6.40×10^6	2.69×10^5	0.38 ± 0.71	2.63 ± 0.58
OC3	3.63×10^6	3.82×10^6	3.5×10^7	-0.17 ± 0.25	0.36 ± 0.17
HC3	9.1×10^6	7.84×10^6	1.15×10^7	0.73 ± 0.18	1.72 ± 0.61

To identify the significance of the C_3 opioid scaffold symmetry toward duplex DNA binding, **OC1**, **OC2**, **MC1** and **MC2** compounds were generated and tested using gel electrophoresis experiments (24, 35, 37). Condensation results, however, revealed negligible C_1 and C_2 activity (Appendix D-3) confirming the requirement of a tertiary opioid substituent to facilitate efficient nucleic acid coordination at low micromolar concentration. Thermal melting analysis on duplex polymers were then completed (Table V-1), and, unlike classic DNA binding agents of netropsin and actinomycin D (35), examined previously under identical conditions by this group, no significant stabilisation energies were identified for the *tris*-opiate compounds.

In order to probe the nature of DNA binding, viscosity studies with salmon testes DNA (ST-DNA) at varying drug load were evaluated (Figure V-2). Classical condensation behaviour by C_3 opioids was observed whereby all three agents exhibited identical, downward curving, hydrodynamic (η/η_o) values. As shown in Figure V-2, the profile of **MC3** is similar to the well-studied DNA compaction agent spermine (SPM), which was run as a control agent alongside the classical DNA intercalator EtBr. Since condensation of dsDNA can be monitored at 350 nm, a wavelength where nucleic acids do not normally absorb unless condensation/aggregation has occurred (24), UV-vis absorption spectrophotometry was employed to further characterise the condensation process.

(Although turbidity of dsDNA can also be monitored at 260 nm, electronic absorption of C_3 opioids in this region precluded this measurement.) All three opioids exhibit concentration-dependent aggregation of dsDNA with binding isotherms of **MC3** and **HC3** being sigmoidal in nature and approximately similar in shape to spermine (Figure V-2). **OC3**, however, has a markedly different profile that increases almost linearly between 1–25 μM before reaching a plateau beyond this titration point. Overall, and in comparison to spermine, greater aggregation was observed for C_3 opioids tested up to 25 μM, beyond which, **OC3** and **MC3** scaffolds can be described as having the highest condensation effects in the series.

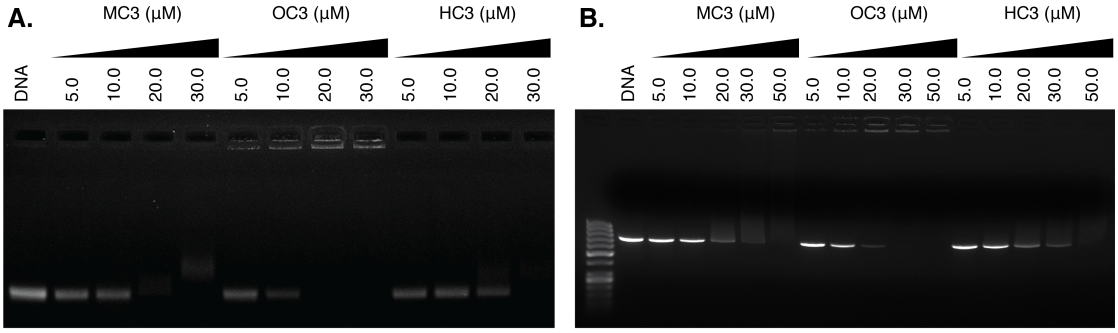

Figure V-3. A. Agarose gel electrophoresis of supercoiled (400 ng) and **B.** a 742 bp dsDNA fragment of pUC19 (400 ng) exposed to increasing concentrations of **MC3**, **OC3**, and **HC3**. Reactions were carried out in the presence of 25 mM NaCl for 5 h at 37°C prior to electrophoretic analysis.

Since condensation by C_3 opioids had been established by viscosity and turbidity measurements, visualisation of DNA compaction was then followed by electrophoresis. Samples were titrated against both supercoiled pUC19 plasmid DNA and a 742 bp dsDNA fragment amplified from pUC19 encompassing the lacZα gene, before incubation for 5 h prior to analysis by agarose gel electrophoresis (Figure V-3). All three opioid scaffolds were found to condense both supercoiled and linear dsDNA; **MC3** and **HC3** have similar profiles with the onset of aggregation at 20 μM, beyond which native DNA bands become fainter in appearance or disappear entirely from view, thus reflecting total condensation. **OC3**, however, exhibits improved condensation effects in comparison to morphine and heterocodeine scaffolds. Here, the initiation of aggregation can be visualised at 5 μM with the condensation process being completed at 20 μM and 30 μM on supercoiled plasmid and linear DNA, respectively. Indeed, on comparing the gels, it is evident that opioid-induced aggregation of supercoiled pUC19 (Figure V-3A) occurs more efficiently than for linear dsDNA (Figure V-3B).

To further probe the condensation mechanism, the interaction of C_3 opioids with pUC19 were examined in the presence of non-covalently bound recognition elements netropsin, which is well-characterised to bind within the minor groove (40), and methyl green—an agent that binds at the major groove (41). In these experiments plasmid DNA was pre-exposed to 20 μM of each recognition element prior to the introduction of opioid sample (5 – 50 μM). No differences were detected in the condensation process between the control (opioid + pUC19) and tested samples in any case, indicating interactions within the minor and major grooves are unlikely as prospective recognition sites for C_3 opioid binding (data not shown). Indeed, no evidence of minor or major groove binding, or of intercalation could be found in the circular dichroism (CD) spectra of **MC3** and **OC3** with ST-DNA (Figure V-4). It was further noted that no conformational change was induced upon opioid binding and condensation. Thus, the profiles for both C_3 scaffolds do not yield spectral shifts expected of classical DNA binding agents but, instead, are similar to surface-binding condensation agents spermine and $[Co(NH_3)_6]Cl_3$ (42) when tested with long DNA polymers. Finally, while the spectrum of **HC3** could not be examined owning to its limited solubility in CD accessible solvents, it is reasonable to assume the binding interaction should not deviate from that observed from **MC3** or **OC3**.

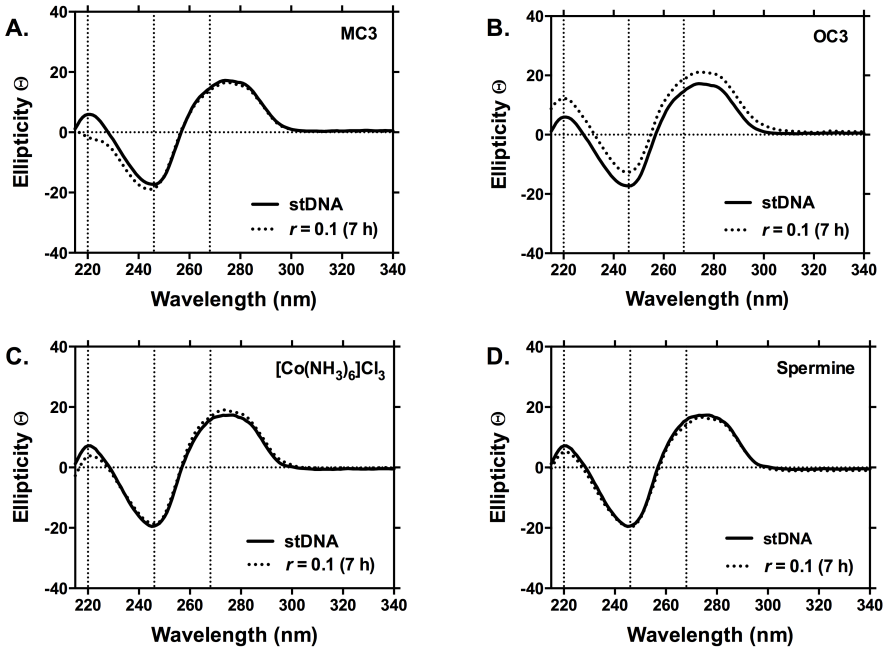

Figure V-4. Circular dichroism (CD) spectra of ST-DNA treated with **MC3**, **OC3** and electrostatic DNA binding controls hexammine cobalt(III) chloride and spermine over 7 h at *r* ([opioid] / [DNA]) values of 0.1.

V. 4.3. Influence of pH and ionic strength on condensation

Since the biophysical evidence gathered on C_3 opioid-DNA binding points toward a surface-binding coordination mode, we considered the possibility of the tertiary amine within the morphine D (piperidine) ring as a possible cationic site responsible for H-bonding and/or electrostatic binding to the phosphate backbone. Indeed, this particular site is well recognised to undergo protonation prior to binding with specific amino acid residues within opioid receptor cavities (43). To examine this hypothesis, the condensation effects of supercoiled pUC19 were initially examined under sodium chloride titration on agarose electrophoresis. Here, 25 μM aliquots of **MC3**, **OC3**, and **HC3** were analysed with increasing NaCl ionic strength (25 – 1000 mM) with supercoiled pUC19 (Figure V-5A). At low salt concentrations (25 – 75 mM) the plasmid was condensed by all three opioids, however, in the presence of ≥100 mM NaCl, aggregation by **MC3** and **HC3** agents was inhibited as evidenced by the fraction of DNA migrating in supercoiled form. In contrast, **OC3** maintained its condensation effects up to 750 mM of titrated NaCl and only at the highest ionic strength examined, 1 M, could a fraction of native supercoiled pUC19 be identified. These results indicate that condensation by C_3 morphine analogues are dependent on ionic charge, and that disruption of this interaction by the introduction of an ionic gradient can, at least partially, reverse DNA aggregation. Furthermore, it is worth highlighting that compaction by **MC3** and **HC3** is disrupted to the same degree by NaCl, while **OC3** is substantially more resistant to changes in ionic strength.

To further probe the involvement of quaternary amine cations in the condensation process, aggregation of pUC19 was then examined under acidic (pH 4.0) and basic (pH 9.0) buffered conditions. As anticipated, a clear enhancement of the condensation process at lower pH with sodium acetate buffer (Figure V-5B) was observed, while under basic conditions (Tris buffer) DNA aggregation was reduced (Figure V-5C). These results indicate that in an acidic environment, the piperidine opioid D ring becomes protonated and collapse of DNA proceeds at lower C_3 concentration. Indeed, on comparing Figure V-3A with Figure V5B and C it is clear that condensation in pH 4 buffered solution occurs with the highest efficiency across all three tested opioids, followed thereafter by condensates at pH 7.2 and then finally pH 9.0 where very little aggregation for both **MC3** and **HC3**. This analysis supports proposal that the amine group within the piperidine opioid ring is the protonation site responsible for condensation and, based on these

condensation results, is highly probable the 3+ polycationic state of the C_3 symmetric opioid scaffold is required to induce aggregation.

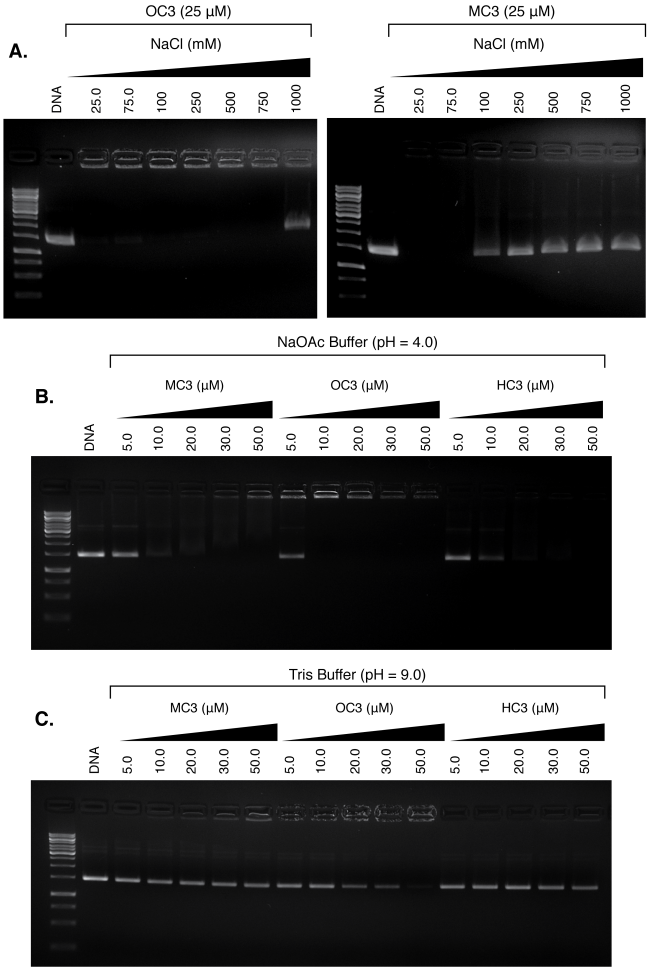

Figure V-5. A. Influence of ionic strength on pUC19 condensation (400 ng) by **OC3** and **MC3** (25 μM) opioid compounds. Condensation reactions on pUC19 (400 ng) by opioid compounds in **B.** acidic NaOAc buffer (80 mM, pH = 4.0), and C. basic Tris buffer (80 mM, pH = 9.0) in the presence of 25 mM NaCl.

V. 4.4. Atomic force microscopy (AFM)

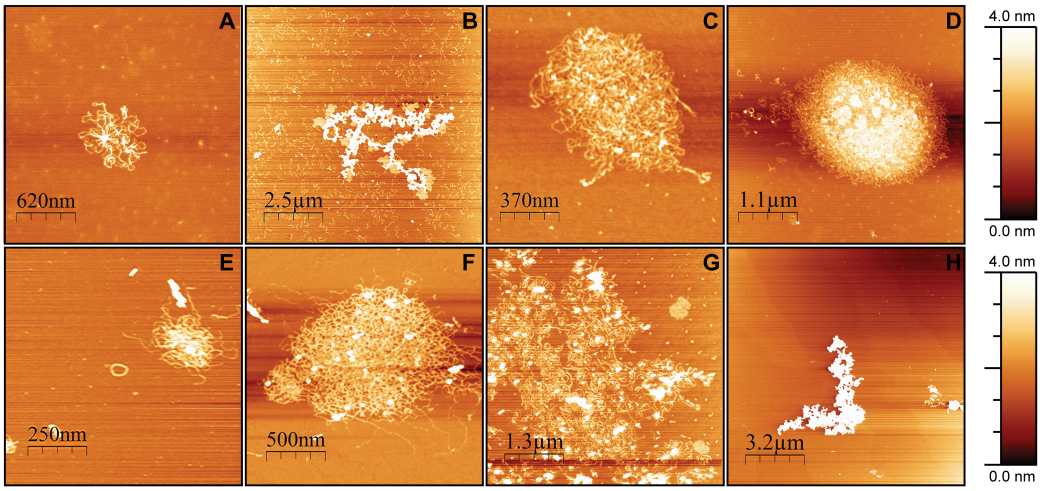

Figure V-6. AFM images of **MC3**-treated supercoiled and HindIII linearised pUC19 DNA; **A-D**: supercoiled pUC19 with 8, 9, 10, and 20 µM **MC3**; **E-H**: linear pUC19 with 5, 10, 20, and 50 µM **MC3**.

AFM imaging provides a direct tool for exploring the effects of ligand binding on DNA morphology (44, 45). Due to its nanoscale resolution there are numerous examples of AFM techniques used to determine the binding mode, affinity and site-exclusion number of DNA in the presence of suitable binding substrates. Recent AFM studies have characterised the binding modes of well-studied ligands such as doxorubicin, ethidium bromide and netropsin (46). Moreover, this technique can successfully probe morphological changes induced in closed circular plasmid and linear forms of DNA, along with RNA. In this work, AFM studies were performed with closed circular and HindIII linearised pUC19 in ambient air using a Tapping-Mode with unmodified silicon cantilevers at a 40 N/m force constant. Furthermore, we established that 5 mM of $MgCl_2$ was required for complete mica adhesion with no appreciable conformational changes to DNA morphology. **MC3** was selected as a representative compound in this series for AFM analysis. In the presence of 8 µM of **MC3**, supercoiled pUC19 exhibited small cluster formation where tight packing is present in the cluster center with DNA strands extending from its midpoint (Figure V-6A). As the concentration of **MC3** increased to 9 µM, a sizeable increase in cluster formation was observed, however, unbound strands of DNA were evident at this point (Figure V-6B). A gradual increase in **MC3** concentration to 10 and 20 µM led to the near disappearance of unbound pUC19, leaving only large and tightly packed globules of ~800 nm and ~3.3 µm spherical dimension, respectively (Figure V-6C and D). Data here supports our earlier gel electrophoresis analysis where 20 µM of **MC3** was required to fully condense the supercoiled plasmid (see Figure V-3A). In the presence

of linearised pUC19, a lower concentration of **MC3** (5 μM) initiated the onset of condensation (Figure V-6E) with both toroidal and cluster formation evident. Toroid condensates, however, were evident at low **MC3** concentration only with larger aggregates, >1 μm, appearing at 10 and 20 μM exposure with compact globules forming thereafter (50 μM). These results agree with our electrophoretic data on linear pUC19 (see Figure V-3B), where 50 μM of **MC3** was established to condense this sequence.

V. 4.5. Microfluidic analysis of endonuclease inhibition

The condensation effects of the opioid series on a 742 bp dsDNA fragment, amplified from the pUC19 vector encompassing the lacZα gene (Appendix D-6), and subsequent access by sequence-recognition type II restriction endonucleases were initially examined by gel electrophoresis. Results showed the inhibition of migration at ~20 μM of C_3 opioid exposure indicating condensation had occurred. An on-chip microfluidic assay using an Aglient 2100 Bioanalyzer was then employed (Figure V-7) to determine whether C3-opoid induced condensation could block sequence-recognition by type II restriction enzymes BamHI, HindIII, SalI and EcoRI. These restriction enzymes were selected based on their single recognition site within our transcript with control experiments (Appendix D-5) establishing no direct interaction between restriction enzymes and C_3 opiates. A DNA 1000 microfluidic chip was employed in this study to detect and quantify excision fragments, resulting in the disappearance of the parent 742 bp band and the emergence of daughter fragments sized between 295 and 447 bp (Figure V-8A). Pre-incubation of the transcript with 50 μM of both **MC3** and **HC3** afforded little protection toward endonuclease accessibility (Figure V-8B and C). An exception, however, was noted for BamHI activity to **HC3** exposed DNA; here, the parent fragment at 742 bp emerged with notable reduction in the excision fragment peak area at 325 and 417 bp. Interestingly, pre-incubation of the transcript with low micromolar loading of **OC3** (10 μM) was found to inhibit endonuclease accessibility by BamHI, SalI and EcoRI. Furthermore, in the case of the BamHI-treated transcript pre-exposed to **OC3**, almost complete protection of the oligo was observed. It was noted, however, that peak area of **OC3** exposed fragments were diminished in comparison to **MC3** and **HC3** experiments, most likely through the enhanced condensation effects of this agent. Finally, in a complimentary study using gel electrophoresis, we identified that the non-specific endonuclease DNase I degraded all C_3-opioid plasmid pUC19 condensates with identical efficiency (data not shown).

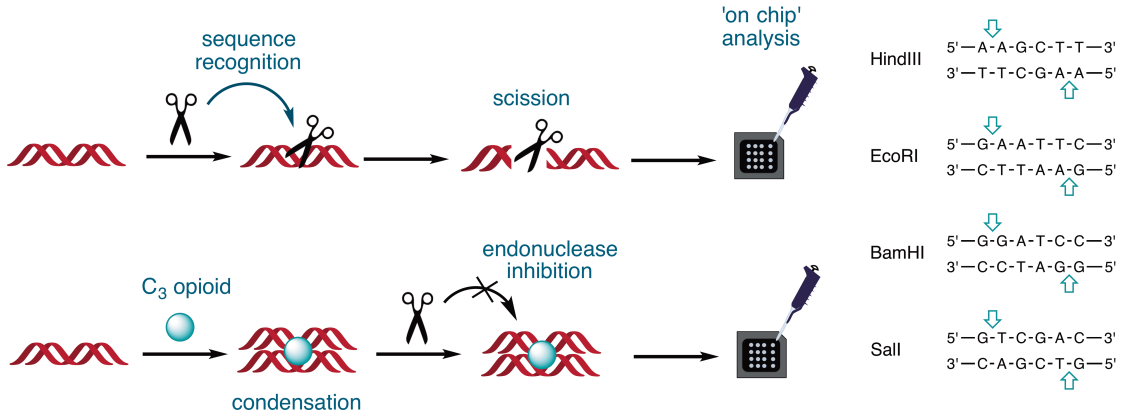

Figure V-7. Experimental design for the Bioanalyzer 2100 to identify site-specific endonuclease inhibition by opioid compounds, HindIII, EcoRI, BamHI, and SalI.

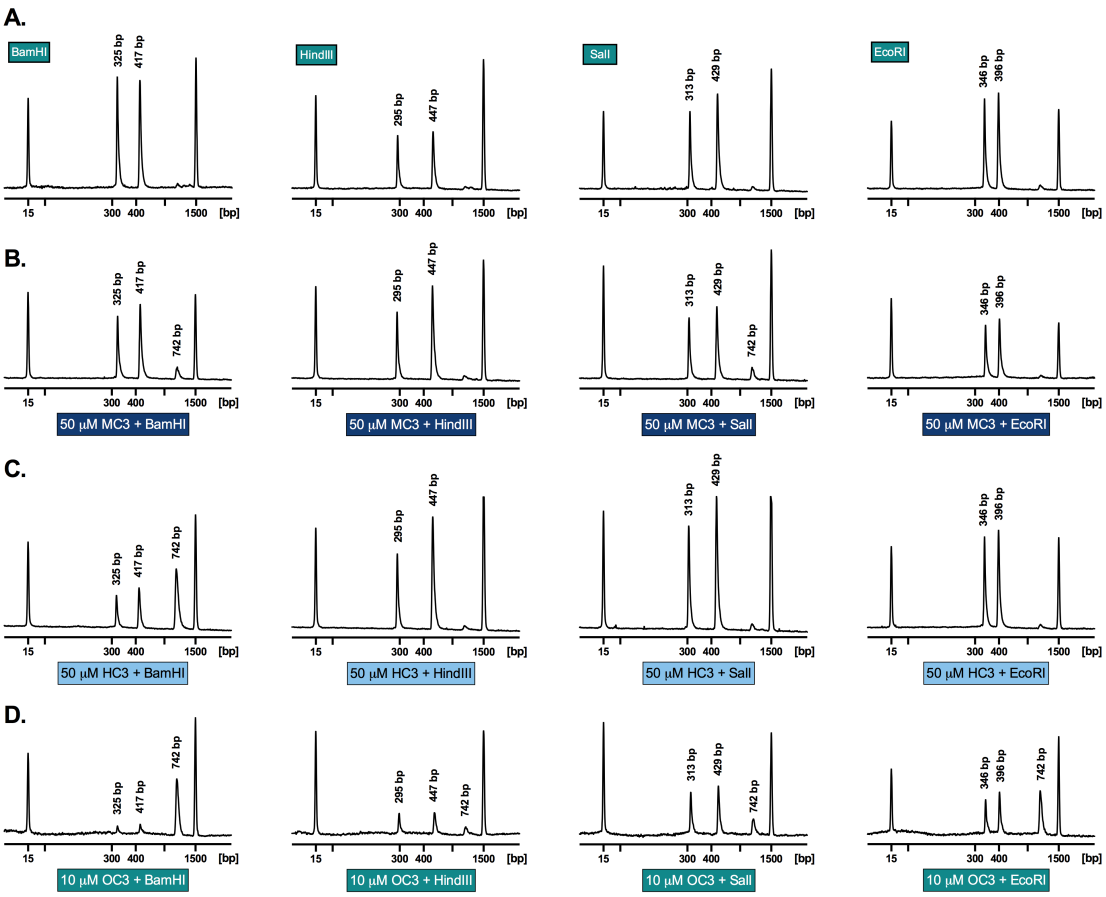

Figure V-8. A. Electrograms generated using the Bioanalyzer 2100 of 742 bp dsDNA fragment with treatment by endonuclease BamHI, HindIII, SalI, and EcoRI. Electrograms of the 742 bp fragment were pre-incubated for 5 h with either **MC3 (B)**, **HC3 (C)**, and **OC3 (D),** followed by exposure over night to the type II restriction endonuclease.

V. 5. Conclusions

To our knowledge opioid compounds have not previously been shown to interact with nucleic acids. This work may therefore open up new applications for these well-established analgesic compounds as semi-synthetic natural products that facilitate nucleic acid recognition. Target compounds were prepared *via* short synthetic routes, which in most cases involved a single step (i.e. from an opioid natural product and commercially available benzyl bromide derivative). The high-affinity DNA binding and condensation properties of this scaffold demonstrate a requirement for a *tris*-opiate, along with a polycationic charge of 3+, as the C_1 and C_2 opiate congeners showed negligible condensation effects by comparison. In this regard, this class of agent falls squarely in line with the majority of established DNA condensation agents where a ≥3+ cationic valence requirement for DNA collapse is generally required (22). Biophysical assays on duplex DNA polymers revealed no intercalative or major/minor groove residency, which led to the probing of C_3-opioids as potential electrostatic and/or H-bonding agents. Thus, our preliminary studies using C_3-morphine (**MC3**) focused on the possibility of the 6′-OH, located in the morphine C ring, as a possible surface binding moiety. Further, while physiological conditions promote interplay between morphine protonation (k^O) and zwitterionic (k^N) isomers (Appendix D-8), the 6′-OH does not engage in acid/base speciation and was therefore considered as a potential phosphate-interacting site (47, 48). To test this axiom, the development of C_3-heterocodeine (**HC3**) and C_3-oripavine (**OC3**) derivatives, where the 6′-OH site is masked by methoxy substituents, was undertaken. Biophysical studies, however, revealed comparable (**HC3**) and enhanced (**OC3**) high-affinity binding to DNA; these data, coupled with condensation properties observed at varying pH and ionic strength, implicate N-protonation of the piperidine (E) ring—a known cationic site that undergoes ionic bond formation with the opioid receptor (43)—as the nucleation site responsible for nucleic acid coordination. A proposed model for DNA binding is shown in Figure 9 where each opiate is protonated (and charged) at the piperidine ring that, in turn, surface binds the vicinal nucleic acid backbone. Based on this proposed model, the binding of C_3 opioids to other nucleic acid structures can be expected and preliminary experiments on the condensation of tRNA by **MC3** (Appendix D-9) evidences this. To corroborate the binding mode described in Figure 9, methylation of each N-piperidine moiety in **MC3** was achieved (Appendix D-7) leading to isolation of the quateranized piperidium cation **MC3-NMe$_2$** as an iodide salt. The condensation effects of

MC3-NMe$_2$ with pUC19, when directly compared to **MC3** (Appendix D-4), resulted in a significantly altered condensation profile. Thus, **MC3-NMe$_2$** did not aggregate DNA at any exposure value (1 – 30 μM) where **MC3** exhibited condensation and only at higher concentrations (>30 μM) was **MC3-NMe$_2$** condensation observed; we propose this interaction is electrostatic in nature and similar to NMe_2-quaternarized nucleic acid binding observed in the literature (49, 50). It is highly likely, therefore, that N-protonation of the *C_3* opioid scaffold is responsible for efficient condensation and that piperidium phosphate hydrogen bonding interactions are required for these high-affinity interactions.

Further examination of *C_3* agents revealed i.) no conformational modification to long canonical DNA polymers, ii.) improved affinity toward aggregation of supercoiled plasmid versus linear DNA conformation, and iii.) an overall aggregation activity profile **OC3** >> **HC3** ≈ **MC3**. To derive some insight into the differences in binding between the oripavine compound and the morphine or heterocodeine analogs, we considered structural data for examples of each class taken from the CSD (51). Figure 10 shows the cation of diacetylmorphine hydrogen chloride monohydrate (FAZDAM, ccdc 242245) and 3,6-dimethoxy-5,17-dimethyl-6,7,8,14-tetradehydro-4,5-epoxymorphinan (LOBGUG, ccdc 985664), for the purpose of comparison a proton has been added to the amine at the calculated position in the latter case. The increased unsaturation in the oripavine means that the "C" ring is flattened relative to the morphine or codeine systems and that one of the hydrogen atoms in an axial position relative to the amine proton is lost. As a consequence, the amine site is clearly less sterically crowded in the oripavine system and this might be expected to make interaction with the DNA phosphate backbone easier. There are also electronic changes in the π system of ring C, which may influence both the pK_a of the amine and electronic aspects of bonding.

The condensation process at neutral pH, studied by AFM analysis with **MC3**, identified toroidal formation of pUC19 at low compound loading, while higher loading promoted tightly packed globule formation in both closed circular and linear DNA structures. The combined effect of high binding constants and condensation of the *C_3*-opioid class was then considered in terms of interrupting protein-DNA recognition (23). Since condensation agents have found widespread utility as transfection agents or carriers of nucleic acids (52, 53), protection of this "cargo" to endonuclease degradation is of considerable importance. While DNase I mediated complete transcript degradation from all three *C_3*-opioid carriers, type II restriction endonucleases inhibition for **HC3** (50 μM) and

OC3 (10 μM) was witnessed at the G-G excision region of BamHI, while **OC3** (10 μM) further protected the G-A excision region of EcoRI. In summary, this work has revealed the discovery of a new high-affinity DNA binding scaffold capable of mediating condensation ostensibly through electrostatic and H-bonding interactions with the phosphate backbone. Our attention now turns to further explore the condensation effects of RNA and alternative DNA structures by these molecules and for their ability to successfully deliver gene vectors.

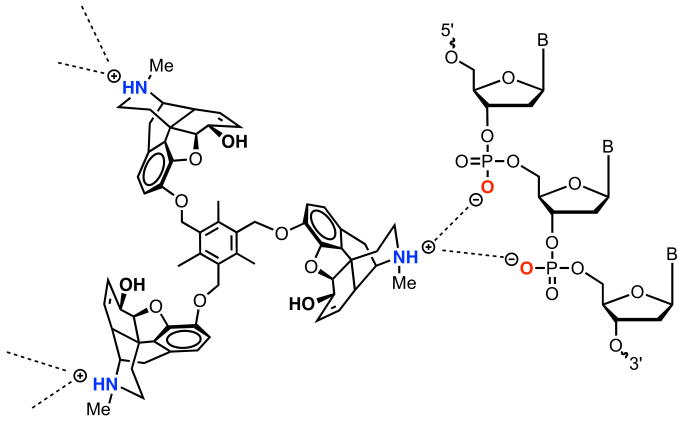

Figure V-9. Proposed ionic binding by the C_3 opioid scaffold to the nucleic acid phosphate backbone.

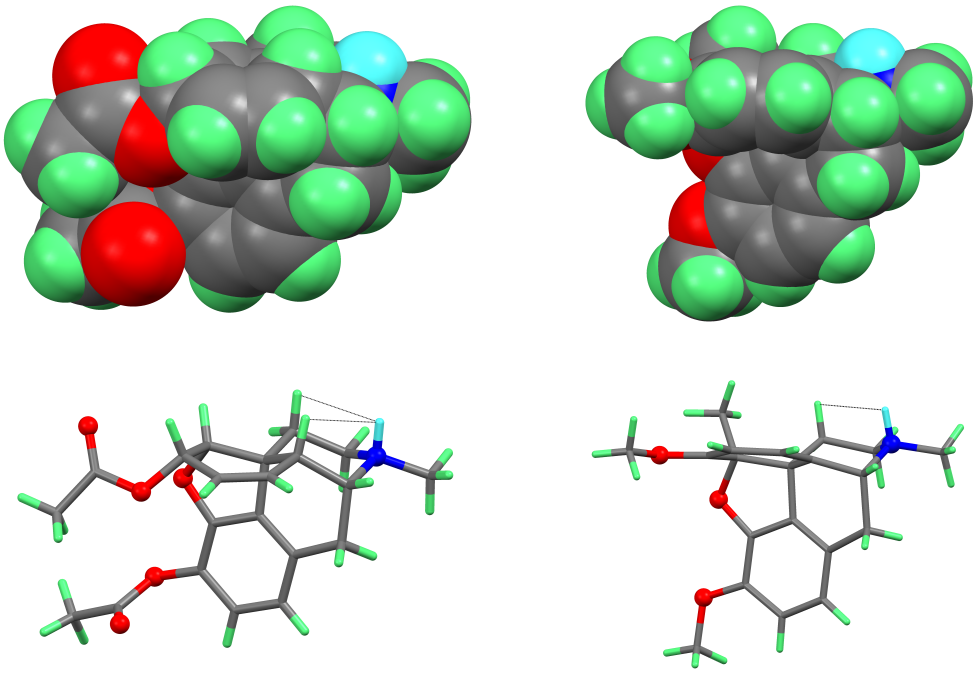

Figure V-10. Structures of protonated diacetylmorphine (FAZDAM left) and protonated 3,6-dimethoxy-5,17-dimethyl-6,7,8,14-tetradehydro-4,5-epoxymorphinan (LOBGUG right) redrawn from the CSD data (the amine proton has been added to the structure at a calculated position for LOBGUG). The amine proton (highlighted in cyan) is more exposed in the oripavine. Dashed lines show the interactions with neighbouring axial protons.

V. 6. Funding

This work was supported by the Irish Research Council (IRC) grant GOIPG/2013/826 and the Marie Skłodowska-Curie Innovative Training Network (ITN) ClickGene (H2020-MSCA-ITN-2014−642023). Equipment used in this study was funded under the Programme for Research in Third Level Institutions (PRTLI) Cycle 5. The PRTLI is co-funded through the European Regional Development Fund (ERDF), part of the European Union Structural Funds Programme 2011-2015. This project has also received funding from the European Union's Seventh Framework Programme for research, technological development and demonstration under grant agreement No. 621364 (TUTIC-Green).

V. 7. References

1. Kelland,L. (2007) The resurgence of platinum-based cancer chemotherapy. *Nat. Rev. Cancer*, **7**, 573–584.

2. Takahara,P.M., Rosenzweig,A.C., Frederick,C.A. and Lippard,S.J. (1995) Crystal structure of double-stranded DNA containing the major adduct of the anticancer drug cisplatin. *Nature*, **377**, 649–652.

3. Pieper,R.O., Futscher,B.W. and Erickson,L.C. (1989) Transcription-terminating lesions induced by bifunctional alkylating agents in vitro. *Carcinogenesis*, **10**, 1307–1314.

4. Strekowski,L. and Wilson,B. (2007) Noncovalent interactions with DNA: An overview. *Mutat. Res.*, **623**, 3–13.

5. Niyazi,H., Hall,J.P., O'Sullivan,K., Winter,G., Sorensen,T., Kelly,J.M. and Cardin,C.J. (2012) Crystal structures of Λ-$[Ru(phen)_2dppz]^{2+}$ with oligonucleotides containing TA/TA and AT/AT steps show two intercalation modes. *Nat. Chem.*, **4**, 621–628.

6. Hurley,L.H. (2002) DNA and its associated processes as targets for cancer therapy. *Nat. Rev. Cancer*, **2**, 188–200.

7. Cai,X., Gray,P.J. and Von Hoff,D.D. (2009) DNA minor groove binders: Back in the groove. *Cancer Treat. Rev.*, **35**, 437–450.

8. Hamilton,P.L. and Arya,D.P. (2012) Natural product DNA major groove binders. *Nat. Prod. Rep.*, **29**, 134–143.

9. Bailly,C., Hénichart,J.-P., Colson,J.-P., Colson,P. and Houssier,C. (1992) Drug-DNA Sequence-Dependent Interactions Analysed by Electric Linear Dichroism. *J. Mol. Recognit.*, **5**, 155–171.

10. Tuite,E. and Nordén,B. (1995) Intercalative interactions of ethidium dyes with triplex structures. *Bioorganic Med. Chem.*, **3**, 701–711.

11. Erkkila,K.E., Odom,D.T. and Barton,J.K. (1999) Recognition and reaction of metallointercalators with DNA. *Chem. Rev.*, **99**, 2777–2795.

12. Liu,H.-K. and Sadler,P.J. (2011) Metal complexes as DNA intercalators. *Acc. Chem. Res.*, **44**, 349–359.

13. Hopcroft,N.H., Brogden,A.L., Searcey,M. and Cardin,C.J. (2006) X-ray crystallographic study of DNA duplex cross-linking: Simultaneous binding to two $d(CGTACG)_2$ molecules by a bis(9-aminoacridine-4-carboxamide) derivative. *Nucleic Acids Res.*, **34**, 6663–6672.

14. Farrell,N.P. (2015) Multi-platinum anti-cancer agents. Substitution-inert compounds for tumor selectivity and new targets. *Chem. Soc. Rev.*, **44**, 8773–8785.

15. Calnan,B.J., Tidor,B., Biancalana,S., Hudson,D. and Frankel,A.D. (1991) Arginine-mediated RNA recognition: the arginine fork. *Science (80-.).*, **252**, 1167–1171.

16. Yamaguchi,N., Zouzumi,Y., Shimada,N., Nakano,S., Sugimoto,N., Maruyama,A. and Miyoshi,D. (2016) A reversible B-A transition of DNA duplexes induced by synthetic cationic copolymers. *Chem. Commun.*, **52**, 7446–7449.

17. Bloomfield,V.A. (1996) DNA condensation. *Curr. Opin. Struct. Biol.*, **6**, 334–341.

18. Teif,V.B. and Bohinc,K. (2011) Condensed DNA: Condensing the concepts. *Prog. Biophys. Mol. Biol.*, **105**, 208–222.

19. Bloomfield,V.A. (1997) DNA Condensation by Multivalent Cations. *Biopolymers*, **44**, 269–282.
20. Grosberg,A.Y. and Kuznetsov,D. V. (1992) Quantitative Theory of the Globule-to-Coil Transition. 1. Link Density Distribution in a Globule and Its Radius of Gyration. *Macromolecules*, **25**, 1970–1979.
21. Vijayanathan,V., Thomas,T., Shirahata,A. and Thomas,T.J. (2001) DNA condensation by polyamines: A laser light scattering study of structural effects. *Biochemistry*, **40**, 13644–13651.
22. Wilson,R.W. and Bloomfield,V.A. (1979) Counterion-Induced Condensation of Deoxyribonucleic Acid. A Light-Scattering Study. *Biochemistry*, **18**, 2192–2196.
23. Prisecaru,A., Molphy,Z., Kipping,R.G., Peterson,E.J., Qu,Y., Kellett,A. and Farrell,N.P. (2014) The phosphate clamp: sequence selective nucleic acid binding profiles and conformational induction of endonuclease inhibition by cationic Triplatin complexes. *Nucleic Acids Res.*, **42**, 13474–13487.
24. Malina,J., Farrell,N.P. and Brabec,V. (2014) DNA condensing effects and sequence selectivity of DNA binding of antitumor noncovalent polynuclear platinum complexes. *Inorg. Chem.*, **53**, 1662–1671.
25. Malina,J., Farrell,N.P. and Brabec,V. (2014) Substitution-Inert Trinuclear Platinum Complexes Efficiently Condense/Aggregate Nucleic Acids and Inhibit Enzymatic Activity. *Angew. Chemie Int. Ed.*, **53**, 12812–12816.
26. Plum,G.E., Arscott,P.G. and Bloomfield,V.A. (1990) Condensation of DNA by trivalent cations. 2. Effects of cation structure. *Biopolymers*, **30**, 631–643.
27. He,S., Arscott,P.G. and Bloomfield,V.A. (2000) Condensation of DNA by multivalent cations: Experimental studies of condensation kinetics. *Biopolymers*, **53**, 329–341.
28. Kankia,B.I., Buckin,V. and Bloomfield,V.A. (2001) Hexamminecobalt(III)-induced condensation of calf thymus DNA: circular dichroism and hydration measurements. *Nucleic Acids Res.*, **29**, 2795–2801.
29. Malina,J., Hannon,M.J. and Brabec,V. (2015) Iron(II) Supramolecular Helicates Condense Plasmid DNA and Inhibit Vital DNA-Related Enzymatic Activities. *Chem. - A Eur. J.*, **21**, 11189–11195.
30. Andrushchenko,V., van de Sande,H. and Wieser,H. (2003) DNA interaction with Mn^{2+} ions at elevated temperatures: VCD evidence of DNA aggregation. *Biopolymers*, **69**, 529–545.
31. Vallejo,R., Barkin,R.L. and Wang,V.C. (2011) Pharmacology of opioids in the treatment of chronic pain syndromes. *Pain Physician*, **14**, E343–E360.
32. Prisecaru,A., McKee,V., Howe,O., Rochford,G., McCann,M., Colleran,J., Pour,M., Barron,N., Gathergood,N. and Kellett,A. (2013) Regulating Bioactivity of Cu^{2+} Bis-1,10-phenanthroline Artificial Metallonucleases with Sterically Functionalized Pendant Carboxylates. *J. Med. Chem.*, **56**, 8599–8615.
33. Barber,R.B. and Rapoport,H. (1975) Synthesis of thebaine and oripavine from codeine and morphine. *J. Med. Chem.*, **18**, 1074–1077.
34. Rapoport,H. and Barber,R.B. (1977) Method of producing thebaine from codeine and oripavine from morphine (US4045440 A).

35. Molphy,Z., Prisecaru,A., Slator,C., Barron,N., McCann,M., Colleran,J., Chandran,D., Gathergood,N. and Kellett,A. (2014) Copper Phenanthrene Oxidative Chemical Nucleases. *Inorg. Chem.*, **53**, 5392–5404.
36. McCann,M., McGinley,J., Ni,K., O'Connor,M., Kavanagh,K., McKee,V., Colleran,J., Devereux,M., Gathergood,N., Barron,N., *et al.* (2013) A new phenanthroline-oxazine ligand: synthesis, coordination chemistry and atypical DNA binding interaction. *Chem. Commun.*, **49**, 2341–2343.
37. Molphy,Z., Slator,C., Chatgilialoglu,C. and Kellett,A. (2015) DNA oxidation profiles of copper phenanthrene chemical nucleases. *Front. Chem.*, **28**.
38. Horcas,I., Fernández,R., Gómez-Rodríguez,J.M., Colchero,J., Gómez-Herrero,J. and Baro,A.M. (2007) WSXM: A software for scanning probe microscopy and a tool for nanotechnology. *Rev. Sci. Instrum.*, **78**.
39. Cunningham,C.W., Thatcher,L.N. and Coop,A. (2006) Methylation of Non-acidic Alcohols of Alkaloids with TMS-diazomethane: Conversion of Codeine to Codeine-6-methyl Ether. *Heterocycles*, **68**, 837–840.
40. McElroy,C.R., Constantinou,A., Jones,L.C., Summerton,L. and Clark,J.H. (2015) Towards a holistic approach to metrics for the 21st century pharmaceutical industry. *Green Chem.*, **17**, 3111–3121.
41. Gore,R.G., Myles,L., Spulak,M., Beadham,I., Garcia,M.T., Connon,S.J. and Gathergood,N. (2013) A new generation of aprotic yet Bronsted acidic imidazolium salts: effect of ester/amide groups in the C-2, C-4 and C-5 on antimicrobial toxicity and biodegradation. *Green Chem.*, **15**, 2747–2760.
42. Jordan,A., Haiß,A., Spulak,M., Karpichev,Y., Kümmerer,K. and Gathergood,N. (2016) Liquids and Tertiary Amines: Green Chemistry Preliminary Biodegradation Data Analysis. *Green Chem.*, **18**, 4374–4392.
43. Neidle,S. (2001) DNA minor-groove recognition by small molecules. *Nat. Prod. Rep.*, **18**, 291–309.
44. Kim,S.K. and Nordén,B. (1993) Methyl green. A DNA major-groove binding drug. *Fed. Eur. Biochem. Soc. Lett.*, **315**, 61–64.
45. Arscott,P.G., Li,A.-Z. and Bloomfield,V.A. (1990) Condensation of DNA by trivalent cations. 1. Effects of DNA length and topology on the size and shape of condensed particles. *Biopolymers*, **30**, 619–630.
46. McFadyen,I.J., Houshyar,H., Liu-Chen,L.-Y., Woods,J.H. and Traynor,J.R. (2000) The steroid 17α-acetoxy-6-dimethylaminomethyl-21-fluoro-3-ethoxy-pregna-3,5-dien-20-one (SC17599) is a selective μ-opioid agonist: Implications for the μ-opioid pharmacophore. *Mol. Pharmacol.*, **58**, 669–676.
47. Hansma,H.G., Golan,R., Hsieh,W., Lollo,C.P., Mullen-Ley,P. and Kwoh,D. (1998) DNA condensation for gene therapy as monitored by atomic force microscopy. *Nucleic Acids Res.*, **26**, 2481–2487.
48. Zhou,T., Llizo,A., Wang,C., Xu,G. and Yang,Y. (2013) Nanostructure-induced DNA condensation. *Nanoscale*, **5**, 8288–8306.
49. Cassina,V., Seruggia,D., Beretta,G.L., Salerno,D., Brogioli,D., Manzini,S., Zunino,F. and Mantegazza,F. (2011) Atomic force microscopy study of DNA conformation in the presence of drugs. *Eur. Biophys. J.*, **40**, 59–68.

50. Mazák,K. and Noszál,B. (2012) Lipophilicity of morphine microspecies and their contribution to the lipophilicity profile. *Eur. J. Pharm. Sci.*, **45**, 205–210.
51. Mazák,K., Hosztafi,S., Rácz,Á. and Noszál,B. (2009) Structural and Physicochemical Profiling of Morphine and Related Compounds of Therapeutic Interest. *Mini-Reviews Med. Chem.*, **9**, 984–995.
52. Jin,C., Qiu,H., Han,L., Shu,M. and Che,S. (2009) DNA transcription into diverse porous silicas by a co-structure directing route: chiral, ring and ordered nanochannel arrays. *Chem. Commun. (Camb).*, 10.1039/b900614a.
53. Squire,C.J., Clark,G.R. and Denny,W.A. (1997) Minor groove binding of a bis-quaternary ammonium compound: The crystal structure of SN 7167 bound to d(CGCGAATTCGCG)2. *Nucleic Acids Res.*, **25**, 4072–4078.
54. Groom,C.R. and Allen,F.H. (2014) The Cambridge Structural Database in retrospect and prospect. *Angew. Chemie Int. Ed.*, **53**, 662–671.
55. Volcke,C., Pirotton,S., Grandfils,C., Humbert,C., Thiry,P.A., Ydens,I., Dubois,P. and Raes,M. (2006) Influence of DNA condensation state on transfection efficiency in DNA/polymer complexes: An AFM and DLS comparative study. *J. Biotechnol.*, **125**, 11–21.
56. Dunlap,D.D., Maggi,A., Soria,M.R. and Monaco,L. (1997) Nanoscopic structure of DNA condensed for gene delivery. *Nucleic Acids Res.*, **25**, 3095–3101.

APPENDIX D.

C_3-Symmetric Opioid Scaffolds are pH-Responsive DNA Condensation Agents

---

D-1: NMR spectroscopy of C_3 derivatives

MC3 spectra:

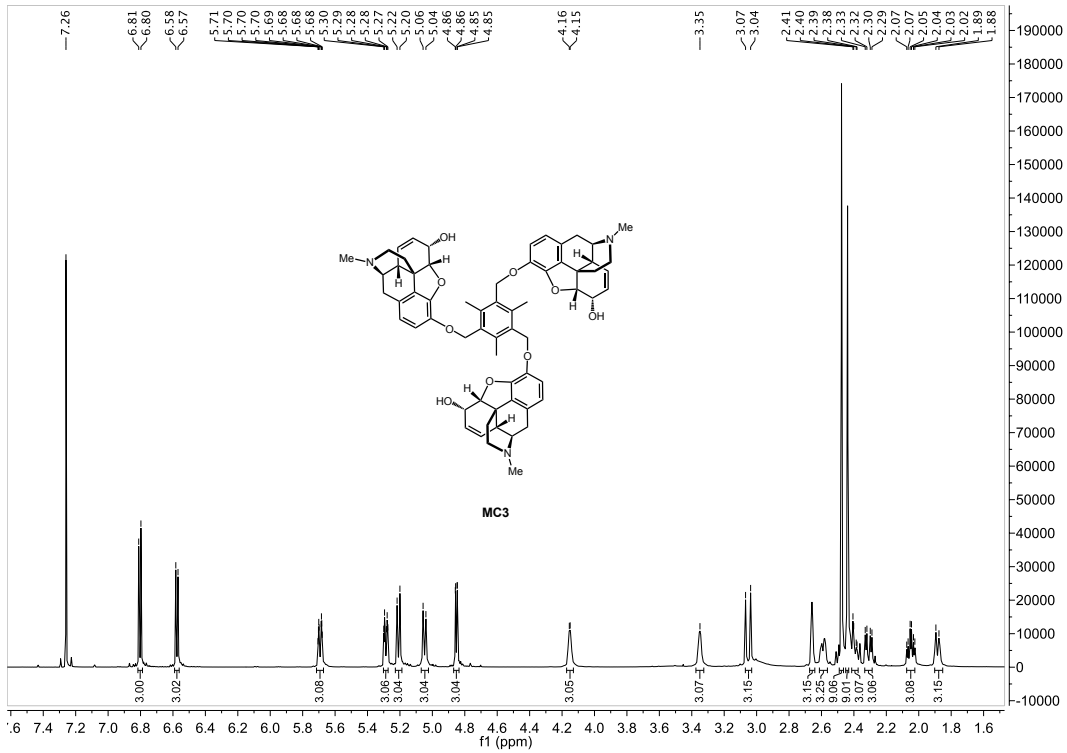

Figure D-1. ^{1}H NMR spectra for **MC3**.

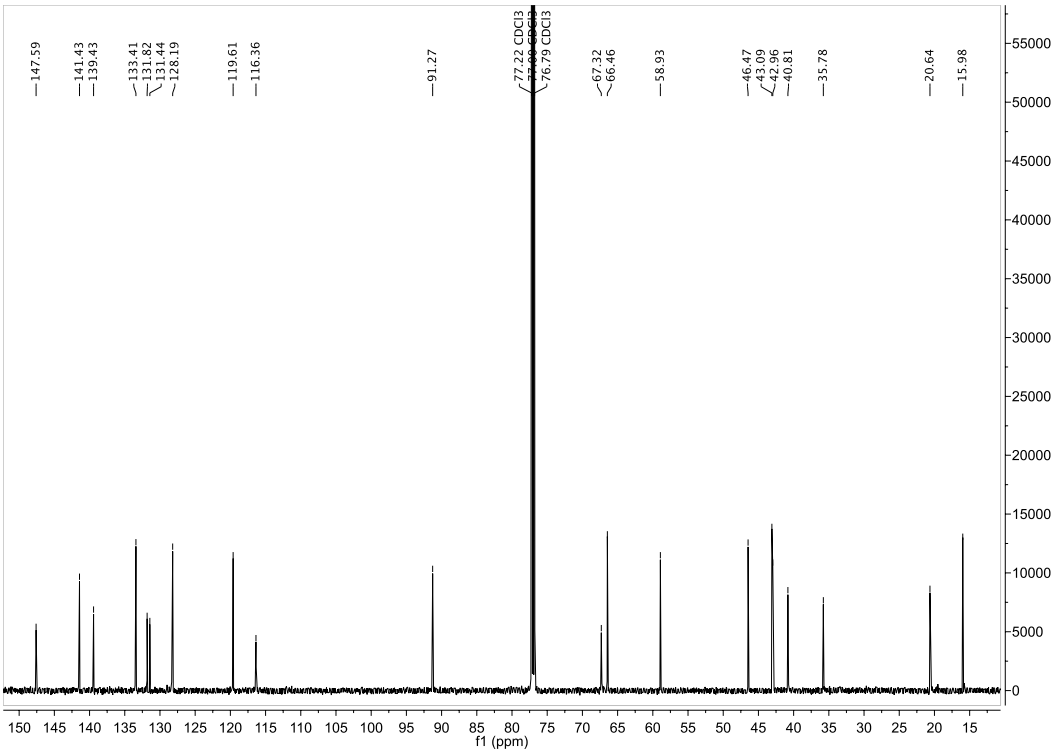

Figure D-2. ^{13}C NMR spectra for **MC3**.

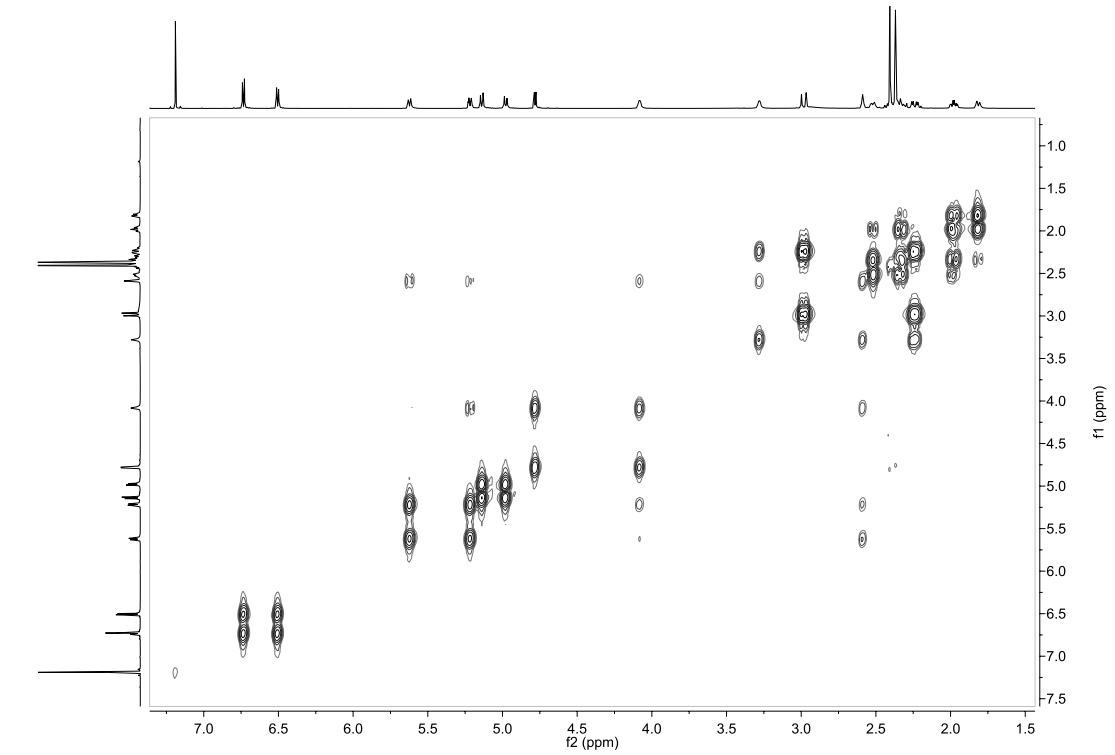

Figure D-3. COSY NMR spectra for **MC3**.

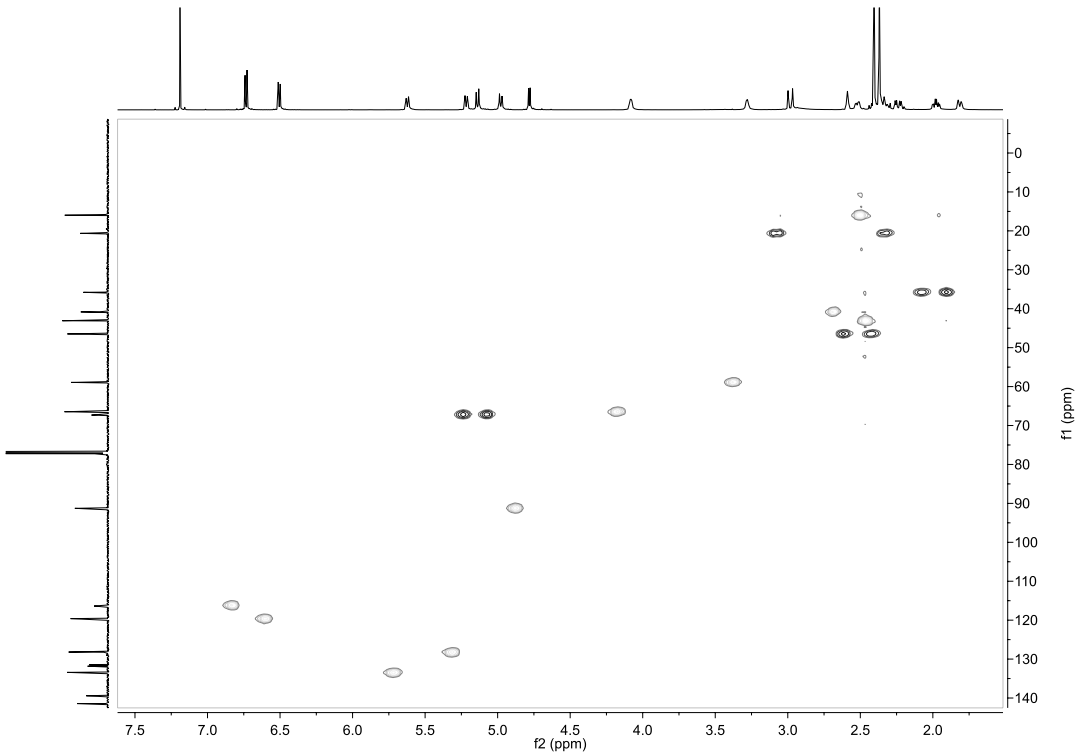

Figure D-4. HSQC NMR spectra for **MC3**.

OC3 Spectra:

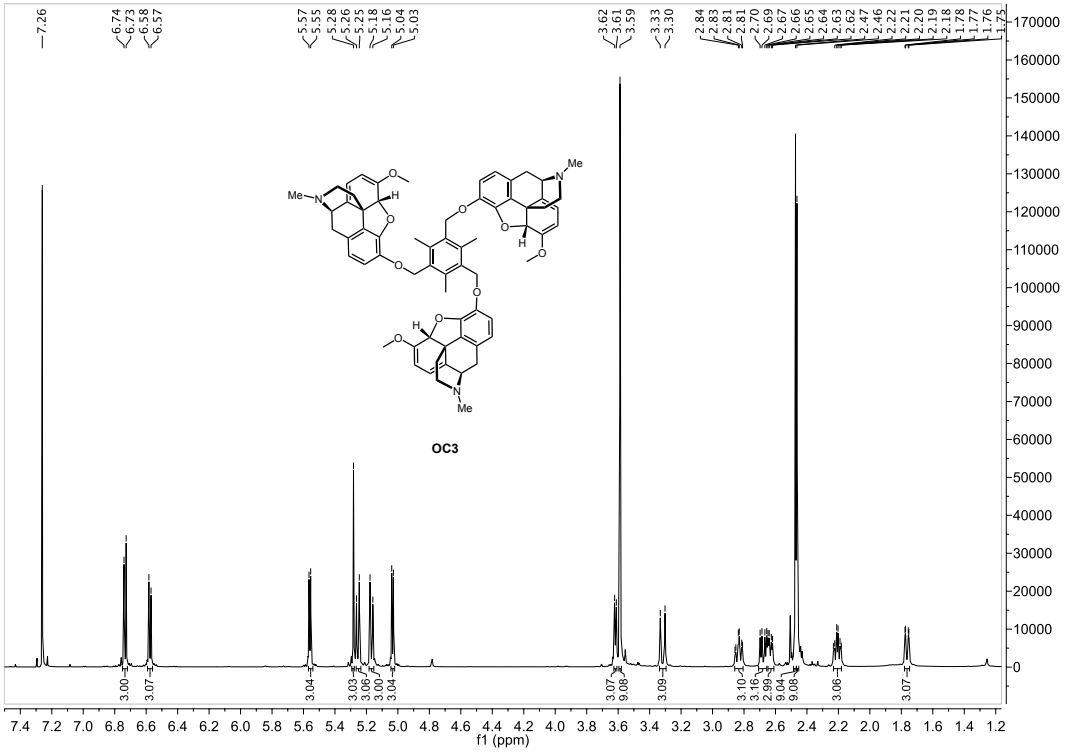

Figure D-5. ^{1}H NMR spectra for **OC3**.

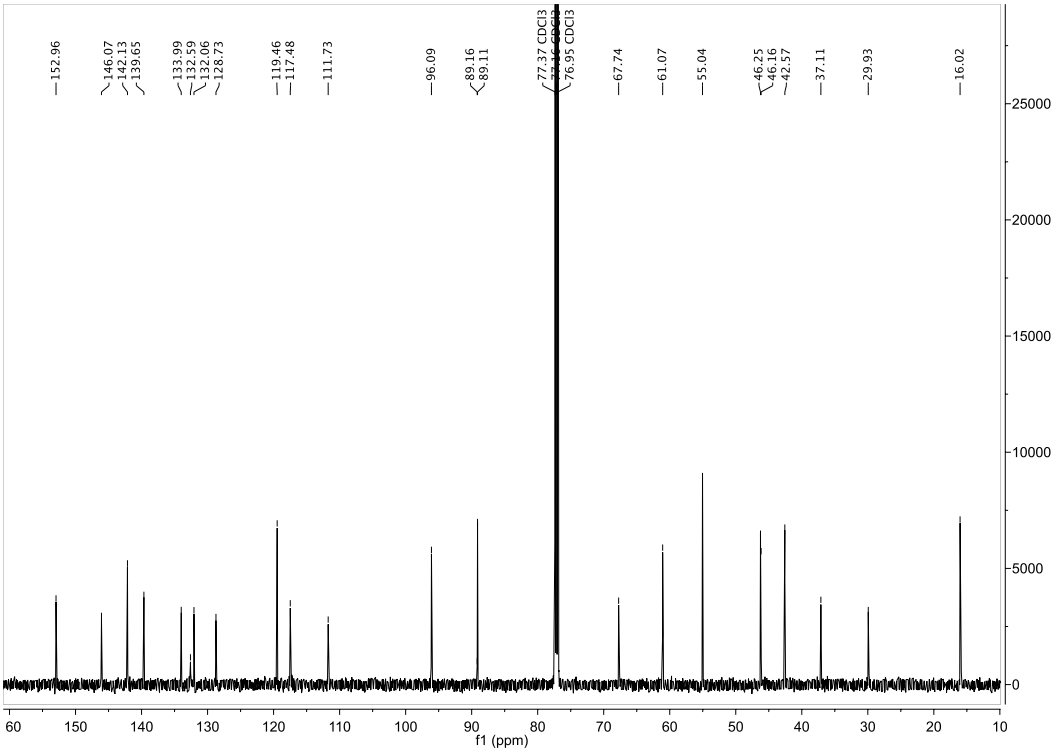

Figure D-6. ^{13}C NMR spectra for **OC3**.

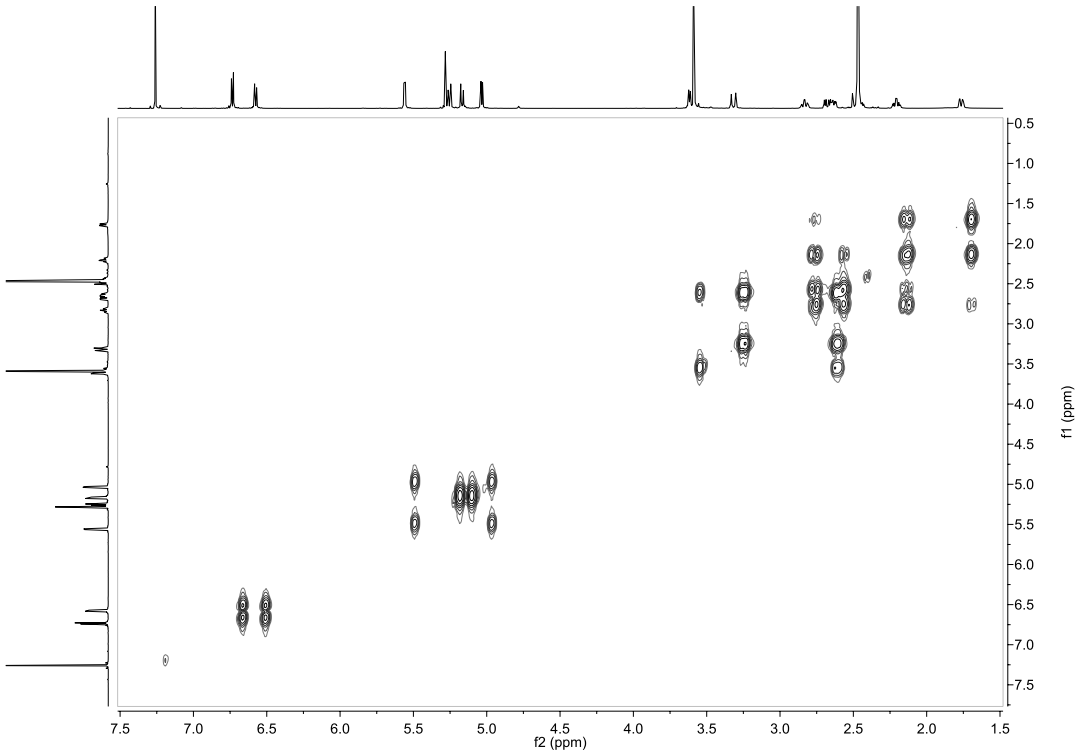

Figure D-7. COSY NMR spectra for **OC3**.

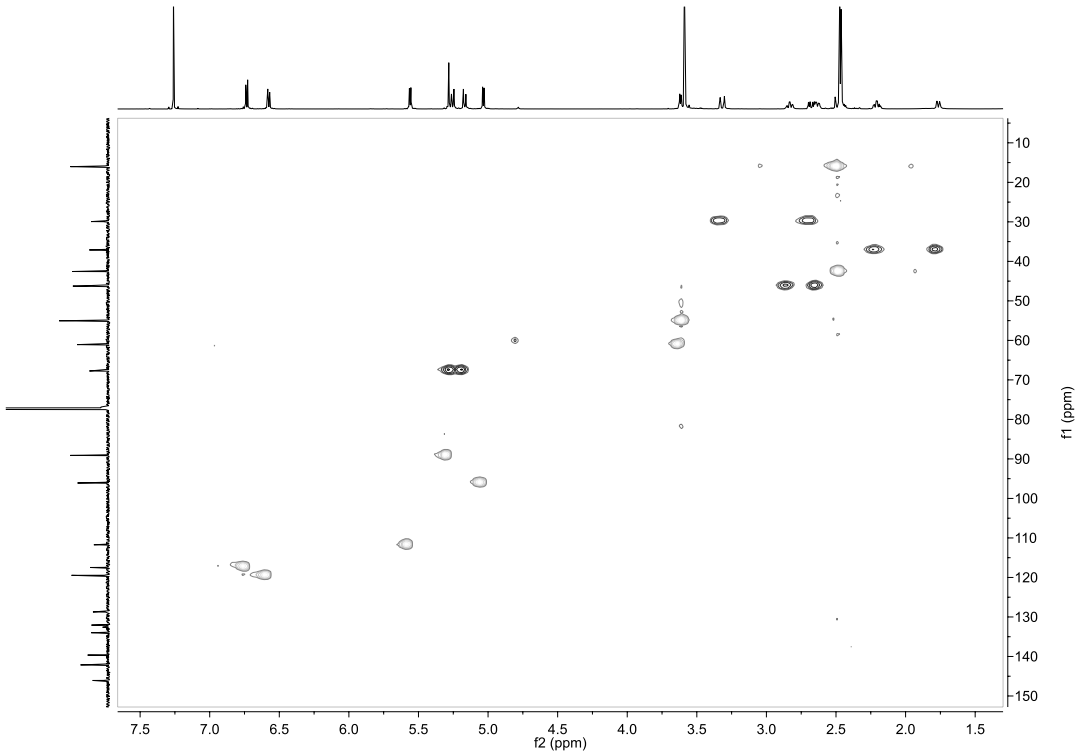

Figure D-8. HSQC NMR spectra for **OC3**.

HC3 Spectra:

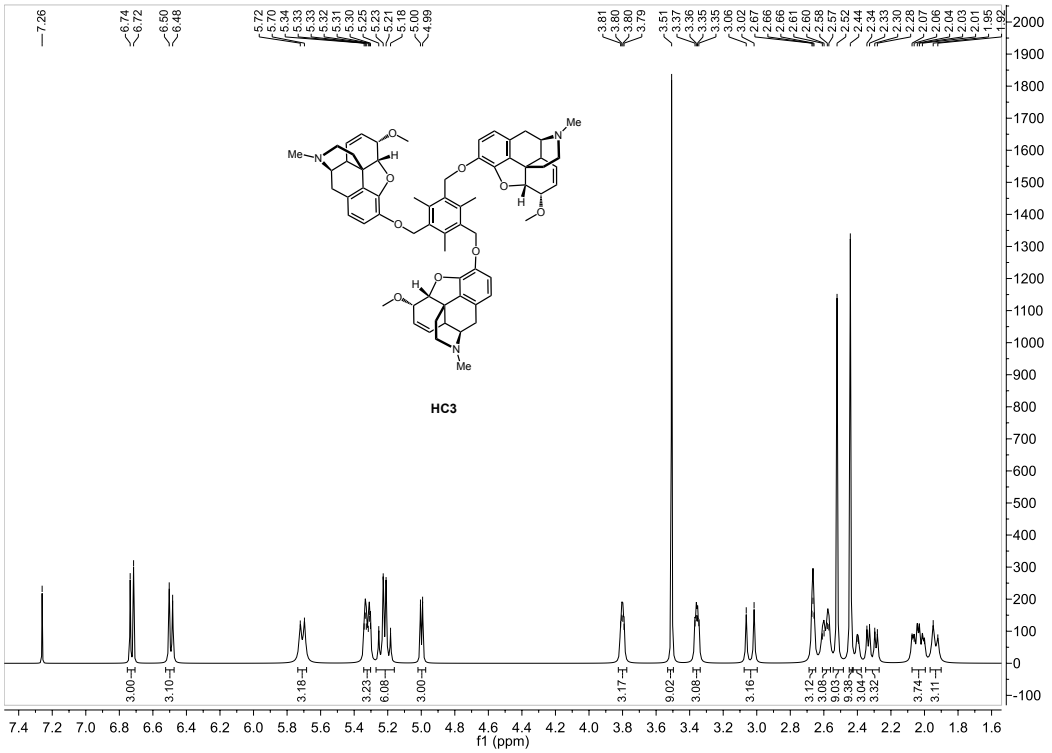

Figure D-9. ^{1}H NMR spectra for **HC3**.

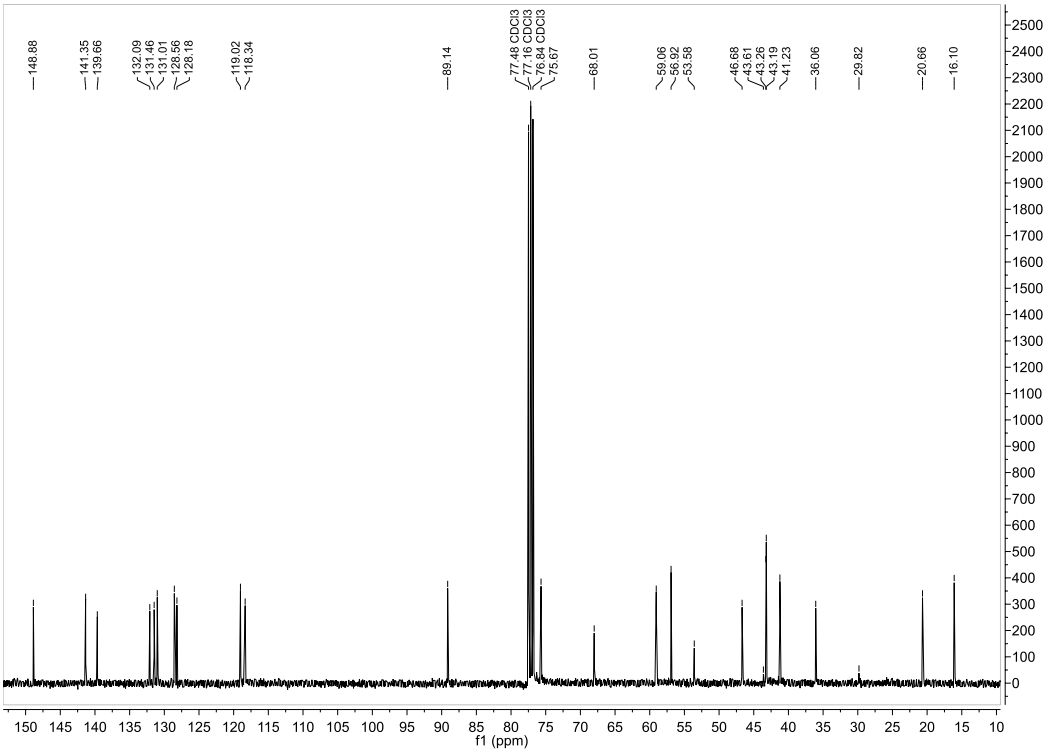

Figure D-10. ^{13}C NMR spectra for **HC3**.

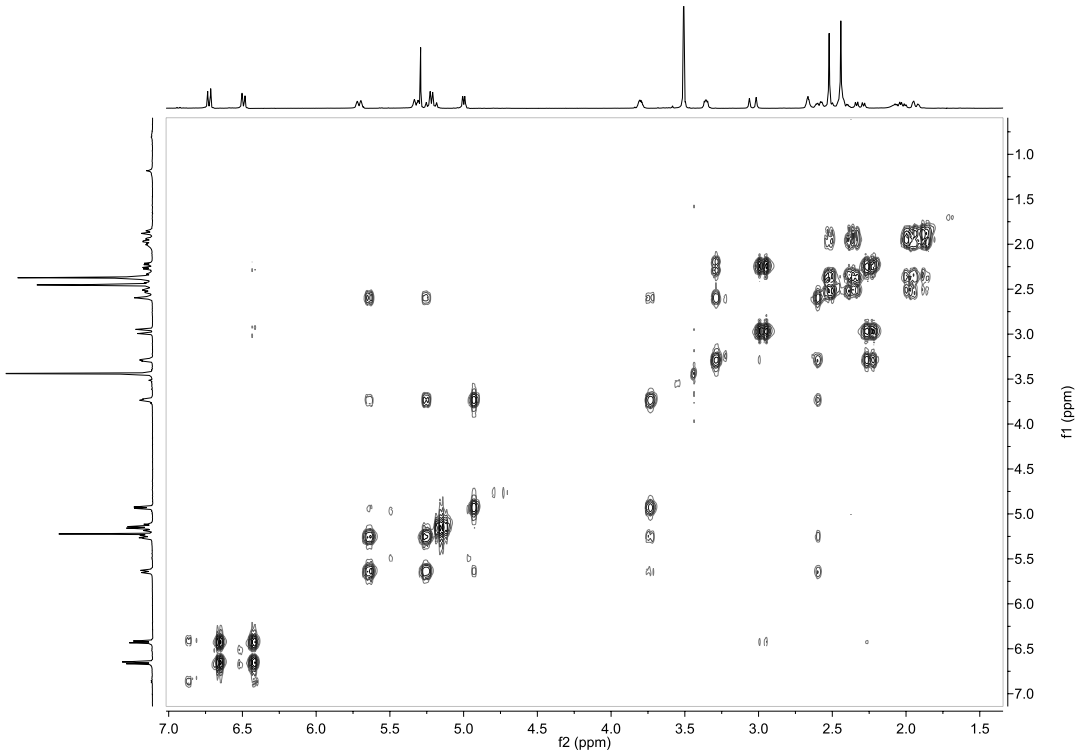

Figure D-11. COSY NMR spectra for **HC3**.

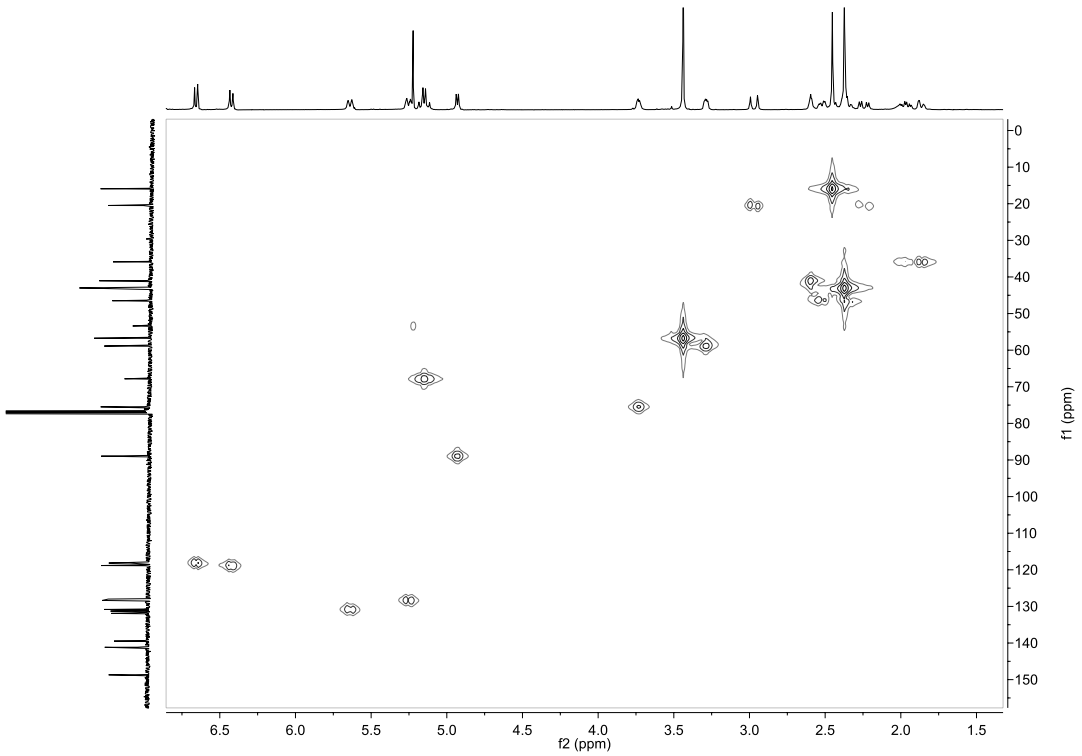

Figure D-12. HSQC NMR spectra for **HC3**.

D-2: Circular dichroism spectra

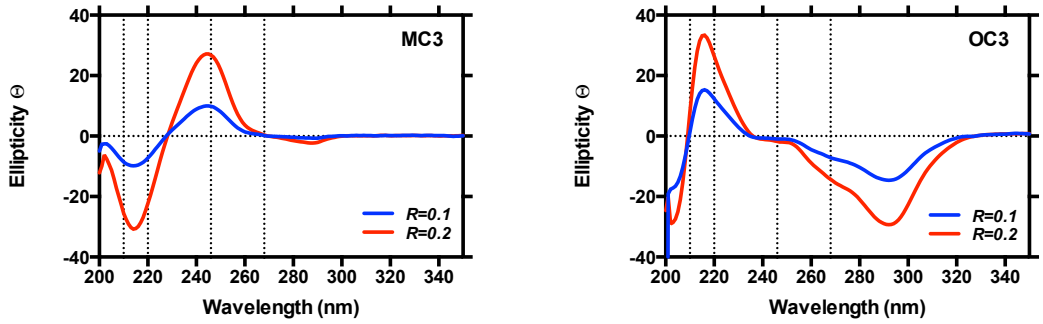

Figure D-13. CD spectra of opioid scaffolds **MC3** and **OC3** in the absence of stDNA at 10 µM and 20 µM loading (at equivalent concentrations to the *r* values of 0.1 and 0.2, respectively).

D-3: Gel electrophoresis with C_1 and C_2 derivatives

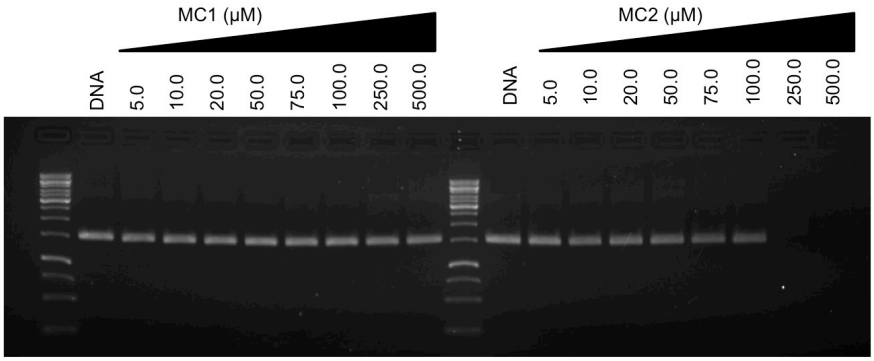

Figure D-14. Agarose gel electrophoresis of supercoiled (400 ng) exposed to increasing concentrations of **MC1**, and **MC2.** Reactions were carried out in the presence of 25 mM NaCl for 5 h at 37°C prior to electrophoretic analysis.

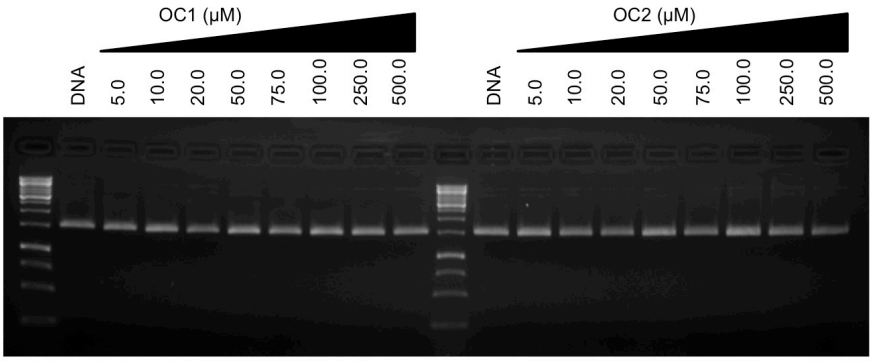

Figure D-15. Agarose gel electrophoresis of supercoiled (400 ng) exposed to increasing concentrations of **OC1**, and **OC2.** Reactions were carried out in the presence of 25 mM NaCl for 5 h at 37°C prior to electrophoretic analysis.

D-4: Gel electrophoresis experiments with MC3 and -NMe_2 derivatives

Both MC3 and the MC3–NMe_2 derivative were initially prepared in DMF and further diluted in 80 mM HEPES buffer (Fisher). Reactions were carried out according to the following general procedure: in a total volume of 20 µl using 80 mM HEPES buffer (pH 7.2) with 25 mM NaCl, 400 ng pUC19 (NEB, N3041) and varying concentrations of test compound (5, 10, 20 and 30 µM), were incubated at 37°C for 5 h. Reaction mixtures were subjected to gel electrophoresis as previously stated.

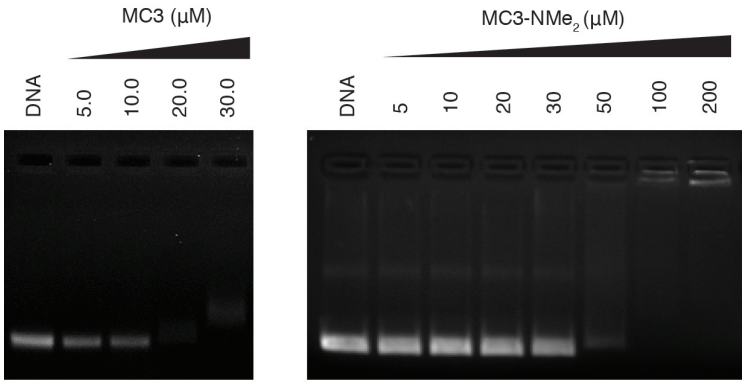

Figure D-16. Agarose gel electrophoresis of supercoiled (400 ng) exposed to increasing concentrations of **MC3** and **MC3-NMe_2**. Reactions were carried out in the presence of 25 mM NaCl for 5 h at 37°C prior to electrophoretic analysis.

D-5: Restriction enzyme interactions with MC3 and -NMe_2 derivatives

Restriction enzymes HindIII, EcoRI, SalI and BamHI (1 µl) were combined with 30 µM of either MC3 or MC3-NMe_2 derivatives in a final volume of 20 µl using 80 mM HEPES buffer (pH 7.2) and incubated for 2 h at 37°C. 400 ng of pUC19 was then added to each reaction mixture and incubated for 1 hr 30 minutes at 37°C and subjected to gel electrophoresis as previously described.

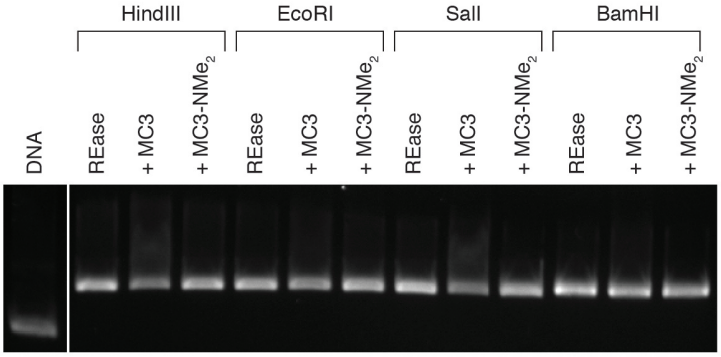

Figure D-17. Agarose gel electrophoresis of selected restriction enzymes pretreated with 30 µM of either **MC3** or **MC3-NMe_2** prior to the addition of 400 ng supercoiled pUC19.

D-6: Bioanalyzer restriction map

TCGCGCGTTTCGGTGATGACGGTGAAAACCTCTGACACATGCAGCTCCCGGAGACGGTCA
CAGCTTGTCTGTAAGCGGATGCCGGGAGCAGACAAGCCCGTCAGGGCGCGTCAGCGGGTG
TTGGCGGGTGTCGGGGCTGGCTTAACTATGCGGCATCAGAGCAGATTGTACTGAGAGTGC
ACCATATGCGGTGTGAAATACCGCACAGATGCGTAAGGAGAAAATACCGCATCAGGCGCC
ATTCGCCATTCAGGCTGCGCAACTGTTGGGAAGGGCGATCGGTGCGGGCCTCTTCGCTAT
TACGCCAGCTGGCGAAAGGGGGATGTGCTGCAAGGCGATTAAGTTGGGTAACGCCAGGGT
TTTCCCAGTCACGACGTTGTAAAACGACGGCCAGTGAATTCGAGCTCGGTACCCGGGGATT
CCTCTAGAGTCGACCTGCAGGCATGCAAGCTTGGCGTAATCATGGTCATAGCTGTTTCCT
GTGTGAAATTGTTATCCGCTCACAATTCCACACAACATACGAGCCGGAAGCATAAAGTGT
AAAGCCTGGGGTGCCTAATGAGTGAGCTAACTCACATTAATTGCGTTGCGCTCACTGCCC
GCTTTCCAGTCGGGAAACCTGTCGTGCCAGCTGCATTAATGAATCGGCCAACGCGCGGGG
AGAGGCGGTTTGCGTATTGGGCGCTCTTCCGCTTCCTCGCTCACTGACTCGCTGCGCTCG
GT**CGTTCGGCTGCGGCGAGCGG**

D-7: Synthesis of C_1 and C_2 derivatives

*Morphine-C_1 (**MC1**)*

Morphine (0.579 g, 2.03 mmol) and potassium carbonate (1.122 g, 8.12 mmol) were suspended in ACN (30 ml) and heated to reflux. α^2-Chloroisodurene (0.337 g, 2.00 mmol) was added in small aliquots to the reaction mixture and vigorously stirred overnight (18 h) under reflux conditions. After allowing the reaction mixture to cool to rt, the reaction solvent was removed by rotary evaporation and crude product dissolved in DCM (50 ml). The organic layer was washed with d.H_2O (40 ml) and the aqueous layer extracted with DCM (3 x 20 ml). All organic layers were combined, then washed with d.H_2O (3 x 20 ml) and with a saturated brine solution (20 ml). The organic layer was dried over magnesium sulphate, filtered and solvents removed by rotary evaporation. The crude product was purified by column chromatography (SiO_2, 95:1:1 to 92:8:1 CH_2Cl_2:MeOH:NH_4OH). The title compound **MC1** was isolated as a white solid in 73 % (0.609 g, 1.46 mmol). mp. 225-226°C. ^{1}H NMR (600 MHz, $CDCl_3$) δ: 6.87 (s, 2H), 6.79 (d, J = 8.1 Hz, 1H), 6.57 (d, J = 8.1 Hz, 1H), 5.67 (ddt, J = 9.9, 3.1, 1.8 Hz, 1H), 5.31 – 5.28 (m, 1H), 5.15 (d, J = 10.3 Hz, 1H), 4.99 (d, J = 10.3 Hz, 1H), 4.86 (dd, J = 6.6, 1.2 Hz, 1H), 4.15 (s, 1H), 3.35 (dd, J = 6.1, 3.2 Hz, 1H), 3.06 (d, J = 18.6 Hz, 1H), 2.77 (s, 1H), 2.66 (p, J = 2.7 Hz, 1H), 2.59 (dd, J = 12.2, 4.1 Hz, 1H), 2.44 (s, 3H), 2.44 – 2.39 (m, 1H), 2.37 (s, 6H), 2.33 – 2.29 (m, 1H), 2.27 (s, 3H), 2.06 (td, J = 12.5, 5.1 Hz, 1H), 1.90 – 1.87 (m, 1H). ^{13}C NMR (151 MHz, $CDCl_3$) δ: 147.65, 141.57, 138.13, 138.09, 133.38, 131.40, 130.23, 128.99, 128.24, 128.18, 119.63, 116.79, 91.16, 77.47, 77.20, 77.12, 76.99, 76.78, 67.00, 66.35, 58.93, 46.48, 43.11, 42.90, 40.81, 35.83, 20.99, 20.61, 19.52. IR (ATR, cm^{-1}): 2928, 2789, 1634, 1500, 1485,

1447, 1380, 1271, 1249, 1152, 1113, 1058, 1037, 1008, 934, 855, 833, 817, 792, 781, 756, 719, 701, 671. $[\alpha]_D = -70°$ (c = 0.152, $CHCl_3$, 589nm, 25°C)

*Morphine-C_2 (**MC2**)*

Morphine (0.536 g, 1.88 mmol) and potassium carbonate (1.038 g, 7.51 mmol) were suspended in ACN (30 ml) and heated to reflux. 2,4,-Bis(chloromethyl)-1,3,5-trimethylbenzene (0.204 g, 0.94 mmol) was added in small aliquots to the reaction mixture and vigorously stirred overnight (18 h) under reflux conditions. After allowing the reaction mixture to cool to rt, the reaction solvent was removed by rotary evaporation and crude product dissolved in DCM (50 ml). The organic layer was washed with d.H_2O (40 ml) and the aqueous layer extracted with DCM (3 x 20 ml). All organic layers were combined, then washed with d.H_2O (3 x 20 ml) and with a saturated brine solution (20 ml). The organic layer was dried over magnesium sulphate, filtered and solvents removed by rotary evaporation. The crude product was purified by column chromatography (SiO_2, 95:1:1 to 92:8:1 CH_2Cl_2:MeOH:NH_4OH). The title compound **MC2** was isolated as a white solid in 35 % yield (0.235 g, 0.33 mmol). mp. 144-146°C. ^{1}H NMR (600 MHz, $CDCl_3$) δ 6.92 (s, 1H), 6.80 (d, J = 8.1 Hz, 2H), 6.58 (d, J = 8.1 Hz, 2H), 5.68 (ddt, J = 9.9, 3.1, 1.4 Hz, 2H), 5.30 – 5.27 (m, 2H), 5.18 (d, J = 10.3 Hz, 2H), 5.02 (d, J = 10.4 Hz, 2H), 4.86 (dd, J = 6.5, 1.1 Hz, 2H), 4.17 – 4.12 (m, 2H), 3.36 (dd, J = 5.4, 2.9 Hz, 2H), 3.05 (d, J = 18.7 Hz, 2H), 2.91 (s, 2H), 2.69 – 2.65 (m, 2H), 2.61 (dd, J = 12.0, 4.1 Hz, 2H), 2.46 (d, J = 5.4 Hz, 9H), 2.41 (dd, J = 12.6, 3.1 Hz, 2H), 2.37 (s, 6H), 2.34 – 2.29 (m, 2H), 2.06 (td, J = 12.5, 5.0 Hz, 2H), 1.91 – 1.87 (m, 2H). ^{13}C NMR (151 MHz, $CDCl_3$) δ: 147.58, 141.48, 138.95, 138.45, 133.39, 131.40, 131.33, 130.20, 128.09, 119.59, 116.55, 91.15, 77.16, 76.95, 76.74, 67.15, 66.34, 58.91, 46.44, 43.02, 42.86, 40.70, 35.70, 20.61, 19.74, 15.34. IR (ATR, cm^{-1}): 2907, 1633, 1602,1493, 1443, 1374, 1349, 1273, 1248, 1200, 1175, 1157, 1118, 1099, 1034, 983, 940, 833, 784, 766, 730. $[\alpha]_D = -78°$ (c = 0.155, $CHCl_3$, 589 nm, 25°C)

Oripavine-C_1 (***OC1***)

A flask was charged with oripavine (0.654 g, 2.19 mmol), tetrabutylammonium hydroxide (40% aqueous solution, 18 ml) and DCM (8 ml) and stirred under nitrogen for 30 mins. A solution of α^2-chloroisodurene (0.371 g, 2.20 mmol) in DCM (4 ml) was added and the biphasic reaction mixture was stirred for 6 h at rt. The reaction solution was transferred into d.H_2O (150 ml) and washed with DCM (4 x 10 ml). Organic layers were combined

and washed with aqueous NaOH solution (0.1 M, 2 x 20 ml) followed by d.H_2O (3 x 20 ml) then saturated brine solution (20 ml). The organic layer was dried over magnesium sulphate, filtered and solvents removed by rotary evaporation. The crude product was purified by column chromatography (SiO_2, 95:1:1 to 92:8:1 CH_2Cl_2:MeOH:NH_4OH), The title compound **OC1** was isolated as a white solid in in 54 % (0.511 g, 1.19 mmol). mp. 74-76°C. ^{1}H NMR (600 MHz, $CDCl_3$) δ 6.86 (s, 2H), 6.73 (d, *J* = 8.1 Hz, 1H), 6.58 (d, *J* = 8.1 Hz, 1H), 5.57 (d, *J* = 6.4 Hz, 1H), 5.29 (s, 1H), 5.19 (d, *J* = 10.4 Hz, 1H), 5.10 (d, *J* = 10.4 Hz, 1H), 5.04 (d, *J* = 6.4 Hz, 1H), 3.63 (d, *J* = 6.7 Hz, 1H), 3.60 (s, 3H), 3.33 (d, *J* = 18.0 Hz, 1H), 2.84 (td, *J* = 12.7, 3.5 Hz, 1H), 2.69 (dd, J = 18.2, 7.2 Hz, 1H), 2.65 (dd, *J* = 12.9, 5.0 Hz, 1H), 2.47 (s, 3H), 2.38 (s, 6H), 2.27 (s, 3H), 2.22 (td, J = 12.6, 5.0 Hz, 1H), 1.77 (dd, J = 12.5, 2.0 Hz, 2H). ^{13}C NMR (151 MHz, $CDCl_3$) δ 153.12, 146.24, 142.42, 138.62, 138.18, 134.14, 132.74, 130.90, 129.23, 128.87, 119.62, 117.48, 111.97, 96.30, 89.30, 77.58, 77.37, 77.16, 67.20, 61.27, 55.20, 46.43, 46.36, 42.73, 37.26, 30.16, 30.04, 21.34, 19.84. IR (ATR, cm^{-1}): 2912, 1602, 1493, 1473, 1369, 1331, 1278, 1232, 1144, 1022, 985, 868, 817, 768, 704. $[\alpha]_D = -124°$ (c = 0.154, $CHCl_3$, 589nm, 25°C)

Oripavine-C_2 (***OC2***)

A flask was charged with oripavine (0.612 g, 2.05 mmol), tetrabutylammonium hydroxide (40% aqueous solution, 18 ml) and DCM (6 ml) and stirred under nitrogen for 30 mins. A solution of 2,4,-Bis(chloromethyl)-1,3,5-trimethylbenzene (0.224 g, 1.03 mmol) in DCM (4 ml) was added and the biphasic reaction mixture was stirred for 6 h at rt. The reaction solution was transferred into d.H_2O (150 ml) and washed with DCM (4 x 10 ml). Organic layers were combined and washed with aqueous NaOH solution (0.1 M, 2 x 20 ml) followed by d.H_2O (3 x 20 ml) then saturated brine solution (20 ml). The organic layer was dried over magnesium sulphate, filtered and solvents removed by rotary evaporation. The crude product was purified by column chromatography (SiO_2, 95:1:1 to 92:8:1 CH_2Cl_2:MeOH:NH_4OH), The title compound **OC2** was isolated as a white solid in 30 % yield (0.172 g, 0.23 mmol). mp. 73-74°C ^{1}H NMR (600 MHz, $CDCl_3$) δ 6.88 (s, 1H), 6.74 (d, J = 8.1 Hz, 2H), 6.58 (d, J = 8.1 Hz, 2H), 5.56 (d, J = 6.4 Hz, 2H), 5.29 (s, 2H), 5.23 (d, J = 10.5 Hz, 2H), 5.13 (d, J = 10.5 Hz, 2H), 5.03 (d, J = 6.4 Hz, 2H), 3.62 (d, J = 6.8 Hz, 2H), 3.59 (s, 6H), 3.32 (d, J = 18.0 Hz, 2H), 2.83 (td, J = 12.7, 3.4 Hz, 2H), 2.68 (dd, J = 18.2, 7.1 Hz, 2H), 2.63 (dd, J = 12.8, 4.8 Hz, 2H), 2.47 (d, J = 5.1 Hz, 9H), 2.37 (s, 6H), 2.21 (td, J = 12.6, 5.1 Hz, 2H), 1.76 (dd, J = 12.5, 2.0 Hz, 2H). ^{13}C NMR (151 MHz, $CDCl_3$) δ 153.02, 146.19, 142.28, 139.50, 138.66, 134.11, 132.78, 131.93, 130.30, 128.87,

119.55, 117.53, 111.79, 96.24, 89.24, 77.58, 77.37, 77.16, 67.53, 61.17, 55.13, 46.37, 46.29, 42.71, 37.26, 30.04, 20.03, 15.57. IR (ATR, cm^{-1}): 2909, 1605, 1491, 1436, 1369, 1367, 1232, 1143, 1021, 983, 867, 816, 746. $[\alpha]_D = -106°$ (c = 0.156, $CHCl_3$, 589nm, 25°C)

N-Methyl Morphine-C_3 (***MC3-NMe$_2$***)

A flask was charged with **MC3** (100 mg, 0.098 mmol) and dissolved in hot EtOH (5 ml), MeI (100 µl, 1.60 mmol) was added and heated under reflux conditions for 18 h. The solution was allowed to cool and the precipitate collected by vacuum filtration. The product was twice recrystallized from MeOH. The title compound **MC3-NMe$_2$** was isolated as a yellow solid in 14% yield (20 mg, 0.013 mmol). ^{1}H NMR (600 MHz, CD_3CN) δ 6.92 (d, J = 8.2 Hz, 3H), 6.66 (d, J = 8.2 Hz, 3H), 5.75 (d, J = 10.0 Hz, 3H), 5.32 (dt, J = 10.0, 2.6 Hz, 3H), 5.23 (d, J = 10.9 Hz, 3H), 5.16 (d, J = 10.9 Hz, 3H), 4.98 (dd, J = 6.5, 1.0 Hz, 3H), 4.36-4.31 (m, 3H), 4.03-3.99 (m, 3H), 3.48 (d, J = 20.5 Hz, 3H), 3.40 (s, 3H), 3.36 – 3.30 (m, 15H), 3.25 (s, 9H), 3.20 (td, J = 13.4, 3.7 Hz, 3H), 2.90 (dd, J = 20.5, 6.0 Hz, 3H), 2.59 – 2.53 (m, 3H), 2.44 (s, 9H). IR (ATR, cm-1): 2944, 1632, 1607, 1494, 1448, 1250, 1186, 1163, 1119, 1037, 1014, 985, 944, 849, 782, 757.

MC1 spectra:

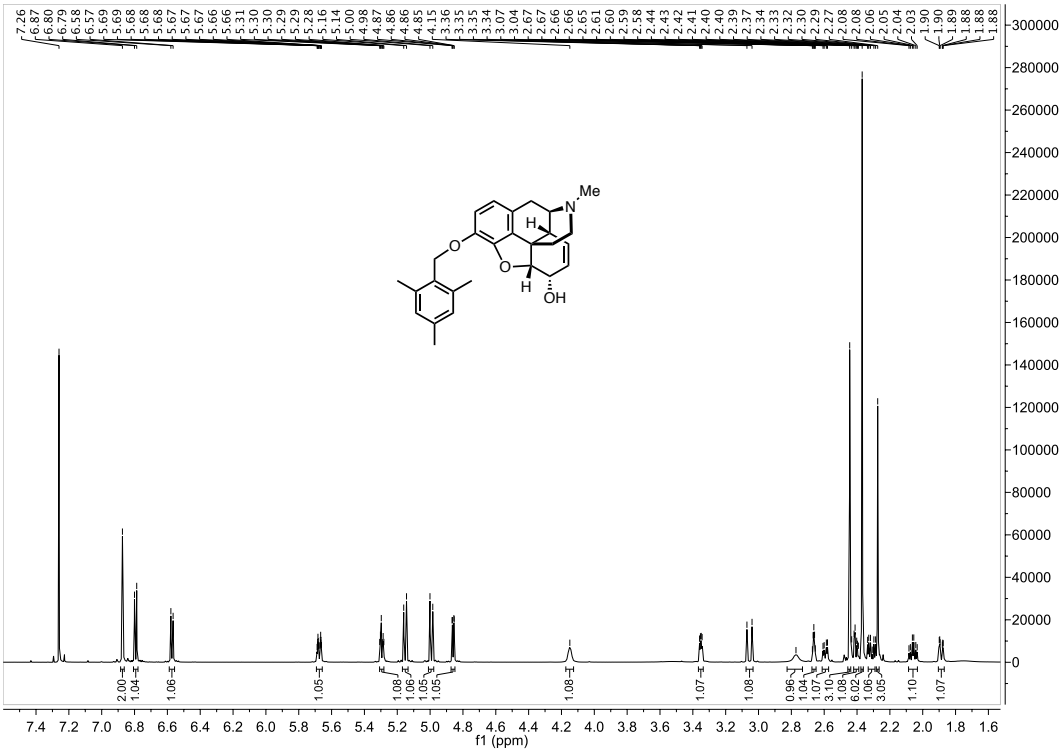

Figure D-18. ^{1}H NMR spectra for **MC1**.

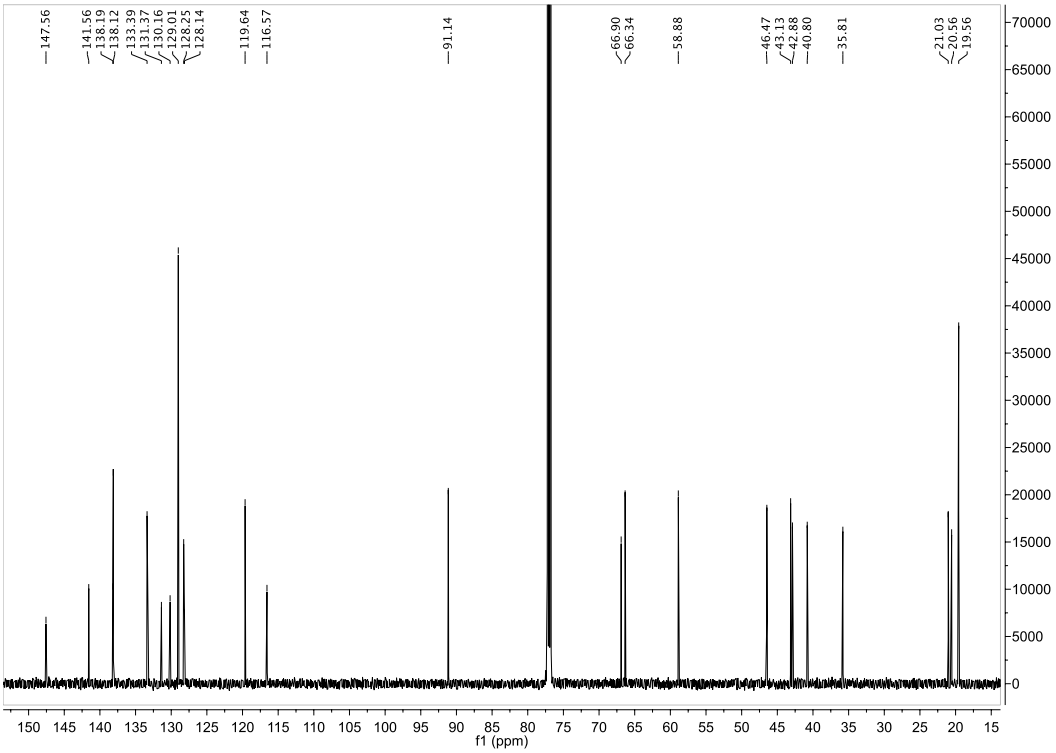

Figure D-19. ^{13}C NMR spectra for **MC1**.

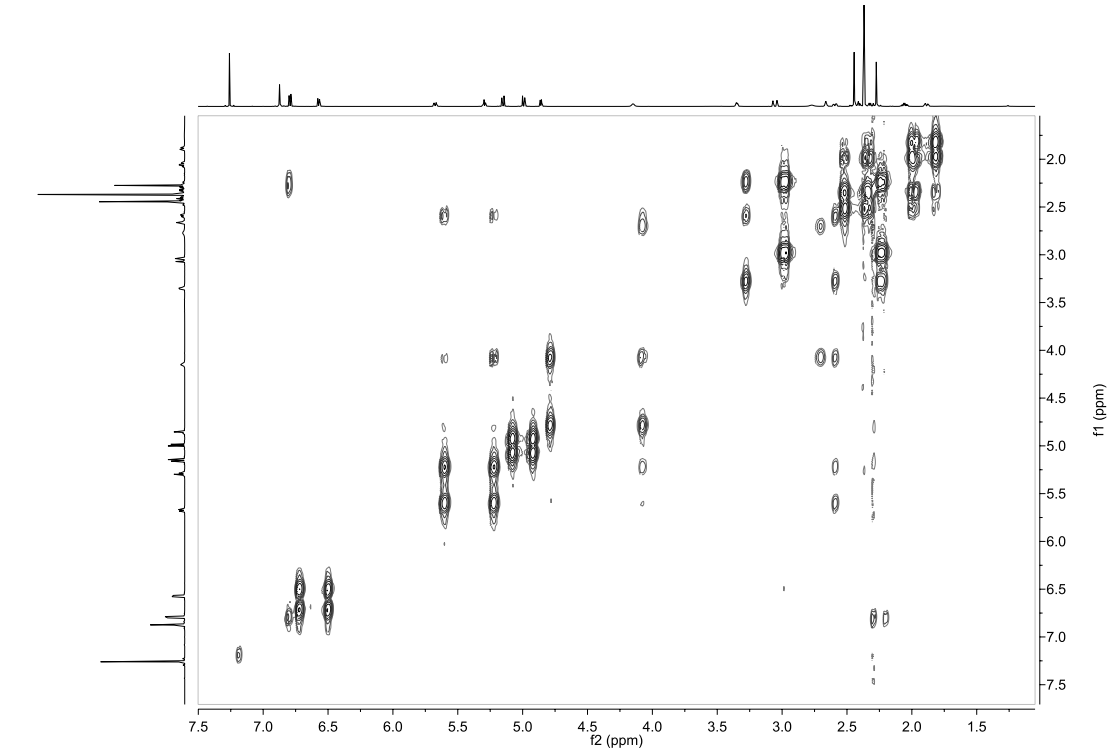

Figure D-20. COSY NMR spectra for **MC1**.

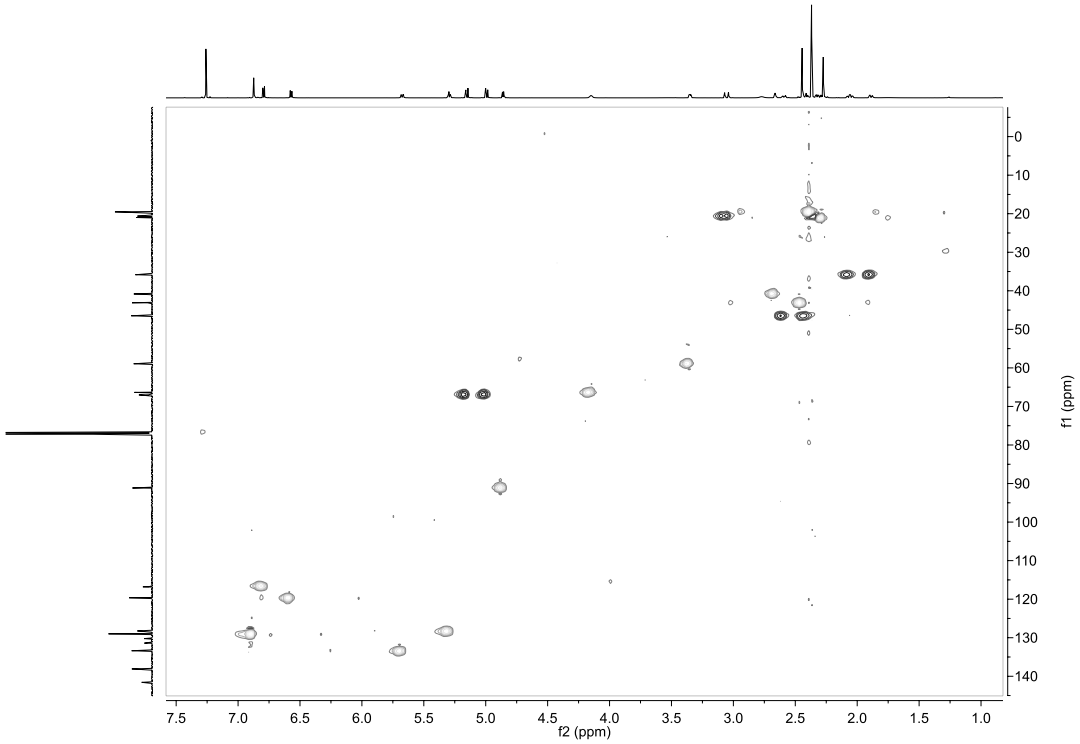

Figure D-21. HSQC NMR spectra for **MC1**.

MC2 spectra:

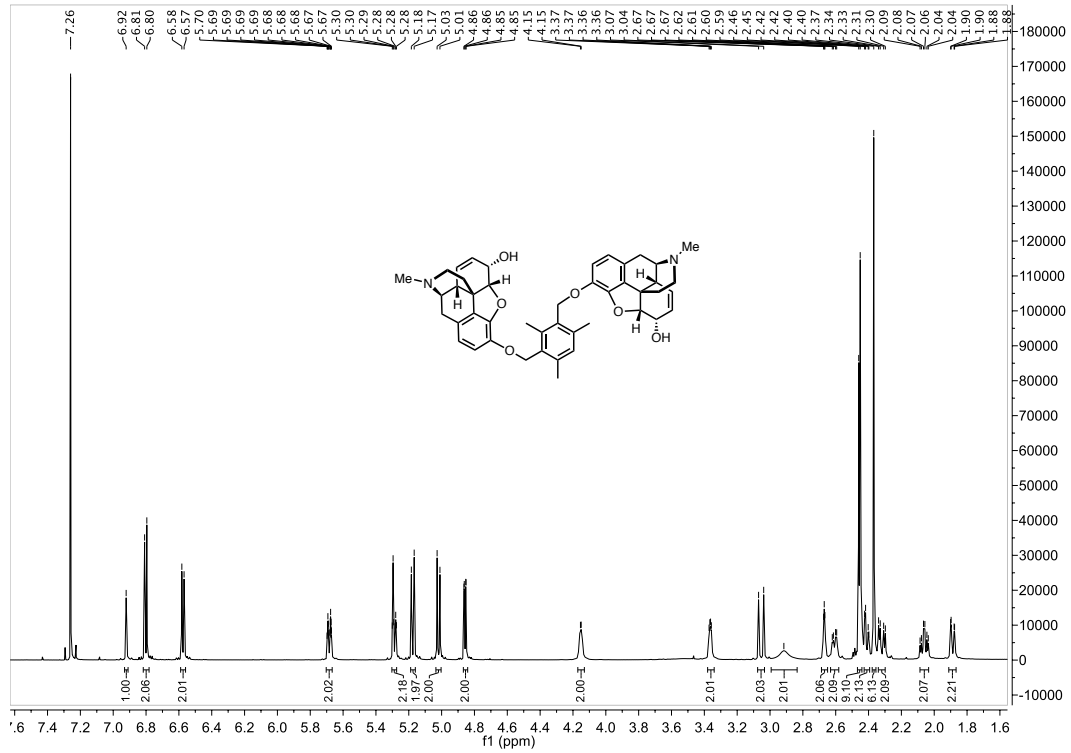

Figure D-22. ^{1}H NMR spectra for **MC2**.

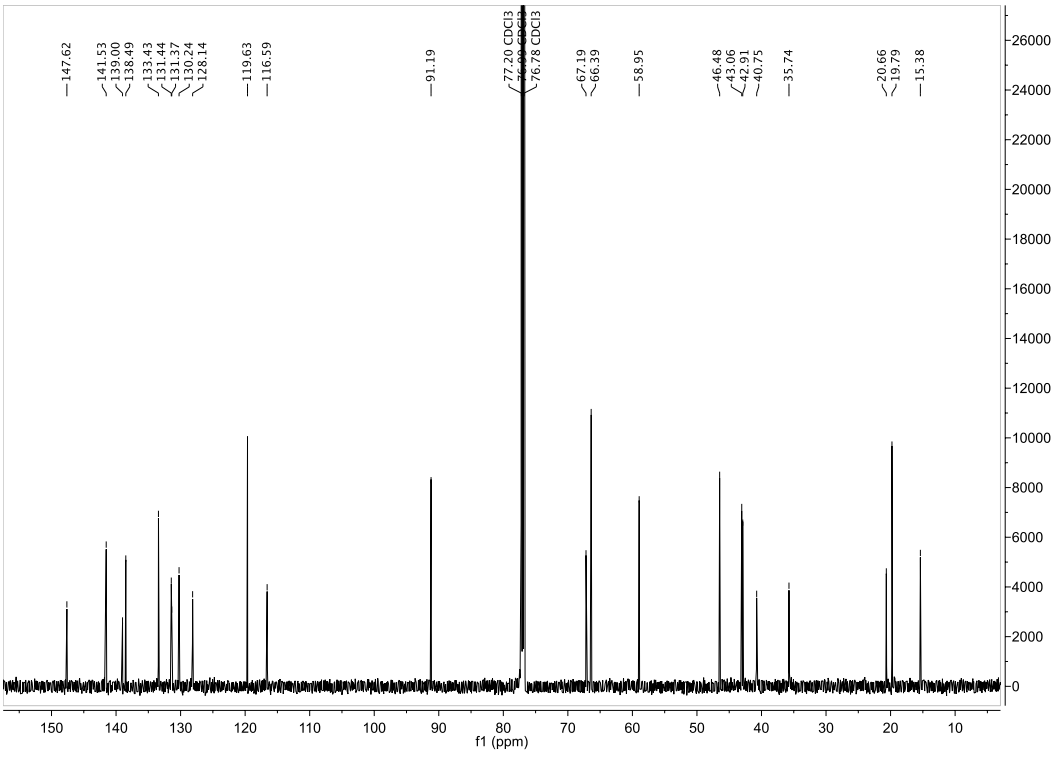

Figure D-23. ^{13}C NMR spectra for **MC2**.

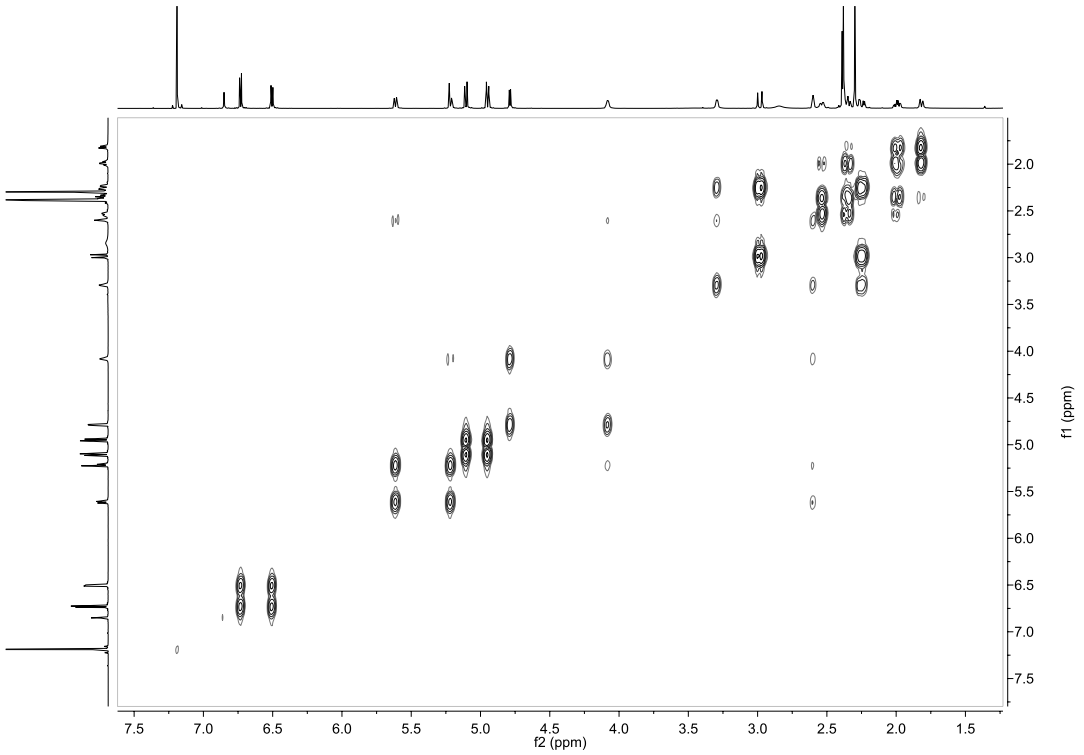

Figure D-24. COSY NMR spectra for **MC2**.

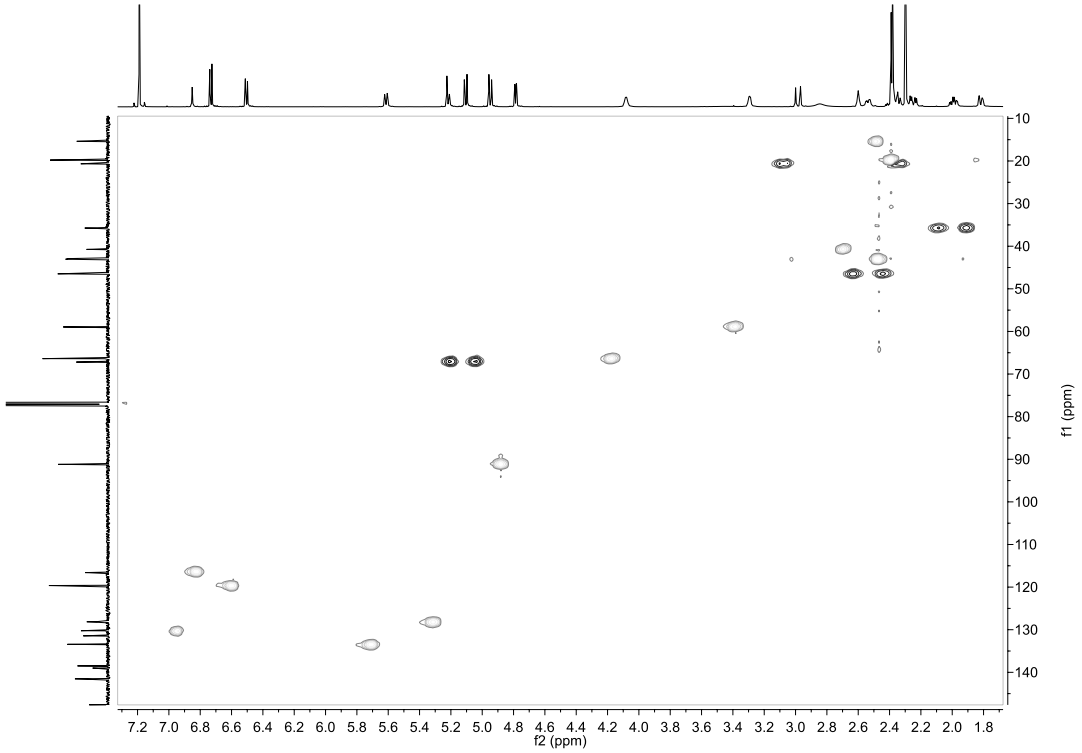

Figure D-25. HMQC NMR spectra for **MC2**.

OC1 Spectra:

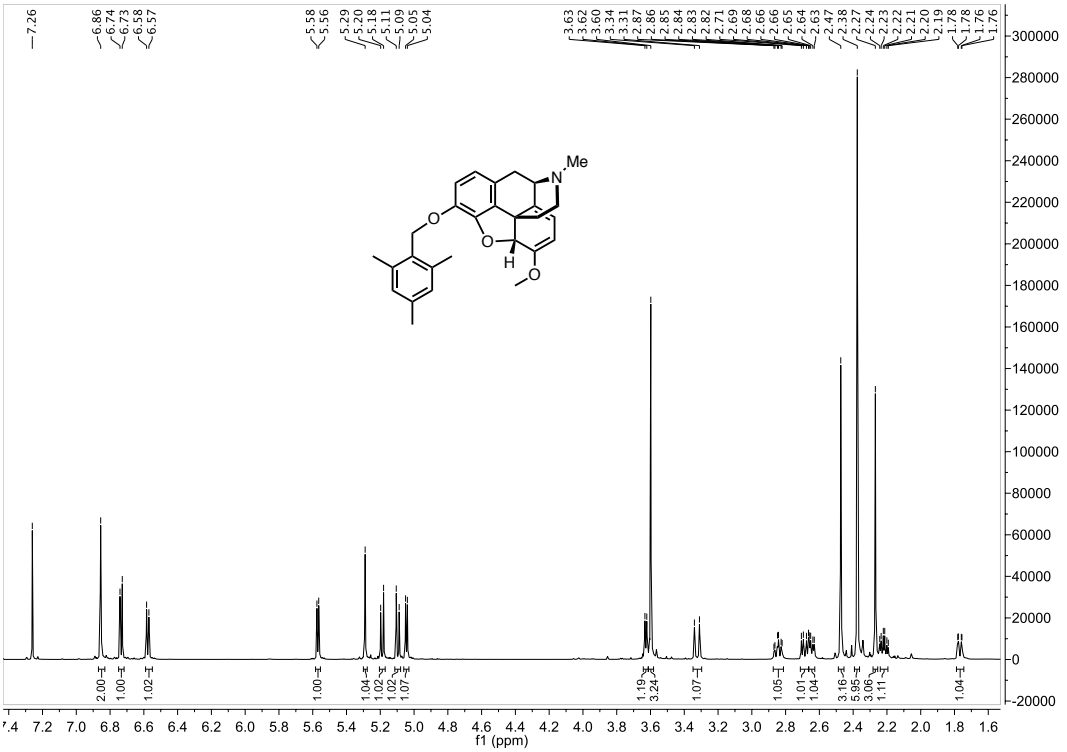

Figure D-26. ^{1}H NMR spectra for **OC1**.

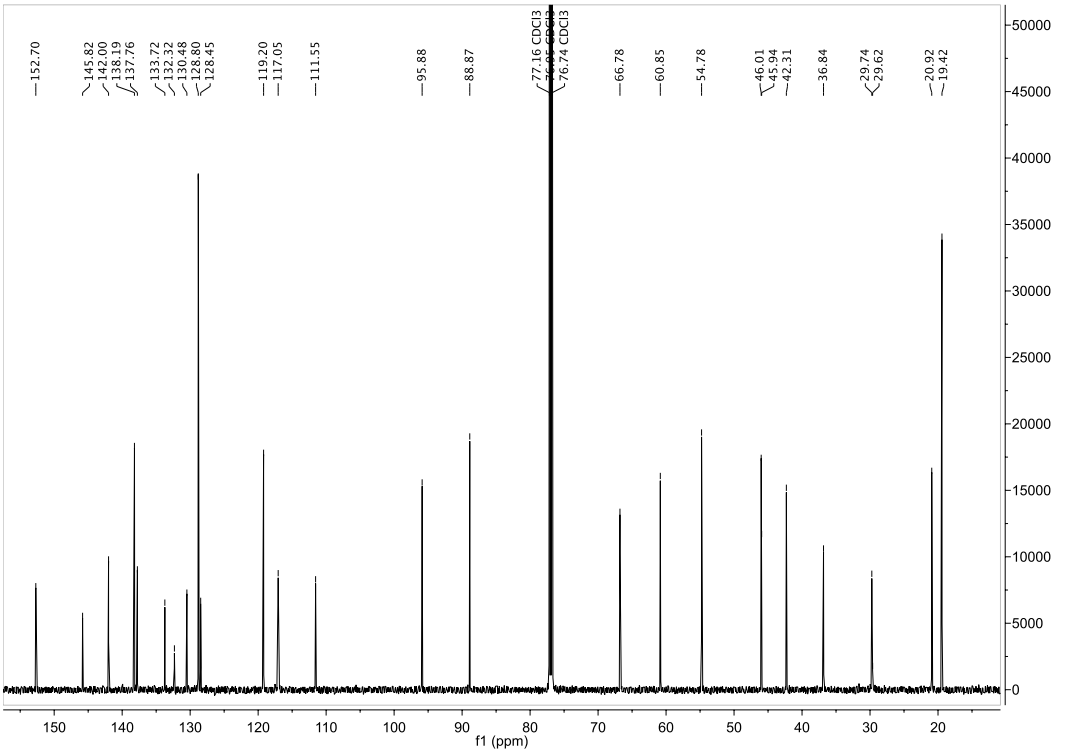

Figure D-27. ^{13}C NMR spectra for **OC1**.

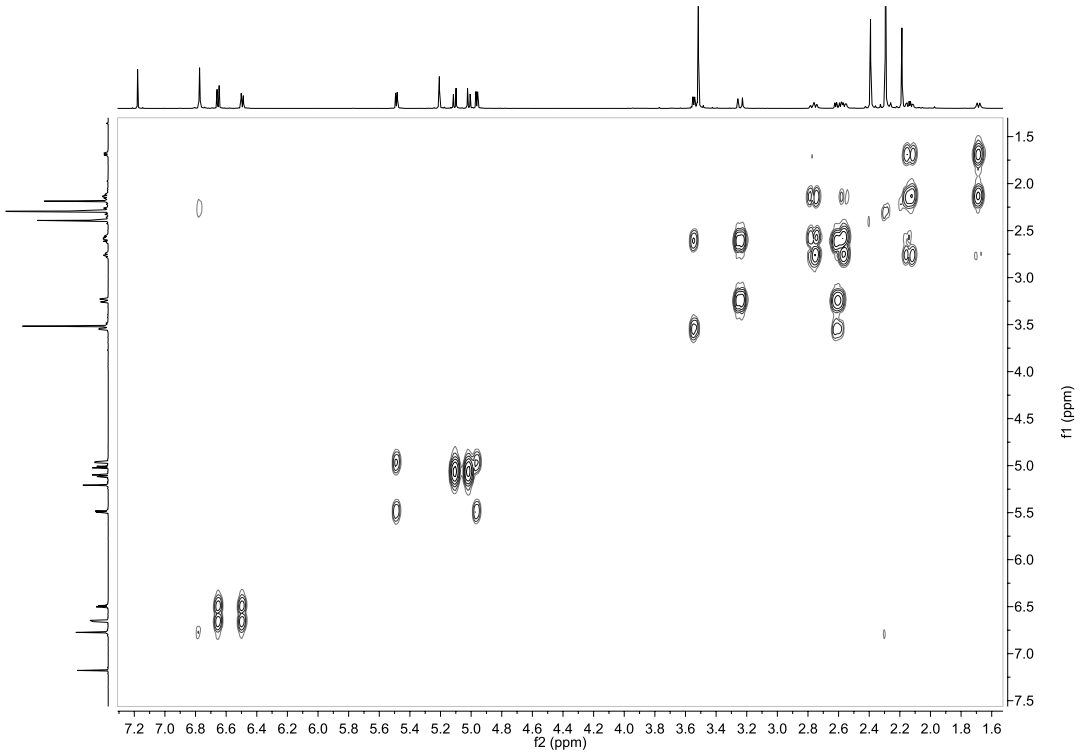

Figure D-28. COSY NMR spectra for **OC1**.

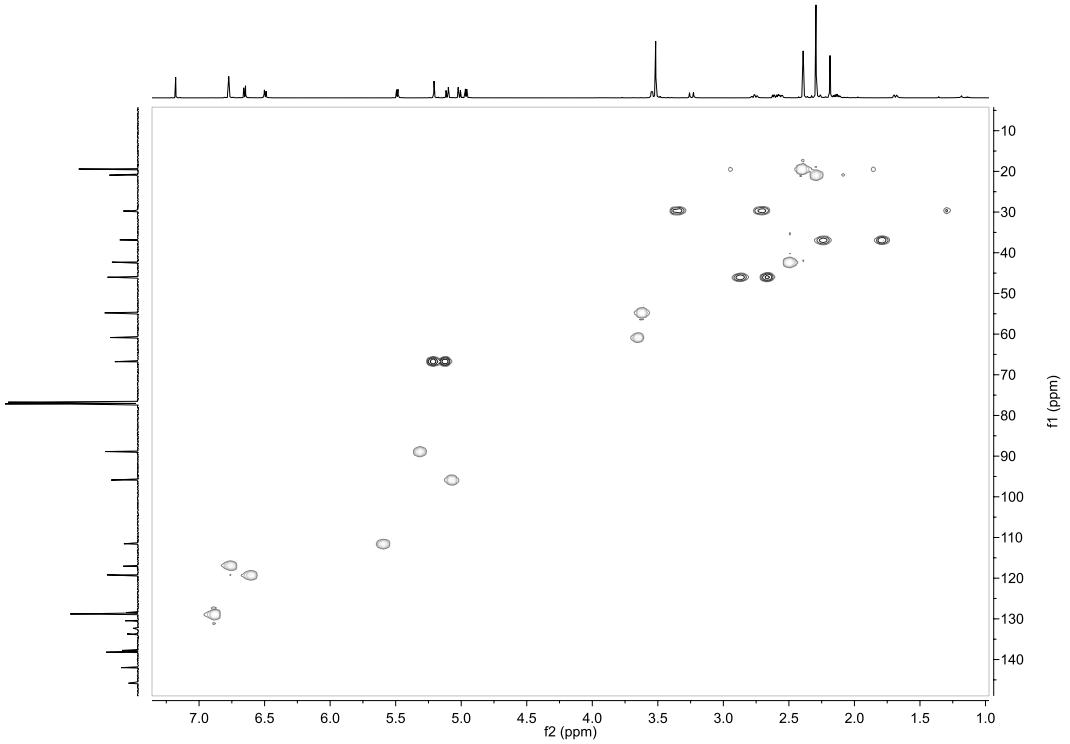

Figure D-29. HMQC NMR spectra for **OC1**.

OC2 spectra:

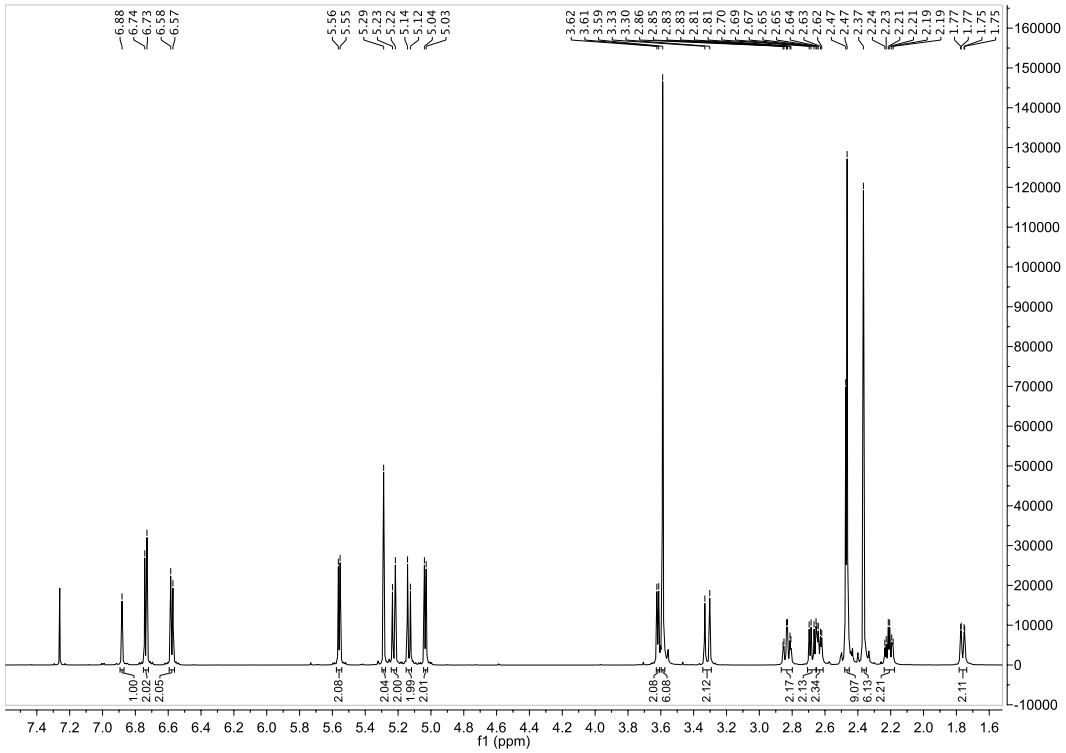

Figure D-30. ^{1}H NMR spectra for **OC2**.

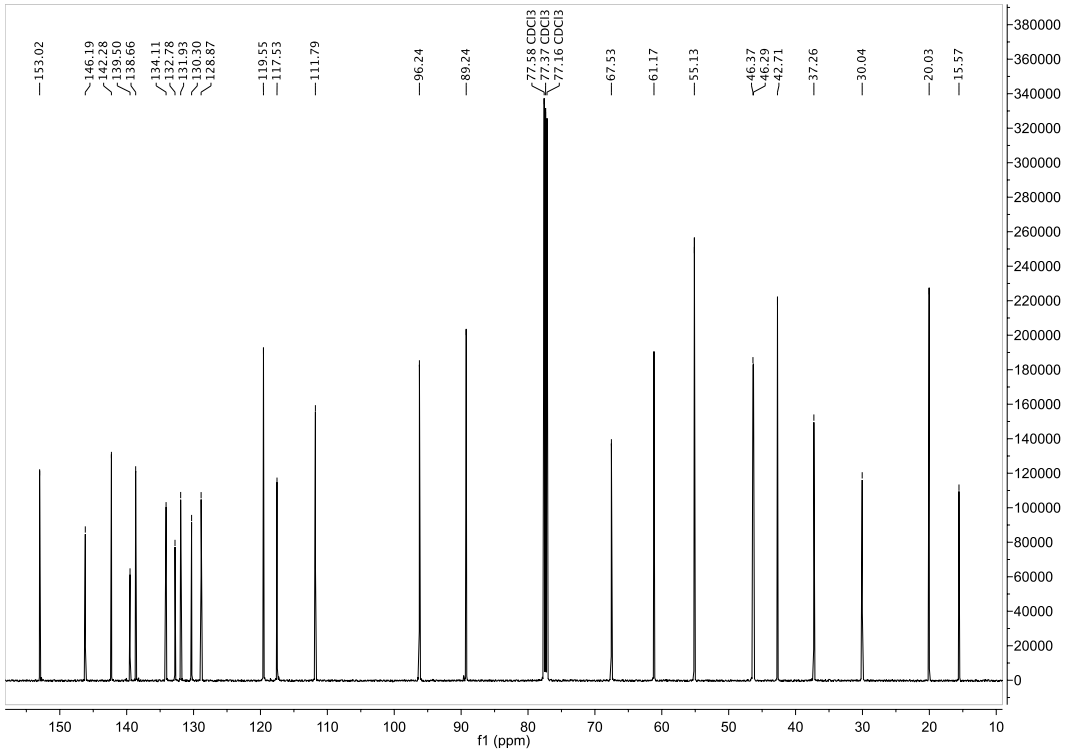

Figure D-31. ^{13}C NMR spectra for **OC2**.

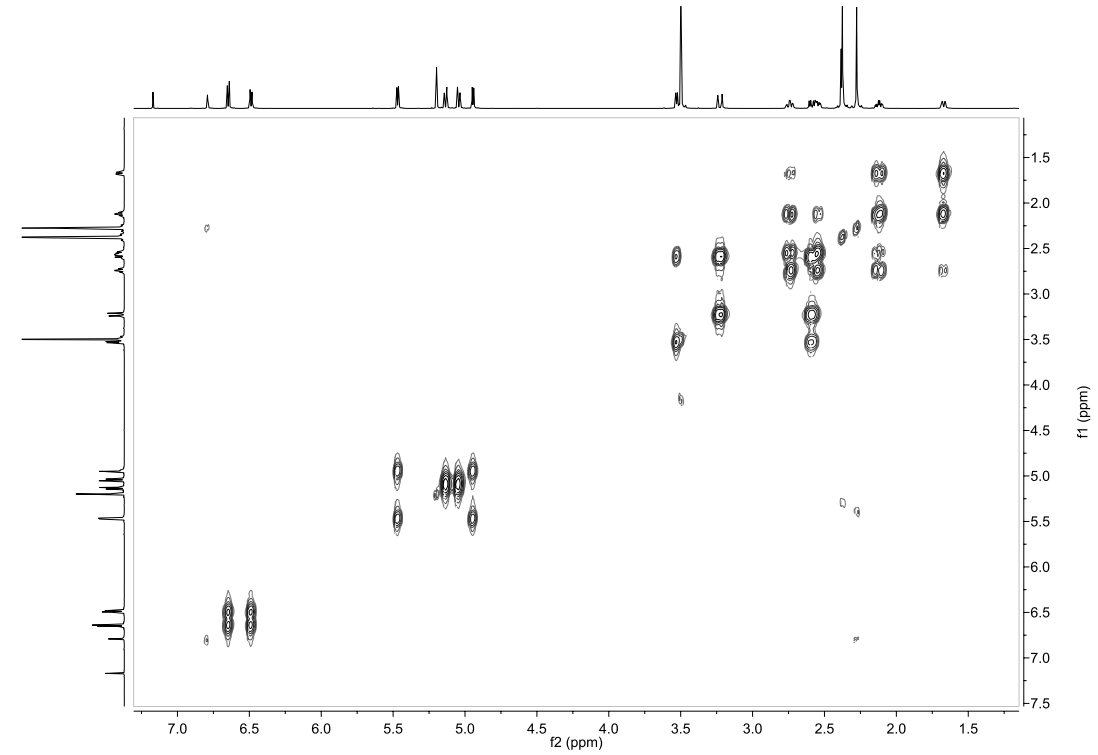

Figure D-32. COSY NMR spectra for **OC2**.

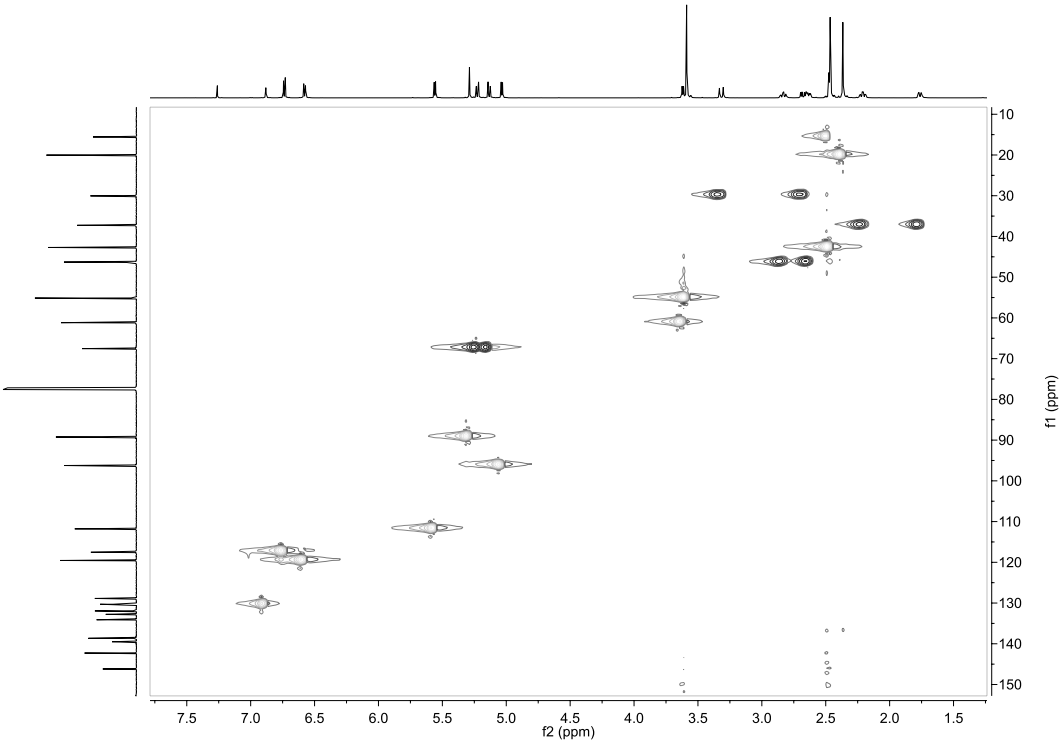

Figure D-33. HMQC NMR spectra for **OC2**.

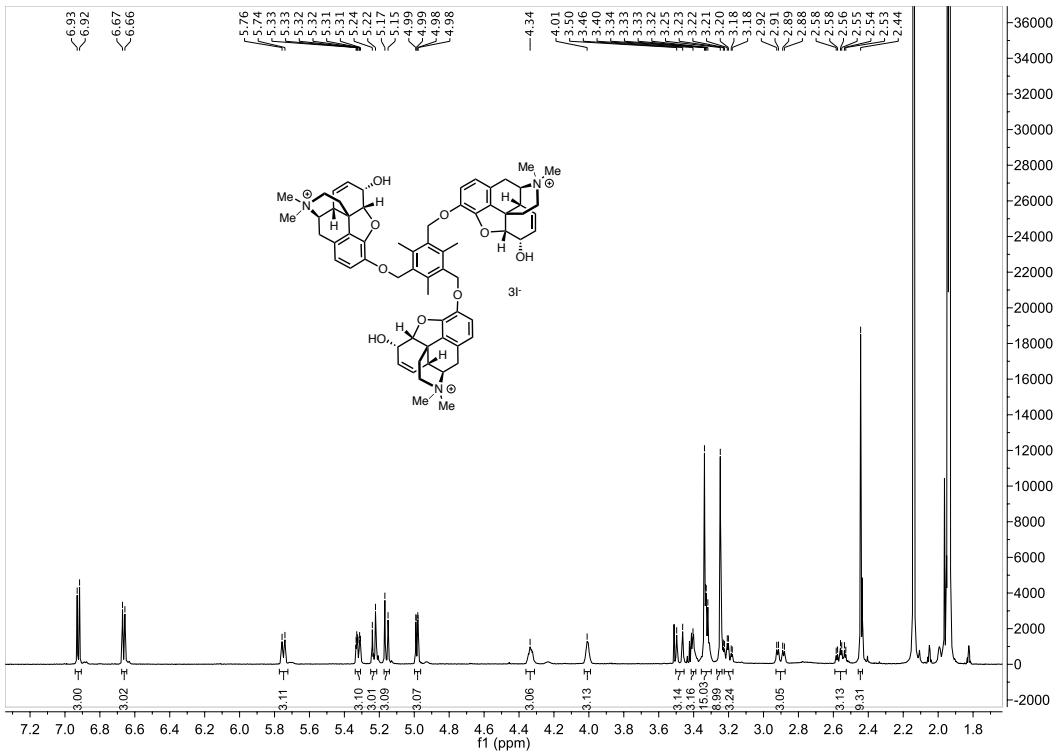

Figure D-34. ^{1}H NMR spectra for **MC3-NMe$_2$**.

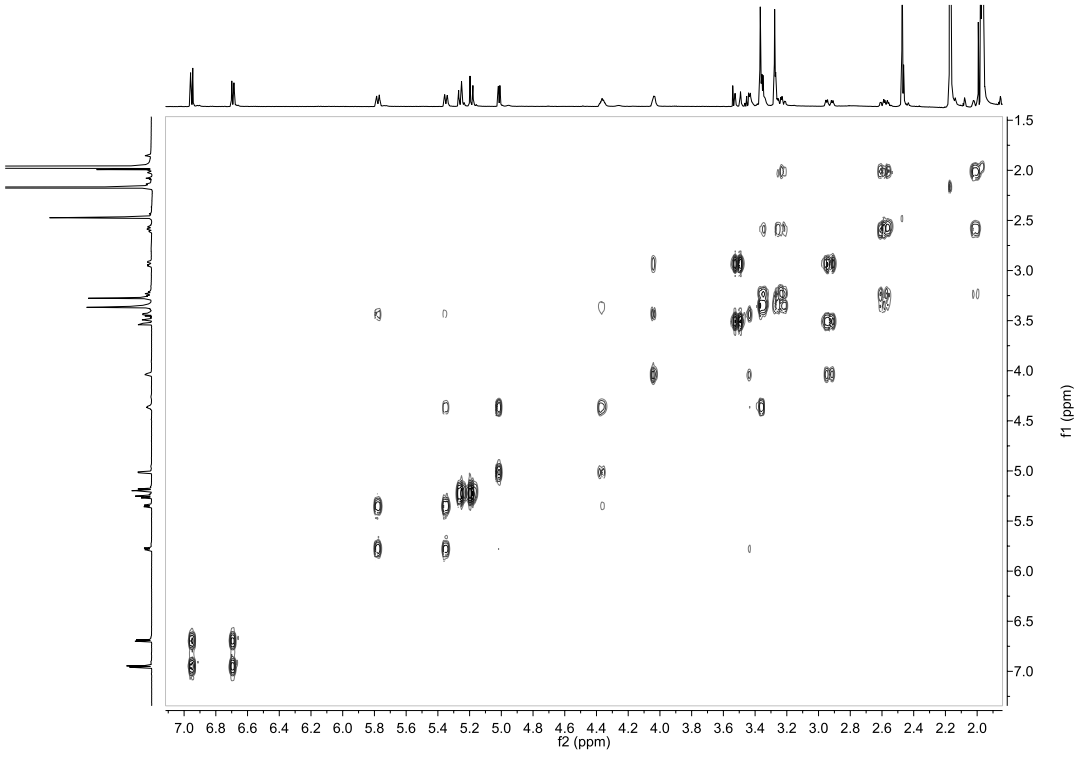

Figure D-35. COSY NMR spectra for **MC3-NMe$_2$**.

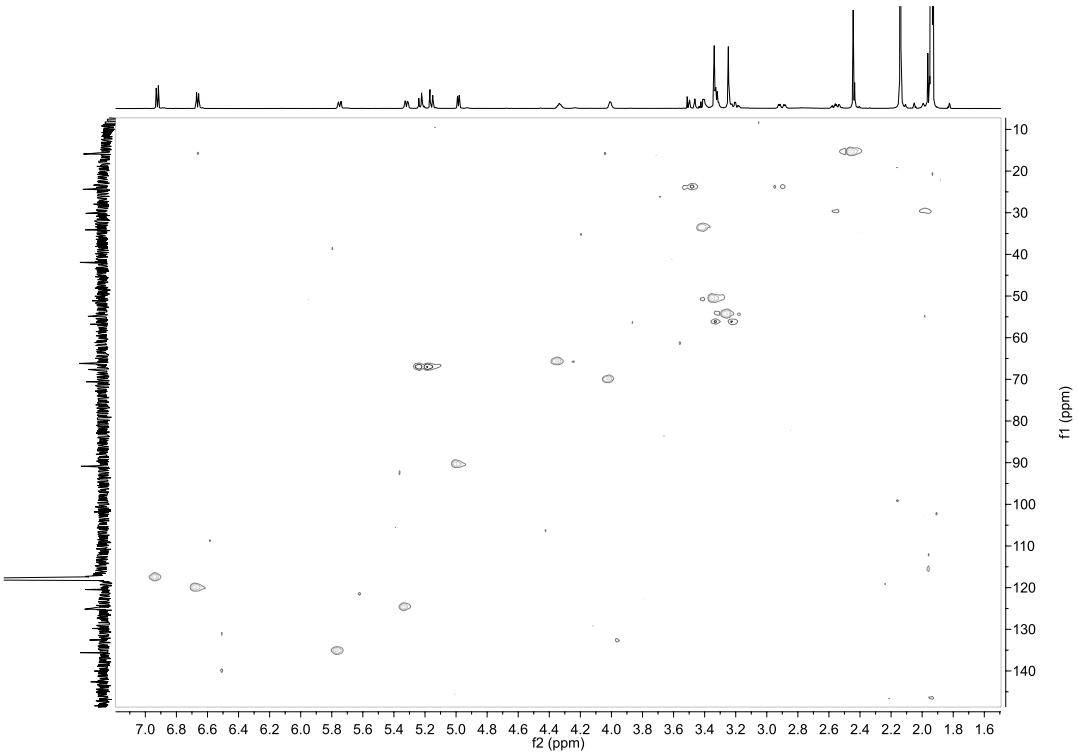

Figure D-36. HSQC NMR spectra for **MC3-NMe$_2$**.

D-8: Morphine isomerization

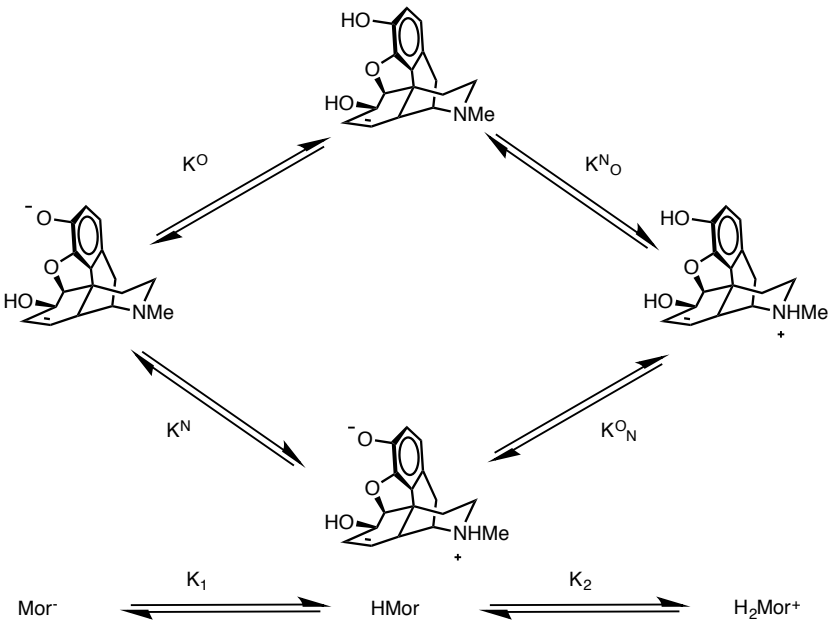

Scheme D-37. Interplay between morphine protonation (k^O) and zwitterionic (k^N) isomers under physiological conditions.

D-9: Gel electrophoresis with yeast tRNA

In a total volume of 20 µl using 80 mM HEPES buffer (pH 7.2) with 25 mM NaCl, 400 ng yeast tRNA (ε_{260} = 9,250 M^{-1} cm^{-1}) (AM7119, Invitrogen) was titrated against **MC3** (0.5 – 50.0 µM). Samples were incubated at 37°C for 5 h and reaction mixtures were subjected to gel electrophoresis as previously stated.

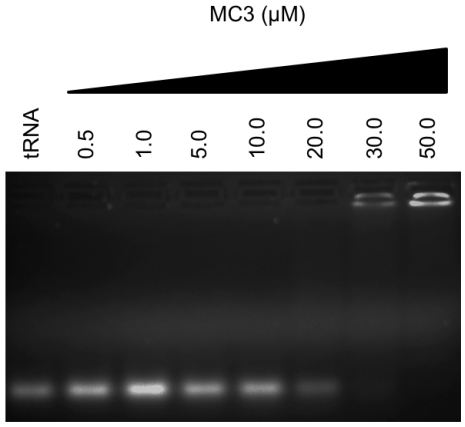

Figure D-38. Agarose gel electrophoresis of yeast tRNA (400 ng) exposed to increasing concentrations of **MC3.** Reactions were carried out in the presence of 25 mM NaCl for 5 h at 37°C prior to electrophoretic analysis.